

AFRL-ML-WP-TR-2001-4074

**LAMINATED OBJECT MANUFACTURING-
BASED DESIGN CERAMIC MATRIX
COMPOSITES**

RAYMOND MEILUNAS

**NORTHROP GRUMMAN CORPORATION
INTEGRATED SYSTEMS SECTOR
TECHNOLOGY DEVELOPMENT
SOUTH OYSTER BAY ROAD
BETHPAGE, NY 11714**

APRIL 2001

FINAL REPORT FOR PERIOD OF 01 JUNE 1998 – 25 SEPTEMBER 2000



Approved for public release; distribution unlimited

**MATERIALS AND MANUFACTURING DIRECTORATE
AIR FORCE RESEARCH LABORATORY
AIR FORCE MATERIEL COMMAND
WRIGHT-PATTERSON AIR FORCE BASE, OH 45433-7750**

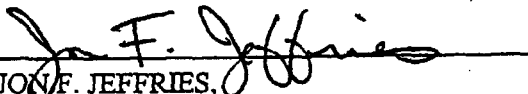
Report Documentation Page		
Report Date 00042001	Report Type N/A	Dates Covered (from... to) -
Title and Subtitle Laminated Object Manufacturing-Based Design for Ceramic Matrix Composites	Contract Number	
	Grant Number	
	Program Element Number	
Author(s) Meilunas, Raymond	Project Number	
	Task Number	
	Work Unit Number	
Performing Organization Name(s) and Address(es) Northrop Grumman Corporation Integrated Systems Sector Technology Development South Oyster Bay Road Bethpage, NY 11714	Performing Organization Report Number	
Sponsoring/Monitoring Agency Name(s) and Address(es) Materials and Manufacturing Directorate Air Force Research Laboratory Air Force Materiel Command Wright-Patterson AFB, OH 45433-7750	Sponsor/Monitor's Acronym(s)	
	Sponsor/Monitor's Report Number(s)	
Distribution/Availability Statement Approved for public release, distribution unlimited		
Supplementary Notes The original document contains color images.		
Abstract		
Subject Terms		
Report Classification unclassified	Classification of this page unclassified	
Classification of Abstract unclassified	Limitation of Abstract UU	
Number of Pages 242		


NOTICE


USING GOVERNMENT DRAWINGS, SPECIFICATIONS, OR OTHER DATA INCLUDED IN THIS DOCUMENT FOR ANY PURPOSE OTHER THAN GOVERNMENT PROCUREMENT DOES NOT IN ANY WAY OBLIGATE THE US GOVERNMENT. THE FACT THAT THE GOVERNMENT FORMULATED OR SUPPLIED THE DRAWINGS, SPECIFICATIONS, OR OTHER DATA DOES NOT LICENSE THE HOLDER OR ANY OTHER PERSON OR CORPORATION; OR CONVEY ANY RIGHTS OR PERMISSION TO MANUFACTURE, USE, OR SELL ANY PATENTED INVENTION THAT MAY RELATE TO THEM.

THIS REPORT IS RELEASABLE TO THE NATIONAL TECHNICAL INFORMATION SERVICE (NTIS). AT NTIS, IT WILL BE AVAILABLE TO THE GENERAL PUBLIC, INCLUDING FOREIGN NATIONS.

THIS TECHNICAL REPORT HAS BEEN REVIEWED AND IS APPROVED FOR PUBLICATION.


JON F. JEFFRIES,
Project Engineer
Industrial Infrastructure Team
Mfg. & Engineering Systems Branch


KENNETH A. FEESER
Leader
Industrial Infrastructure Team
Mfg. & Engineering Systems Branch


BRANCH BODEN
Chief
Mfg. & Engineering Systems Branch
Manufacturing Technology Division

Do not return copies of this report unless contractual obligations or notice on a specific document require its return.

REPORT DOCUMENTATION PAGE			Form Approved OMB No. 0704-0188	
Public reporting burden for this collection of information is estimated to average 1 hour per response, including the time for reviewing instructions, searching existing data sources, gathering and maintaining the data needed, and completing and reviewing the collection of information. Send comments regarding this burden estimate or any other aspect of this collection of information, including suggestions for reducing this burden, to Washington Headquarters Services, Directorate for Information Operations and Reports, 1215 Jefferson Davis Highway, Suite 1204, Arlington, VA 22202-4302, and to the Office of Management and Budget, Paperwork Reduction Project (0704-0188), Washington, 0020503.				
1. AGENCY USE ONLY (Leave blank)	2. REPORT DATE April 2001	3. REPORT TYPE AND DATES COVERED Final Report for 1 June 1998 to 25 September 2000		
4. TITLE AND SUBTITLE Laminated Object Manufacturing-Based Design for Ceramic Matrix Composites		5. FUNDING NUMBERS C F33615-98-C-5121 PE 62712E PR 8Y10 TA 04 WU 00		
6. AUTHORS Raymond Meilunas				
7. PERFORMING ORGANIZATION NAME(S) AND ADDRESS(ES) Northrop Grumman Corporation Integrated Systems Sector Technology Development South Oyster Bay Road Bethpage, NY 11714		8. PERFORMING ORGANIZATION REPORT NUMBER		
9. SPONSORING/MONITORING AGENCY NAME(S) AND ADDRESS(ES) Materials and Manufacturing Directorate Air Force Research Laboratory Air Force Materiel Command Wright-Patterson AFB, OH 45433-7750 POC: Jon Jeffries, AFRL/MLMS, (937) 904-4353		10. SPONSORING/MONITORING AGENCY REPORT NUMBER AFRL-ML-WP-TR-2001-4074		
11. SUPPLEMENTARY NOTES				
12a. DISTRIBUTION/AVAILABILITY STATEMENT Approved for Public Release; Distribution is Unlimited.			12b. DISTRIBUTION CODE	
13. ABSTRACT (Maximum 200 words) <p>This report summarizes the significant accomplishments of the Laminated Object Manufacturing Based Design for Ceramic Matrix Composites Program. The overall objective of the twenty-seven month long effort was to further develop LOM based solid freeform fabrication for the rapid design and manufacture of CMC components for DoD applications. Program goals included the development of (1) a new LOM based design methodology for CMC, (2) optimized preceramic polymer CMC material forms specific for LOM processing, (3) LOM system upgrades to increase fabrication efficiencies and improve part tolerances/accuracy, and (4) demonstration of the combined design methodology and materials and hardware improvements via the rapid design and LOM fabrication of a CMC prototype component. This program was funded through DARPA Contract No.F33615-98-C-5121, administered by the Air Force Wright Laboratory. Program participants included Northrop Grumman Corp. (Prime), Helisys Inc., and the University of Dayton Research Institute (UDRI). The technical approach included tasks in LOM based CMC design methodology development, material and LOM system development, and methodology demonstration. The demonstration component was an engine exhaust washed, high temperature blastshield representative of structures anticipated on future military vertical short takeoff and landing (VSTOL) and low observable (LO) aircraft with shielded exhaust.</p>				
14. SUBJECT TERMS Laminate object manufacturing, solid freeform fabrication, composite processing, design methodology, rapid prototyping, ceramic matrix composites, Blackglas™, Nextel™, exhaust washed structures			15. NUMBER OF PAGES 226	
			16. PRICE CODE	
17. SECURITY CLASSIFICATION OF REPORT UNCLASSIFIED	18. SECURITY CLASSIFICATION OF THIS PAGE UNCLASSIFIED	19. SECURITY CLASSIFICATION OF ABSTRACT UNCLASSIFIED	20. LIMITATION OF ABSTRACT SAR	

Table of Contents

<u>Section</u>	<u>Page No.</u>
LIST OF FIGURES.....	iv
LIST OF TABLES	xii
FOREWORD	xiii
1.0 INTRODUCTION.....	1-1
2.0 APPROACH.....	2-1
3.0 SUMMARY OF RESULTS.....	3-1
3.1 Design Methodology Development	3.1.1-1
3.1.1 LOM Forming Concept	3.1.1-1
3.1.2 CCDP/LOM Interface Development.....	3.1.2-1
3.1.3 CAD/LOM Procedure Development (Task 1.1.2)	3.1.3-1
3.1.4 Design Methodology Validation.....	3.1.4-1
3.2 LOM/CMC Process Validation.....	3-2
3.2.1 Material System Development (Task 1.2.1).....	3.2.1-1
3.2.2 LOM System Development.....	3.2.2-1
3.2.3 LOM System Demonstration.....	3.2.3-1
3.3 CMC Prototype Demonstration.....	3-3
3.3.1 Design of Demonstration Component	3.3.1-1
3.3.2 Fabrication of Demonstration Component (Task 1.3.2)	3.3.2-1
4.0 OVERALL SUMMARY & CONCLUSIONS.....	4-1
5.0 APPENDICES.....	5-1

List of Figures

<u>Figure</u>	<u>Page No.</u>
2-1 Nextel™/Blackglas™ AV-8B CMC Blastshield Design Concept	2-7
3.1.1-1 Schematic of New LOM/Forming Process Sequence	3.1.1-4
3.1.1-2 Classification of Part Shapes in terms of Gaussian or Compound Curvatures.....	3.1.1-7
3.1.1-3 Examples of CMC Parts with 0 Gaussian Curvature A) Nicalon/ Blackglas™ Fairing Channel, B) SiC/SiC Engine Flameholders, C) DIMOX™ Body Armor Plate	3.1.1-8
3.1.1-4 Examples of CMC Parts with Positive Gaussian Curvature: A) Blackglas Radome, B) Nicalon/Blackglas Blastshield, C) Nextel/Blackglas Engine Tailcone.....	3.1.1-8
3.1.1-5 Example of CMC Part with Negative Gaussian Curvature: Nicalon/Blackglas duct section.	3.1.1-9
3.1.1-6 Examples of F/A-18 parts suitable for automated forming.....	3.1.1-14
3.1.1-7 Examples of C-17 parts and tooling suitable for LOM/Forming	3.1.1-16
3.1.1-8 Section of JSF Tooling Fixture	3.1.1-17
3.1.1-9 Schematic of Composites Forming Cell for LOM.....	3.1.1-18
3.1.1-10 LOM Composites Forming System.....	3.1.1-19
3.1.1-11 Thermocouple positions on flat pattern of blast shield tool.....	3.1.1-20
3.1.1-12 Detail of LOM Composites Forming System w/ glass fiber/polymer laminate.....	3.1.1-21
3.1.1-13 LOM Composites Forming System during temperature calibration.....	3.1.1-22
3.1.2-1 User Interface Screen displaying ply layer from LOMNEF file for 8"x 8" cruciform stiffened subcomponent panel.....	3.1.2-6
3.1.3-1 ExampleDesign Software Suite for LOM/Forming of CMC Components	3.1.3-2
3.1.3-2 LOM/Forming Design Methodology Procedure with updated Part Formability Evaluation Module	3.1.3-5
3.1.3-3 Overview of the elements of a Composite Part Formability Evaluation.....	3.1.3-5
3.1.3-4 Component Gaussian Curvature Analysis (Rhino3D software).....	3.1.3-10
3.1.3-5 Examples of ply patterns required for mapping over hemisphere	3.1.3-11

List of Figures (cont.)

<u>Figure</u>	<u>Page No.</u>
3.1.3-6 Examples of screen outputs in FiberSIM for component producibility assessment and flat pattern generation	3.1.3-13
3.1.3-7 Engine Tailcone Model for FiberSIM Formability Simulation	3.1.3-16
3.1.3-8 FiberSIM analysis output of generic tailcone geometry mapped with a single woven composite ply	3.1.3-17
3.1.3-9 FiberSIM analysis output of plan view of deformation pattern of a generic weave draped over tail-cone geometry	3.1.3-17
3.1.3-10 FiberSIM forming simulation for demonstration tailcone.....	3.1.3-19
3.1.4-1 CMC Subcomponent Design Sequence	3.1.4-1
3.1.4-2 CMC sub-component LOMNEF design data files	3.1.4-2
3.1.4-3 Ply Table for 4"x 4" Flat Cruciform Sub-element	3.1.4-3
3.2.1-1 Effect of Aging at Room Temperature on the Compressibility of '-5%' Prepreg.....	3.2.1-7
3.2.1-2 Effect of Aging at Room Temperature on the Compressibility of 'Standard' Prepreg.....	3.2.1-9
3.2.1-3 Effect of Aging at Room Temperature on the Compressibility of '+5%' Prepreg.....	3.2.1-11
3.2.1-4 Effect of Aging at Room Temperature on the Compressibility of '+10%' Prepreg	3.2.1-12
3.2.1-5 Effect of Resin Content on Compressibility of Fresh High Initial Viscosity Prepreg (Batch No. 22439)	3.2.1-13
3.2.1-6 Effect of Aging on the Compressibility 'Standard' 493C High Initial Viscosity Resin (Batch No. 22439)	3.2.1-14
3.2.1-7 Effect of Aging on the Compressibility '-5%' 493C High Initial Viscosity Resin Batch No. 22439)	3.2.1-15
3.2.1-8 Effect of Resin Content on the Compressibility of 493A/B Prepreg	3.2.1-16
3.2.1-9 Effect of Aging on Compressibility of -5% 493A/B Resin Prepreg.....	3.2.1-17
3.2.1-10 Effect of Aging on Compressibility of Standard 493A/B Resin Prepreg	3.2.1-18
3.2.1-11 Effect of Aging on the Compressibility of +5% 493A/B Resin Prepreg.....	3.2.1-18
3.2.1-12 Effect of Application of 489 as a Tackifier on the Compressibility of 493A/B Prepreg...	3.2.1-23

List of Figures (cont.)

<u>Figure</u>	<u>Page No.</u>
3.2.1-13 Effect of Application of Epoxy Tackifier on the Compressibility of 493A/B Prepreg	3.2.1-23
3.2.1-14 Effect of Freezer Storage on Compressibility of 493 A/B Prepreg.....	3.2.1-24
3.2.1-15 Compressibility curves for Nextel 312/Blackglas 489 prepreg material.....	3.2.1-26
3.2.1-16 Effect of resin content on the compressibility of Nextel 720/COI prepreg in the as-received condition.....	3.2.1-30
3.2.1-17 Effect of Out-time on the compressibility of Nextel 720/COI Prepreg with 55 grams per square foot of resin applied.....	3.2.1-32
3.2.1-18 Effect of Out-time on the Compressibility of Nextel 720/COI Prepreg with 50 grams per square foot of resin applied.....	3.2.1-32
3.2.1-19 Effect of Out-time on the compressibility of Nextel 720/COI Prepreg with 45 grams per square foot of resin applied.....	3.2.1-33
3.2.1-20 Viscosity as a function of time for COI resin	3.2.1-34
3.2.1-21 Viscosity as a function of time for Blackglas 493A/B and 493C resins	3.2.1-35
3.2.1-22 DSC scans on 489C Blackglas resin tested after various out times	3.2.1-37
3.2.1-23 DSC scans on 493C Blackglas resin tested after various out times	3.2.1-37
3.2.1-24 Viscosity as a function of time for 489C resin.....	3.2.1-39
3.2.1-25 Dynamic Mechanical Analysis samples infiltrated with (a) Photoresist resin and (b) TCC 630 epoxy resin	3.2.1-46
3.2.1-26 Dynamic Mechanical Analysis samples infiltrated with TCC 630 epoxy; (a) infiltrated under atmospheric pressure without subsequent post cure, (b) atmospheric pressure with post cure (c) 100 psi over pressure and post cured (d) 100 psi over pressure with 1/4" center holes (e) 100 psi over pressure with 1/4" center holes using high temperature hardener.....	3.2.1-48
3.2.1-27 Thermo mechanical behaviors of candidate infiltration resins as evaluated by Dynamic Mechanical Analysis.....	3.2.1-51
3.2.1-28 Thermo mechanical behavior of LOM Paper samples infused with TCC 630 Epoxy.....	3.2.1-53
3.2.1-29 Thermo mechanical behaviors of LOM Paper samples infused with Epofix potting compound and Blackglas resin.....	3.2.1-55

List of Figures (cont.)

<u>Figure</u>	<u>Page No.</u>
3.2.1-30 (a) Section of pressure infiltrated (100 psi) LOM test block with single .062" dia. through hole, (b) vacuum/pressure infiltrated LOM test block (sectioned) with through hole array, (c) vacuum/pressure infiltrated 11"x 11" LOM test block (sectioned) with through hole array, (d) vacuum/pressure infiltrated 9"x 9" LOM forming tool.....	3.2.1-57
3.2.1-31 a) Vacuum/Over Pressure Resin Infiltration Process: Step 1	3.2.1-59
3.2.1-31 b) Vacuum/Over Pressure Resin Infiltration Process: Step 2	3.2.1-60
3.2.1-31 c) Vacuum/Over Pressure Resin Infiltration Process: Step 3	3.2.1-60
3.2.1-32 (a) 3D CAD model of LOM blastshield forming tool and (b) final resin infiltrated part. .	3.2.1-63
3.2.1-33 Shape offset analysis of LOM tool before and after temperature calibration on composites forming system (offsets in mils)	3.2.1-65
3.2.2-1 Modified LOM2030H system with laser scanner subsystem.....	3.2.2-6
3.2.2-2 Laser Scanner Module on LOM 2030H system.....	3.2.2-7
3.2.2-3 3D representation of the calculated Z-axis Look Up Table.....	3.2.2-12
3.2.2-4 Difference between calculated and original Z axis lens Look-up Table.....	3.2.2-12
3.2.2-5 Division of the working field into quadrants.....	3.2.2-13
3.2.2-6 Division of a quadrant into 5x5 array of control points.	3.2.2-14
3.2.2-7 Visual Interface Dialog Box for scanner calibration.	3.2.2-15
3.2.2-8 Image of target calibration points shot by the laser into one quadrant.	3.2.2-15
3.2.2-9 CCD camera data at the junction of quadrants 1,2,3,4,7,8.	3.2.2-16
3.2.2-10 Verification of calibration by detecting the coordinate of a shot delivered into a quadrant origin.	3.2.2-17
3.2.2-11 Example of grid misalignment at quadrant boundaries before Inter-Regional Calibration procedure.....	3.2.2-18
3.2.2-12 Example of laser calibration shots on LOM paper used for Inter-Regional Calibration procedure.....	3.2.2-18
3.2.2-13 Grid alignment at quadrant boundary after Inter-Regional Calibration procedure.	3.2.2-19

List of Figures (cont.)

<u>Figure</u>	<u>Page No.</u>
3.2.2-14 Multi-quadrant laser cutting evaluation on glass fiber fabric after Inter-Regional Calibration procedure.....	3.2.2-20
3.2.2-15 DVT CCD camera system mounted on scanner gantry.....	3.2.2-22
3.2.2-16 processing steps for LOM fabrication of half scale fiberglass blastshield laminate: a) lamination of fabric with heated roller, (b) multi-quadrant laser cutting of part circular boundary, (c) +45° rotation of ply stack, d) -45° rotation of ply stack.....	3.2.2-24
3.2.2-17 LOM fabricated half scale, fiberglass blastshield laminate after decubing.....	3.2.2-25
3.2.2-18 Corner cuts in Nextel™312/Blackglas™493AB prepreg sheet utilizing laser scanner on LOM 2030H prototype unit: (a) 90° corner, (b) .0625" corner radius.....	3.2.2-27
3.2.2-19 Laser cutting tests at various scanner velocities in 45% resin content Nextel™/Blackglas™ prepreg.....	3.2.2-28
3.2.2-20 Laser cuts made in standard resin content prepreg with (a) Synrad and (b) Coherent laser	3.2.2-29
3.2.2-21 Multiple scanner passes in Nextel™/Blackglas™ prepreg (45% resin content) with tackifier: (a) first pass, (b) second pass, (c) third pass, (d) fourth pass.....	3.2.2-31
3.2.2-22 Multiple scanner passes in Nextel™/Blackglas™ prepreg (45% resin content) without tackifier: (a) first pass, (b) second pass, (c) third pass, (d) fourth pass.....	3.2.2-31
3.2.3-1 SEM photomicrographs of fracture surface of Nextel™ 312/Blackglas™ panel LOM 990203.....	3.2.3-2
3.2.3-2 Photomicrographs of microstructure of Nextel™ 312/Blackglas™ panel LOM 21799-3.....	3.2.3-3
3.2.3-3 Illustration of laser cutting damage minimization through LOM fabrication of part top to bottom Curved Panel Fabrication	3.2.3-5
3.2.3-4 A) Uncured 8" x 8" Curved Cruciform Panel Vacuum Bagged on Al Forming Tool; B) Vacuum Curing Oven with LOM Part/Forming Tool.....	3.2.3-6
3.2.3-5 8" x 8" Curved Cruciform Panel after cure/consolidation and decubing.....	3.2.3-6
3.2.3-6 Pyrolysis model simulation of pressure rate variation due to accumulated gases in a closed system at three heating rates.....	3.2.3-8
3.2.3-7 Pyrolysis Cycle Rate of Gas Evolution (Beta Cycle: Lab Implementation).....	3.2.3-9
3.2.3-8 Initial LOM fabricated Blackglas 493/Nextel 312 sub-component panels	3.2.3-9

List of Figures (cont.)

<u>Figure</u>	<u>Page No.</u>
3.2.3-9 Green State 4"x 4" Curved Panel with edge/surface irregularities due to laser char zone	3.2.3-11
3.2.3-10 Cross-sections taken from raised edge of 8"x 8" curved cruciform Nextel™/Blackglas™ CMC subcomponent panel (shown in insert).....	3.2.3-13
3.2.3-11 Pulsed (400fsec) laser cut in Nextel™312/Blackglas™ 493 A/B prepreg: laser cuts at (a) 0°, (b) 45°, and (c) 90° orientations to ply edge, 15-25 passes per cut, 485μJ/pulse with a fluence of 9.7 J/cm2 (Scale: 1 graduation = 100μm.).....	3.2.3-16
3.2.3-12 Detail of femtosecond (400fsec) laser cut in Nextel™/Blackglas™ prepreg at 90° orientation to ply edge (Scale: 1 graduation = 100μm.).....	3.2.3-16
3.2.3-13 (a) Top and (b) side view of 4" x 4" Nextel™/Blackglas™ cruciform panel fabricated on prototype LOM scanner system.....	3.2.3-19
3.2.3-14 8" x 8" Nextel™/Blackglas™ curved cruciform panel fabricated on prototype LOM scanner system	3.2.3-19
3.2.3-15 8" x 8" "Single Stiffener Mechanical Test Panels (a) 1 and (b) 2; curved cruciform panels (c, d) formed/cured on resin infused LOM tool (Notice the remnants of diamond decubing pattern in skin sections of c and d).	3.2.3-22
3.2.3-16 "Diamond" decube offset pattern for (a) ply 1, (b) ply 2, and (c) ply 3.....	3.2.3-22
3.2.3-17 Alternate decube offset pattern for (a) ply 1, (b) ply 2, and (c) ply 3.....	3.2.3-23
3.3.1-1 AV-8B Metal production blastshield and 1997 baseline CMC blastshield	3.3.1-1
3.3.1-2 LOM CMC blastshield	3.3.1-3
3.3.1-3 CMC Properties	3.3.1-3
3.3.1-4 Arrangement of stiffener elements on LOM CMC model.....	3.3.1-4
3.3.1-5 Boundary conditions for baseline CMC model.....	3.3.1-5
3.3.1-6 Boundary conditions for LOM CMC model.....	3.3.1-6
3.3.1-7 Modified ultimate static pressure distribution	3.3.1-7
3.3.1-8 Static stresses.....	3.3.1-8
3.3.1-9 Thermal profile—hot day adjusted ground test measured temperatures, after smoothing....	3.3.1-9
3.3.1-10 Thermal stresses	3.3.1-10

List of Figures (cont.)

<u>Figure</u>	<u>Page No.</u>
3.3.1-11 Frequency and mode shape analysis, case 7 LOM CMC model.....	3.3.1-11
3.3.1-12 Frequency analysis summary.....	3.3.1-12
3.3.1-13 Acoustic pressure load.....	3.3.1-13
3.3.1-14 Power spectral density—acoustic loading.....	3.3.1-14
3.3.1-15 Acoustic stresses	3.3.1-15
3.3.1-16 Skin flexure strength and modulus, with and without hole—Panel 1.....	3.3.1-16
3.3.1-17 Skin flexure strength and modulus, with and without hole—Panel 2.....	3.3.1-17
3.3.1-18 Skin-stiffener flexure tests results	3.3.1-18
3.3.1-19 Stiffener section flexural tests.....	3.3.1-19
3.3.2-1 Surface nodes for blastshield demonstration component	3.3.2-2
3.3.2-2 Edge and attachment nodes for blastshield demonstration component	3.3.2-3
3.3.2-3 CCDP screen display of blastshield flat ply patterns with offset decube pattern.....	3.3.2-4
3.3.2-4 LOMSlice screen display of demonstration blastshield (a) skin ply and (b) stiffener ply	3.3.2-5
3.3.2-5 Nextel TM /Blackglas TM prepreg laminate (a) vacuum bagged over blastshield tool and (b) after cure in oven.....	3.3.2-8
3.3.2-6 Partially decubed section of cured blastshield showing offset decube pattern.....	3.3.2-9
3.3.2-7 Blastshield Demonstration Component 1 after decubing.....	3.3.2-9
3.3.2-8 Detail of stiffener section of decubed blastshield Demonstration Component 1 showing ply wrinkling	3.3.2-10
3.3.2-9 Pyrolyzed Nextel TM /Blackglas TM Blastshield Demonstration Component 1.	3.3.2-12
3.3.2-10 Composites forming module with a) uncured blastshield prepreg laminate on resin infused LOM tool, b) transparent diaphragm under initial vacuum, c) under partial vacuum, and d) under full vacuum; e) curing of blastshield laminate under heat lamps and f) final, cured Demonstration Component 2 before decubing.....	3.3.2-14
3.3.2-11 Nextel TM /Blackglas TM Blastshield Demonstration Component 2 after decubing (before first pyrolysis).....	3.3.2-15

List of Figures (cont.)

<u>Figure</u>	<u>Page No.</u>
3.3.2-12 Detail of stiffener elements in cured Nextel™/Blackglas™ Blastshield Demonstration Component 2 after decubing (before first pyrolysis).....	3.3.2-15
3.3.2-13 Nextel™/Blackglas™ Blastshield Demonstration Component 2 after pyrolysis.....	3.3.2-16
4-1 Elements of LOM-Based CAD/CAM Procedure for CMC Blastshield.....	4-2

List of Tables

<u><i>Table</i></u>	<u><i>Page No.</i></u>
3.1.1-1 Coordinates of Thermocouple locations given in Figure 3.1.1-11	3.1.1-20
3.1.1-2 Equilibrium temperatures on low temperature calibration.	3.1.1-23
3.1.1-3 Positions of heating lamps for low and high temperature cure segments.....	3.1.1-23
3.1.1-4 Equilibrium temperatures on high temperature calibration.	3.1.1-24
3.1.2-1 Input Data File Definition	3.1.2-3
3.2.1-1 Flexural Property Summary of Nextel 312/Blackglas CMC Panels Processed by NGC Bethpage.....	3.2.1-28
3.2.1-2 LOM Paper Mandrel Stability Tests.....	3.2.1-42
3.2.3-1 Mechanical test results for Nextel TM /Blackglas TM panels	3.2.3-2

FOREWORD

This Program was funded by the Advanced Research Projects Agency (ARPA) and was administered for the government by the Wright Laboratory of the Air Force. We are indebted to Mr. Jon Jeffries and Dr. Edmund Moore of the Air Force Research Laboratory and Dr Kevin Lyons and Dr. William Coblenz of DARPA who had government responsibility for overseeing the technical and administrative aspects of the Program. Their sage and constructive guidance was an invaluable resource in focusing the Program and in helping to resolve the technical issues that were encountered. The author would also like to acknowledge the many individuals from the participating organizations who contributed to the work reported herein. Michael Feygin and Sasha Shkolnik from Helisys, Inc., were responsible for major advances in the hardware and software upgrades to the commercial LOM 2030H system to allow efficient processing of aerospace grade composite materials. Mukesh Agarwala, Don Klosterman, Alan Lightman, and Nora Osborne from UDRI played a significant role in the helping to identify the critical material and hardware technical issues in the preliminary phase of the program. The author would like to thank Northrop Grumman colleagues Magdy Barsoum, Don Box, Jim Dart, Charles Foreman, Greg Dillon, Mary Colby, Joe Martarana, John Rheil, John Madsen, Jim Whiteside, Tom Donnellan, Cynthia Holley, Bob Christ, and Jerry Nardiello.

The author would like to acknowledge Steve Luby and Ed Bernardan from Composite Design Technologies, Inc. (CDT), now called VISTAGY, for helping with devising the composite forming evaluation and testing the concept using their FiberSim code. The authors would also like to acknowledge Bob Jurf of Composite Optics Inc. who supplied the NextelTM/oxide sol-gel based prepreg forms evaluated in the program.

1.0 INTRODUCTION

This program was initiated in response to DARPA Research Announcement BAA #97-35 on Solid Freeform Fabrication and Design. The overall program concept was to provide a demonstration of reduced time and cost for validation of advanced Ceramic Matrix Composite (CMC) design concepts through novel Solid Freeform Fabrication (SFF) and design technologies. Major program goals included extending SFF system capabilities to new materials, improved tolerances and surface finishes, and larger area, non-planar build layers (i.e. components), as well as integration of these enhanced capabilities with new design optimization software. All of these major goals were accomplished in the program. This Report summarizes the scope of work that was performed and accomplishments that were achieved over the 27-month program period. The specific program tasks are described in the following paragraphs.

The overall goal of this program was to develop an innovative structural design methodology to improve the product development cycle for ceramic matrix composite (CMC) components. The approach for achieving this goal is to combine an existing composite laminate design optimization software methodology with a low-cost, CMC prototyping capability based on Laminated Object Manufacturing (LOM) SFF. This new design process will enhance the structural efficiency and reduce design time and cost for aerospace CMC structures. To demonstrate this enhanced CMC product development capability, a prototype of an aircraft CMC blastshield component was designed and fabricated using LOM.

The program contained three main tasks: a Design Methodology Development task for LOM based prototyping, a LOM CMC Process Validation task, and a CMC Prototype Demonstration task. The Design Methodology task contained three CAD/LOM related sub-tasks that include software interface development, CAD design procedure evaluation, and a design methodology effort. In this task a software interface between an integrated composite design software program, designated Computerized Composite Development Project (CCDP), and a

LOM machine modified to fabricate ceramic matrix composites was developed and implemented. The design software was then utilized to generate databases for the LOM machine of increasing complex CMC laminates containing multiple ply orientations and drop-offs.

The second task, LOM CMC Process Validation, was performed in parallel with the first, and was directed towards extending the capability of the LOM technique to the fabrication of large curved shapes typical of large aerospace components. Both Nextel™ 312/Blackglas™ and oxide/oxide composite systems were initially investigated. The Materials System Development subtask included development of appropriate material forms, i.e., prepregs that meet the dual requirements of LOM processability and CMC mechanical performance. The LOM System Development subtask included system process development activities and equipment modification.

The third subtask, LOM System Demonstration entailed a demonstration of the usefulness of the developed LOM based design methodology. In this subtask, an enhanced LOM system was used to fabricate sub-components designed in the first task. The results from subsequent sub-component testing was incorporated into the design methodology database to aid in the design definition of the planned demonstration component that was designed and fabricated in the final task. The demonstration component is an engine exhaust washed high temperature blastshield representative of structures anticipated on future military vertical short takeoff and landing (VSTOL) and low observable (LO) aircraft with shielded exhaust.

2.0 APPROACH

Approach

This effort developed and demonstrated a paperless design methodology utilizing Laminated Object Manufacturing (LOM) based processing to fabricate complex ceramic matrix composite (CMC) structural components. The approach involved the development and integration of two fundamental capabilities. The first capability included modification of the computer aided design (CAD) process to include prototype fabrication, and the development of interfaces between the design software environment and the appropriate prototyping system. The second capability involved the development of LOM materials and processes that are applicable for typical continuous fiber CMC aerospace structures. A need exists for the development of an innovative design environment in which the use of LOM based SFF should provide significant improvement to the product development cycle for CMC. Current design practice for CMC is hindered by lack of sufficient material property data and by the limited understanding of composite failure behavior. Consequently, CMC designs are overly conservative and expensive, and CMC utilization in structural applications is limited. This program described in this final report involved the development of a new design process that should enhance the structural efficiency and reduce the design time and cost for aerospace CMC components. These advantages will accelerate the insertion of CMC components onto advanced DoD platforms.

Technical Scope

This effort consisted of three main tasks: a Design Methodology Development Task for LOM based prototyping, a LOM CMC Process Validation Task, and a CMC Prototype Demonstration Task. The design methodology task contained three CAD/LOM related sub-tasks that include software interface development, CAD design procedure evaluation, and a design methodology effort. The second task was directed towards extending the capability of the LOM technique to fabrication of large curved shapes typical of large aerospace components and included CMC material and system process development activities and equipment modification.

The third task involved a demonstration of the usefulness of the LOM based design methodology. The modified LOM system was used to fabricate sub-components designed in the first task. The results from subsequent subcomponent testing were incorporated into the design methodology database to aid in the design definition of the demonstration component that was designed and fabricated in the final task.

Background

Implementation of CMC components by the aerospace community has been hampered by the lack of acceptance of the technology by the design community. This reluctance to apply CMC materials in advanced systems designs is due to a number of inter-related obstacles that include a lack of complete CMC design allowables, a lack of an analytical understanding of CMC failure mechanisms, and limited design experience.

In the past, other materials such as polymer matrix composites have faced similar barriers to implementation. These barriers have been overcome through the development of suitable rigorous analysis of material behavior in the anticipated application environment. The analyses are supported by similarly rigorous experimental validation of material and structural behavior. Unfortunately, these development efforts are time and cost intensive, and acceptance and implementation of polymer composites have been achieved only in an evolutionary manner over a 30-year time period.

An alternative approach, which has also been successfully employed in polymer composite technology, is the generation and test of prototype designs under realistic test conditions. These prototypes have been used to gain insight into performance characteristics where the analysis tools available were insufficient to describe the material and structural response. The effort involved in the design and fabrication of these prototypes is not trivial: cost and schedule to complete the design, fabrication, and test of these components can be quite significant.

One evolutionary change to the design process that has enhanced innovation in composites technology is the development of an integrated computer based design framework. Northrop Grumman has developed a system, called CCDP, which allows multi-functional design optimization, based on consideration of a wide range of product attributes, such as performance, producibility, maintainability, and cost. Within the design environment, functional organizations such as stress, design, manufacturing, and integrated logistics support (ILS), can participate seamlessly in component or system design activities. In polymer composites, the CCDP has been integrated with automated fabrication equipment, such as ply cutting and automated tape placement systems. The benefits from the implementation of the CCDP system have been well documented in previous Northrop Grumman composite production programs. The CCDP is used routinely in conjunction with stereolithography for rapid prototyping and tooling applications. Further development of the CCDP system is the focus of continued activity in multi-functional design optimization tools.

Although utilizing the CCDP capability in a CMC design framework will facilitate implementation, there is still the problem that the generation of CMC prototype components is severely limited by the cost and time associated with traditional CMC fabrication techniques. The design community requires a rapid, low cost CMC prototype manufacturing capability that can quickly fabricate designs of comparable quality compared to those produced via traditional CMC fabrication techniques. Ideally, this capability would reduce the time and costs associated both with tool development and prototype fabrication, each of which is a costly, time-consuming activity.

The LOM rapid prototyping process offers the potential to provide this capability within the CCDP framework. LOM is an SFF technique used to make 3D geometric shapes by sequentially stacking, bonding, and laser cutting layers of material. LOM has the largest working envelope of any available SFF technique and the only Rapid Prototype (RP) technique suitable for working with continuous fiber reinforced materials forms. The rationale for using the process

is based on LOM's inherent capability for handling sheet materials such as ceramic fiber reinforced composite prepregs, for producing geometrically complex near net shape objects, and for operating with a high degree of automation. LOM technology has been successfully applied to a range of ceramic and metal powder systems to fabricate fully functional ceramic and metal components. However, the use of LOM for fabrication of large continuous fiber reinforced composite structures has been relatively unexplored.

The use of the LOM process for CMC has been the basis for an earlier Defense Advanced Research Agency (DARPA) funded SFF program (DARPA/ONR Grant No0014-95-1-0059). One of the most novel developments of this earlier DARPA program is the curved layer LOM building process. The ability to use curved layers instead of planar layers to create objects is a significant advance, not just in LOM technology, but also in the entire arena of SFF. The rationale for developing a curved layer LOM process is based on the need to maintain fiber continuity in curved composite structures. Other benefits of the curved layer process are reduced amount of expensive raw material waste when compared to the flat layer process and better surface finish due to elimination of a surface "staircase" effect. This program has further enhanced and simplified this basic Curved LOM process into a more commercially viable (and hence implementable) form that significantly expands the range of CMC component types that the technology can address.

The combination of the LOM process with the CCDP system offers tremendous potential for accelerating implementation of CMC into aerospace applications. This new design tool will allow simultaneous evaluation of new materials and new design concepts, and potentially revolutionary advances in structural component concepts. The generation of such a design tool will allow rapid design and fabrication of competing prototypes within a new product development cycle. The benefits of this new SFF based design tool is demonstrated in the program by the design and LOM fabrication of a demonstration CMC blastshield using the low cost NextelTM/BlackglasTM CMC material system. This design demonstration builds from two

earlier CMC technology development efforts and serves as a realistic test case of how this new design methodology could be utilized in future aircraft modification efforts.

In an earlier CMC development effort, Northrop Grumman as part of a cooperative research and development program with McDonnell Douglas Aerospace (MDA, now Boeing), designed, fabricated and flight tested a NicalonTM/BlackglasTM CMC blastshield for the AV-8B Harrier VSTOL aircraft. The blastshields are located behind the aft rotating exhaust nozzles on each side of the fuselage and protect the fuselage structure from hot exhaust gases. Because of the intense acoustic and thermal environment, the current stainless steel blastshields have a limited life. Work conducted to date has shown that CMC blastshields can provide increased durability, significant increase in life, and reduced weight compared to the metal production units. A replacement NicalonTM/BlackglasTM CMC blastshield, designed and fabricated by Northrop Grumman, was successfully ground tested by MDA on an AV-8B technology demonstration aircraft in 1997 followed by a successful flight test. Though the conclusion of the program resulted in the flight-testing of a significant CMC airframe component in a challenging environment, the high material and fabrication costs of the NicalonTM/BlackglasTM CMC system inhibited further consideration of transitioning the article to the AV-8B fleet.

One significant result of the flight test of the NicalonTM/BlackglasTM CMC heatshield, though, was that the maximum temperature the test article attained (800F) was significantly less than that initially predicted (1300°F) and hence designed to accommodate. This allowed the program to propose evaluating a lower cost CMC material system, the preceramic polymer derived NextelTM/BlackglasTM system as an alternate design case for demonstration. This lower cost system was deemed not suitable for the earlier development program, as its maximum long-term use temperature is 1000°F. In evaluating this low cost CMC system the program leveraged the considerable material characterization, processing experience and CMC database accumulated in the earlier Northrop Grumman led DARPA Low Cost Ceramic Composites (LC³) Program

(MDA972-93-2007). This five-year effort focused on development of the materials and processing required for the low cost preceramic polymer Blackglas™ and Nextel™ ceramic fiber systems as applied to DoD and commercial CMC applications. Because of this extensive background on Blackglas™ composites, this material served as a useful baseline system for the program. In addition to the extensive processing and properties database, the ease of producibility of this material makes it an excellent candidate for the LOM process. The LC3 program focused on optimizing the Nextel™/Blackglas™ system for Resin Transfer Molding (RTM) and Resin Vacuum Infusion (RVI) processing using 2.5-D and 3-D woven fiber preforms. This program expanded that database by developing and characterizing the system as a prepreg (sheet) form and further optimized the system for laser cutting type processing.

In addition to investigating prototyping of the blastshield with a lower cost CMC material system, an alternate structural design case was also simultaneously evaluated. The conceptual design of this component is shown in Figure 2-1. This new design is similar to but slightly smaller than the Nicalon™/Blackglas™ blastshield. The earlier Nicalon™/Blackglas™ blastshield contained 5 horizontal stiffeners with a total of 15 attachment nodes. The design for the blastshield demonstration article evaluated in this program used integral, intersecting stiffeners to transmit static and acoustic pressures to the fuselage attachment bolts and brackets. These pressures result in bending moments in the stiffeners that are highest near the attachments. The stiffeners provide sufficient out-of plane bending stiffness to the blastshield so that its dynamic response frequencies are above engine harmonic frequencies. This significantly reduces the acoustic RMS stresses in the blastshield, which increases its fatigue life. The new design also reduced the number of attachment nodes from 15 to 9, which provided an additional weight savings due to the need for fewer attachment bolts and brackets.

The performance benefits through simultaneous insertion of both the lower cost Nextel™/Blackglas™ CMC material system and a more complex, structurally efficient stiffener sub-element design in the overall component design was evaluated. The earlier

Nicalon™/Blackglas™ CMC design served as the baseline for the demonstration article designed and LOM fabricated in this program. Northrop Grumman has an archived database on the design and fabrication of the earlier AV-8B CMC blastshield. Using this component as the demonstration article allowed evaluation of the potential benefits achievable through the use of LOM based design and fabrication procedures.

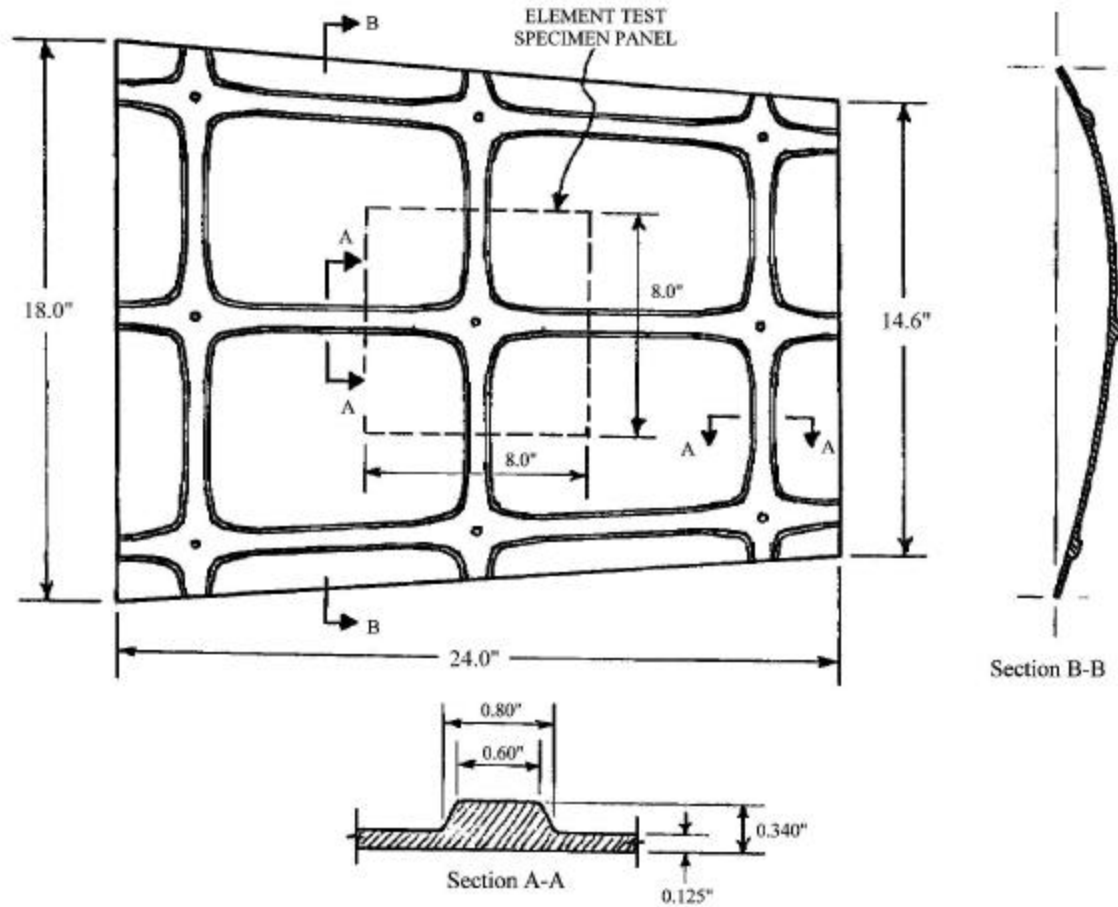


Figure 2-1 Nextel™/Blackglas™ AV-8B CMC Blastshield Design Concept

3.0 SUMMARY OF RESULTS

3.1 Design Methodology Development

3.1.1 LOM/Forming Concept

The overall objective of this task was to add a LOM based SFF module to the Computerized Composites Development Project (CCDP) software system and utilize the capability in a CMC design capacity. The task contained three subtasks to achieve this goal, which included CCDP/LOM Software Interface Development, Computer Aided Design (CAD) CAD/LOM Procedure Development, and finally the new Design Methodology Validation. The design methodology that was to be developed in the program (as discussed in the initial proposal) was to be formulated from the Curved LOM Solid Freeform Fabrication (SFF) process developed at UDRI under previous DARPA sponsorship. Early in the program, though, several interrelated technical issues necessitated a re-evaluation of the benefits of utilizing the Curved LOM process as the basis for the new methodology. These issues included:

- Limitations of Curved LOM process for generation of complex curved structures.
- Hardware and software inadequacies of Curved LOM system that impede further hardware/software upgrades.
- Limited commercial viability of current Curved LOM process (due to above concerns)

The Curved LOM system in its current form was not considered attractive for industrial implementation. The range of parts that can be produced by curved LOM is small, making a commercial version of the machine of limited market value. This restricted range of part shapes is directly related to an inherent shortcoming in the curved LOM build sequence. In the current implementation of curved LOM, a flat sheet is first laminated over a tool surface, then laser cut to its desired shape. For successful lamination of the sheet onto the tool the curvature of the tool must be relatively simple to avoid wrinkling or buckling in the ply. In the nomenclature of 3D

geometric mapping analysis, curved LOM is largely restricted to part shapes composed of only *developable* surfaces or surfaces possessing very limited double curvature. To form flat sheets over more complex shapes (which might have severe double curvature) without ply buckling, cuts and/or darts may be necessary at specific locations in the material before lamination. To extend curved LOM to a greater range of part shapes, an alternate build sequence is needed which incorporates some ability to cut, dart, or shape a ply before it is formed onto a tool.

Difficulties in implementing modifications to the curved LOM system to improve part tolerances and surface finish (through tangent cutting) also warranted consideration of a program redirection. It was initially proposed that LOM part tolerances can be enhanced significantly by converting the XY laser positioning gantry on the curved LOM unit to a scanning galvanometer based mirror system. A galvo scanner provides better laser positioning accuracy, which results in more uniform corner cutting and better edge definition in finished parts. The scanner system also increases cutting speeds (by a factor of four), which helps significantly to reduce build times for large parts. Both hardware and software problems on the curved LOM system, though, seriously hindered the incorporation of a laser scanner on this unit. The structural frame of the machine is fairly compliant which offsets any laser positioning accuracy improvement provided by an attached scanner.

The software implementation of gantry motion on the curved LOM system also needed to be modified from a point-to-point to a contour mode of control. This extensive software modification task was needed not only to eliminate excess laser cutting damage (charring) but also to enable proper interfacing of the galvo scanner controller with the LOM unit's laser and motion controllers. Finally, improvement in cutting speed is also not realized when a scanner is utilized in conjunction with a curved LOM (3D) laser cutting operation. Curved LOM laser cutting is achieved by the coordinated, simultaneous control of the XY gantry velocity and the z platform

motion. The laser cutting speed is thus ultimately limited by how fast and accurately the relatively large and heavy LOM build platform (plus part) can be positioned, not the scanner speed. Though all the above technical challenges can ultimately be solved, their resolution unfortunately still does little to enhance the commercial viability of the current curved LOM process.

An alternate LOM process was instead proposed that eliminated the above technical problems, expanded the range of curved composite part shapes for LOM, and enabled all proposed program objectives to be accomplished. The major benefit of the new LOM process was that it resulted in a more commercially attractive Curved LOM process and system that the vendor, Helisys Inc., was willing to market. The basic concept behind the redirection plan was to combine the commercial 2D LOM build process with a final composites forming step to produce curved composite components. Composites forming is a manufacturing process wherein a flat composite sheet or laminate is transformed into a three dimensional shape by a deformation process. The 3D shape is generated by deforming the laminate while compacting the material in a matched mold (press forming) or by contouring the plies over a tool surface with a flexible diaphragm (diaphragm forming). The major benefit of composites forming is that it can substantially decrease the manufacturing costs of a composite component by eliminating time-consuming hand lay-up procedures.

The Curved LOM technique is essentially an example of an automated diaphragm forming operation, as the basic Curved LOM lamination sequence onto a tool mandrel is a forming process. The major difference between Curved LOM and conventional composites diaphragm forming is that in the Curved LOM process the individual plies are sequentially laminated over the tool to generate the curved part while in conventional forming the entire flat laminate is deformed onto a tool in one step. The major rationale for development of the Curved LOM process was to enable the generation by LOM of curved, continuous fiber reinforced composite structures in

which the reinforcement remained continuous across the curvature of the part. The modified curved LOM process evaluated in the program (henceforth referred to as LOM/Forming) still achieves this goal but in a more direct and simplified manner.

A schematic of the LOM/Forming concept is depicted in Figure 3.1.1-1. In this new LOM process the series of flat pattern cutouts needed to fabricate a curved composite structure is first generated using appropriate CAD/CAM software (such as CCDP or the commercially available FiberSIM program). Utilizing this ply stack data, the LOM system is next utilized to fabricate a flat (2D) laminate preform incorporating any cuts or darts in individual ply layers necessary for successful mapping of the laminate over a curved surface. In a final step the entire stack of plies is formed over the tool surface with a conformable vacuum diaphragm and cured in place. The final vacuum forming/cure step could take place directly on the LOM build platform, or in a separate forming module specially designed for use with a LOM system.

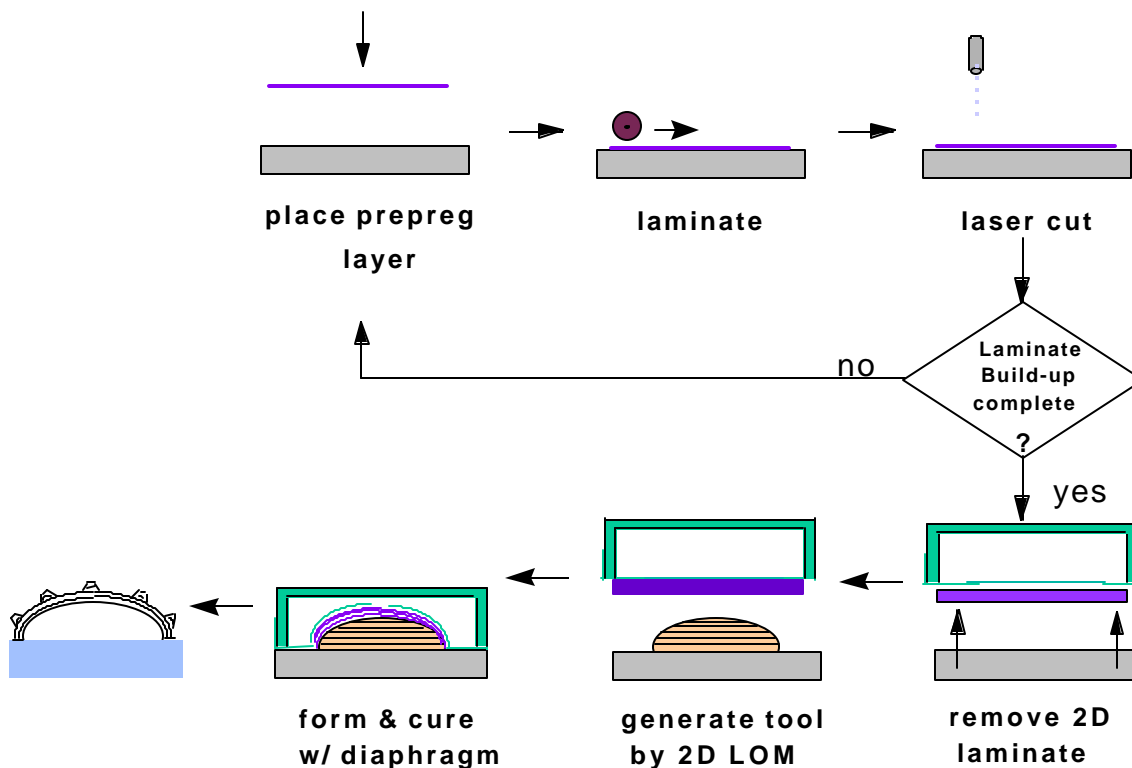


Figure 3.1.1-1 Schematic of New LOM/Forming Process Sequence

The implementation of the LOM/Forming concept in the redirected program proceeded as follows. The LOM system hardware upgrade and scale-up subtasks were shifted from the Curved LOM system at UDRI to a commercial 2030H LOM unit located at Helisys, Inc. The base 2030H system was upgraded with a precision galvo laser scanner as well as a 200W CO₂ laser. The software used to drive the laser cutting process on the model 2030H was also vastly improved compared to the much older version on the Curved LOM unit. Integrating the upgraded software with a precision laser scanner helped to rectify laser-cutting problems that had impeded process development activities early in the program.

The material feed system on the 2030H remained a roll-based source, as this design was more appropriate for fabricating large structures by LOM. A sheet feeder mechanism is beneficial mainly when prototyping smaller parts by LOM as it helps to reduce the amount of waste material generated in the process. Control of ply fiber orientation was achieved with a rotary mechanism attached to the LOM build platform. To vary the fiber direction in a specific layer of the composite part a two-step rotation was required. During the LOM lamination sequence for that ply the build surface is first rotated to the correct fiber orientation (relative to the source roll direction). Material is next laminated onto the build layer, then a boundary cut around the entire part to detach the source material from the roll. The build surface is then rotated back to its home position at which point the boundaries and crosshatch regions for that layer are laser cut. The LOM system software on the 2030H was also modified to accept both .STL and CCDP generated part design files.

Utilizing a LOM/Forming process to generate curved composite parts offers several advantages over the earlier curved LOM technique. The advantages are:

- Extends LOM capability to composite structures with significant complex curvature
- More relevant to commercial composite analysis/design software

- Allows better utilization of scanner technology to increase part accuracy and build speed
- Easily adaptable to existing commercial LOM units (i.e. upgrade vs. purchase of new curved LOM system)

A more detailed discussion of each advantage follows:

Extended Range of Curved Parts Suitable for LOM/Forming

One of the major advantages of the LOM /Forming process is that it creates the possibility for prototyping more complex parts than those currently possible using the Curved LOM method. This advantage stems from the ability, with the new process, to alter the geometric shape of individual plies of a laminate before forming the final 3D shape. In identifying the various types of curved parts, which could now be generated by LOM/Forming, it proves helpful to first define several geometric properties of surfaces and their classifications. A key property of a surface that directly influences how easily it can be formed from a flat sheet is its Gaussian curvature. Gaussian curvature is the compound curvature and its value is simply the product of the curvatures in the two principal directions. It can be shown that for any point on a surface the direction of maximum curvature will be at 90° to the direction of minimum curvature. These orthogonal directions are the directions of the principal curvatures. Parts can be classified by their Gaussian curvature as shown in Figure 3.1.1-2. Single curvature parts with zero Gaussian curvature (Category 1) are developable, which means that no net stretching or compression is required to form them. Single curvature composite parts require interply shear only, a deformation mode exactly the same as that seen when a stack of pages are bent. Because of this, composite parts in this category should never be subject to a wrinkling problem and can typically be prototyped by the original Curved LOM process. Examples of single curvature shapes are surface sections of cylinders or cones. Figure 3.1.1-3 displays several examples of CMC parts

with single curvature.

The second two classifications of parts, those with non-zero Gaussian curvature, prove the more interesting to consider for prototyping by LOM/Forming. Positive Gaussian curvature parts (Category 2), have the same sense curvature in both principal directions. Forming these shapes will always require a net compression of the neutral (or middle) surface. Obviously bending is also required. This group of parts includes spherical segments, ellipsoids and other shell-type geometries. Because buckling (generally) occurs where compression is required, positive Gaussian curvature parts are the most prone to this undesirable type of deformation. Examples of CMC parts with positive Gaussian curvature are shown in Figure 3.1.1-4.

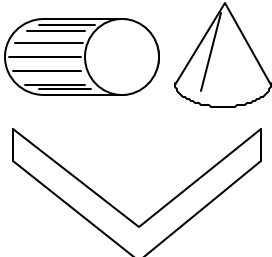
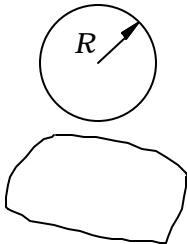
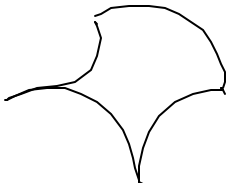
	CATEGORY 1	CATEGORY 2	CATEGORY 3
Gaussian Curvature:	zero everywhere	positive	negative
Surface:	singly curved	doubly curved	doubly curved
Developability:	developable	nondevelopable	nondevelopable
Neutral Plane Deformation:	pure bending	bending plus compression	bending plus tension
Examples:	cylinder, cone, bend	Shells	Saddle
			

Figure 3.1.1-2 Classification of Part Shapes in terms of Gaussian or Compound Curvatures

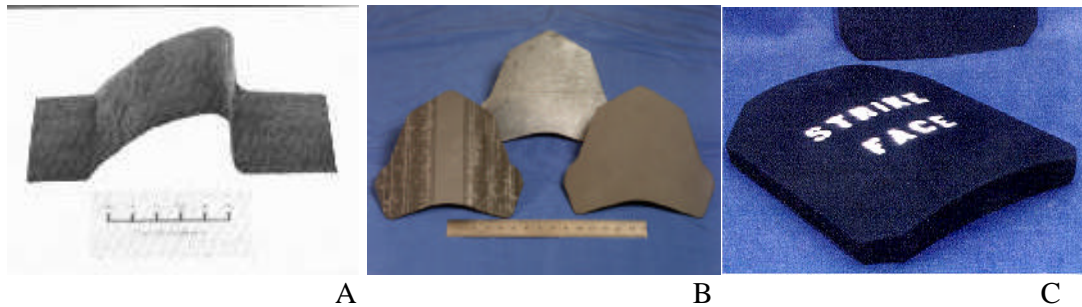


Figure 3.1.1-3 Examples of CMC Parts with 0 Gaussian Curvature A) Nicalon/ Blackglas™ Fairing Channel, B) SiC/SiC Engine Flameholders, C) DIMOX™ Body Armor Plate

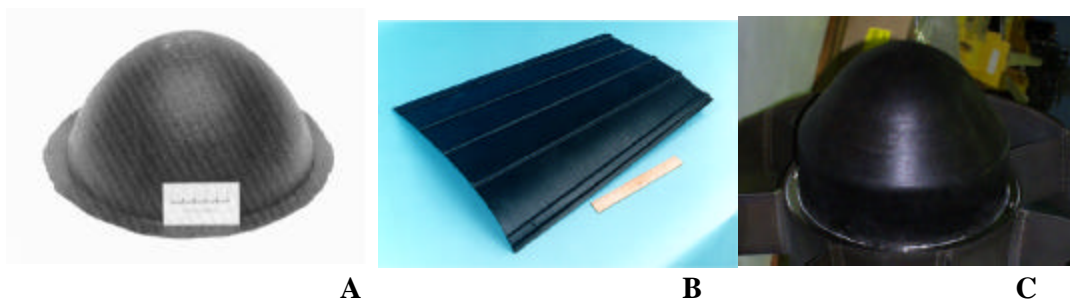


Figure 3.1.1-4 Examples of CMC Parts with Positive Gaussian Curvature: A) Blackglas Radome, B) Nicalon/Blackglas Blastshield, C) Nextel/Blackglas Engine Tailcone

Saddle shapes (Category 3), have negative compound curvature and forming them requires bending and a combination of tension and compression. The magnitude of the compressive strain, which is the critical parameter for forming, is a function of the mismatch between the absolute values of the principal curvatures i.e. if the positive curvature on a ‘saddle’ type shape is equal in magnitude to the negative curvature, then the perimeter will be in net tension everywhere during forming and the part will therefore be relatively easy to form. If these magnitudes differ greatly, then proportionately more compressive strain is required to make the shape, forming becomes more difficult. An example of a CMC part with negative Gaussian curvature is depicted in Figure 3.1.1-5.

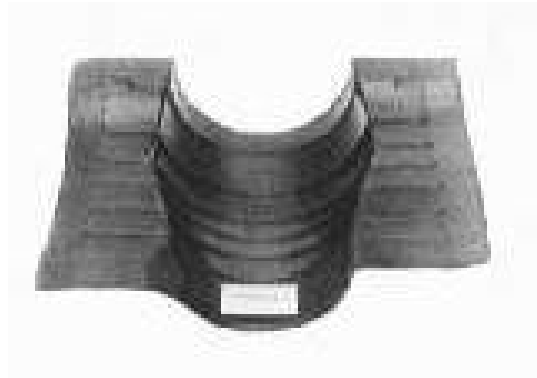


Figure 3.1.1-5 Example of CMC Part with Negative Gaussian Curvature: Nicalon/Blackglas duct section.

Any composite part that has non-zero Gaussian curvature requires deformation to occur within the plane of the part when it is formed. The kinematics of this in plane deformation is controlled by several interrelated material and structural properties of the composite, which include type of fiber and matrix, fiber orientation and architecture, and part geometry. Woven and aligned materials achieve this in-plane deformation in different ways. In the case of woven material there is a limit to the level of in plane deformations that can be developed before the grid ‘locks up’ and further deformation proceeds out of plane in the form of wrinkles. Beyond this critical limit, part shapes can still be achieved by making cuts and darts in the flat pattern where high deformations are expected before forming. These are the range of part geometries not suitable for prototyping by curved LOM but may be generated by the LOM/Forming process. One can not determine if a part shape is formable without cutting or darting simply by determining its Gaussian curvature, though, as consideration must be made of the material properties of the system. Certain non-developable surfaces (i.e. blastshield) require very small in plane deformations to form and do not require cuts or darts in the plies. The material properties of the laminate preform plays just as critical a role in determining a parts formability as does its geometry.

Enhanced Utilization of Commercial Composite Analysis Software

Another advantage of the LOM/Forming process is that it enables various software

programs that are useful for determining the deformation behavior of fiber reinforced materials to now be utilized for LOM prototyping. The development of accurate models that consider both geometric and material properties to identify shapes that cannot be formed (and appropriate redesigns to limit defect creation in these parts) is currently an area of extensive research in the composites forming community. This body of work is directly applicable to the technical issues associated with curved LOM and serves as a useful guide in the development of a design procedure for the LOM/Forming process. Several fiber composite analysis codes useful in composites forming production (and hence LOM/Forming) have also become commercially available in recent years.

The formability evaluation above of different shape categories is based on a gross kinematic analysis and is not specific to any material. Composites deform in a manner completely different from homogeneous materials. Single curvature composite parts require interply shear only, while non-zero Gaussian curvature parts require deformation to occur within the plane of the part. The deformation limits for a particular fiber reinforced composite shape and material system can now be accurately predicted using commercially available deformation codes such as FiberSim and DRAPER. These programs can also be used to determine the optimal locations to place cuts and/or darts in a laminate to assist the forming process. These fully developed codes can be utilized during the part design process to maximize the chances of success before LOM processing.

The critical strains that cause wrinkling in woven materials can be determined experimentally, by simple shearing tests. Samples of the woven cloth are clamped around the perimeter in a frame that is pin-jointed at the corners. The material can then be deformed in shear, and the shear angle that leads to the onset of out-of-plane deformation can be recorded. This is then a material input parameter in such programs as FiberSim and DRAPER. These

analysis codes can just as easily be utilized with the Curved LOM process to predict the formability of a particular composite shape. The results, though, can only be used to decide if the part can or cannot be fabricated by LOM. When used in conjunction with LOM/Forming, the analysis can now be used to optimize the part design to enhance formability

Improved Part Tolerances and Build Speed

Another advantage of the redirection plan was that it eliminated the technical problems that hindered incorporation of a laser-positioning scanner on an older LOM unit. Replacing the LOM X-Y gantry drive mechanism with a galvo mirror positioning system offers major advantages in increased laser positioning accuracy and speed which results in more exact parts built in less time. The benefits of a laser scanner, though, can only be realized if these precision optics are mounted on a rigid, stable platform. This is achieved in the redirection plan by utilizing the enhanced structural frame incorporated on the redesigned LOM 2030H unit.

By restricting the laser cutting operation to the X-Y build plane the LOM/Forming process also enables faster cutting speeds to be utilized which results in reduced part build times. A galvo mirror scanner is inherently much faster than the linear positioning motors used on the Curved LOM system for X-Y gantry and Z position control. For the original curved LOM process simply replacing the X-Y positioning mechanism with a scanner, though, does not translate into increased cutting speeds as the z platform is still translated by a linear motor. As the angular position of the scanner and linear position of the z platform must be coordinated for accurate cutting during curved LOM, the cutting speed is ultimately set by the maximum rate at which the z platform can be adjusted.

Potential Commercial Markets / Parts

The final advantage of the LOM/Forming process/system is its greater commercial potential than that of the curved LOM unit. These specific commercial markets and associated

components suited for prototyping by LOM/Forming vary. In general, ceramic matrix and polymeric composite components where investigation of design options is prohibitively expensive are the primary parts suited for LOM/Forming based prototyping. Some examples of potential CMC components were depicted in Figures 3.1.1-3, -4 and -5. Several examples of polymer matrix composite parts are identified in the following discussion. The potential customers for the technology to which the program has marketed is the aerospace industry, particularly the composites design and manufacturing communities with previous experience in CMC processing and composites forming. Potential applications also exist in the non-aerospace military, automotive, marine, and energy sectors i.e. any area with applications for low cost, rapid design and manufacture of CMC (and PMC) components.

The modification of the 3-D LOM process to include a lamination procedure followed by a forming step builds on an expanding database established for implementation of various automated forming techniques. Accumulated knowledge from several years of research and process development on polymer matrix composites has led to a solid understanding of the physical processes involved in forming. This establishes an accepted rationale for differentiating between candidate parts, in terms of formability. Generally the difficulty in forming a given part is principally a function of the geometric complexity, determined by the degree of compound curvature, and the part size. Material factors are also important.

Northrop Grumman has evaluated the potential for diaphragm forming processes to reduce production costs for composite parts that are currently hand laid up. Evaluation of this earlier work is useful for identifying applications for LOM/Forming. Figure 3.1.1-6 shows a number of F/A-18 parts considered suitable for forming. These are covers and skin sections, and the one in the bottom left is an aft dorsal cover that has been the subject of a number of process trials in which cost savings on the order of 50% have been demonstrated. All of these have

principal dimensions on the order of 2 to 3 feet. Essentially the aft dorsal cover was made by a process very similar to LOM, with the significant difference being the lack of an automated fiber stacking system. While LOM could also form the basis of an agile manufacturing process, there is no doubt that the ability to make structural prototypes of such typical parts would be a major advantage in the design cycle.

Another advantage of the LOM/Forming process is that it potentially opens up the possibility of forming more complex parts than those likely to be available in the original forming process configuration. Cutting and darning the preforms may be necessary in order to make parts that are just beyond the complexity of those shown above. This may allow some very complex structural prototypes to be made, irrespective of the technology later used to manufacture them. For example, parts being considered for RTM, in which tooling costs are exorbitant, could be prototyped cheaply before tool development.

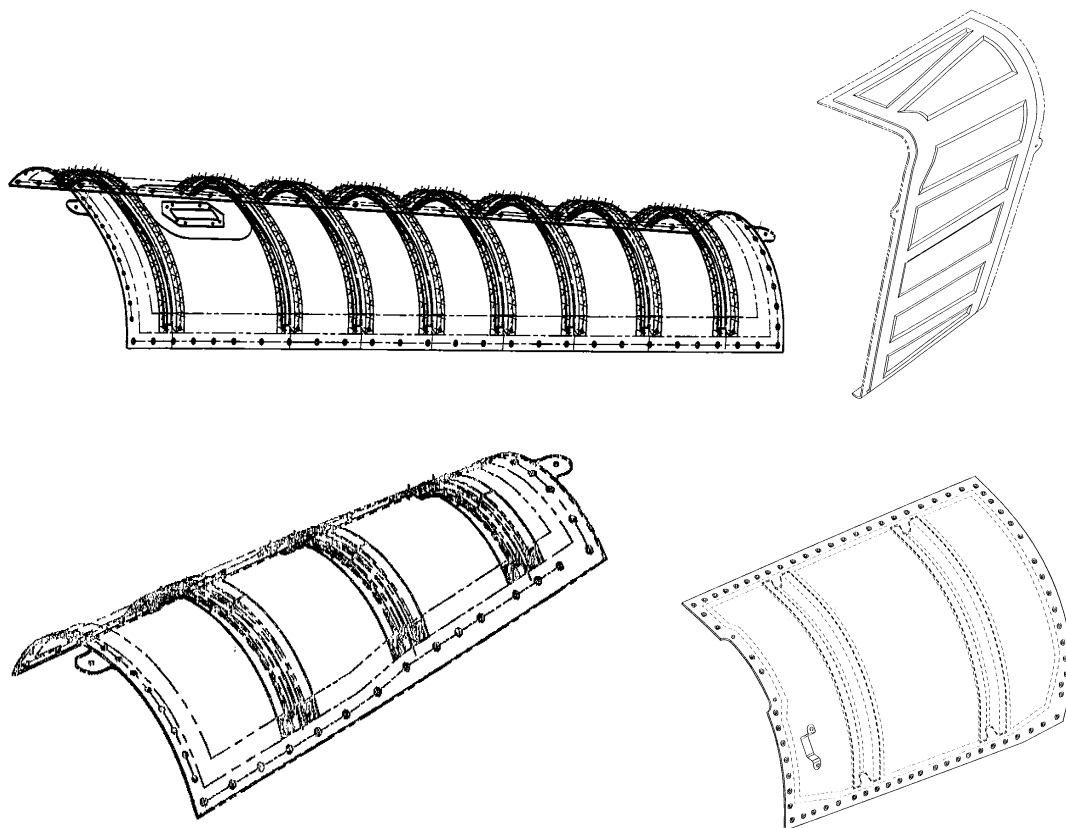


Figure 3.1.1-6 Examples of F/A-18 parts suitable for automated forming

Successes demonstrated for forming on the F/A-18 program will migrate to other programs. A potential need for the LOM rapid prototyping technology being developed has been identified in the Northrop Grumman C-17 program as part of a Composites Affordability IPT. As the CCDP composite design software is also part of this NG business unit, this application is a particularly attractive initial insertion opportunity for the program. Figure 3.1.1-7 shows parts and tooling (in each case the scale bar is a one foot ruler) from the C-17 program identified as suitable for fabrication by LOM/Forming. These parts are currently manufactured by hand lay-up. These parts are considered ideal for forming technology and therefore also LOM/Forming. Again, the development of a flexible manufacturing cell based on LOM may provide a useful production technique, in addition to a rapid prototyping technique capable of producing these types of parts with a more streamlined design process.

The JSF program has also been identified as having a need for an advanced rapid prototyping capability for both tooling and demonstration structural articles. An SFF type Laminated Object Manufacturing process, or some scaled derivative thereof, will be of particular interest to the JSF community, in the development of the Preferred Weapons Systems Concept demonstrations, as well as in the establishment of agile manufacturing capabilities for platform production. Figure 3.1.1-8 shows an example of a section of a JSF tooling fixture, which has been identified as a candidate part for a LOM/Forming demonstration. Several JSF components, which are candidates for CMC implementation, have also been identified that could be fabricated by LOM/Forming. These include an APU/ECS duct cover, tail inboard horizontal stabilizer leading edges, lift nozzle door, and lift improvement devices (LIDS). Other potential customers are, of course, the various engineering companies and laboratories that currently possess commercial LOM systems. These sites include Boeing (3 units), Lockheed Martin, Raytheon, NASA Marshall Space Flight Center, NAWC China Lake, NAVAIR, NRL, Army Natick RD&E Center, and Army Tank Automotive Command. As Boeing is currently utilizing commercial LOM prototyping in their JSF development efforts, they should also be receptive to the LOM/Forming concept.

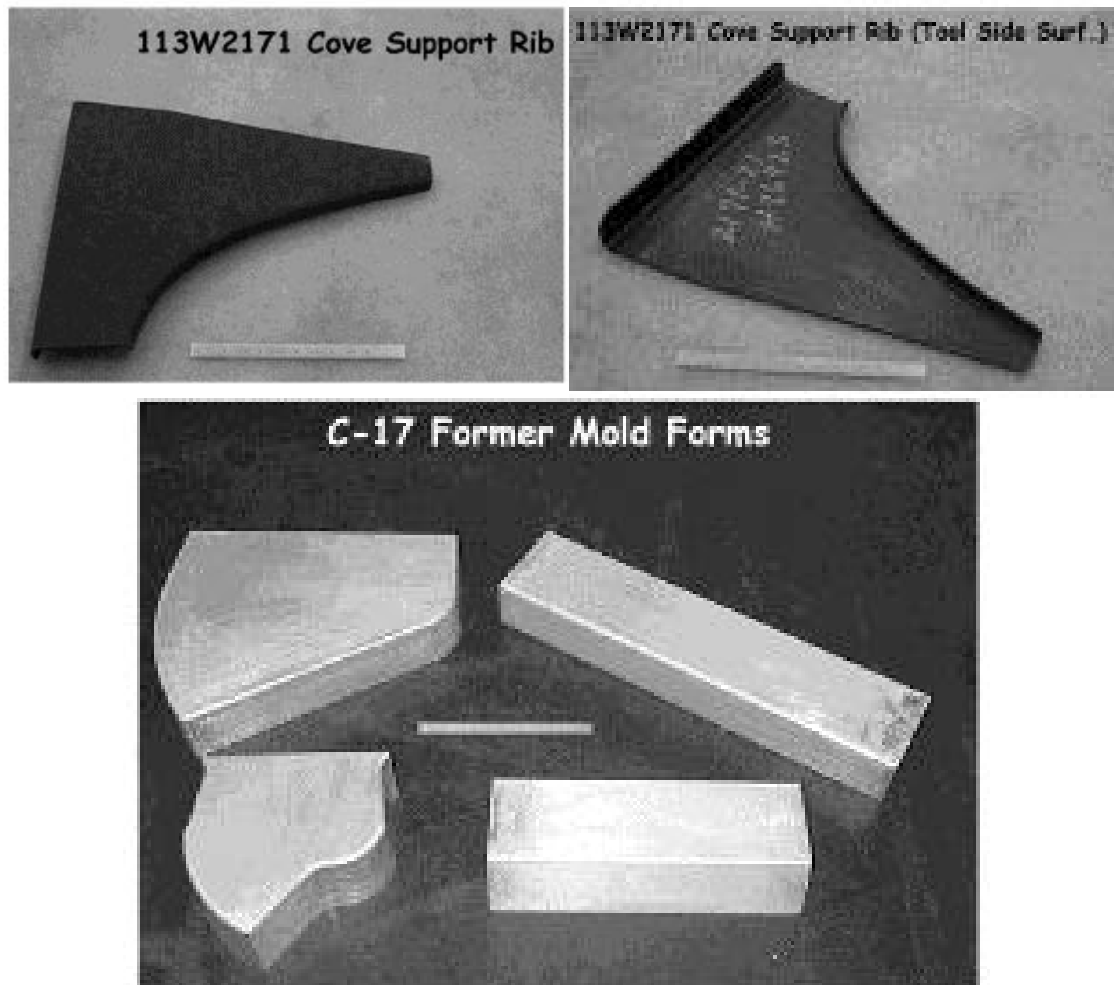


Figure 3.1.1-7 Examples of C17 parts and tooling suitable for LOM/Forming

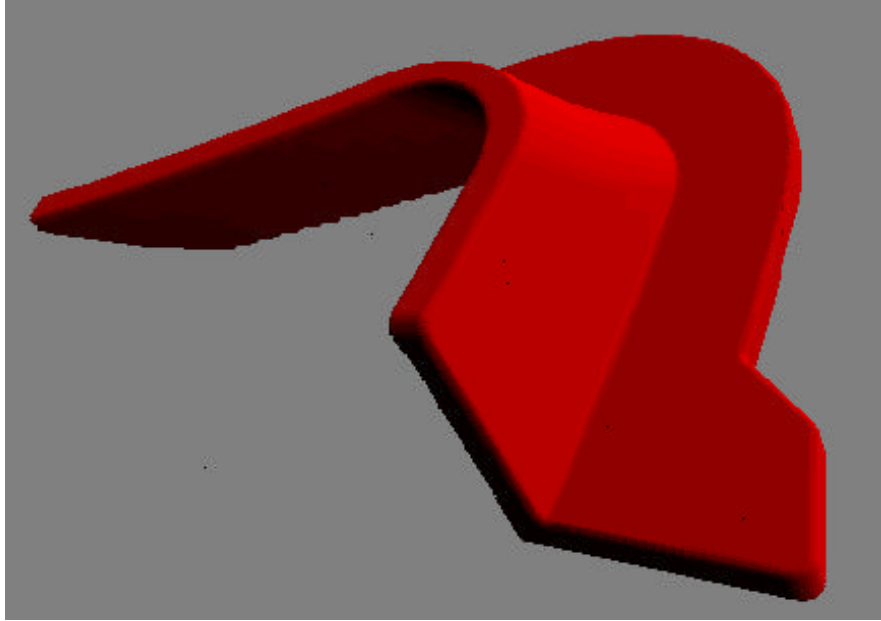


Figure 3.1.1-8 Section of JSF Tooling Fixture

LOM Forming Cell - Construction/Calibration

The LOM/Forming process developed in the program entails the flat layer lamination of Nextel™/Blackglas™ composite plies by the LOM unit and subsequent deformation into final part geometry by a vacuum diaphragm-forming step. In this program a double diaphragm composites forming system was designed, constructed, and used in the above forming application to produce the final CMC blastshield demonstration component. Figure 3.1.1-9 shows a schematic of the Composites Forming Cell. The system consists of a vacuum box (internal

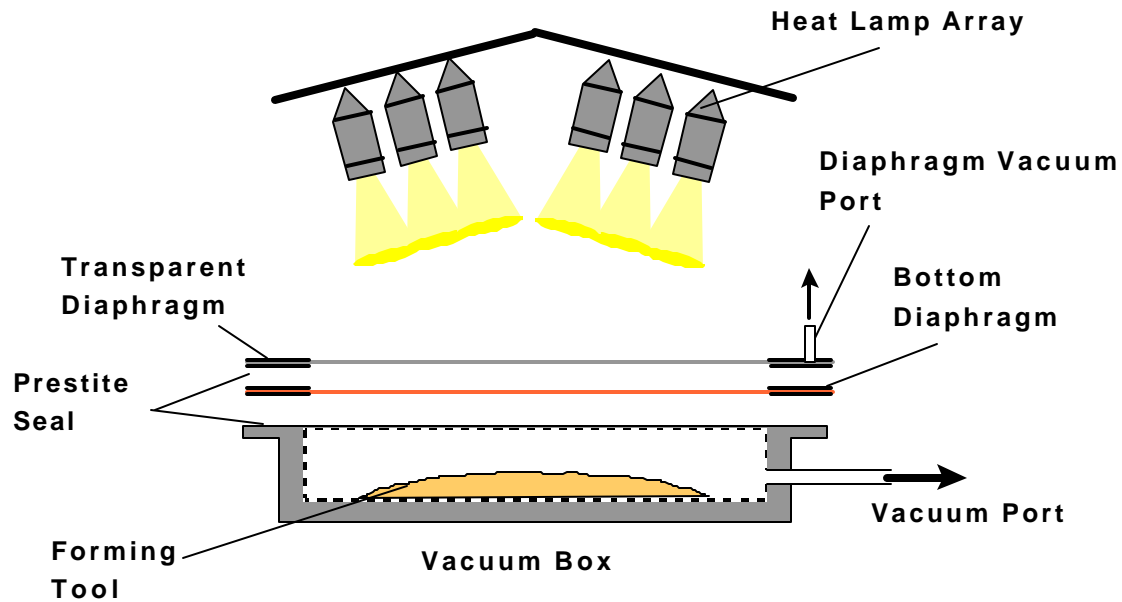


Figure 3.1.1-9 Schematic of Composites Forming Cell for LOM.

dimensions 30.5”L x 21.5”W x 8”H), two 0.075” thick silicone rubber diaphragms bonded to individual 3” wide Al frames, and a heat lamp array consisting of six 375 watt IR lamps mounted on adjustable sockets. The bottom silicone rubber diaphragm is opaque while the top diaphragm is constructed of transparent silicone rubber to enable efficient radiant heat transfer between the IR lamps and the composite laminate to be cured on the system. The Al frame of the top diaphragm also contains a vacuum port to enable a vacuum to be sustained between the top and bottom diaphragms.

Figure 3.1.1-10 displays the prototype Composites Forming Cell loaded with the final blastshield LOM forming tool. Each heat lamp is attached to a threaded rod bolted through a section of multi-holed C channel for individual lamp height adjustment and variation of lamp-to-lamp spacing. Better temperature control and uniformity over the part surface area also is achieved in the forming system (compared to the previously developed Northrop Grumman Composites Forming Unit) by the ability to rotate and pivot the individual lamp housings.

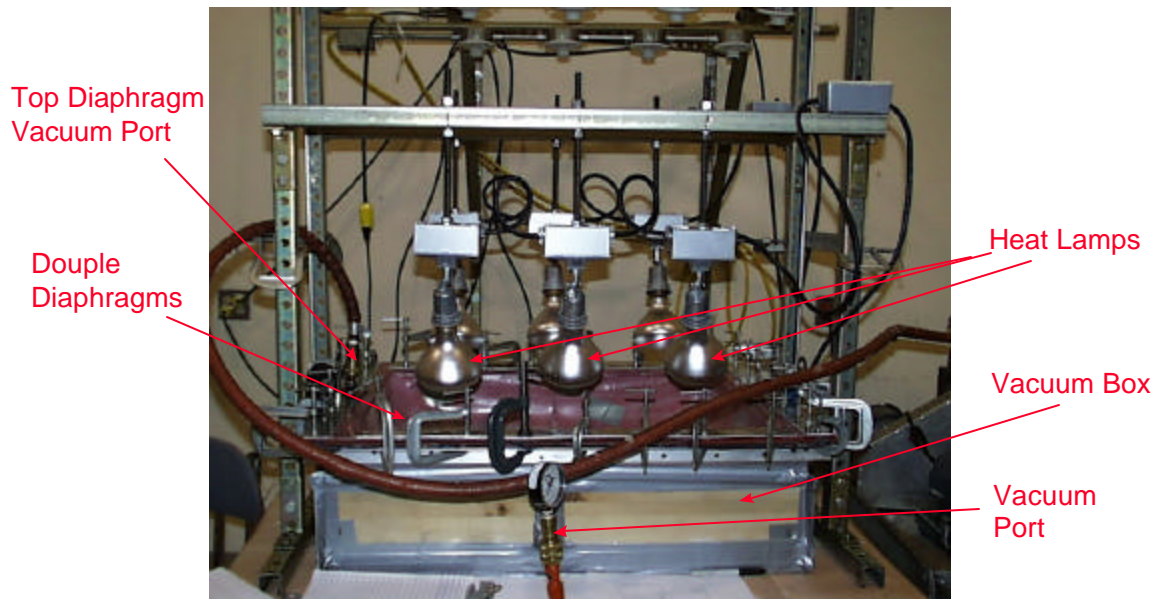


Figure 3.1.1-10 LOM Composites Forming System

An initial temperature calibration of the forming system was obtained using only the blastshield LOM tool under vacuum. This calibration served mainly to determine the gross height locations required of the individual heat lamps such that the LOM tool reached 301°F, the upper hold temperature of the Blackglas™ polymer cure cycle. A more thorough thermal calibration of the system was obtained using the LOM forming tool and a 16-ply preform made using a fiberglass cloth and a vinyl ester resin. Earlier work had shown that the heating characteristics of the vinyl ester/glass composite system were very similar to those of the Nextel™/Blackglas™ material under investigation. Therefore this material was again used to determine the optimal heating light configuration for the new forming cell. Curative was not added to the preform, in order to allow several heating profiles to be obtained from the laminate. Type K thermocouples were placed on top and beneath the laminate at various locations to determine both the in-plane and through thickness temperature gradients. The recommended cure cycle for Blackglas™ resin calls for an initial slow heat ramp to 131°F and a hold for three hours followed by a further heating to 301°F and a final two hour hold. Separate infrared heat lamp arrangements needed to be

determined for both the low and high temperature cure steps, as well as an evaluation of the temperature ramp rates and in plane and through thickness temperature gradients obtained over the course of the cure schedule.

Thermocouples were placed with identical spatial arrangements above the part and below the lower diaphragm. The positions of the thermocouples relative to an origin chosen on the midline or 'backbone' of the part are shown in Figure 3.1.1-11. The co-ordinates of these positions are given in Table 3.1.1-1. Note that thermocouples A through E was placed on top

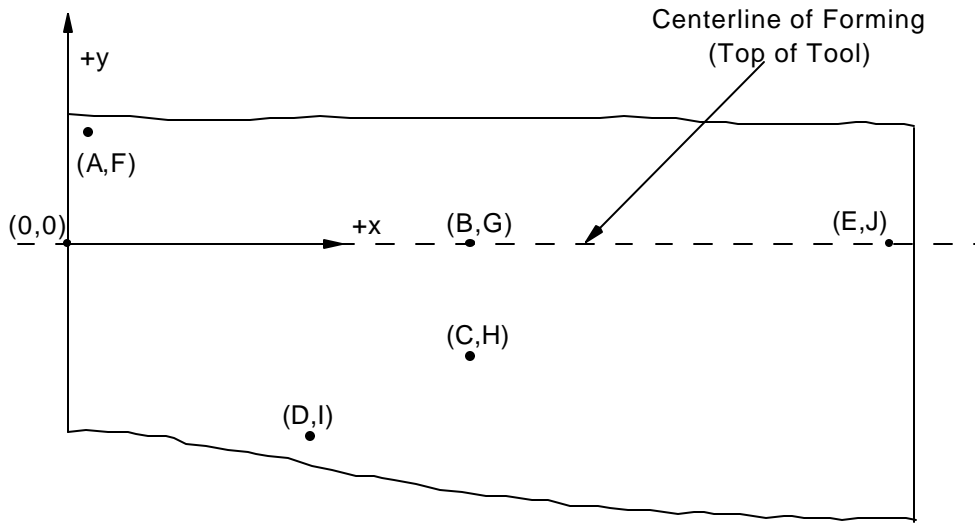


Figure 3.1.1-11 Thermocouple positions on flat pattern of blast shield tool.

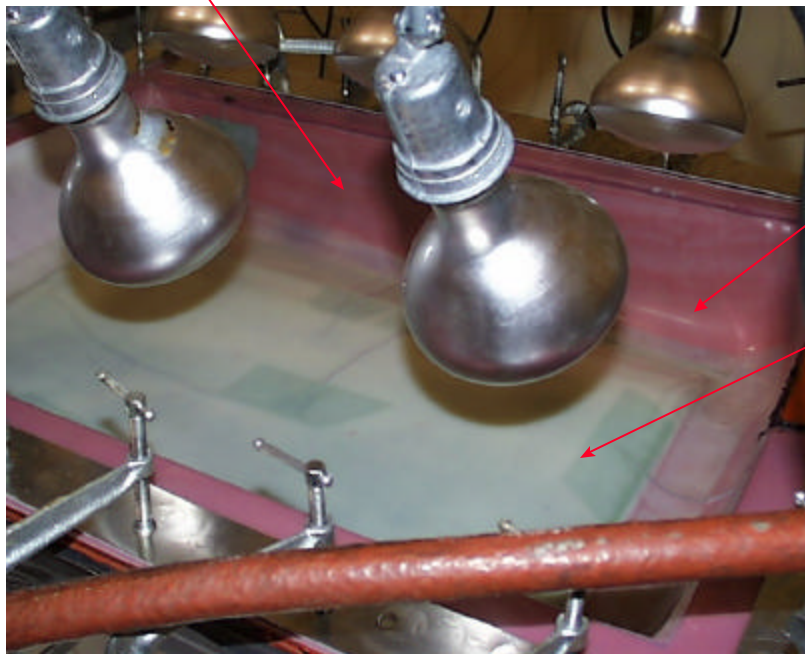
Thermocouples	X (inches)	Y (inches)
A & F	1.0	6.5
B & G	11.5	0.0
C & H	11.5	-4.5
D & I	8.25	-8.0
E & J	22.5	0.0

Table 3.1.1-1 Co-ordinates of Thermocouple locations given in Figure 3.1.1-11.

of the laminate, and thermocouples F through J were placed beneath the lower diaphragm. The arrangement shown was chosen in order that data be collected at a number of key locations on the part, including edges, part center, directly beneath heat lamps, and between heat lamps. Figure

3.1.1-12 shows a close-up view of the LOM Forming Cell containing the LOM forming tool and glass/vinyl ester laminate under vacuum. Figure 3.1.1-13 shows the forming system with the heat lamps on during the temperature calibration of the system. Several light position arrangements were tried for the lower temperature calibration. Initially 375 Watt IR lamps were used, but these provided light energy at too high an intensity when operating anywhere within the spacing constraints of the new forming cell. Therefore a second set of lights, powered at

Bottom Diaphragm



Top
Transparent
Diaphragm

LOM Tool
w/ Laminate

Figure 3.1.1-12 Detail of LOM Composites Forming System w/ glass fiber/polymer laminate.



Figure 3.1.1-13 LOM Composites Forming System during temperature calibration.

250 Watts each were installed, and again several calibrations performed. The equilibrium temperatures of the final calibration are shown in Table 3.1.1-2. All temperatures were found within an acceptable range for curing the Nextel™/Blackglas™ prepreg. The very small temperature variation through the thickness of the laminate and lower diaphragm is somewhat surprising. However this is a relatively small temperature increase, which was effected over a period of about an hour and a half. The final positions of the lights for this lower temperature calibration are given in tabular form along with those for the higher temperature calibration in Table 3.1.1-3. The positions of the six overhead IR lamps are given as a series of XYZ coordinates referenced to the origin (0,0) given in Table 3.1.1-3. The tilt angles, α , of the lights are also given. These angles are relative to a vertical plane that passes through the centerline of the part, and positive angles imply tilting of the light inward in the direction of the laminate and tool.

Thermocouple	A	B	C	D	E
Equilibrium Temp. (°F)	141	134	147	121	134
Thermocouple	I	J	K	L	M
Equilibrium Temp. (°F)	136	133	139	122	131
Delta (°F) (Top-Bottom)	-5	-1	-8	+1	-3

Table 3.1.1-2 Equilibrium temperatures on low temperature calibration.

Low Temperature Calibration						
Light Number	1	2	3	4	5	6
X	2.25	11.25	20.25	2.25	11.25	20.25
Y	7.5	7.5	7.5	-10.25	-10.25	-10.25
Z	29	29	29	29	29	29
α	10°	0°	10°	10°	10°	10°
High Temperature Calibration						
Light Number	1	2	3	4	5	6
X	2.25	11.25	20.25	2.25	11.25	20.25
Y	7.5	7.5	7.5	-10.25	-10.25	-10.25
Z	7.5	7.5	7.5	7.5	7.5	7.5
α	20°	20°	20°	20°	30°	30°

Table 3.1.1-3 Positions of heating lamps for low and high temperature cure segments.

A similar process was employed to determine the optimum position of the lights for the higher temperature stage of the cure cycle. In this case the lights were lowered substantially (see Table 3.1.1-3) and the higher energy bulbs (375W) were employed. After a number of lighting arrangements were tested, equilibrium temperatures shown in Table 3.1.1-4 were obtained. Again, these are acceptable for processing of the NextelTM/BlackglasTM material, but in this case there is a more noticeable gradient between the part and the top of the LOM tool. The equilibrium values shown were obtained after more than an hour and a half of heating. The results represent an increase in heating capacity over the earlier machine, in that temperature as high as 300°F were not previously available. The insulating effect provided by the lower diaphragm is important, since it reduces the thermal exposure of the tool, and therefore likely increases its service life. Using a thicker diaphragm or additional insulating layers could of course, increase this protection. Details of using the completed forming module to form and cure the full size NextelTM/BlackglasTM blastshield are described in Section 3.3.2.

Thermocouple	A	B	C	D	E
Equilibrium Temp. (°F)	315	299	294	289	280
Thermocouple	F	G	H	I	J
Equilibrium Temp. (°F)	300	280	286	282	270
Delta (°F) (Top-Bottom)	-15	-19	-8	-7	-10

Table 3.1.1-4 Equilibrium temperatures on high temperature calibration.

3.1.2 CCDP/LOM Interface Development

The purpose of this subtask was to develop an interface (new non-STL file format and software code) that would translate the output of the Computerized Composites Development Project (CCDP) laminate design software (Computer Aided Design for Composites, CADCOMP & Ply Definition, PLYDEF) into a format suitable for input and execution by the LOM machine. Northrop Grumman composite laminate design software, CCDP, was utilized to generate design data, as Computer Aided Design (CAD) files, of CMC components to be fabricated by LOM. These files contained all the pertinent design specifications needed to fabricate the part (ply lay-up sequence, ply orientation sequence, etc.). The CAD files are input to the LOM system for CMC component manufacture. The current practice in the Rapid Prototyping (RP) field, as well as in the SFF field, is to convert the CAD design file to an STL file format for input to the appropriate RP or SFF machine. In converting the CCDP-derived design data to an STL format, though, important component build specifications, such as ply orientation and lay-up sequence, are lost. Consequently, a non-STL, CCDP-derived output file that retained the pertinent composite design specifications (mainly ply orientation information) was developed for input to the LOM unit.

The new file format was structured to address two program needs: 1) to circumvent the use of an STL file format for input to a LOM system and instead allow direct import of a generic ASCII data file, which could be generated by a variety of Commercial Off-The-Shelf (COTS) or proprietary modeling systems (not just CCDP) as desired by DARPA and USAF; 2) to incorporate several new processing parameters to this input file for future use with LOM system component upgrades.

In the new data input scenario, 3D models of composite parts (which are to be fabricated by the curved LOM system) will be first created using in-house 3D modeling software, and all

slicing (ply definition) will be accomplished using this software. As such, the slicing algorithm in LOMSlice 2.0 Program is by-passed and this “pre-sliced” generic ASCII data file will be inputted directly into machine control software. This ASCII data file will be delivered to the software for each ply (slice) comprising the part and will be formatted as shown in Table 3.1.2-1. This new file format, designated LOM Neutral Exchange Format (LOMNEF), is similar to the standard CSF data file used by the current LOM system except for the following differences:

- The file defines fiber alignment angle for each ply; so that alignment can be implemented by appropriate indexing of the table rotary mechanism.
- The file incorporates several placeholders (lines 6 through 9) for additional LOM processing parameters that may be necessary in future LOM system upgrades.
- The file contains the decubing/debulking paths so the Helisys software need not generate them.

Input Data File Definition	
0)	Designation of the beginning of a ply (ply) [ply=ply#, ply=0 implies end of file]
1)	Count of ply boundary paths (nb)
2)	Count of points making up each ply boundary path (nbp)
3)	For or at each ply path boundary point:
	• (x,y,z) location coordinates
	• (i,j,k) unit length tangent cut vector coordinates
	• (p) laser power (P>0 implies laser is on, p=0 implies laser is off)
	• (f) motion feedrate
4)	Count of ply decube/debulking path points (ndp)
5)	For or at each ply decube/debulking point:
	• (x,y,z) location coordinates
	• (i,j,k) unit length tangent cut vector coordinates
	• (p) laser power (p>0 implies laser is on, p=0 implies laser is off)
	• (f) motion feedrate
6)	Ply compaction time (t)
7)	Ply compaction pressure (k)
8)	Ply compaction temperature (c)
9)	Material selection (m)
10)	Feed table fiber alignment angle (a) (in degrees)
11)	Material pickup from feed table flag (u)
12)	Material deposit onto lay-up platform flag (d)
13)	Sled motion or positioning along rails (s)

Table 3.1.2-1 Input Data File Definition

The structure of the new file format above was devised so that the interface is not tied to the CCDP software code and is thus applicable to other COTS design or analysis programs. The platform neutrality of the LOM/CCDP data exchange format was developed such that component design data inputs from a variety of sources (commercial, in-house) could be utilized for LOM SFF prototyping. This neutral data exchange format was developed specifically for LOM. The exchange format is not tied to CCDP in any way. It was developed specifically for LOM product fabrication processes and features. The design features used in the neutral exchange format were

based on those of the "ISO-Standard STEP/PDES AP209 Protocol for Laminate Composites: Analysis to Design". Standard for the Exchange of Product model data (STEP) is an international standard for the computer-interpretable representation and exchange of product data. STEP is increasingly replacing the more familiar IGES neutral exchange format standard used to define product information because of its enhanced capabilities.

The objective of STEP (and the earlier IGES protocol) is to describe part definition data throughout the life cycle of a product, independent of the computer platform or system on which it resides and to provide for a seamless exchange of part design description among multiple platforms. It is in the spirit of this multiple user applicability without regard for user platform that the LOM exchange was formulated. In addition, some input data sources may include input design data for more component and process features than other systems. The neutral exchange format for LOM was structured to accommodate such differences among the source systems; and can be implemented incrementally as the systems mature. The only features not included in the exchange format are those specific and unique to LOM itself. CCDP represents the first (hopefully, of many) design data source systems that offer a LOMNEF translator.

The necessary LOM system software was developed and tested which accepts product definition data from the LOMNEF input file and utilize such data, as depicted in Table 3.1.2-1, to generate system and motion control commands sufficient to perform the indicated operations by the LOM system. This software was structured to function as a design data post-processor or a control system pre-processor; essentially duplicating the LOMSlice software, only without having to perform any of the slicing or debulking calculations. Hence, it is a scaled down version of the LOMSlice software, having a new input data module and nearly the same output modules. This software enhancement allows the user a choice of either file format without eliminating any of the functionality of LOMSlice to process standard STL-type data input.

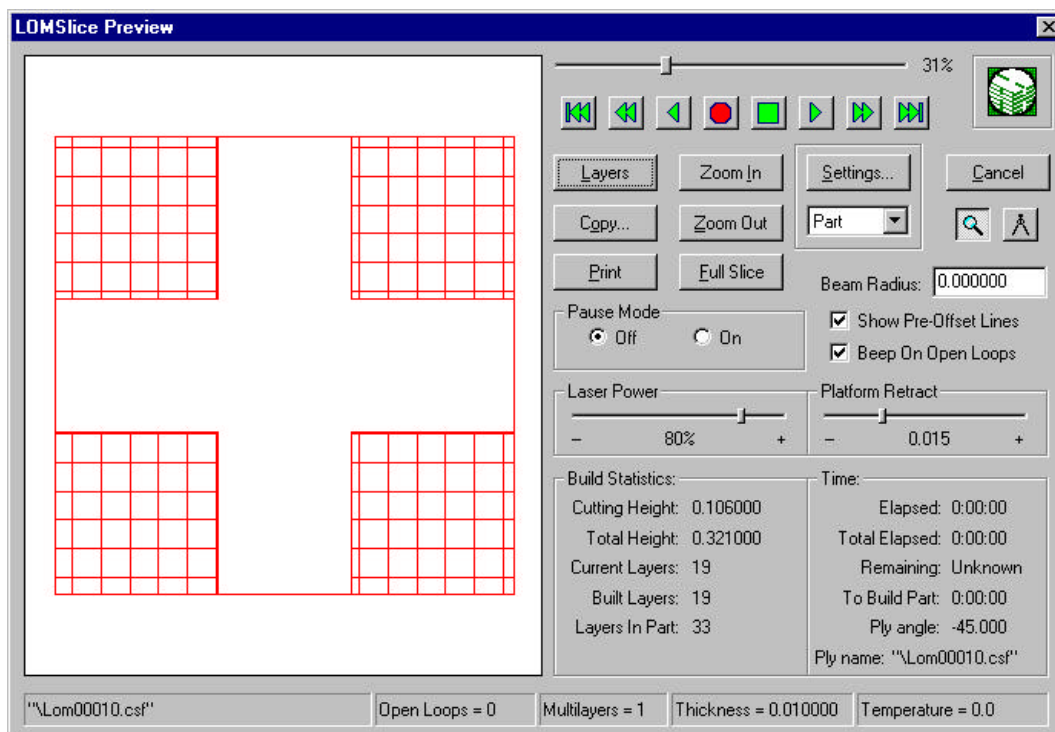
The initial implementation of the new software incorporated only one new design feature, ply (slice) fiber orientation, and did not include the indicated processing of the following product definition data features but, instead displayed them on the operator's console for visibility and tracking:

- 6) Ply compaction time (t)
- 7) Ply compaction pressure (k)
- 8) Ply compaction temperature (c)
- 9) Material selection (m)
- 11) Material pickup from feed table flag (u)
- 12) Material deposit onto lay-up platform flag (d)
- 13) Sled motion or positioning along rail(s)

Helisys performed the system enhancements, as needed to incorporate product definition features 6-9 and 11-13 listed above. The unit length tangent cut vector coordinates (i, j, k) and motion feedrate (f) parameters also were ignored by the system at this time: At a later date, additional software/hardware modifications may be implemented to allow computer controlled variable ply compaction and tangent cutting. Features 6-9 and 11-13 are placeholders in the software for future functionality upgrades.

Modifications were also made to the CCDP system to incorporate a CCDP to LOM translator to convert PLDEF and CADCOMP output data into the LOMNEF file format. The CCDP design code also required modification to update build-up surface thicknesses for the LOM material sheet size, as opposed to updating only surface regions covered by a ply. This was necessary because excess material is removed later during debulking. A CCDP to LOM plotting program was also written. This program is used to provide visual verification that the designed LOM part is correct. Modifications to LOMSlice software on the LOM 2030H system were also

completed so the program could interpret both STL and CCDP derived part design data files and prompt the user for which file type to process. Software was created that generates an interface between the LOMNEF file format and internal operations of the LOMSlice 2.0 machine control program on the 2030H unit. The code automatically recognizes the LOMNEF format and uses it in the multi-quadrant laser-cutting mode. The visual interface shows the specific LOMNEF defined plies on the screen (and its required orientation) as they are being produced. Figure 3.1.2-1 displays the user interface screen for one ply from the LOMNEF file for an 8" x 8" cruciform stiffened subcomponent panel. The operation of the rotary table mechanism needed for orientation of composite layers is discussed in Section 3.2.2.



LOM_FLAT_STFND_2 CCDP Data File; Ply 11, -45° Orientation

Figure 3.1.2-1 User Interface Screen displaying ply layer from LOMNEF file for 8"x 8" cruciform stiffened subcomponent panel

3.1.3 CAD/LOM Procedure Development (Task 1.1.2)

The initial goal of this subtask was to develop CAD design procedures that integrate CAD models, CADCOMP and PLYDEF software routines and the LOM machine to enable generation of design descriptions for composite sub-element and components to be fabricated by LOM. During the course of the program, the subtask was expanded to include (1) definition of a software tool suite for performing design and prototyping via LOM/Forming and (2) development of a formability criteria for composite parts in relation to the overall design procedure for the LOM/Forming process.

Design/Analysis Software Suite for LOM/Forming Process

To ensure the LOM/Forming based design methodology developed in the program could be readily utilized by the general DoD, CMC, and aerospace composites communities, the protocol was not strictly tied to a specific design software code (i.e. CCDP). The methodology was made general enough such that it could be applied using a range of other proprietary or COTS design and analysis programs. Though the program demonstrated the methodology using CCDP, this specific design ‘program’ will not be included in the LOM commercial software package. Sufficient software architecture flexibility was built into the system to interface with customer preferred design codes. Through use of the LOMNEF translator, alternate COTS software can be substituted for the CCDP system in the various steps of the LOM/Forming CAD/CAM process. One can define a general LOM/Forming software tool suite based on the essential elements required in this overall design/manufacturing process. Figure 3.1.3-1 displays the basic software elements for a LOM/Forming design tool for CMC components. The minimal tool suite the user requires to design and LOM prototype a composite component includes a part 3D modeling program (i.e. CATIA, AutoCAD, ProE), a flat ply pattern generator, (i.e. FiberSIM, CADCUT, Rhino3D), and an IUA (Interactive User Application) module which is a common

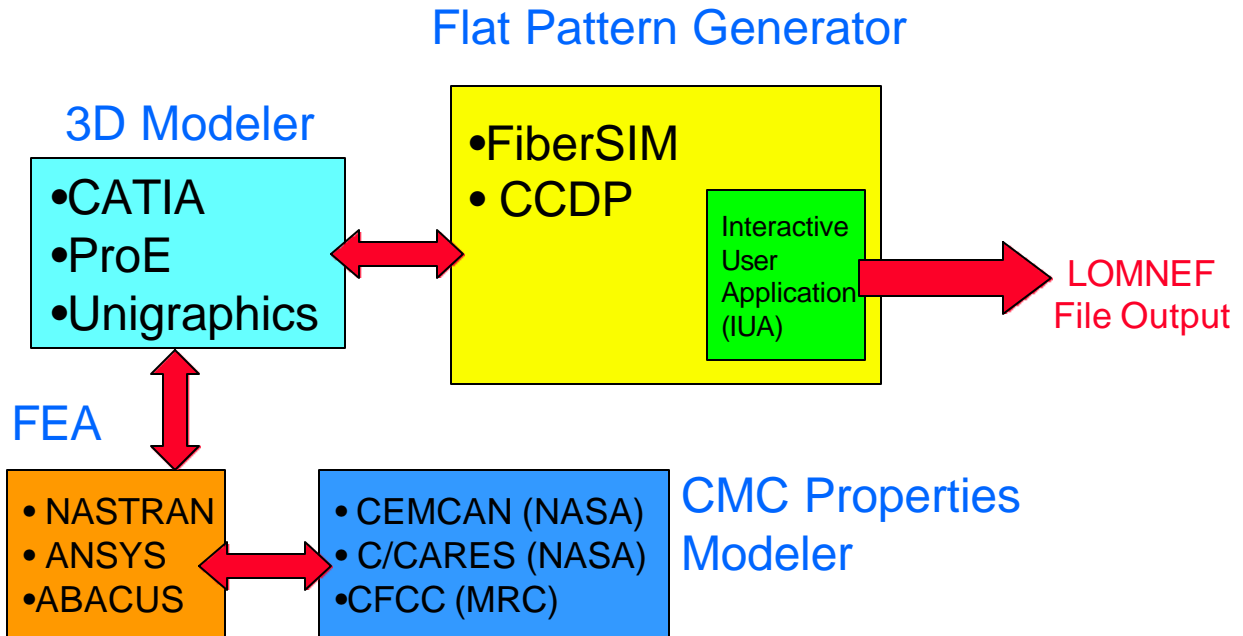


Figure 3.1.3-1 Example Design Software Suite for LOM/Forming of CMC Components

component of most 3D modeling software programs. The IUA allows the designer to custom generate the necessary software translator to convert the design data into the required LOMNEF file format for output to the LOM unit. In a realistic CMC or composite structural analysis and design scenario, the 3D modeling software would typically be linked with a specific commercial FEA code (NASTRAN, ANSYS, ABACUS, COSMOS/M) to evaluate the mechanical performance of the component under the applied application loads. A CMC component designer might also utilize several analysis codes developed specifically to model the properties of CMC material systems and structures (which work in association with the various commercial FEA codes). Some examples include the probabilistic based CEMCAN (Ceramic Matrix Composite Analyzer) and C/CARES (Composites/ Ceramics Analysis and Reliability Evaluation of Structure) CMC property prediction codes developed by NASA (Glenn) or the micromechanics based CFCC (Continuous Fiber Ceramic Composite) code developed by Materials Science Corp. (MSC).

Using the combined 3D modeling, FEA, and CMC property prediction software various CMC design cases can be quickly evaluated. Flat Pattern Generation software developed

specifically for continuous fiber reinforced composite materials (Such as FiberSIM from CDT Inc. or CADCUT) is next used to generate the flat ply patterns needed to successfully form the composite prepreg ply stack into the 3D part shape without wrinkling. This design data is next converted to the LOMNEF file format for input to the LOM unit to rapidly convert a new CMC design concept into a real part. As part of the Helisys' commercialization plan for the next generation LOM/Forming system, documentation will be provided to a new user defining the required steps to design and fabricate a part by LOM/Forming, the requirements for the IUA LOMNEF translator, as well as example components or shapes and the software utilized to make these components. An example of a design/LOM prototyping exercise using specific COTS software (instead of CCDP) will also be provided in the documentation.

CAD/LOM Procedure Development

A preliminary LOM based design methodology for CMC parts was generated when the program was first proposed. A schematic of the methodology that has been modified to include evaluation of composite part formability is shown in Figure 3.1.3-2. A critical element that was missing in the earlier design/analysis sequence (as described in the proposal) was a step to determine the formability of the composite part of interest. As the formability of the composite part determines if the component can be prototyped by curved LOM or LOM/Forming, this step should be performed early in the design/analysis protocol, preferably at the conceptual design stage. An efficient and accurate formability evaluation, though, requires analysis at two stages of the part design process. The first formability analysis occurs in the preliminary component design stage. The overall geometric characteristics of the part are first assessed to determine the suitability of its shape for LOM/Forming based prototyping. A more detailed formability evaluation is required again once the laminate properties have been established for the component (number of plies, ply geometry, architecture, and stacking sequence) to enable a realistic simulation. This

new predictive capability for composites forming combined with the LOM/Forming SFF ability should help to significantly reduce the time and cost associated with prototyping of composite structures. A summary of the important elements of the formability evaluation methodology outlined in the program follows.

Composite Part Formability Evaluation

Though an understanding of the formability of fiber reinforced composite structures is by no means complete, a set of criteria or rules can be defined to predict fairly well if a structure can be fabricated. The current knowledge base on composites formability prediction is derived from both analytical modeling results for specific part shape classifications and reinforcement architectures and practical experience in composites forming of polymer composites components. Figure 3.1.3-3 displays the associated elements of a Composite Part Formability Evaluation, which includes the interrelated material and geometric properties of the part, an analysis model/program, and the information one would like the analysis to determine.

Forming Analysis

Two modeling approaches are currently utilized for evaluating sheet forming processes; one based on geometric mapping calculations and the other on continuum mechanics type models. The mapping approach views forming as a purely geometric transformation by which the initially flat sheet (or sheets) is mapped onto the curved, three-dimensional surface of the tool in a single step. The primary information obtained is kinematic in nature and includes the fiber orientation in the final part and any strains developed in the formed material. The strain information can be used to infer where defects (ply wrinkling, buckling) might occur which could then be offset by slight modifications to the ply shape or part geometry. Mechanics approaches use both equilibrium equations that balance the forces within the composite against the applied loads and constitutive equations that give the stress in the composite as a function of

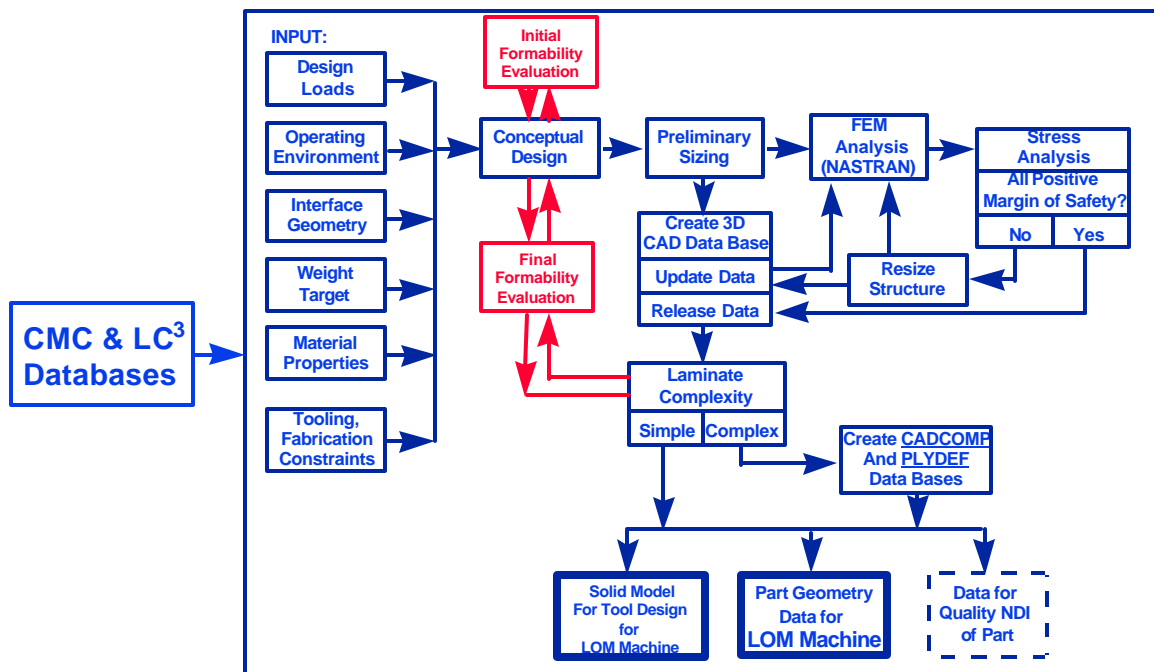


Figure 3.1.3-2 LOM/Forming Design Methodology Procedure with updated Part Formability Evaluation Module

Composite Formability Evaluation

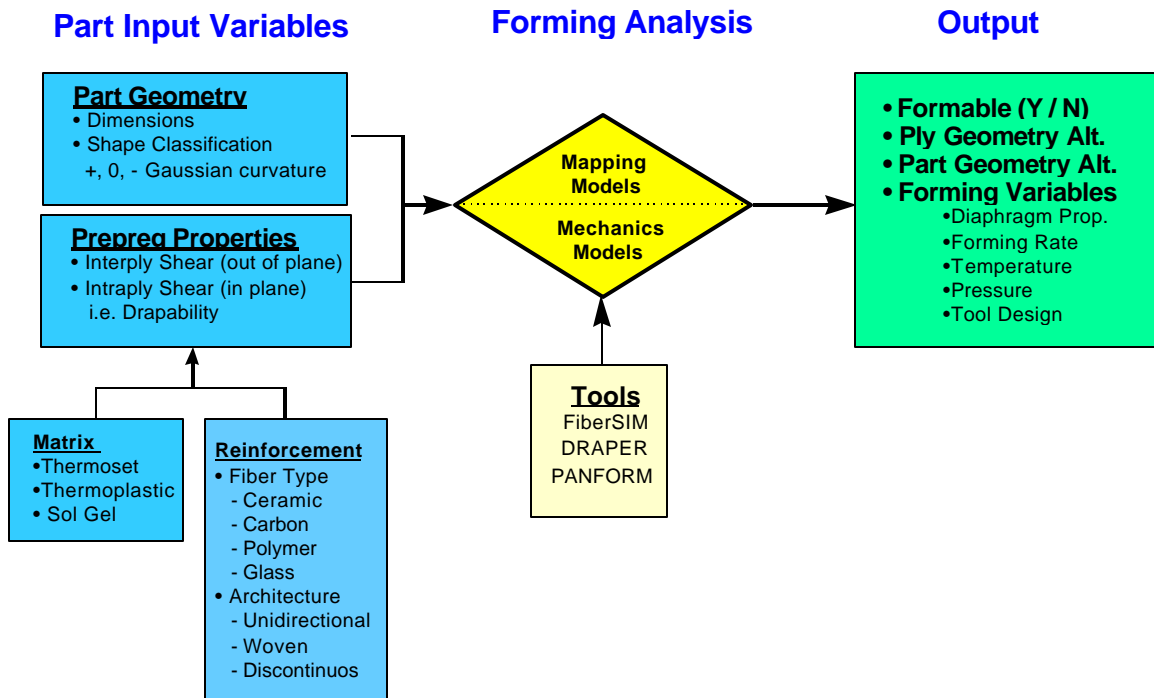


Figure 3.1.3-3 Overview of the elements of a Composite Part Formability Evaluation

strain or strain rate. Mechanics approaches give kinematic information similar to mapping models. They also give much more information about the stress state in the material that can be used to better predict the formation of defects. As mechanics models are more complicated than mapping models they are much less developed at this time and fairly cumbersome and time consuming to run. To date there is no complete mechanics type model that can represent a multilayer laminate being formed into a three dimensional shape. Most commercially available sheet forming codes (FiberSim, DRAPER), thus utilize mapping based numerical or analytical models for their analysis. As such, for the current program the criteria to determine part formability was strictly based on mapping approaches (using the FiberSim code).

Part Input Variables

Both the size of the part and its shape (in terms of Gaussian curvature) dictates the type of forces (tension, compression, shear) developed in the laminate during the forming step and the deformation levels (both in plane and out of plane) required of the plies. The interply (out of plane) and intraply (in plane) shear behavior of the prepreg are the critical properties that determine the level of deformation that can be sustained in the part before defects are generated. These shear values are in turn a function of the combined properties of the matrix and fiber reinforcement of the prepreg. Viscosity is the critical matrix property that influences the shear behavior of the ply. As the matrix viscosities of most thermoset prepreps are low, the forming behavior of these systems is largely determined by the fiber reinforcement. The heating capability of the forming apparatus is an issue with thermoplastic-based prepreps, as they must be processed at elevated temperatures to attain the low matrix viscosities required for forming.

The type and architecture of the fiber reinforcement generally plays the greatest role in determining the forming behavior of the prepreg. The stiffness of the fiber reinforcement directly

influences ply drapability. The type of fiber architecture defines the constraints of the mapping problem and the most appropriate analysis model to use. In the mapping approach one calculates the correspondence between a defined set of points in the flat composite sheet and points on the tool surface. The primary constraint in the analysis is that the reinforcing fibers cannot stretch. The material is thus inextensible in the main fiber direction. Material with aligned discontinuous fibers that stretch somewhat in the fiber direction, therefore, cannot be analyzed with mapping approaches since they do not follow this inextensibility constraint. Mechanics based models are better suited for formability analysis of these materials.

The constraints of fiber inextensibility influence the mapping analysis so strongly that ultimately it is the properties of the fiber reinforcement that largely dictates part formability for both aligned (unidirectional) and woven systems. The mapping behavior of plies with unidirectional fibers behaves distinctly different from woven materials (due to the fiber inextensibility constraint) as woven materials have fibers running in cross directions. Separate numerical and analytical solutions are required for each case. During mapping the distance between unidirectional fibers is assumed to be fixed and the fibers simply slide parallel to one another. For woven fabrics the assumption is that neither the warp nor fill directions may stretch and they may pivot but not slip at crossover points. When a woven fabric is sheared, though, the spacing between the warp fibers must decrease to keep the length of the fill direction fibers constant. Mapping models developed for woven materials generate results that accurately reproduce experimental findings and serve as the framework for commercially available analysis codes. Mapping calculations for unidirectional materials are not as accurate as that for woven systems as the assumption of constant fiber spacing during forming is not held. The predicted shear levels and fiber paths are typically overestimated and serve more as a worst-case estimate.

Formability Analysis Output

The information the analysis should provide is a determination if 1) the part can be formed as is, 2) the part can never be formed, or 3) the part can be formed after suitable alteration of ply shape or part geometry. The nature of the required alterations should be specified. Though the results will not include actual process variables for the forming step, the formability criteria established would help to determine what those optimal conditions should be.

The design methodology for SFF of composite parts utilizing a LOM/Forming process was updated to include a part formability evaluation step. A method was devised on how to use a commercially available composites analysis program, FiberSIM, to perform this formability determination. Full commercialization of a LOM/Forming system requires a computer design interface that captures the accumulated processing knowledge on composites forming for practicable material systems. A realistic evaluation of the applicability of LOM technology to a particular design/prototyping challenge must include consideration of basic processing as well as cost and time issues. Parallel development of composites forming technology at Northrop Grumman and elsewhere has enabled a potential extension of the part shapes and sizes available to LOM technology. However, in order that this advantage is exploited fully, convenient computer based representations of process limits must in some way be encoded into the design process. The purpose of this sub-task is to establish a processing knowledge database to provide a rapid evaluation of the suitability of a particular part for LOM processing. This starts with an assessment of part formability, and assuming that the shape is admissible, provides additional discriminatory information on cost and time. The result is an interface that allows the user to make critical processing/prototyping decisions in advance of first part/tool fabrication.

Initial Component Formability Analysis: Gaussian Curvature Evaluation

The simplest evaluation to perform on a given part shape to determine its suitability to be

fabricated by the LOM/Forming process is to initially determine the type and degree of curvature of its surface. Most commercial CAD 3D modeling software packages (CATIA, ProE, Rhino3D) have built in features for performing curvature analysis of surfaces. Figure 3.1.3-4 displays examples of the curvature analysis output for various part shapes using Rhino 3D. Red in the figure indicates the degree of negative curvature, blue positive curvature, and green zero curvature. The half cylinder depicted in Figure 3.1.3-4(a) represent the simplest case of zero curvature, i.e., a developable surface. As described earlier, a fully developable surface should be easily formable without the need to cut or dart the laminate plies. As the degree of positive or negative curvature (or combination of both) increases, the composite part becomes more difficult to form. The Gaussian curvature of a surface, though, in of itself is not the sole criteria for determining if a composite part is formable. Information about the type of fiber architecture, number of plies, stacking sequence, and rheological properties of the prepreg plies in relation to the overall size of the part is also needed for a full formability analysis.

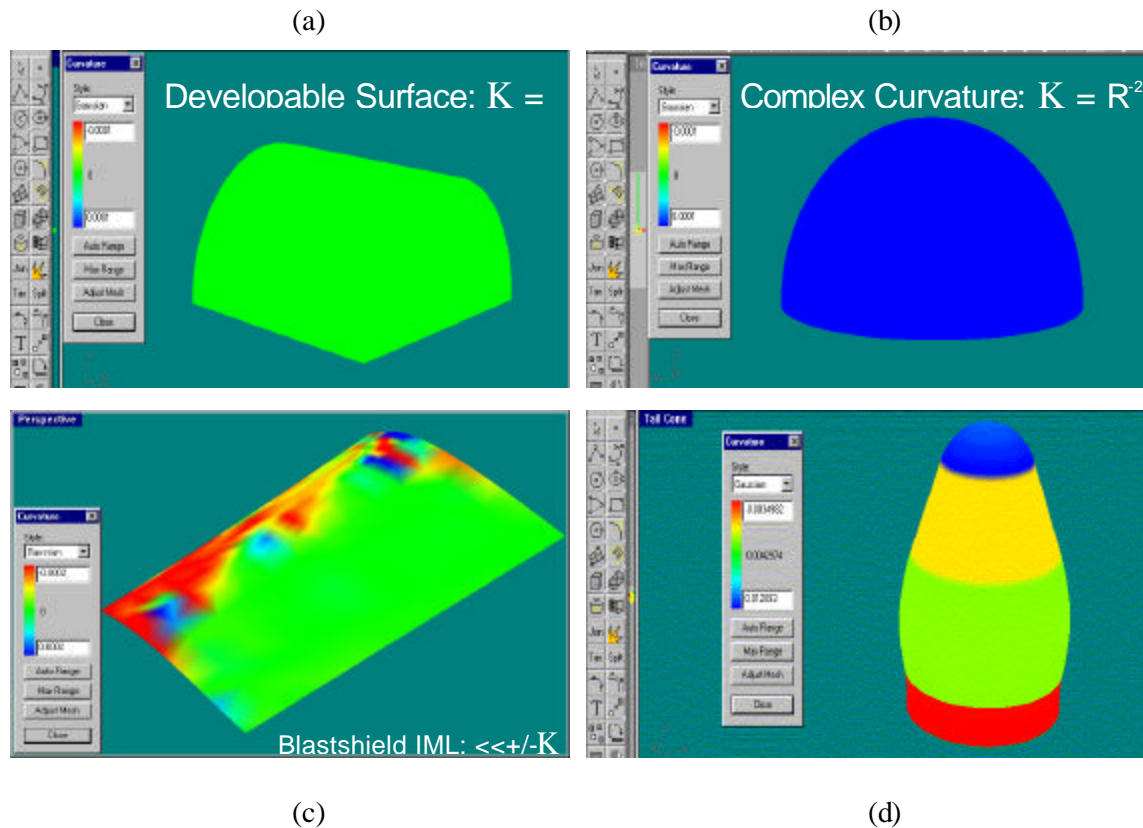
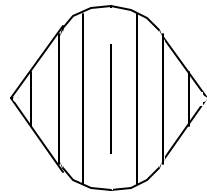


Figure 3.1.3-4 Component Gaussian Curvature Analysis (Rhino3D software)

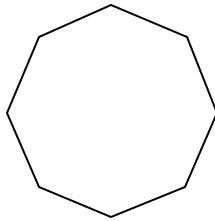
Figure 3.1.3-4(b) is a case in point for a hemisphere with positive Gaussian curvature. Previous composites forming experience shows this part shape is formable, but the required geometry of the flat ply is dictated by the fiber architecture. Figure 3.1.3-5 displays the necessary ply geometry when using unidirectional tape vs. that of a woven material for mapping onto a hemispherical part shape.

Examples of Ply Patterns Required for Mapping Over Hemisphere

Flat Pattern Geometry

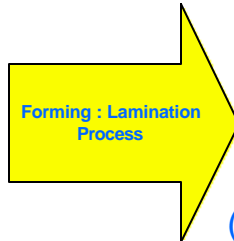


Unidirection Ply

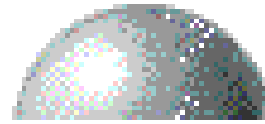


Woven Ply

Fiber Architecture Dictates Ply Pattern Required for Forming
Over Complex Curved Surface with Minimal Fabric Distortion



Part Tool Geometry



Hemisphere Surface
(Positive Gaussian Curvature)

Figure 3.1.3-5 Examples of ply patterns required for mapping over hemisphere

Most engineering forms of interest typically will have more complex curvatures containing both negative and positive features. Figure 3.1.3-4(c) displays the curvature analysis for the blastshield demonstration component, which indicates the surface is largely developable with areas of slight negative curvature. These results indicate that LOM/Forming of the blastshield should not be difficult, though, further analysis in the regions of negative curvature might be appropriate. Figure 3.1.3-4(d) displays another part shape, an aircraft engine tailcone, containing both negative and positive curvature. In this case, though, experience or intuition would suggest that this part shape most likely is a poor candidate for the LOM/Forming process. In many cases, though, determining part formability will not be so clear-cut from simple evaluation of curvature. More rigorous mapping simulation tools are needed which take into account the combined influences of part shape (curvature) and size, and prepreg properties (ply architecture and stacking sequence, matrix rheology, etc). The program investigated using a commercially available 3D mapping simulation tool for polymer composites, Fiber SIM marketed by CDT Inc. for performing more

sophisticated formability evaluation requiring details of intra and inter ply deformation mechanisms

Final Component Formability Analysis: FiberSIM Evaluation

An accurate composite laminate formability simulation must take into account the different, dominate deformation mechanism occurring for a single ply lamination sequence on a 3D tool form compared to a stack of plies. In the former the principal processing limit is determined by the ability of a given composite material form to achieve in-plane deformations. In the latter the capacity to allow inter ply sliding attains greater significance, though in-plane deformations remain important.

In-plane shear of woven materials is well characterized and a relatively large number of analytical and numerical models are available. Among the more highly developed computer codes are the ‘Draper’ program from the University of Delaware Center for Composite Materials, and the FiberSIM code by Composite Design Technologies, Inc. From the viewpoint of industrial application the latter code has been used by a number of companies including Northrop Grumman to determine flat pattern ply shapes necessary for hand lay-up of complex parts. A typical output from FiberSIM is shown in Figure 3.1.3-6. The mapping principal employed, in common with most fabric mapping utilities, is based on pin-joint modeling. The tows in the warp and fill directions are assumed to be pinned at their intersections, and thus no relative motion between them is possible. From the definition of at least two known initial orthogonal fiber paths the entire mapping can be determined. However there is an obvious limit to the type of deformation necessary to complete the mapping. This in-plane shearing deformation particular to woven fabrics is known as ‘trellising’. Depending on well defined architectural features such as the relative numbers of warp and fill yarns and the weave pattern (e.g. plain or satin) a quantifiable ‘locking’ angle will apply, beyond which further deformation forces out of plane wrinkling. The user/designer must understand this type of behavior and evaluate it for the material system being considered, though

databases based on simple shearing tests exist.

The facility illustrated in the figure is directly applicable to LOM since these in-plane deformation considerations will exert influence on the practicability of the process for potential

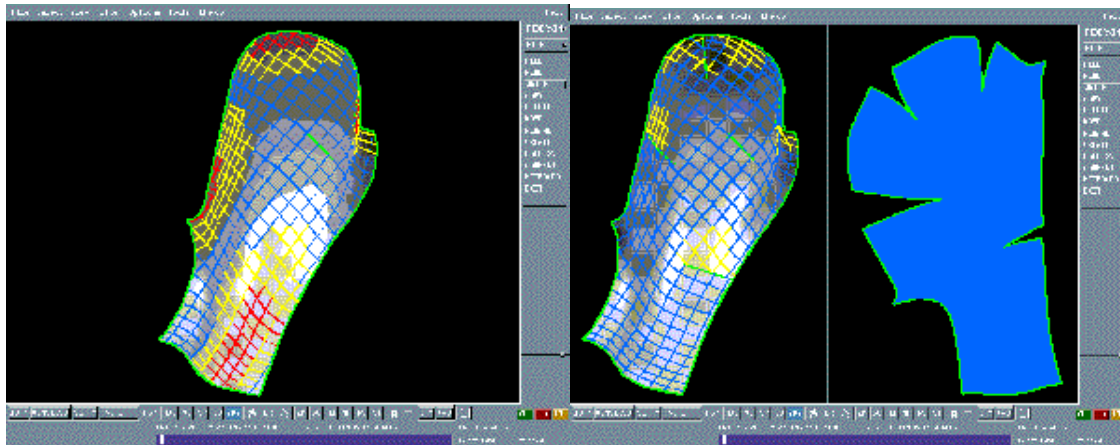


Figure 3.1.3-6 Examples of screen outputs in FiberSIM for component producibility assessment and flat pattern generation (from Composite Design Technology Inc. Homepage - www.cdt.com/ceeds.html#FEATURE-BASED_DESIGN).

part shapes. However in most instances the required inter-ply shear will be of greater concern. It has been shown that the difficulty of forming a laminated prepreg ply stack into a complex shape is directly related to the magnitude of the interply shear. Relatively sophisticated differential geometry analyses have been successfully applied to provide closed form solutions for the in-plane shear required on a number of part shapes of interest to aerospace and other industries, though most published work has been for aligned fiber systems. However, it is felt that the demands of flexibility placed by the range of geometries envisioned in this project are best met using numerical techniques.

The program demonstrated that these critical inter-ply shears could be quickly calculated using the FiberSIM program. Essentially, the code was used in reverse to develop flat ply patterns for different fiber orientations mapped over the same geometry. Once developed onto the flat, 'markers' were placed on each ply that had identical x-y coordinates but were displaced in the z

direction by one ply thickness. The mapping over the contour under evaluation was then regenerated, and the relative separation of the sets of markers provided a mapping of the magnitudes, and potentially directions, of the inter-ply shears. These numbers alone provide insight into the formability of a given component. Where large shears are required difficulty in forming is anticipated. However to determine the associated stress field, which is the ultimate goal, the rheological behavior of the resin that bears these inter-ply shears must be determined. Simple ply pull-out tests can be used that allow the shearing forces to be determined as a function of fiber orientation, temperature, deformation rate and through-thickness loads. When the stress field is evaluated, knowledge of the buckling loads of the material allows a definitive statement to be made on the formability of the component under consideration.

It has been shown in several studies that the formability of a given part geometry is directly related to the amount of interply shearing required to make the part. The degree of ply slippage available to any particular material system is determined by the fiber architecture and the resin rheology. The required interply shear is related to the degree of double or compound curvature on the part. More complex parts, in terms of double curvature, are more difficult to form. It was proposed that a fiber-mapping program, such as FiberSIM by Composite Design Technologies in Waltham, MA, could be adapted to enable rapid evaluation of interply shear patterns for arbitrary shapes. While the fundamental analytical basis for interply shear determination is established differential geometry theory, the accurate parameterized mathematical surface descriptions necessary for closed form solutions can be cumbersome, and so generalization is more readily available through numerical methods. FiberSIM, for example, works within established 3D solid modeling codes such as CATIA, Unigraphics and ProEngineer, and allows rapid determination of fiber mappings and therefore, potentially, associated shear patterns.

The part formability evaluation using FiberSim was demonstrated using a generic turbofan engine tailcone model as a test case. Though the demonstration component for the program was a CMC blastshield, the earlier gaussian curvature analysis indicated this overall part shape was developable and not a particularly challenging composite forming exercise. The tailcone geometry was chosen as it contains a large degree of negative curvature towards the base of the structure and represents a significant composites forming challenge. Though it is anticipated that the FiberSim results would indicate that the part would not be readily formable in its current geometry, the simulation exercise, nevertheless, served to demonstrate the type of output one can expect from the analysis.

The 3D shell model of the tailcone is shown in Figure 3.1.3-7 and represents the tool surface over which the test plies were draped. Figure 3.1.3-8 shows the FiberSim simulation output of a single ply shear pattern for a generic plain weave fabric draped over the tailcone tool surface. This is representative of the type of output available from FiberSIM. In this case, the fiber mapping is initiated at the apex of the cone and propagated down to the base. The mapping was terminated before the base of the cone is reached, but the results presented show the typical in plane shear patterns noted for advanced composites. The angle of deformation, sometimes referred to as the trellis angle, increases as the mapping propagates away from the top. In practical terms, this implies that some physical limit for the fabric being considered would be reached, and further deformation would force an out-of-plane displacement in the form of a wrinkle. The situation could be alleviated by applying a cut or dart in this high deformation region, and FiberSIM as a standard product feature allows the effect of such expedients on the flat pattern to be determined. The facility to pre-calculate the optimal flat pattern geometry is the principal feature of FiberSIM, as it applies directly to established hand lay-up processes. The same fiber mapping as that presented in Figure 3.1.3-8 is shown in plan view in Figure 3.1.3-9. As in

the former the color-coding represents the levels of in-plane shear in different areas of the part. The red regions are highlighted as such because fiber deformations in these areas are at levels that may not be sustained by the chosen fabric without wrinkling. One needs to either introduce a cut or dart in these regions or re-evaluate the mapping with a fabric with a looser and thus more drapable weave. However, the critical element from the perspective of the LOM program is the ability to develop these single ply patterns for arbitrary shapes.

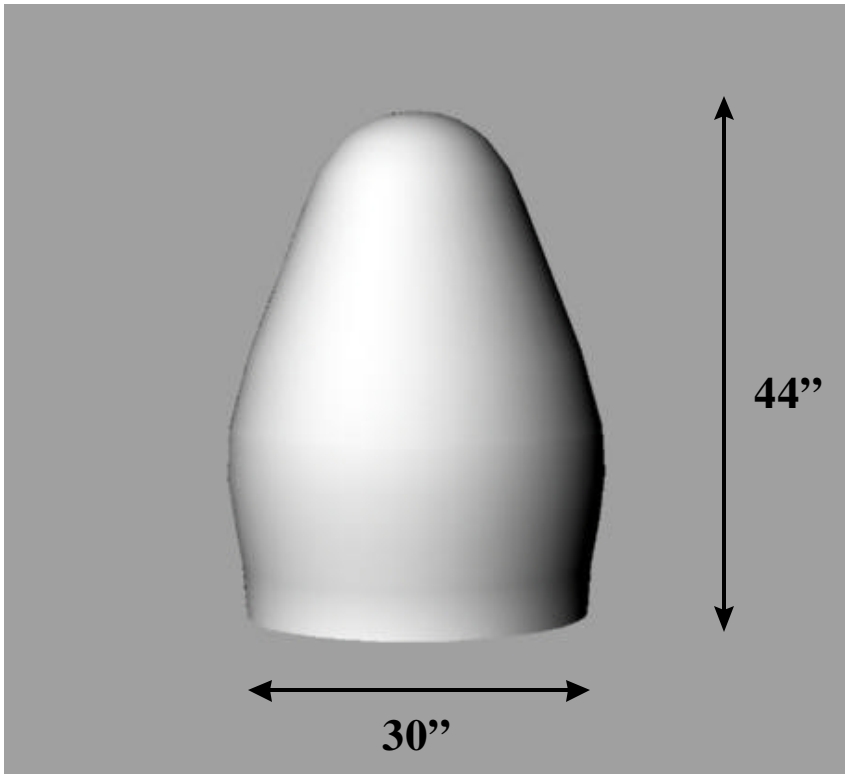


Figure 3.1.3-7 Engine Tailcone Model for FiberSIM Formability Simulation

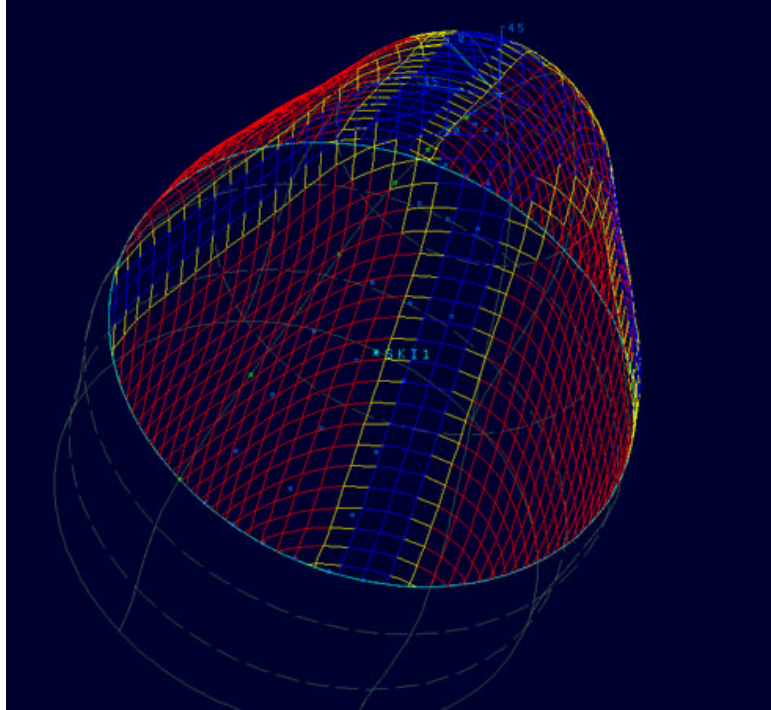


Figure 3.1.3-8 FiberSIM analysis output of generic tailcone geometry mapped with a single woven composite ply

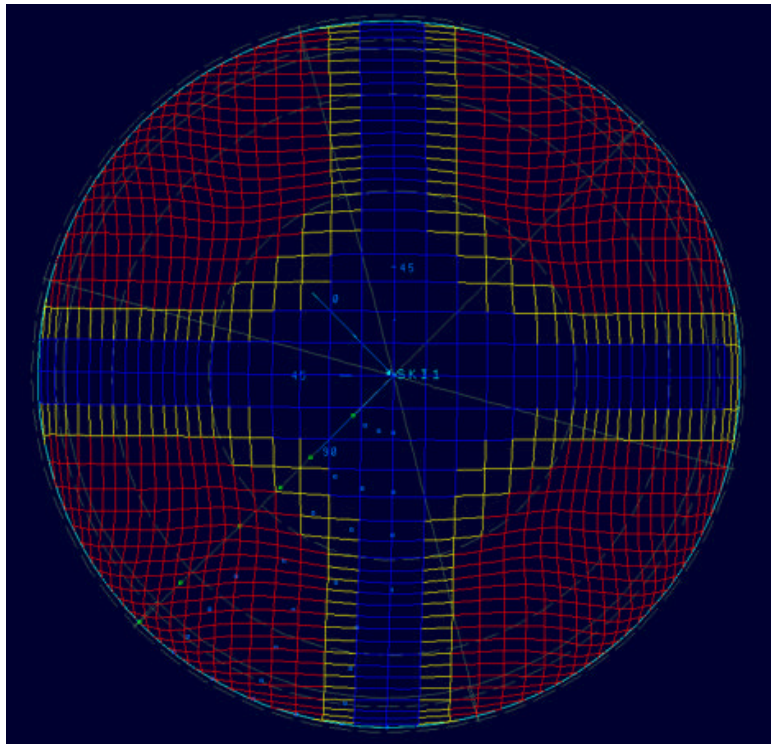


Figure 3.1.3-9 FiberSIM analysis output of plan view of deformation pattern of a generic weave draped over tail-cone geometry

Figure 3.1.3-10 displays a FiberSIM interply shear simulation using the proposed grid technique for a 0/90, + /- 45, 0/90 three ply stack up over the tool surface. The simulation was accomplished using the software features currently available in the code. The figure shows a top view of the overlapping flat patterns and their relative movement in going from the formed (3D) state back to a flat (2D) configuration. The white ply is the 0/90 prepreg, the blue the +-45 sheet. The colored lines connecting the shifted markers give an indication of the shear deformation (strain) in that particular area of the middle ply. The green markers indicate where the middle +-45 ply will be in tension and therefore should not wrinkle; the red markers indicate compression and a likely area for wrinkling to occur. The yellow indicate ply lateral movement over the tool where there may be minor problems. The rationale for the above interpretations is as follows. The behavior of the grid markers is dictated by the overriding constraint that the weave is inextensible in its main fiber directions i.e. the reinforcing fibers are not able to stretch along their length through the forming step. All in plane ply deformation is thus restricted to that accomplished by changing the angles between the warp and fill fibers, that is by shearing or trellising at the fiber crossover points.

Take for example the path of one marker point on the 0/90 ply (white) in Figure 3.1.3-10 (designated as 1) that is located 45 degrees off the 0/90 direction. During the forming step the shearing motion causes point 1 ply marker to shift through space to coincide with point 2 marker for the +-45 ply. The shear motion in this area subjects the +-45 ply sandwiched between the 0/90 plies to tension. The off angle trellising motion of the 0/90 ply gives rise to a state of compression in the primary

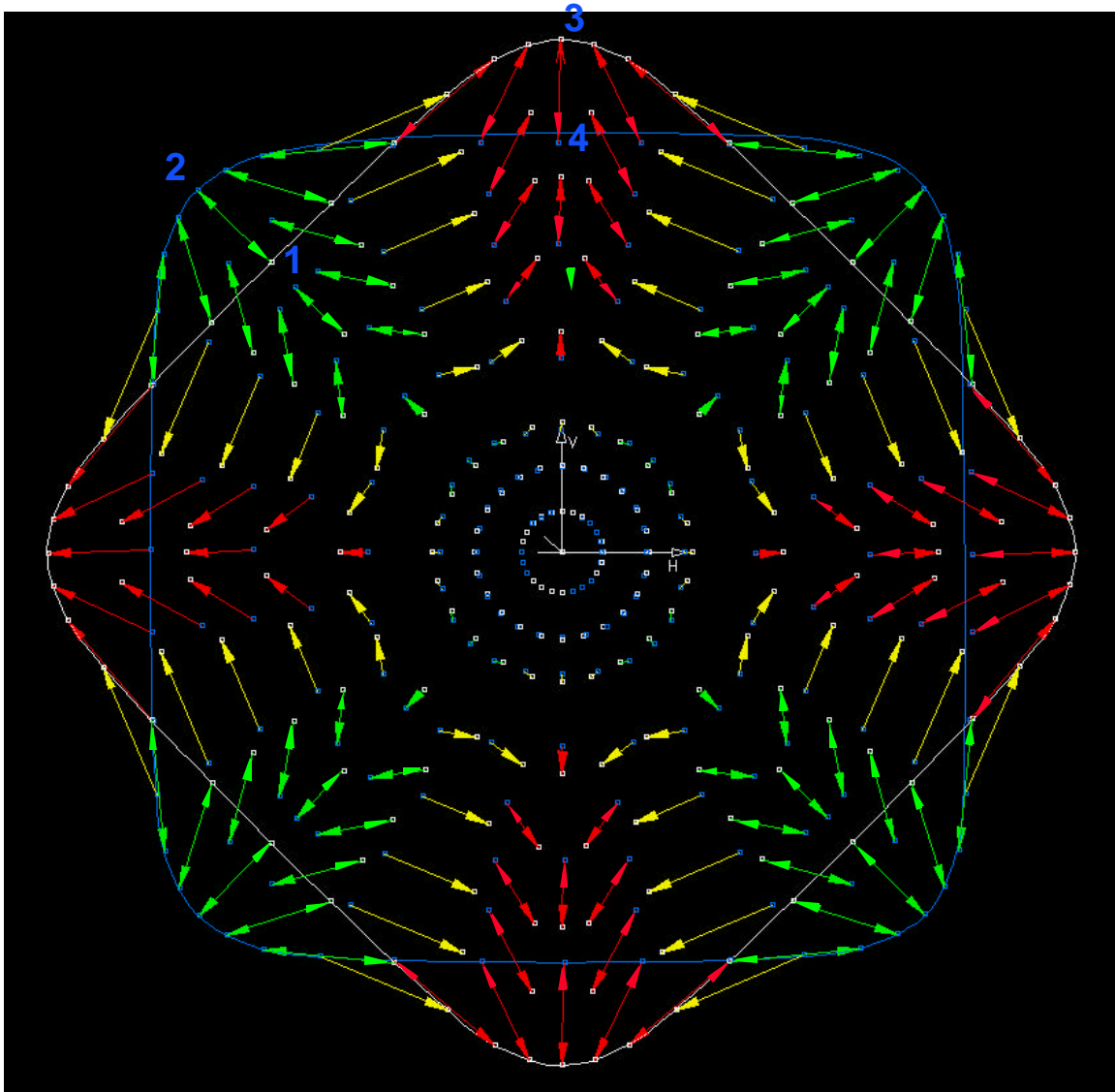


Figure 3.1.3-10 FiberSIM forming simulation for demonstration tailcone.

fiber directions. Marker 3 in Figure 3.1.3-10, which now must move to coincide with marker 4, indicates this type of motion. As the fibers cannot shrink under the compressive force, stress is reduced by out of plane ply wrinkling.

It should be emphasized that the above mapping simulation for composites forming in no way predicts the actual stress in the formed laminate layer. The simulation only provides geometric information about the forming process, i.e., how the plies and reinforcing fibers are oriented in the final part, how much shear strain the material experiences, and where each

material point lies on the tool surface. The simulation also assumes that the material can shear by any amount that is required to form the part. Experimental observations show, though, that defects arise when very large shear strains occur so measures of strain can be used to infer the likelihood of wrinkling or buckling. To make an accurate prediction of the formability of the structure, experimental measurements are needed of the shear properties of the woven prepreg to determine if the material can sustain the shear deformation indicated by the mapping simulation.

As suspected, the simulated shear deformations that are required in forming the tailcone are quite large indicating that this particular geometry and weave architecture is not a good candidate for LOM/Forming. The designer has a choice of modifying the geometry or utilizing a looser weave material (5 harness satin instead of 3 harness satin).

This new predictive capability serves as a key component of a LOM/Forming Design Methodology Procedure. This composites forming simulation combined with the LOM/Forming SFF capability should help to significantly reduce the time and cost associated with prototyping of composite structures such as CMC parts.

These initial positive results indicate that the formability simulation can be performed with the current analysis routines in the commercial version of the FiberSIM software. The operator, though, currently must do the series of analysis steps needed to perform the simulation, manually. Integrating the new composites formability simulation into the commercial FiberSIM software package as an automated feature has yet to be evaluated. CDT has indicated they first need a better idea of the size of the potential market for the new capability and/or the degree of interest of their current customer base before committing to incorporating such an automated feature into the existing code. In the future other simulation packages for composites manufacture that allow forming stresses to be determined (to complement the shear strain information provided by FiberSIM) needed to identified for LOM/Forming applications. PAMFORM by Engineering

Systems International (ESI, Inc.) is a code of particular interest. Recent developments to the PAMFORM code should be reviewed, and its suitability for inclusion in a LOM/Forming tool suite should be evaluated.

3.1.4. Design Methodology Validation

The purpose of this task was to validate the CAD/LOM design methodology by using the CCDP system to generate design descriptions of increasingly complex CMC subcomponent panels, then utilize the new LOM translator capability in CDDP to convert the data to the LOMNEF file format for eventual prototyping by the LOM system. The subcomponent design sequence is shown in Figure 3.1.4-1. This effort was performed in parallel with Task 1.2.3 LOM System Demonstration, the latter task that involved LOM fabrication of the Nextel™ 312/Blackglas™ 493AB subcomponent panels based on the LOMNEF file descriptions.

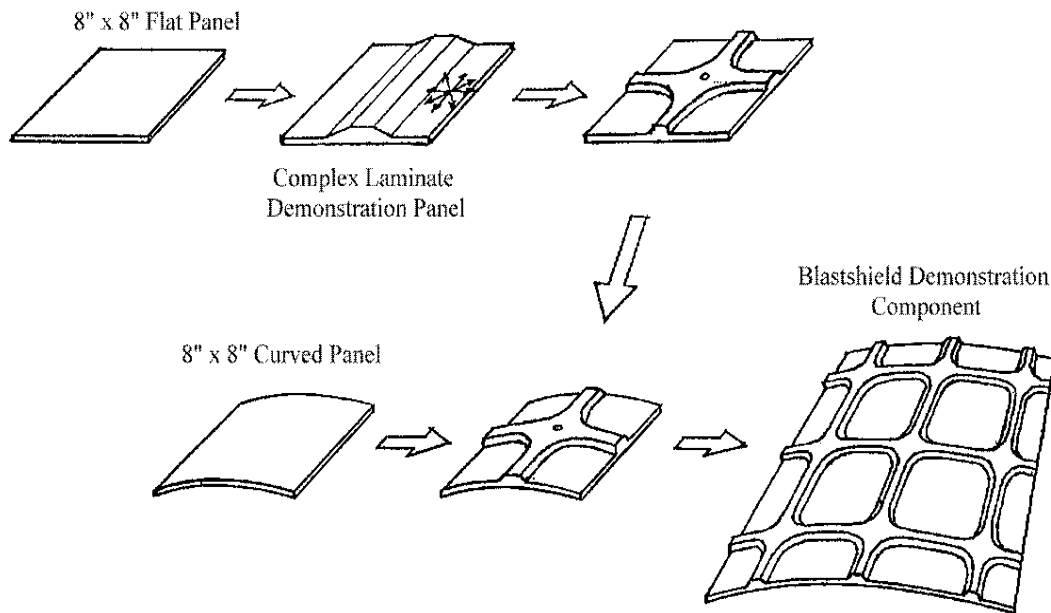


Figure 3.1.4-1 CMC Subcomponent Design Sequence

Figure 3.1.4-2 displays the series of subcomponent LOMNEF design data files generated by CCDP. The laminates were divided into 4"x 4" and 8"x 8" series of subelements consisting of 32 plies with 0°, 45°, 90° ply orientations. The parts increase in complexity from a flat panel, flat panel with cruciform stiffener, curved panel, and finally curved panel with cruciform stiffener. The ply build-up regions had a taper of 1/4" over a 16 ply build-up for the stiffener corresponded to two different crosshatch dimensions (0.1, 0.2 inches). Figure 3.1.4-3 displays the

sections and the radius of curvature for the curved panels was 7" with a surface rise of 0.29" above the XY plane. Two files were generated for each stiffened panel (flat and curved) that









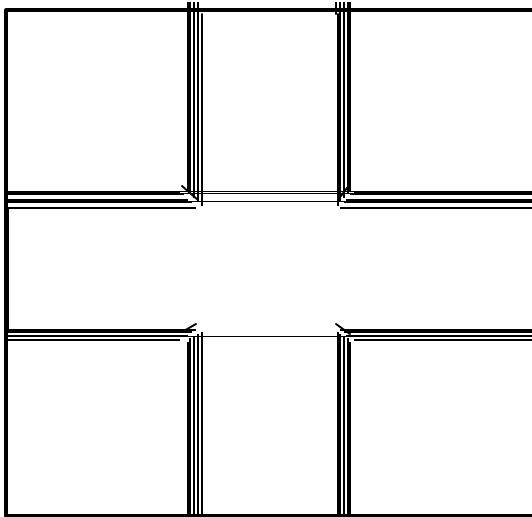
<u>Data File</u>	<u>Part Description</u> (32 ply, 0°,45°,90°)
• LOM_FLAT_SKIN	 4"x4" Flat Panel
• LOM_FLAT_HBAR_4x4 rev	 4"x4" Single Stiffener Panel; 0.2" Crosshatching
• LOM_FLAT_PLUS_4x4 rev	 4"x4" Cruciform Panel; 0.2" Crosshatching
• LOM_FLAT_PLUS_8x8 rev	 8"x8" Cruciform Panel; 0.2" Crosshatching
• LOM_FLAT_SKIN	 4"x4" Curved Panel
• LOM_FLAT_HBAR_4x4	 4"x4" Curved Panel w/ Stiffener; 0.2" Crosshatching
• LOM_FLAT_STFND_2	 4"x4" Curved Cruciform Panel; 0.5" Crosshatching
• LOM_FLAT_PLUS_8x8	 8"x8" Curved Cruciform Panel; 0.5" Crosshatching

Figure 3.1.4-2 CMC sub-component LOMNEF design data files

corresponded to two different crosshatch dimensions (0.1, 0.2 inches). Figure 3.1.4-3 displays the ply orientation sequence for the LOMNEF data file of the flat laminate with cruciform sub-element (LOM_FLAT_STFND_2). The LOMNEF design files were generated early in the program for processing on the Curved LOM system and hence contained both flat and curved panel descriptions. With the adoption of the LOM/Forming process in the program, only the flat panel design descriptions were needed for 2D laminate fabrication on the LOM system.

Data File Description:
 4"x4" Flat Cruciform Panel
 32 Plys; 0.2" Crosshatch



LOM_FLAT_STFND_2 CCDP

Ply Table

Ply #	θ	Ply #	θ
0	0	16	0
1	+45	17	+45
2	-45	18	-45
3	90	19	90
4	0	20	0
5	-45	21	-45
6	+45	22	+45
7	90	23	90
8	90	24	90
9	+45	25	+45
10	-45	26	-45
11	0	27	0
12	90	28	90
13	-45	29	-45
14	+45	30	+45
15	0	31	0

Balanced & Symmetric
 About Midplane

Figure 3.1.4-3 Ply Table for 4"x 4" Flat Cruciform Sub-element.

3.2 LOM/CMC PROCESS VALIDATION

3.2.1 Material System Development (Task 1.2.1):

The focus of this task was divided into two areas: (1) development of the prepreg properties for the NextelTM/BlackglasTM and COI oxide/oxide systems necessary to allow successful lamination of CMC prepreg in the LOM process and (2) development and evaluation of low cost LOM tooling materials suitable with the NextelTM/BlackglasTM processing requirements, i.e. cure T, time and vacuum forming pressure. To summarize the prepreg development efforts: versions of 493 BlackglasTM resin were used to make prepreg material, and the compressibility of these variants was evaluated. Fiber volume fractions in the range of 0.4 were generally attainable with all systems, though high viscosity prepregs (such as those made with 493C BlackglasTM) incurred a compressibility penalty when highly resin loaded. Because of its overall higher compressibility and its extended out-time properties the NextelTM312/BlackglasTM493A/B system became designated material for further process development activity. Evaluation of the NextelTM/BlackglasTM system was also expanded to include consideration of tack properties. BlackglasTM 489 (versions A, B and C) was also evaluated, both as a prepregging material and as a potential tackifier for the 493 variants. The material development study has also included a preliminary evaluation of an oxide-oxide prepreg material consisting of NextelTM 720 fibers and a proprietary sol-gel based matrix developed by Composite Optics Inc. The suitability of this material's characteristics for LOM processing was considered poor at the present time. The COI oxide/oxide system was thus not further evaluated in the program.

To summarize the LOM tooling material efforts: A tool modification technique involving the infusion of standard LOM paper parts with the TCC epoxy resin for improving the thermal capability of this material has been developed. The technique has been successfully scaled up to a larger part, and a practicable 'production-type' methodology has been developed.

Nextel™ 312/Blackglas™ Composite Prepreg Evaluation

One of the purposes of this sub-task is to determine the prepreg properties necessary to allow successful lamination of Nextel™ 312/Blackglas™ prepreg in the LOM process. The Blackglas™ resin system used in this program represents a distinct departure from the previous polymeric binders utilized for LOM. Previous prepregs or tapes developed for LOM (as part of an earlier DARPA funded program) were prepared from fiber impregnated thermoplastic polymers that have distinctively different processing characteristics than that of Blackglas™. These tapes are essentially solid, non-tacky flexible sheets that are sequentially laminated together in the LOM process by the application of heat and pressure. Each successive layer is bonded to the underlying stack by melting the plies together. Blackglas™ resin, though, is a thermosetting polymer system and as such is converted into a solid form by an irreversible time/temperature controlled polymerization or curing reaction. This resin system, therefore, adds new materials issues to be dealt with related to prepreg preparation, handling, and LOM processability.

There are basically 3 critical prepreg properties pertaining to LOM that must be first characterized and then optimized. These are tack, drape, and compressibility. Tack is defined as the tendency of a prepreg layer to adhere to a substrate or other prepreg layer. Drape is the tendency of the material to deform to a given desired geometry. Compressibility, as the term applies to composite lay-up, defines the force necessary to compact a prepreg to a required fiber volume fraction. While all three parameters affect the processing behavior of prepreg in the LOM process, the latter effectively determines the critical mechanical properties of the finished component. For this program, the overall goal was to develop a Nextel™312/Blackglas™ prepreg with a compressibility that will allow the material to be compacted to 40% - 50% fiber volume fraction using only the force that can be realistically generated on the current LOM test bed frame (< 100 psi).

In addition to the prepreg properties of tack, drape, and compressibility, the working time or “out time” of the material is also of critical concern. An increase in resin viscosity occurs as the Blackglas™ system cures that directly results in variations in prepreg tack, drape and compressibility over time. The study reported herein documents the variation in prepreg compressibility as a function of resin type, content, and degree of cure. Prepreg tack is also subjectively evaluated in relation to the above variables.

Two commercially available Blackglas™ 493 resin systems, Blackglas™ 493A/B and 493C, were evaluated for use in prepreg preparation. Each has advantages and disadvantages as a matrix phase in a prepreg suitable for LOM processing. Blackglas™ 493A is the basic polysiloxane monomer. Blackglas™ 493B is the monomer catalyst that is used to cure the 493A into a polymer. The 493A/B system is characterized by an initial low viscosity (~20 cp) and a long working time (> 20 h) and is typically utilized in Resin Transfer Molding (RTM) processing of Blackglas™ materials. Blackglas™ 493C is supplied as a mixture of 493A and an unspecified amount of 493B catalyst which is partially staged in roughly 45 - 65 weight percent iso-octane solvent. This system has been formulated specifically for use in Blackglas™ prepreg preparation. The solvent component of the resin gives the system an initial low viscosity (~ 80cp), which is desirable for the prepreg preparation process. As the solvent evaporates from the prepreg, the resin viscosity increases which imparts the desired degree of tack to the material.

It is well established that the fiber type, architecture, fiber sizing, fiber handling method, and the matrix resin properties affect the compressibility of a prepreg material. A number of studies have shown the extremely non-linear compaction behavior of composite prepreg materials, and a few satisfactory models have been developed. Results obtained in this study show behavior not previously reported for prepreg material.

Prepreg Ply Preparation.

The sample plies were prepared by first taping a single layer of Nextel™ 312 fabric to a thin aluminum base plate that was covered with a single layer of non-porous Teflon coated fabric. Mylar tape was used around the perimeter. Based on the fabric area and areal weight, the required amount of Blackglas™ material was weighed and mixed (if necessary). In the case of the low viscosity 493A/B system the resin was applied evenly onto the fabric using a syringe. With the 493C material the resin was applied more gradually and worked into the fabric by pushing it evenly over the surface using a 'squeegee' or similar tool.

Two separate batches of 493C resin were procured. The first (batch no. 22439) had a higher initial viscosity (15,000 cp) than the second (batch no. 22585; 80cp). The resin contents of the prepregs produced were selected to be reasonably representative of aerospace requirements. A 'standard' prepreg was defined as one consisting of 60% by volume of fibers and 40% resin. To make the prepreg, the required area of Nextel™ cloth was weighed and used to determine the total volume of fibers (density of Nextel™ 312 fibers is 2.69 g/cm³). This volume was then used to determine the required volume of resin, using the density of 493 resin. In the case of 493C resin, allowance was made for the fact that the isooctane solvent is lost from the system over about the first half-hour of exposure. In addition to the 'standard' prepreg other fiber content variations were made. A prepreg containing 5% less fibers by volume was made in order to investigate the effects of using excess resin in the system. This is referred to as the '-5%' material. Fiber rich prepregs were made to simulate the effects of using relatively dry prepreg. These are referred to as the '+5%' and '+10%' prepregs. Thus if these materials were consolidated to the point where all air but no resin was eliminated from the system, they would contain 30, 35, 40, and 45 % resin by volume. The '+10%' prepreg was not made from the higher initial viscosity batch of 493C resin.

Sample Cutting and Lamination

On the basis of previous compressibility studies on this and other fiber materials, it was expected that four plies of NextelTM material would yield a reasonable representation of compressibility behavior. Samples were prepared by cutting four plies from the prepreg sheet manufactured by the procedure given above. In the present study, a 3" x 3" area was selected for compressibility studies. A template having these exact dimensions was placed on the prepreg ply, and an Exacto-knife with a fresh blade was used to cut around the perimeter. Samples were laminated with the warp yarns facing up on all plies, and each ply was oriented in the same direction. After cutting, each ply still adhered to the Teflon fabric layer. Each ply was very carefully peeled off and placed on top of the ply stack. The stack was then placed on top of a 1 inch thick 4" x 4" block that had a central 3" x 3" grid marking for placement of the prepreg plies. This block was machined with parallel faces. A 3" x 3" block, also precisely machined for parallelism was placed on top of the plies and this entire assembly was then placed into an Instron electro mechanical test machine for compressibility determination.

Determination of Machine and Fixture Compliance.

It was extremely important to determine the compliance of the test set-up. Therefore, the compression blocks (4" x 4" and 3" x 3" described above were placed between the compression platens of an Instron test machine with a 20,000 lb. load cell. Calibration indicated an accuracy of better than $\pm 1\%$ in the range of loads of concern. The load/deflection curve for the test blocks alone was determined by applying 1,500 lbs. of load with a controlled deflection rate of 0.030 "/min. The zero position of the displacement transducer was also set at a contact load of 20 lbs. (or approximately 2.2 psi). The load/deflection data captured during this compliance test was fit to a 3rd order polynomial to allow for machine deflection at all values of load application on prepreg

material. It is important to note that the lower compression platen of the machine was gimbaled, thus alleviating non-parallelism concerns that would affect the compressibility results.

Compression Testing

The prepreg ply stack and compression blocks were placed between the compression plates of the Instron Mechanical test machine. A slight contact pressure of about 1 psi was applied before the compression tests were initiated at a controlled deflection rate of 0.030” per minute. Load deflection data were captured, and with knowledge of the fiber areal weights, total fabric area, and fiber density, the required plots of fiber volume fraction versus applied pressure were obtained.

Results and Discussion

493C Resin -Batch No. 22585 - Low Initial Viscosity

This batch of 493C resin had a much lower initial viscosity than the other batch. It therefore exhibited a much higher level of compressibility and a longer ‘working life’. Standard, +5%, +10% and -5% prepregs were made from this batch of material. Each of these prepregs was aged for different time periods in air at room temperature. On the basis of an initial rheometry scan it was decided to age the materials for 3, 6, 12 and 24 hours. These aging times were selected to achieve an approximate doubling of resin viscosity in each time period. In all cases the prepreg was cut into 3” x 3” plies and exposed to room temperature before being laminated. Two samples of each prepreg were tested after each aging treatment. The repeat test was, in all cases, carried out within 5 minutes of the first.

The consolidation behavior of the somewhat resin rich ‘-5%’ prepreg material over time is shown in Figure 3.2.1-1. Predictably, the highest overall compressibility is seen with the fresh or ‘0 Hours’ aging. This is a prepreg material with consolidation behavior that would be expected to

be dominated by the resin. In the 'fresh' condition the resin viscosity is very low (~80 cp). Therefore, since a relatively small pressure is required to cause this resin to flow out of the system, the observed compressibility is seen to be more representative of that normally associated with dry fibers. As the prepreg is progressively aged and the viscosity rises, the pressure required to force the resin out of the system also rises, and the overall compressibility of the material is proportionately reduced.

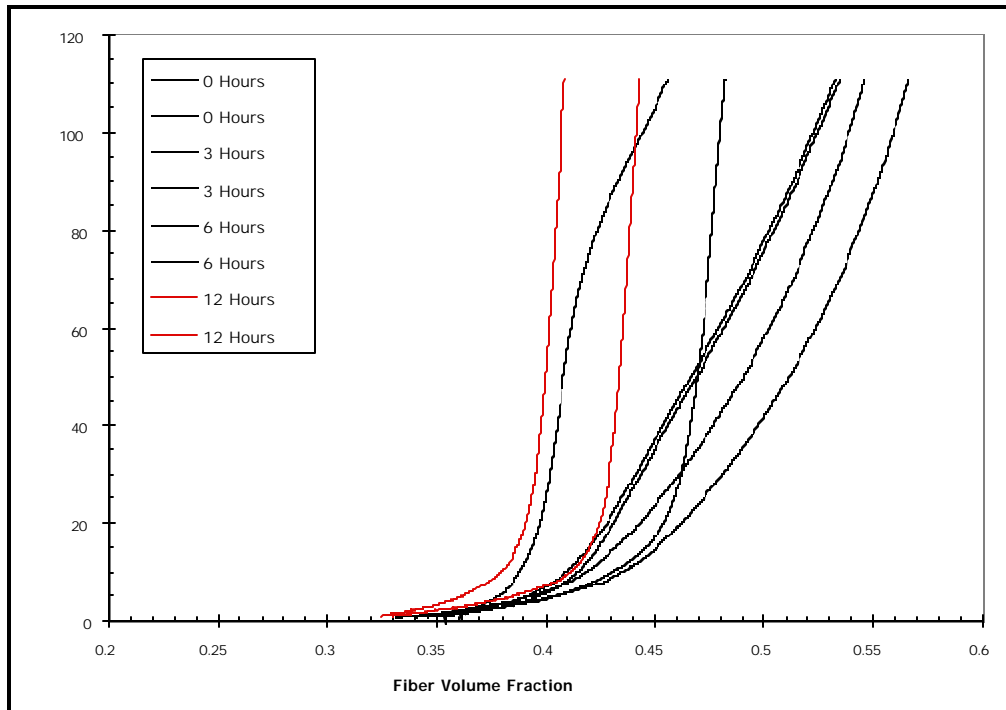


Figure 3.2.1-1 Effect of Aging at Room Temperature on the Compressibility of '-5%' Prepreg

There are two other features in Figure 3.2.1-1 that are worthy of note. There is a great disparity, in most cases, between the compressibility of samples taken from the same prepreg sheet. For instance, the material aged for 6 hours could require anything from 10 to 60 psi to consolidate to 40% fiber volume fraction, depending on which of the sample curves is used for reference. This broad variation in behavior for similar samples is exhibited by all prepreps except, as shown subsequently, by the most fiber rich. This suggests that the variation is due to non-uniformity in resin content over the area of a prepreg layer and is not surprising, given the

fabrication technique employed. It is easily conceivable that, especially in the case of the resin rich prepregs, resin content on the surface of the fabric could vary substantially. This is less of a problem when the viscosity is low, as the resin can be easily squeezed out. But as the viscosity climbs, the impact on consolidation behavior accruing from variation in resin content becomes more significant. The second important point raised by the data in Figure 3.2.1-1 is that the shape of the consolidation curve can vary greatly. The data for 0 hours is very typical of that associated with elastic fiber deformation. However, one of the 6-hour samples shows an s-shape that has not been noted in previously published data. Some suggestion of this type of behavior is present in the 3-hour data and is also seen in data for other resin content prepregs.

The s-shaped behavior described above can be explained in a number of ways. It is very likely that, as the resin viscosity increases and approaches that of gelation, the force necessary to eliminate the resin increases proportionately. One definition of gelation is that it is a process by which a fluid develops the ability to bear a shear stress. One of the 6-hour curves shows a distinctive yield type behavior. This may be the point at which the critical shear stress necessary to cause flow is exceeded. Assuming that the resin in each of the aged prepregs could be induced to flow further by increased pressure application, it is possible that the 12-hour data would exhibit the same s-shape if extended to higher values of applied stress. The s-shaped feature in compressibility data will be a topic of further investigation.

The consolidation behavior of the 'standard' prepreg is shown in Figure 3.2.1-2. This data and that plotted for the '+5%' prepreg in Figure 3.2.1-3 shows consolidation behavior not previously reported. These two prepregs appear to become more compressible at lower pressures as the aging treatment progresses. This is counter to the proposition that resin viscosity increase leads to a reduction in the compressibility. The mechanisms most likely to explain this behavior are chemical/physical shrinkage or redistribution of the resin over time. While the degree of

shrinkage occurring as a result of early gelation has not been established it is not believed likely to be of a sufficient magnitude to explain the relatively large differences in compressibility noted. Therefore a redistribution of resin is thought to be the most likely mechanism.

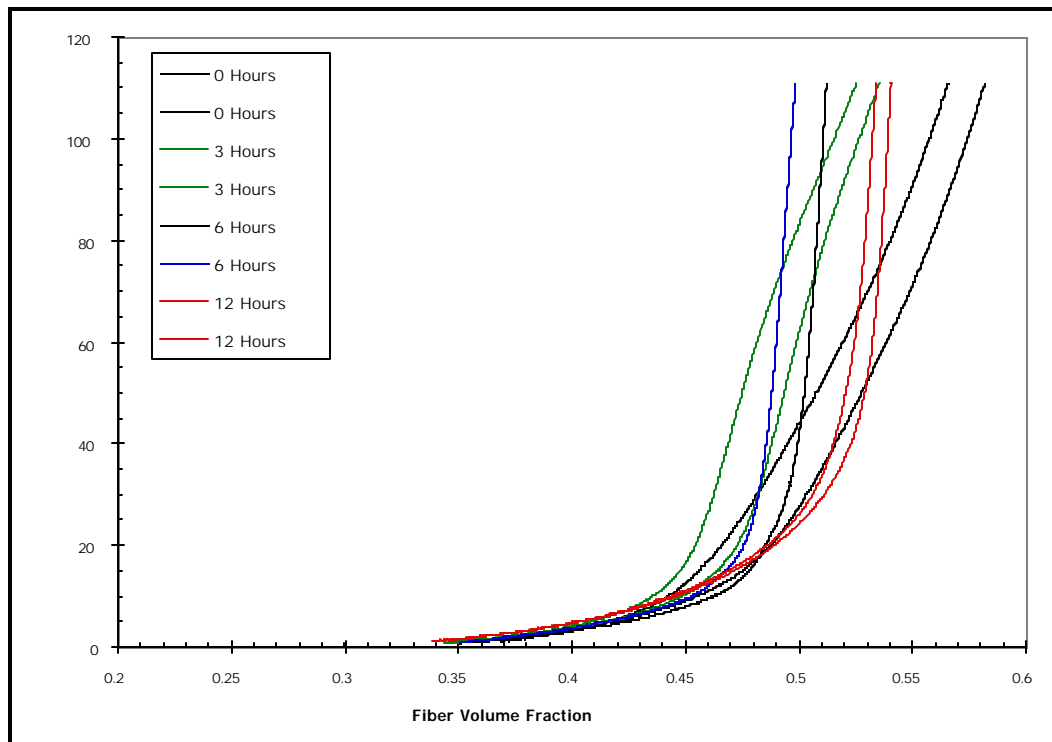


Figure 3.2.1-2 Effect of Aging at Room Temperature on the Compressibility of 'Standard' Prepreg

Nextel™ fibers and Blackglas™ pre-ceramic polymer resin have similar and relatively low surface energies. This condition is not the most favorable for surface tension driven wetting, which would be the predominant mechanism present in the prepregging operation employed. It is likely that the resin quickly permeates the inter-tow regions, but much more slowly enters the tows themselves. Therefore as the aging treatment progresses the surface resin, that was thought to strongly influence the low-pressure consolidation in the resin rich prepreg, can now be almost completely absorbed by the tows over time in the more resin poor materials. Subjectively there is a distinct difference in the observed wetting behavior exhibited by 493A/B and 493C systems. Though wetting studies have not been carried out, it appears that the 493 A/B system wets the

Boron Nitride coated fibers more readily than 493C. 493C was developed specifically for prepregging. The addition of the iso-octane was intended to both reduce viscosity and increase wetting. However, the solvent is lost from the system as the prepregging operation proceeds. Therefore it is possible that the wetting characteristics change as the prepreg is being made. This may also partially explain the variability in compressibility that is a particular feature of the 493C resin. It certainly suggests that time varying resin distribution is a reasonable mechanism that might explain the anomalous changes in compressibility over time. It can then be argued that higher pressures will be necessary to eliminate the resin from the system, since flow channels within the tow are much smaller than those between the tows. This lends credibility to our argument that the s-shape seen on the 3-hour data and to a lesser extent in the six-hour test would be present at very high pressures after 12 hours of aging. Figure 3.2.1-3 also shows the time dependent increase in compressibility seen with the 'standard prepreg, and again there is significant variation in compressibility for similar prepreps.

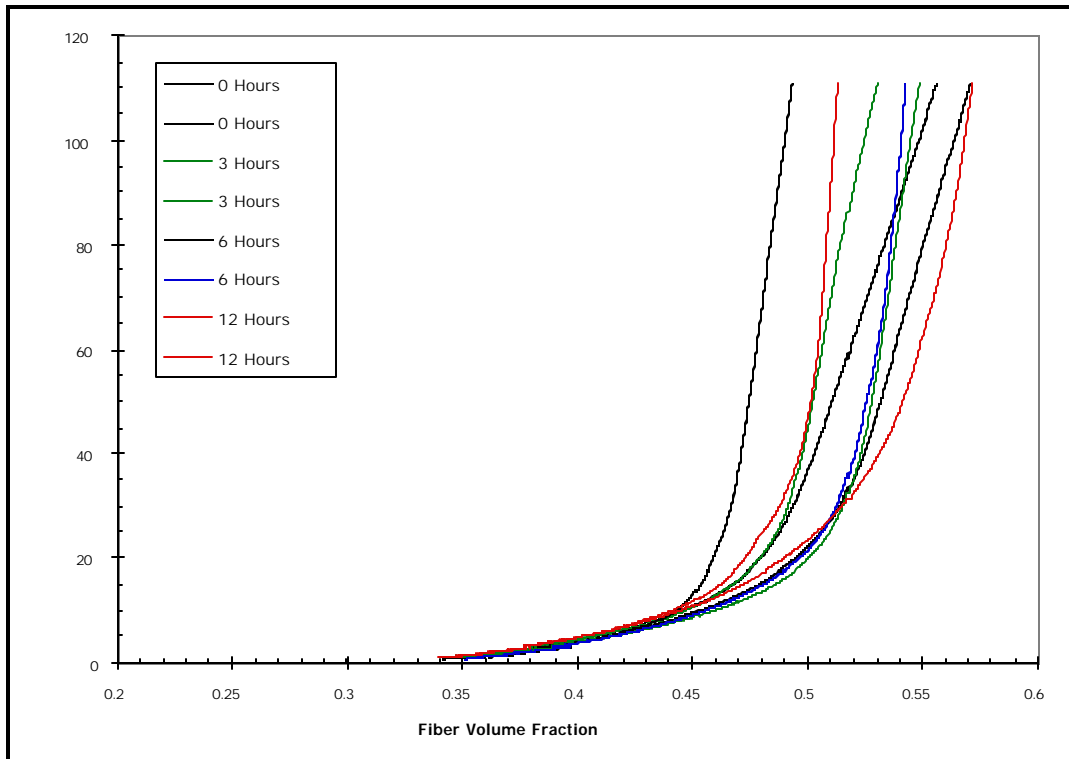


Figure 3.2.1-3 Effect of Aging at Room Temperature on the Compressibility of '+5%' Prepreg

The data for the most 'resin poor' prepreg are shown in Figure 3.2.1-4. Previous contentions that compressibility behavior is strongly influenced by the resin properties are borne out by this data. The variation shown between samples is less, for instance, than that seen in the 3-hour data of the '-5%' prepreg, and is similar to that shown for all prepregs that were tested when fresh. The major difference between the '+10%' prepreg and the fresh material is in the final slopes. At lower consolidation pressures there is little difference in behavior. At higher pressures the data suggests that the fresh materials will reach higher fiber volume fractions than the dry prepreg. This may indicate that the resin in the 'dry' materials does not influence the compressibility substantially until a fiber volume fraction of about 0.52 is reached. This high level of compressibility at low pressures is obviously very desirable in the LOM process. However these dry prepregs have a low level of tack, based on subjective observations. This problem may be alleviated by the use of a prepreg tackifier, and thus the high level of compressibility may be combined with acceptable lay-up properties.

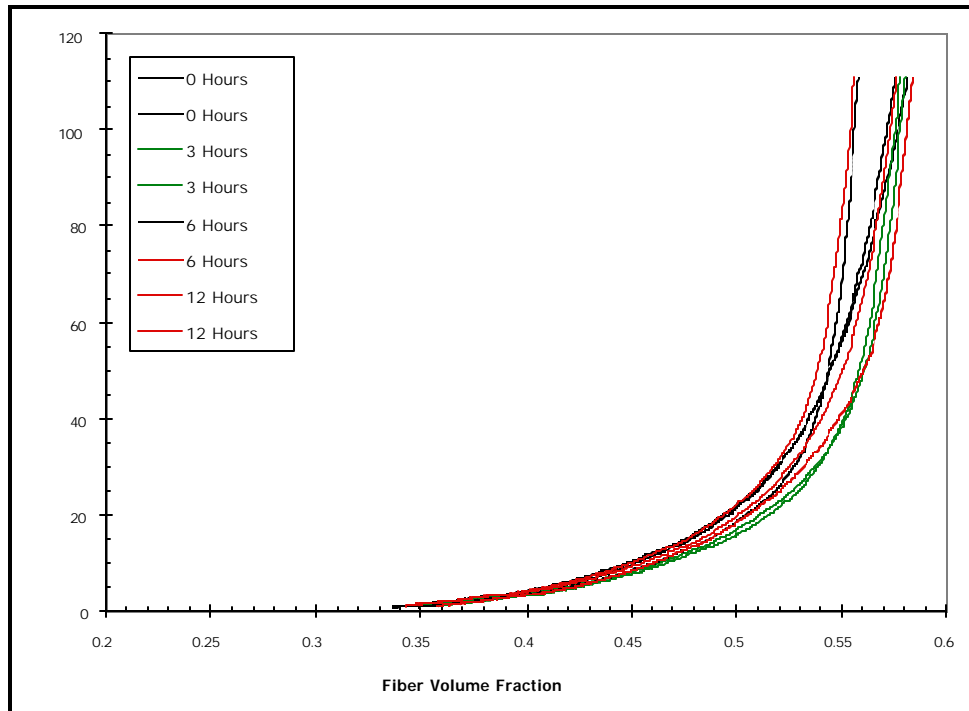


Figure 3.2.1-4 Effect of Aging at Room Temperature on the Compressibility of '+10%' Prepreg

In summary, resin content is shown to have a strong effect on compressibility. Aging in air at room temperature generally reduces compressibility, though a redistribution of resin may be attributable to an observed disturbance in this trend. Preliminary results suggest the 'standard' and '+5%' 493C prepregs that are aged for 6 to 12 hours seem the most practicable for the LOM process, exhibiting the best apparent combination of compressibility and tack.

A tackifier used in the Northrop Grumman LC³ Program for CMC processing will be initially evaluated for this application. Subjectively, the 'standard' and '+5%' aged for either 6 or 12 hours showed the higher level of tack and were thought to be practicable forms, if the tackifier proves to have no unwanted effects on the material properties after pyrolysis. This observation will be tested when the tack test has been perfected for these materials.

493C Resin - Batch No. 22439 - High Initial Viscosity

Standard, +5% and -5% prepregs were made from the batch of 493C resin that had a relatively high initial viscosity. The effect of resin content on the compressibility of the prepreg as

a function of fiber volume fraction is shown in Figure 3.2.1-5. These materials show a much lower level of compressibility than that observed for Batch No. 22585. Following arguments developed above, this is attributable to the resin dominated behavior of the prepreg. From the point of view of LOM application, this material holds little promise, as even the resin poor version of the prepreg cannot be practicably consolidated much beyond 45% fiber volume. This fresh prepreg behaves, therefore, like the low viscosity resin prepreg that had been aged for approximately three hours. Also, the consequences of including excess resin in the prepreg appear serious in this case. The resin rich ‘+5%’ formulation has an extremely low level of compressibility, and is certainly not suitable for LOM application.

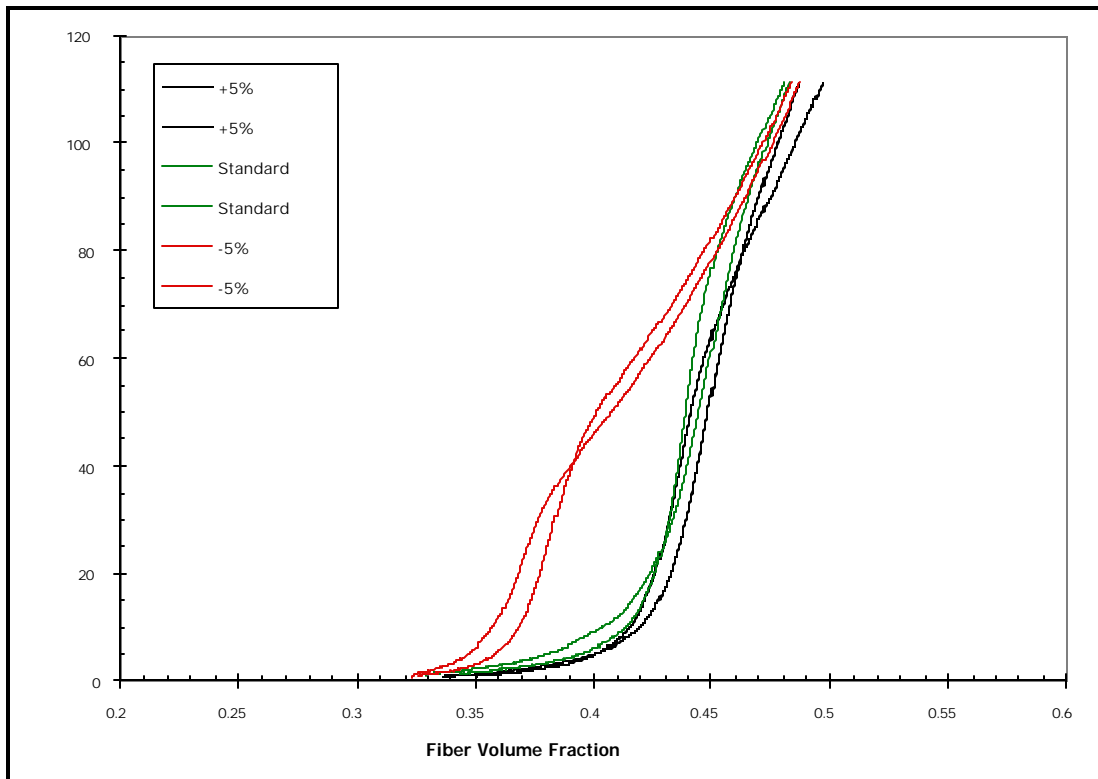


Figure 3.2.1-5 Effect of Resin Content on Compressibility of Fresh High Initial Viscosity Prepreg (Batch No. 22439)

Prepreg samples were also aged in air at room temperature for 8 hours. The results for the ‘standard’ and ‘-5%’ prepregs are shown in Figures 3.2.1-6 and 3.2.1-7, respectively. The compressibility is shown to be further reduced by the aging treatments. In general these materials

exhibited an acceptable level of tack, but from the point of view of LOM application, they require impractical, high consolidation pressures.

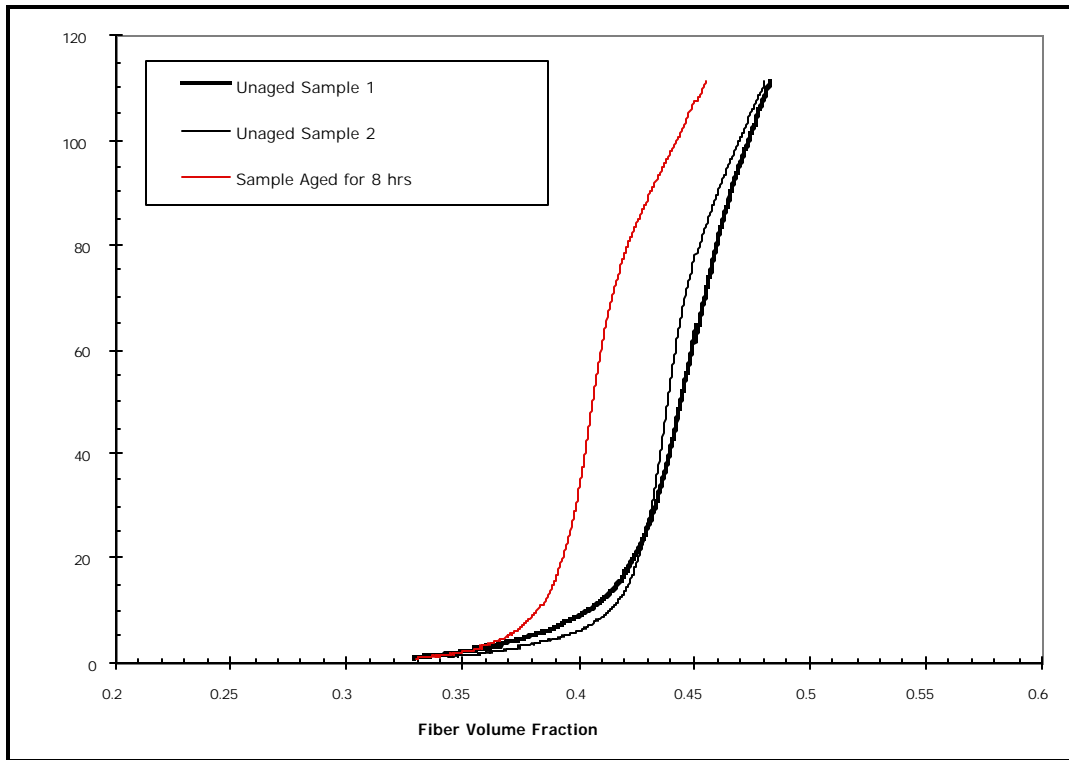


Figure 3.2.1-6 Effect of Aging on the Compressibility 'Standard' 493C High Initial Viscosity Resin (Batch No. 22439)

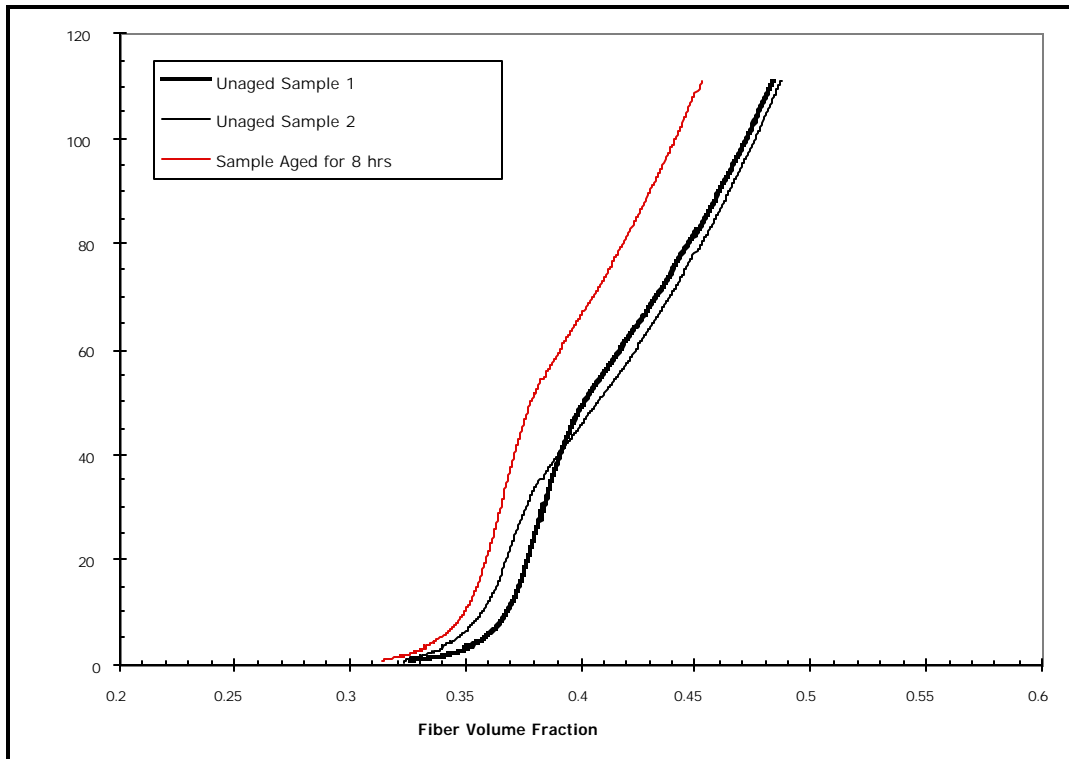


Figure 3.2.1-7 Effect of Aging on the Compressibility '-5%' 493C High Initial Viscosity Resin Batch No. 22439)

493A/B Resin Prepregs

A 493A/B resin was prepared for prepregging by mixing 100 parts by weight of 493A with 2 parts of 493B. This system has a very low viscosity that was maintained over a very long period of time (more than a day). Again prepregs were prepared corresponding to the -5%, standard, and +5% materials. The viscosity of this resin was similar to that of the low viscosity 493C material. The 3 different resin content materials were compression tested in the 'fresh' condition and after 20 hours of aging in air at room temperature.

The effect of resin content on compressibility is shown in Figure 3.2.1-8 and appears negligible. Interestingly, the range of pressures required to achieve 50% fiber volume is, in this case, much lower than for the corresponding prepregs made from the 493C Batch 22585, which has a similar initial viscosity. In addition, the variability in compressibility for the 493A/B resin is remarkably small. The lower variability in the data suggests a smaller influence of the 493A/B

resin. On the other hand, the somewhat higher levels of compressibility noted with some forms of the 493C system suggest that this system may be less influenced by the resin under certain circumstances. These slight variations might be explained by differences in initial resin distributions. Perhaps the 493A/B resin more quickly and consistently achieve a uniform distribution than the 493C. This and many other features of the material behavior require further investigation.

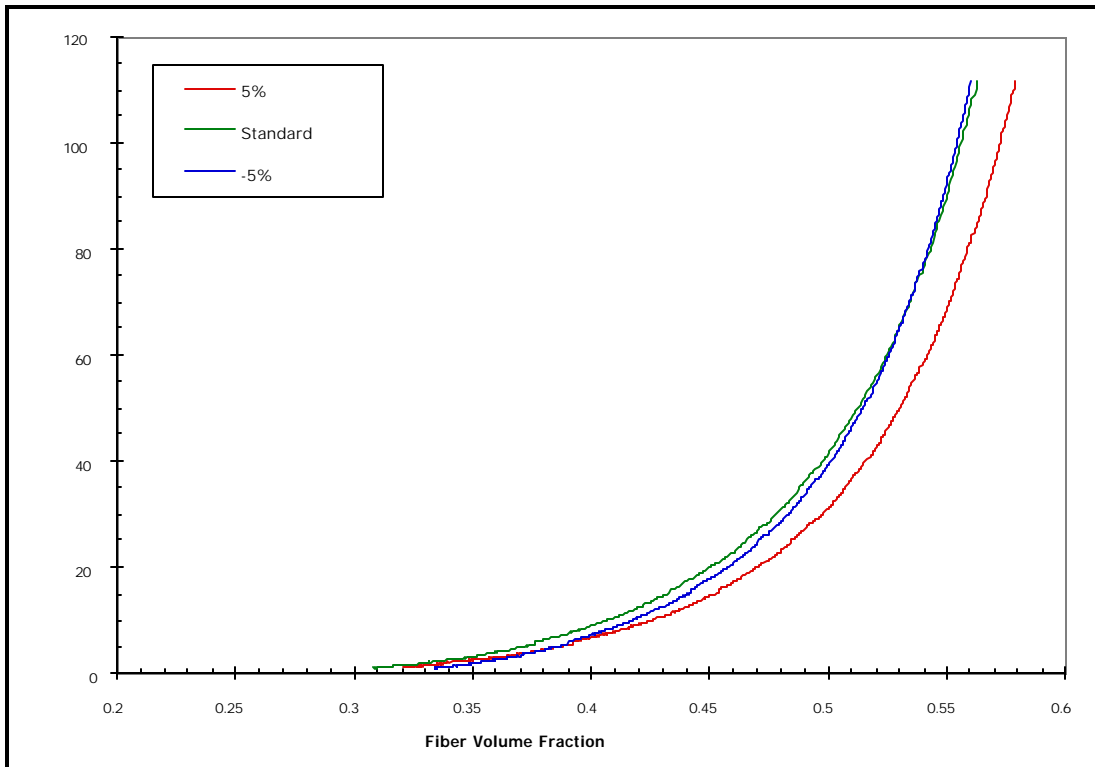


Figure 3.2.1-8 Effect of Resin Content on the Compressibility of 493A/B Prepreg

The effect of 20 hours of aging at room temperature on the compressibility of the various resin content prepreps is shown in Figures 3.2.1-9 through -11. Again the data is extraordinarily free of variation. Aging for this amount of time has no effect on the compressibility of the 493A/B system. On the basis of preliminary rheological testing, little, if any, increase in resin viscosity would be expected in this time period.

The 493A/B samples were not found to have any appreciable degree of tack, though this is once again a subjective statement. Compressibility is satisfactory though on the basis of a comparison between the 493 A/B data and the '+10%' 493C prepreg, the resin does exert an influence on compaction for the range of fiber volumes investigated. The combined properties of high and uniform compressibility behavior (both from sample to sample and over extended aging times) make the 493A/B system very attractive for LOM processing.

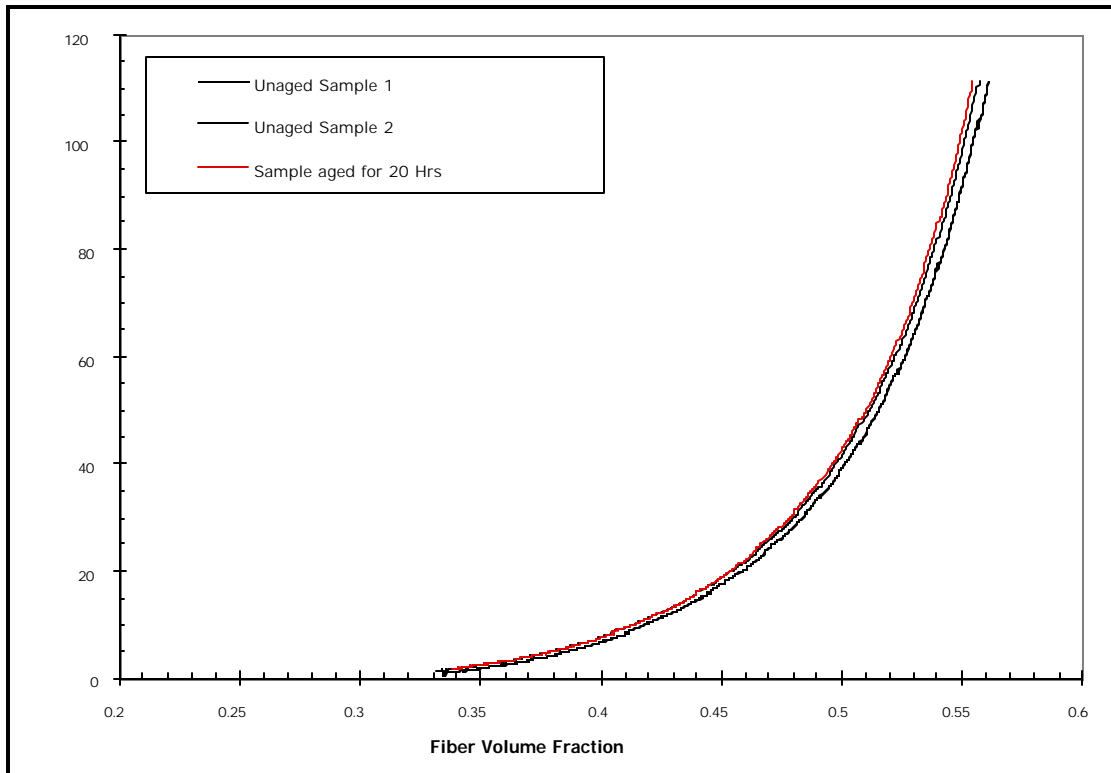


Figure 3.2.1-9 Effect of Aging on Compressibility of -5% 493A/B Resin Prepreg

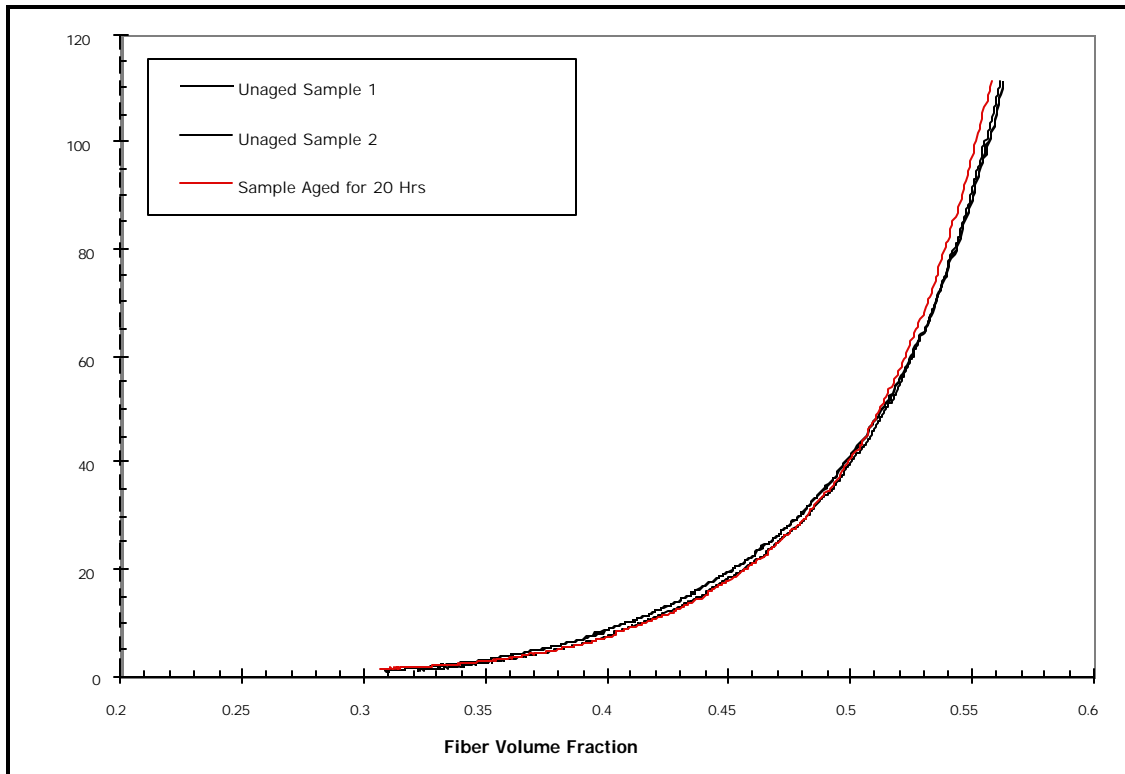


Figure 3.2.1-10 Effect of Aging on Compressibility of Standard 493A/B Resin Prepreg

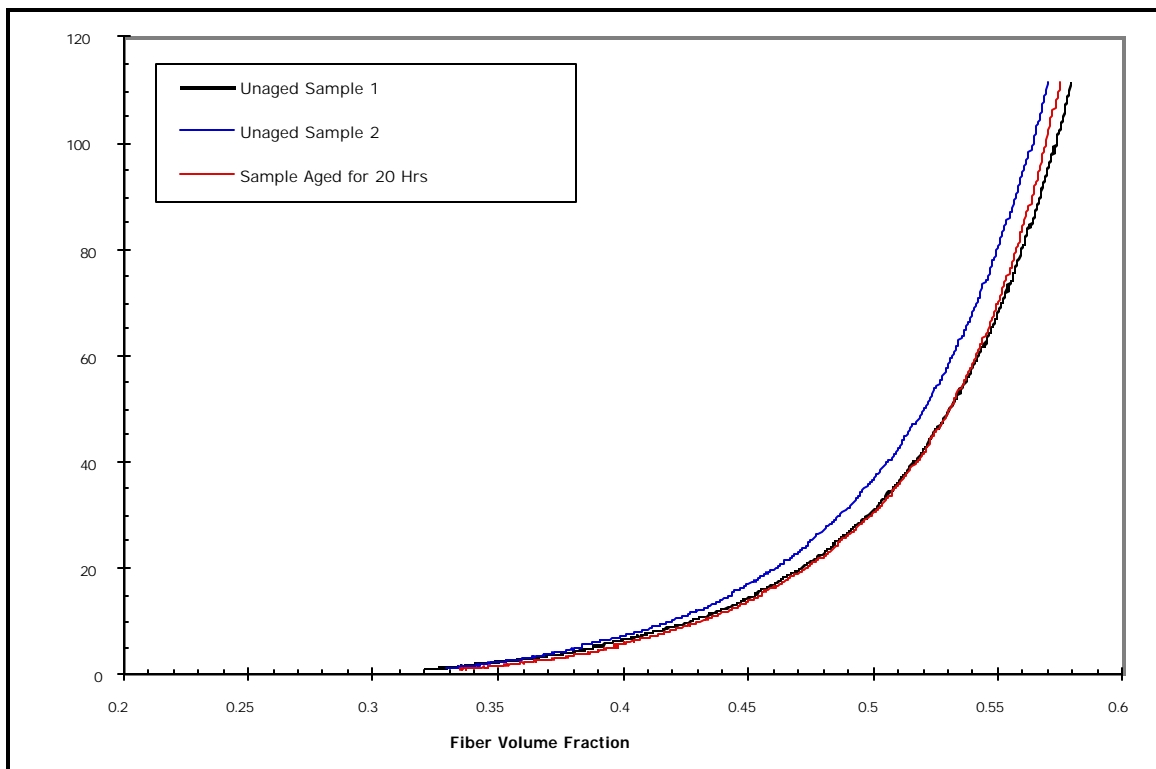


Figure 3.2.1-11 Effect of Aging on the Compressibility of +5% 493A/B Resin Prepreg

Tack Property Evaluation

Preliminary observations have shown that the use of a tackifier will be beneficial in the LOM process. The effects of the use of a tackifier on the compressibility of prepreg material must be investigated.

The configuration of the LOM process when applied to Ceramic Matrix Composites will, of course, depend greatly on the properties of the prepreg. Compressibility will determine the extent to which the material compacts under pressure, and thus will have implications for the machine load application mechanism, and also the attainable properties of the finished part. In the previous report it was shown that with the facility to apply 20-25 psi to the laminate during lay-up, Blackglas™ 493 resins could reach 40-45% fiber volume fraction. This is important in determination of the ply locations during lay-up, but does not entirely dictate the final fiber volume fraction. Load application during cure will have at least as important an effect on component thickness. However, in order that the physics of consolidation be fully understood it is critical that the fiber/resin compaction state be completely characterized throughout the part production cycle. In this way the inevitable fiber volume non-linearities induced in the through-thickness direction by successive lamination pressure applications can be accounted for and minimized/eliminated in optimized cure and pyrolysis operations.

While fiber volume fraction has a large effect on the properties of the final part, the tack properties of the prepreg material will determine, to a significant degree, the material handling requirements of the LOM process. Mechanisms that hold, transport, laminate, and pressurize the prepreg layers will have to be designed with the tack properties of the material in mind. The versions of 493 Blackglas™ assessed in the previous reporting period had very low tack. This creates concern over movement of the laminated material during ply deposition. Room

temperature aging of the material, while effecting some slight improvement in adhesion between plies, did not yield a material with suitable tack properties. Hence the expedient of in-process application of tackifier became relevant. The effects of tackifier loading on both compressibility and final part properties were therefore determined. For similar reasons the oxide-oxide system was tested. These prepreg materials supplied had higher tack, and in view of higher potential final application temperatures were considered an appropriate candidate for LOM of CMC.

For process development purposes prepreg materials have been made at Northrop Grumman and shipped to UDRI for LOM testing. In the fresh condition the BlackglasTM 493 matrix resins have low viscosity. The storage practice adopted in the program is the standard for the aerospace industry, in which prepreg is placed in 0°F freezers when not in use. Out time is carefully logged so that material changes occurring due to room temperature exposure can be determined. Freezer life is not unlimited, however, as curing reactions will proceed, at a retarded rate, even at such low temperatures. This is of concern for the BlackglasTM prepregs, as well as the effects of resin redistribution. In Status Report No. 1 resin movement over time was proposed as a possible mechanism by which some surprising increases in compressibility occurred during ambient temperature aging of the 493C system. In view of the fact that a distinct physical change is not seen to occur in the 493C resins when placed in 0°F storage (viscosity remains relatively low) the compressibility of the 493A/B prepreg after 4 months was determined. Results, given in the next section, suggest that some redistribution of resin occurs, yielding an overall higher level of compressibility.

Changes in compressibility and tack that occur over time are usually attributable to either resin distribution or rheology. A number of tests were carried out in an effort to characterize these changes. Techniques included dynamic mechanical analysis and differential scanning

calorimetry. Results show that compressibility can be related to resin rheology, but subjective evaluations of tack have not correlated with thermal or rheological data.

Finally, based on compressibility and preliminary tack property results for the various prepreg variations studied, a tentative LOM processing sequence has been formulated for the NextelTM/BlackglasTM material system. BlackglasTM 493A/B resin will be utilized for prepreg used in LOM processing due to its high and uniform compressibility and extended out-time behavior. The initial low tack of the 493A/B prepreg will also be beneficial in automating the backing sheet removal/ply sheet feeder mechanism on the LOM unit. An automated spray system on the LOM unit will be developed to deposit suitable tackifier on the surface of each ply after placement on the build platform to ensure sufficient tack for subsequent lamination of the next ply. Once all ply layers have been laminated, the part will next be cured on the LOM Forming system using the standard BlackglasTM 493A/B temperature/pressure schedule.

Compressibility Testing of BlackglasTM Prepreg Materials

BlackglasTM 493 prepreg materials were shown to have adequate compressibility to achieve satisfactory fiber volume fractions in the LOM process. However neither 493 A/B nor 493C possessed sufficient tack properties that would prevent movement of plies relative to each other during lamination. Therefore some effort was devoted to selecting a 'tackifier' that could be dispensed during lamination to hold the plies in place. As this introduced a third material into the lamination process it was necessary to characterize its effects on compressibility. Techniweave Inc. had specially developed an epoxy-based tackifier for this purpose as part of the DARPA LC³ program. This tackifier was developed in that program to hold complex geometry plies together in a preform shape before resin infiltration. The Techniweave tackifier was shown to function very well with the BlackglasTM 493/ NextelTM 312 material system with no degradation in final CMC

mechanical properties. Samples of Blackglas™ 489 material (A/B/C/D resins) were also obtained, along with some 489C/ Nextel™ prepreg, from another program. Blackglas™ 489 is an earlier formulation of the Blackglas™ preceramic polymer system than the 493 version. Both the 489 and 493 versions are processed in the same manner and produce final CMC materials with the same mechanical properties. The advantage of the 493 system is its much lower cost than the 489 version. As prepregs made from Blackglas™ 489C exhibit a much higher level of tack than 493C versions, it was decided to include it in the investigation in order to gain some insights into tack development in Blackglas™ systems. It was also thought desirable to use tackifiers based on this system, as it would possess similar chemistry to the matrix resin.

Compression testing was carried out exactly as described for the earlier Blackglas™ 493 A/B and C compressibility tests. To evaluate the effects of tackifiers on compressibility, four ply laminates were made from 493 A/B prepreg (previously designated +5% prepreg) in which different amounts of tackifier were sprayed on each layer. Samples were tested within a few minutes of lay-up. The results are shown in Figures 3.2.1-12 and 3.2.1-13. Both the 489 and Techniweave tackifiers have similar effects on compressibility. While compressibility above 50% fiber volume is affected, even the relatively heavy loading of resin represented by a 5 second spray does not reduce compressibility to a significant degree in the region of interest in this program. In hand lay-up lamination experiments, a 1 to 2 second spray of the epoxy tackifier was shown to provide satisfactory tack, so on the basis of these measurements it can be assumed that tackifier application does not have an important effect on compressibility.

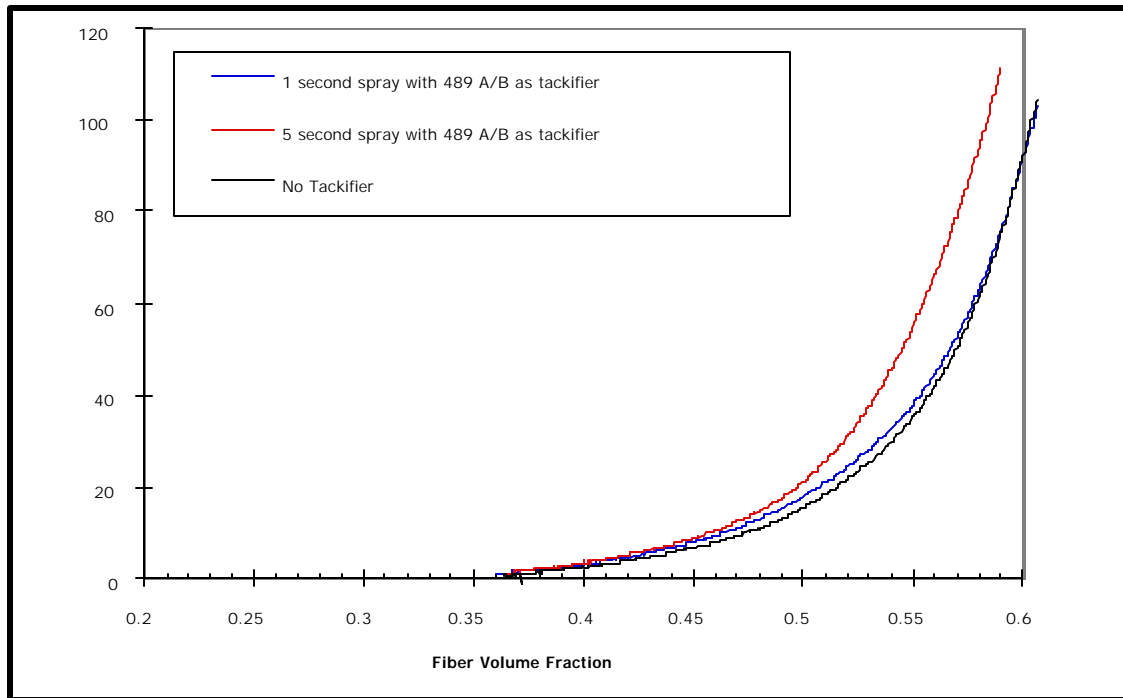


Figure 3.2.1-12 Effect of Application of 489 as a Tackifier on the Compressibility of 493A/B Prepreg

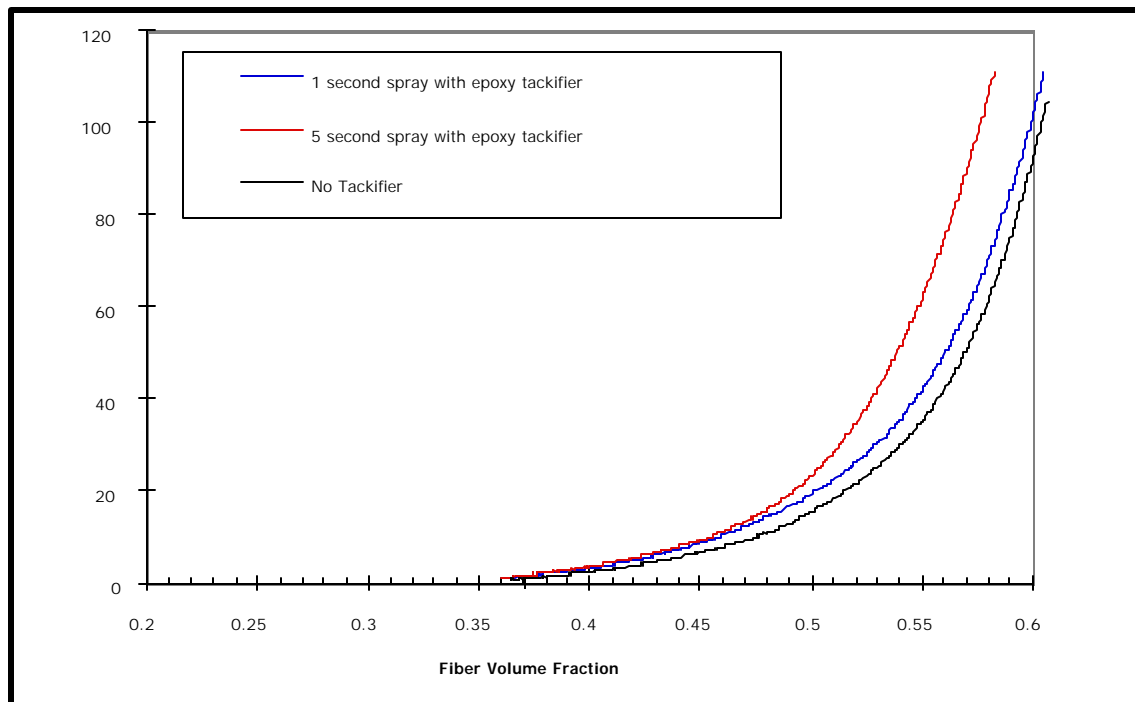


Figure 3.2.1-13 Effect of Application of Epoxy Tackifier on the Compressibility of 493A/B Prepreg.

The results shown in Figures 3.2.1-12 and 3.2.1-13 have a common baseline curve that was determined using the slightly fiber rich (+5%) 493 A/B prepreg. This material had been

stored at 0°F for four months. This baseline curve is plotted again for comparison in Figure 3.2.1-14 where the data for the various 493 A/B prepregs in the ‘fresh’ condition are also given. A significant increase in compressibility has occurred over this time period, to the point where the compaction behavior is virtually identical to that exhibited by the dry fibers. This strongly suggests that the matrix resin has been redistributed or even lost from the prepreg onto the backing material. If it can be shown that the prepreg has retained enough resin to maintain adequate prepreg integrity through cure and initial pyrolysis, and if an in-process tackifier application proves practical, this increased compressibility is, of course, positive. Prepregs could be made well before LOM processing allowing sufficient wet-out time, and ply registration could be assured by tacking in place. However, further work is required to establish that such a processing scenario is practical.

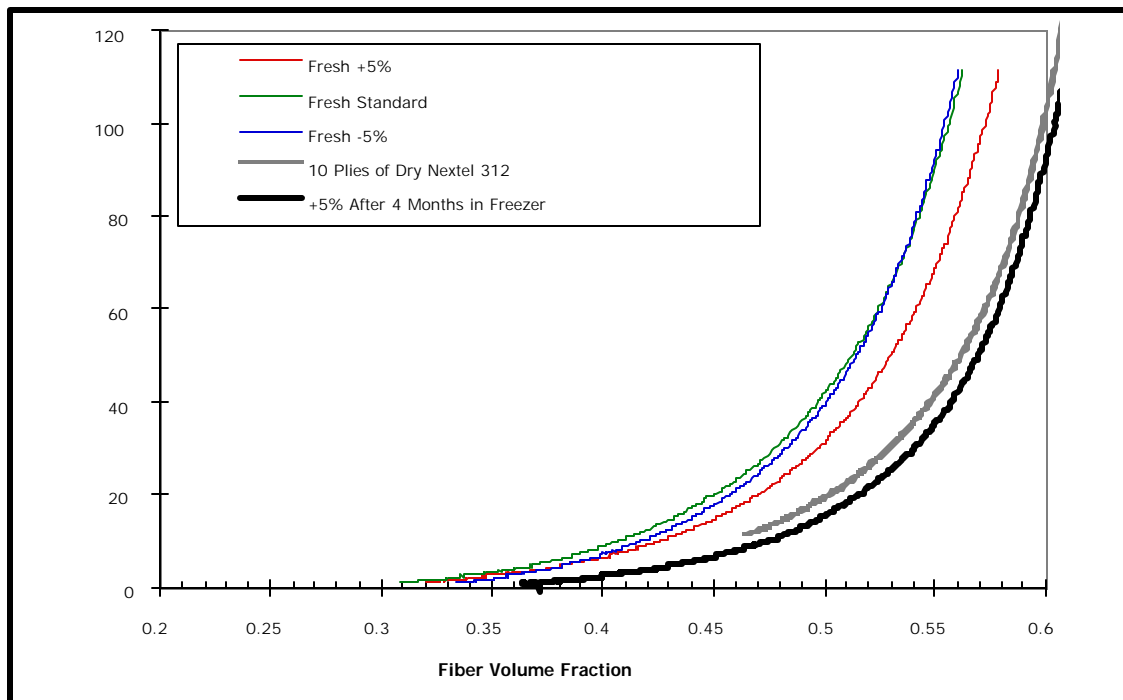


Figure 3.2.1-14 Effect of Freezer Storage on Compressibility of 493 A/B Prepreg

Prepreg material that was made at Allied Signal using 489C BlackglasTM and NextelTM 312 fibers was acquired from a Northrop Grumman West Coast facility. This material was

initially assessed for LOM fabrication by UDRI and was found to exhibit tack properties in excess of what was considered appropriate for the process. It was thought the material's high degree of tack would impose considerable difficulties in devising an automated LOM process sequence for ply backing sheet removal and transport from the feed tray to the LOM unit's build platform. The compressibility of this material was determined and the results are given in Figure 3.2.2-15. Relative to all BlackglasTM 493 materials tested to date this material has by far the lowest compressibility. In the as-received condition this matrix resin seemed to be very viscous. The results clearly show that this high viscosity prevents the development of high fiber volume fractions at pressures and time scales that are feasible for the LOM process. Of course it can still be argued that adequate fiber volume fractions still could be achieved during the cure process subsequent to lay-up. Based on these tack and compressibility results, though the 489C system is not considered suitable as a prepreg resin in this program as the cure step will be performed on the LOM system. The 489C system, though, might be effective as a tackifier agent for the 493 system.

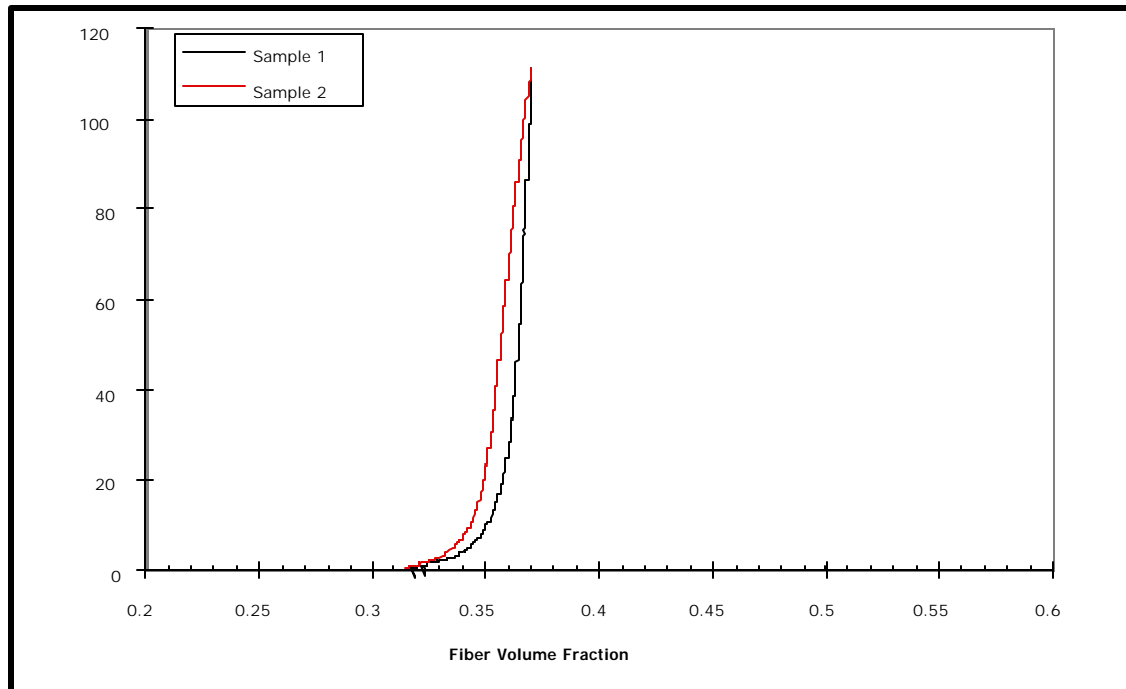


Figure 3.2.1-15 Compressibility curves for Nextel™ 312/ Blackglas™ 489 prepreg material

The results shown in the figure were obtained at different deformation rates. Sample 1 was tested at 0.003 inches per minute while sample 2 was tested at a deformation rate ten times faster. The data show the sensitivity to rate expected for this type of system, though, because of the high viscosity, the effect is less pronounced than might be expected with the 493 system.

Assessment of Tack Properties

In view of the fact that 493 Blackglas™ materials do not possess sufficient tack for present configurations of the LOM process a number of materials were evaluated as tackifiers. Initially it was hoped that room temperature aging of the prepreg would enhance the tack properties. Though some slight increase was noted, adhesion between plies during lay-up did not approach the levels deemed necessary. Two materials are considered reasonable candidates as tackifiers, depending on the process configuration. An epoxy based tackifier developed by Techniweave Inc. proved to be the most effective. Samples of 493 A/B prepreg were layed up with this tackifier sprayed onto one surface of each ply. This effectively prevented movement

between plies. The major drawback to using the Techniweave tackifier is that it does not have the same chemistry as the BlackglasTM resin, and thus may lead to delaminations after cure or pyrolysis or reduced char yield. These concerns were addressed by pyrolysis and testing of laminates made using the Techniweave tackifier; both in previous studies performed by the DARPA LC³ program and in this program. Table 3.2.1-1 shows mechanical test data for the results of these tests compared to the LC³ mechanical flexural property database. Panel # 2-29 in the table was prepared in the LC³ program and is a 10-ply sample of NextelTM 312/ BlackglasTM 493A/B, which had the Techniweave tackifier, applied between laminate layers. As can be seen from the table, the tackifier did not degrade the mechanical properties of the laminate as both the as processed (A/P) and heat treated specimens had comparable flexural properties as other BlackglasTM /CMC test panels fabricated without the tackifier. This test panel from the LC³ program, though, was prepared by a Resin Transfer Molding (RTM) process in which the NextelTM fabric layers were first stacked in an RTM mold and the pre-ceramic polymer injected under pressure into the mold and cured. The panel was then removed from the mold and subjected to the standard BlackglasTM pyrolysis/reinfiltration schedule. To more accurately simulate how the tackifier would be utilized during LOM processing in this program, a series of lamination experiments also were performed using NextelTM 312/ BlackglasTM prepreg and a curing set-up, which better approximated the LOM system.

Table 3.2.1-1 Flexural Property Summary of Nextel™ 312/ Blackglas™
CMC Panels Processed by NGC Bethpage

Panel #	Fiber Architecture	Fabric Lot #	Nitridation Run #	Condition	Specimens Tested	Peak Stress (KSI)	Modulus (MPSI)	% Strain (%)
2-22-2	BRM 6%TTT51*	1-691	67	A/P	4	27 (2)	10.4 (0.2)	0.3 (0.0)
				600°C/100hr	4	24 (2)	7.4 (0.2)	0.5 (0.0)
2-22-3	BRM 6%TTT51*	1-691	67	A/P	4	25 (1)	10.2 (0.5)	0.3 (0.0)
				600°C/100hr	4	25 (1)	7.6 (0.1)	0.5 (0.0)
2-29	2-D Tackifier Applied to Ply Surfaces	6-069	50	A/P	4	34 (4)	10.0 (0.6)	0.4 (0.0)
				600°C/100hr	4	30 (2)	6.9 (0.2)	0.5 (0.1)
2-30	Techniweave T-Formed	6-069	50	A/P	4	15 (3)	10.2 (0.2)	0.2 (0.0)
				600°C/100hr	4	28 (1)	8.0 (0.2)	0.4 (0.0)
2-31	Techniweave T-Formed	6-069	50	A/P	4	14 (1)	10.7 (0.3)	0.1 (0.0)
				600°C/100hr	4	24 (2)	7.8 (0.1)	0.3 (0.0)
2-32	2-D	7-052	67	A/P	8	17 (1)	12.3 (0.5)	0.1 (0.0)
				600°C/100hr	4	22 (1)	9.5 (0.2)	0.2 (0.0)
2-15-7	2-D Witness Coupon	6-069	57	A/P	4	35 (2)	10.9 (0.4)	0.4 (0.0)
LOMT 1	2D Tackifier Applied to Ply Surfaces	7-052	67	A/P	3	29 (1)	12.0 (0.3)	0.3 (0.0)
LOMT- 2	2-D	7-052	67	A/P	3	32 (0)	12.2 (0.6)	0.3 (0.0)

A tabletop laminator/heater apparatus was constructed at Northrop Grumman similar in design to the laminator/heater assembly being installed on the Curved LOM unit at UDRI. Ten 3"x3" plies of Nextel™ 312/ Blackglas™ 493A/B prepreg were coated with Techniweave tackifier, stacked, and cured in the table top apparatus under vacuum with the standard Blackglas™ cure schedule. A similar panel without the tackifier was also cured in the apparatus. Both samples were subsequently pyrolyzed and reinfiltrated and their flexural mechanical properties measured. These mechanical test results are also included in Table 3.2.1-1. Panel LOMT 1 is the sample prepared with Techniweave tackifier and Panel LOMT-2 without tackifier. The flexural properties of both panels are in the range of other Nextel™ 312/ Blackglas™ 493 test specimens and again indicate that the Techniweave tackifier does not seriously degrade the mechanical properties of the CMC.

The properties of BlackglasTM 489C as a tackifier were also investigated. BlackglasTM 489C has the advantage of being derived from the same chemistry as 493 and has significant tack. As such during pyrolysis this tackifier would not decompose into carbon as the Techniweave tackifier but into a silicon-oxycarbide glass comparable to the 493 matrix. When used on dry NextelTM 312 fabric the 489C was found to be a very effective tackifier. However, when applied to prepreg, it was found that the presence of 493 A/B resin renders it ineffective. This leaves open the possibility, though, of laminating dry NextelTM 312 fabric, not prepreg, with 489C tackifier and then infiltrating with the 493 A/B resin after the initial pyrolysis. This, of course, presumes that adequate tackifier can be applied during lay up to assure structural integrity of the laminate after the first pyrolysis.

Compressibility Testing of Composite Optics Oxide-Oxide Prepreg

Composite Optics supplied the oxide-oxide prepreg with three different matrix loadings. The material is a sol-gel derived aluminosilicate matrix that is slurried and prepregged into a NextelTM 720 fabric. The system is water based and can be 'staged' to a desired level of tack before being cured at 300°F and finally sintered at 2000°F. Prepregs were supplied with 45, 50 and 55 grams per square foot matrix loading corresponding to approximately 55, 50 and 45% fiber volume respectively. The compressibility of each of these prepregs was evaluated in the as-received condition and after various out-times. As a water-based sol-gel material, the samples are not amenable to freezer storage.

The compressibility curves for the as-received materials are shown in Figure 3.2.1-16. The most important point to be noted from the data is that the lowest and highest volume matrix content prepregs achieve 40% fiber volume under about the same applied pressure, though by different routes. The lowest compressibility is oddly exhibited by the medium volume matrix

content prepreg. The pressures required to achieve this consolidation are on the cusp of practicability for the presently designed LOM unit and probably not attainable with large parts unless the frame of the system is redesigned to support greater loads. This is, of course, somewhat mitigated by the generally higher mechanical properties and increased application temperatures offered by the COI CMC when compared to the NextelTM312/ BlackglasTM CMC system. Therefore adequate performance might be achieved at a lower fiber volume than those required with the NextelTM / BlackglasTM CMC system. One of the major advantages of the COI CMC system is its higher strength (both at room and elevated temperatures) which through utilization of the LOM based design process may offer the engineer the liberty of designing a COI CMC based blastshield that can perform as satisfactorily as a NextelTM 312 /Blackglas version at a much lower fiber volume fraction.

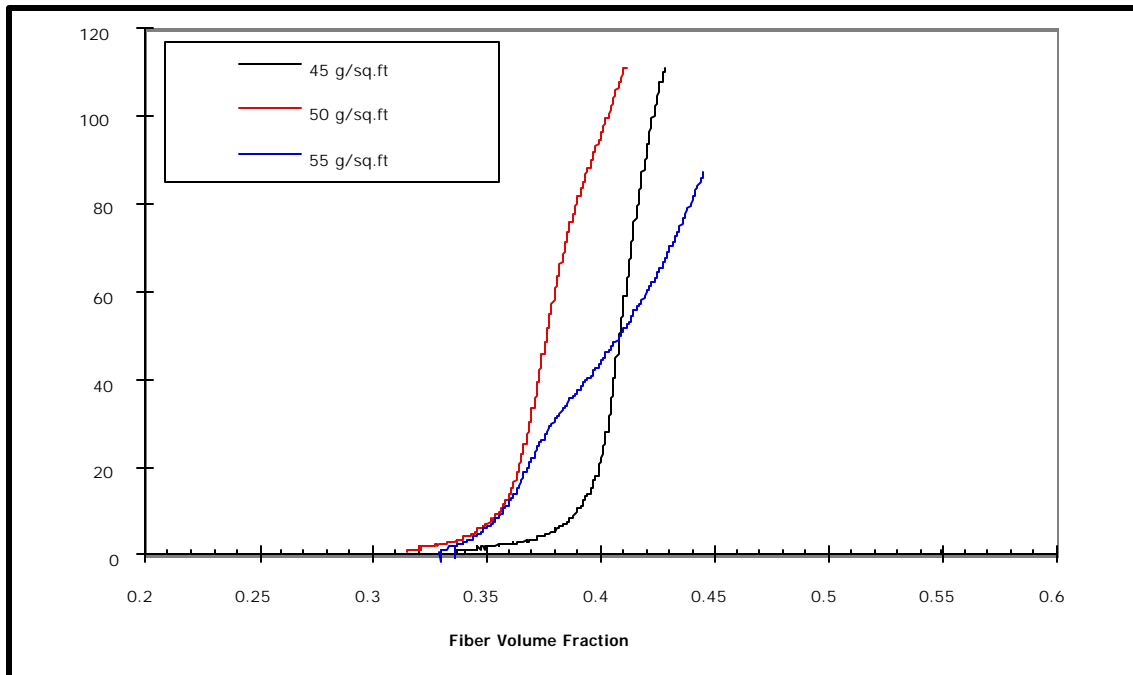


Figure 3.2.1-16 Effect of Resin Content on compressibility of NextelTM 720/COI Resin Prepreg in the as-received condition.

The results presented are somewhat anomalous, though perhaps amenable to similar resin distribution arguments previously presented. Given that the matrix is essentially a water-based

slurry, it might be expected that matrix distribution in this case could have an even more significant effect on compressibility than with BlackglasTM preregs. Water is lost relatively rapidly from prepreg material once the backing sheet is removed. In fact working life is a particular concern with this material, though if applied in the LOM process it is likely that prepreg plies would remain on the backing sheet until just before lamination.

Out-time studies were performed on each of the COI preregs. The results are shown in Figures 3.2.1-17 to 3.2.1-19. The 50 and 55 g/sq. ft versions generally show little variation in compressibility with out-time up to about 37% fiber volume. In fact, with the exception of the 50 g/sq. ft sample treated for 114 hours, these two sets of data taken together show remarkable uniformity in this region. By comparison the most matrix poor material, the data for which are plotted in Figure 3.2.1-19, shows a very clear trend of reduced compressibility with advancing out-time. In fact this trend holds true for all fiber volume fractions of the 45 g/sq. ft material. No such statement can be made regarding the other two materials at higher fiber volume fractions. The matrix rich material shows an initial decrease in high fiber volume compressibility but then provides an essentially identical consolidation curve for each subsequent out-time. The intermediate material seems to become more compressible in the high fiber volume region, though no definite trend is evident. It is somewhat puzzling that the low matrix content material does not yield a curve with the reduced slope at higher pressures that is characteristic of the other two materials. It is possible that the behavior is related to the lubricity of the matrix. With less matrix present, friction between fibers may prevent the further consolidation that occurs at high pressures in highly matrix-loaded preregs.

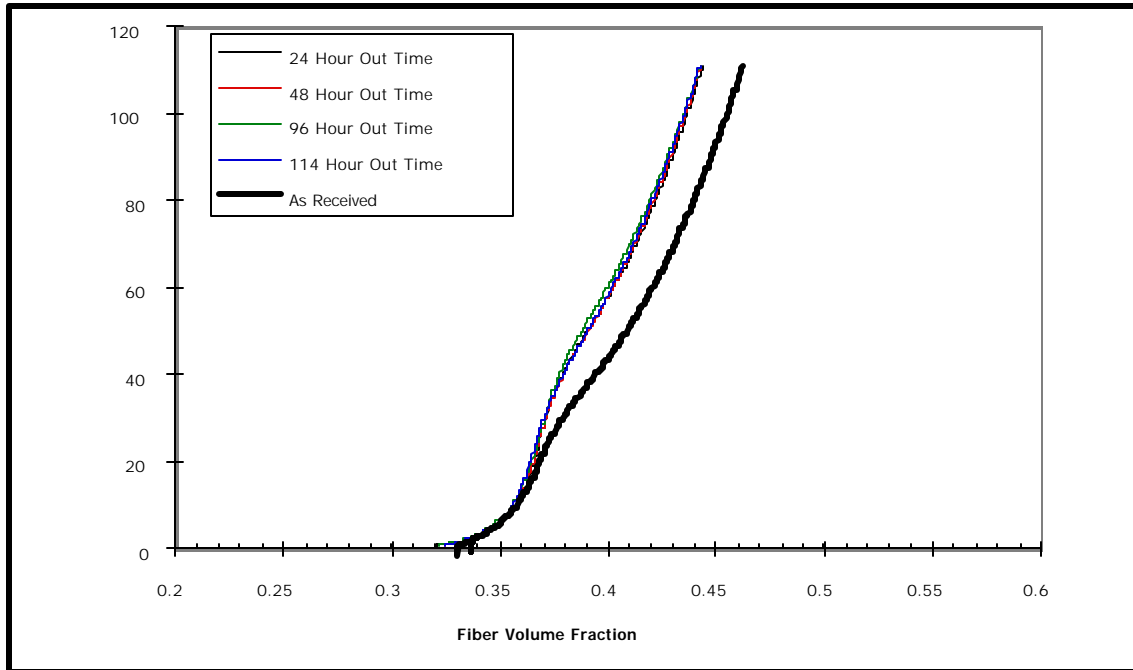


Figure 3.2.1-17 Effect of Out-time on the compressibility of Nextel™ 720/COI Prepreg with 55 grams per square foot of resin applied.

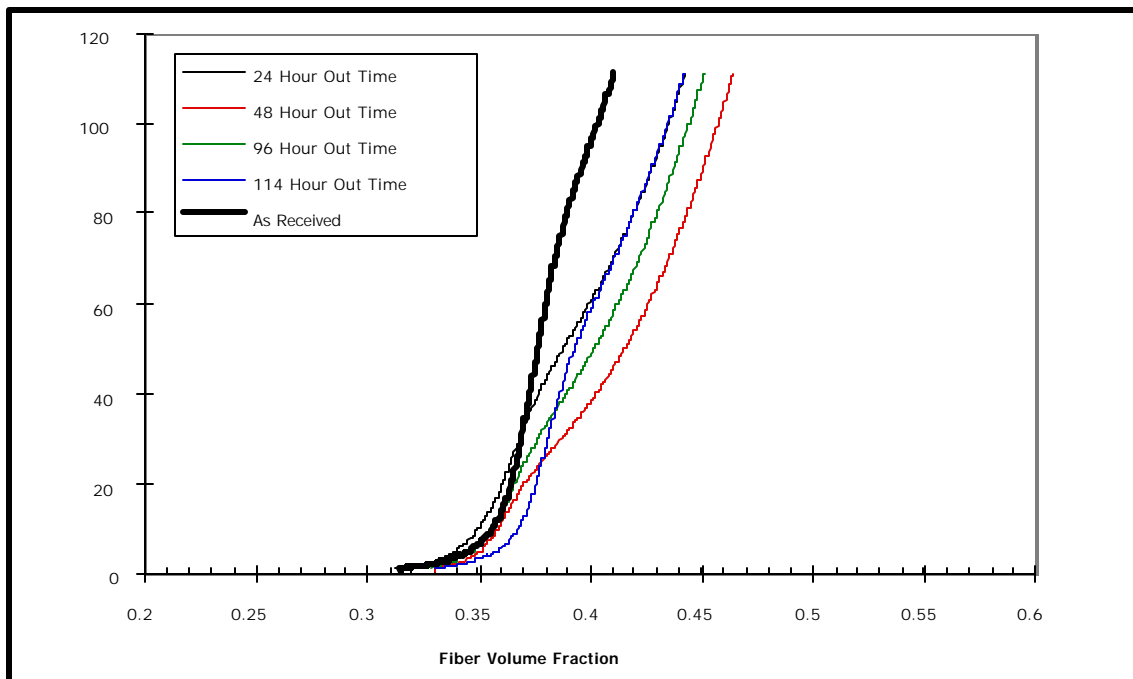


Figure 3.2.1-18 Effect of Out-time on the Compressibility of Nextel™ 720/COI Prepreg with 50 grams per square foot of resin applied.

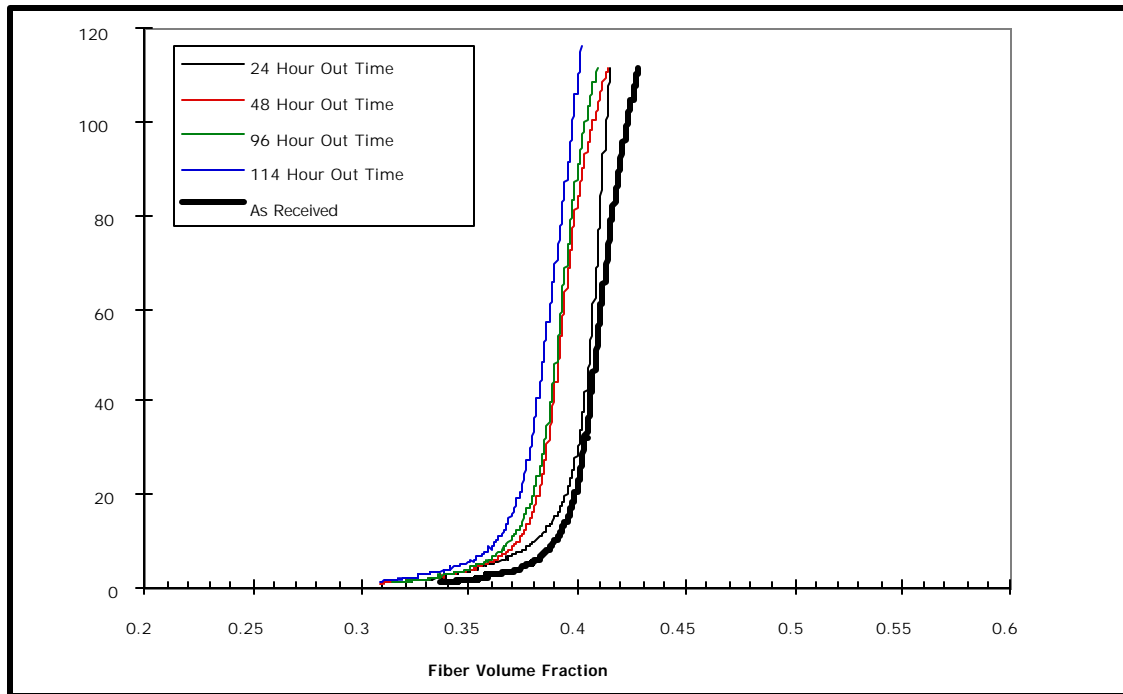


Figure 3.2.1-19 Effect of Out-time on the compressibility of Nextel™ 720/COI Prepreg with 45 grams per square foot of resin applied.

The Composite Optics resin prepreg was also tested and the results are shown in Figure 3.2.1-20. The viscosity is very high and apparently does not vary much over time. However the COI material dries out very quickly when exposed to the atmosphere. This forms a hard skin on the outside of the parallel plates, which gradually increases in stiffness with continued moisture evaporation until it cracks under the oscillatory strain. A new 'layer' of material is exposed and the process repeats itself. This leads to the sudden fluctuations in apparent viscosity seen on the plot.

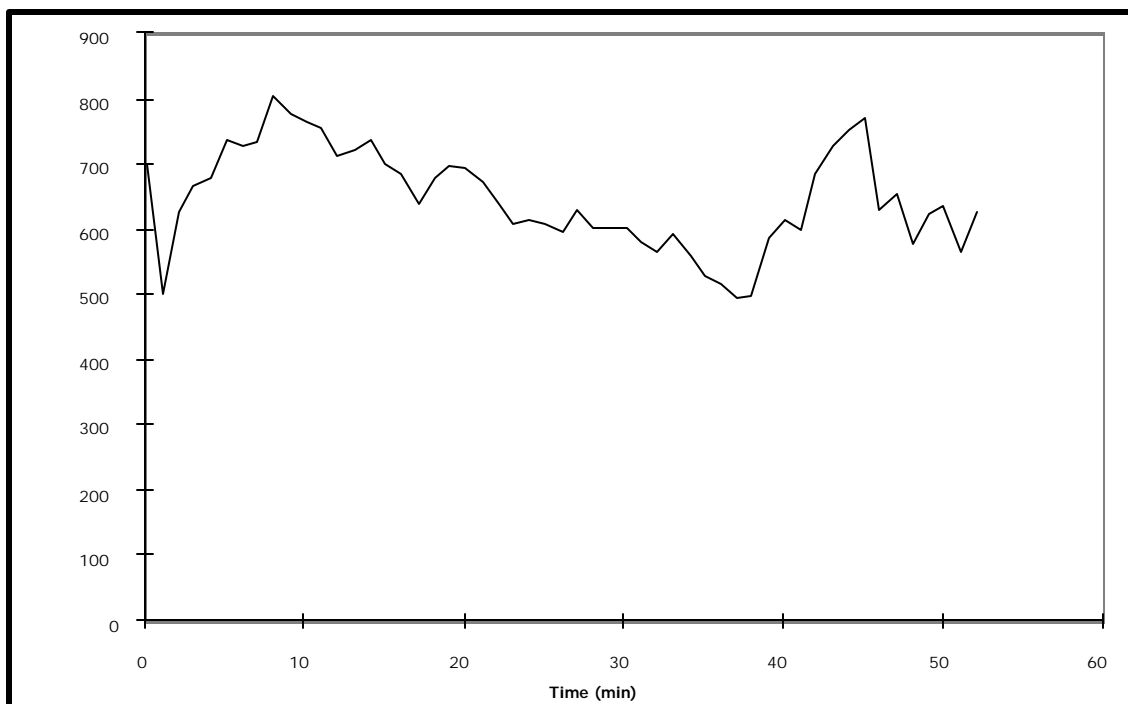


Figure 3.2.1-20 Viscosity as a function of time for COI resin

Some doubt exists regarding the suitability of the standard torsional rheometer test configuration in determining the viscosity profiles of these materials, particularly 493C and COI resin. All tests were carried out using a Rheometrics RDA II Dynamic Mechanical Analyzer. Fluid samples were tested between parallel plates with separations ranging from 0.1 to 0.8 mm depending on the anticipated range of viscosity results. The plate diameter was 40 mm. Due to some low initial viscosities and machine sensitivity considerations a cup-and-plate test geometry was employed with a 60% maximum strain and a strain rate of 50 radians per second. The time scan shown in Figure 3.2.1-21 shows a very gradual increase in viscosity of the 493C resin with no obvious physical transitions such as that occurring after about 20 hours exposure of the 493A/B. However when the test plates were separated it was obvious that the 493 actually had gone through a gelation process, though the gel formed appeared to have low shear properties. It is possible that a higher measurement strain needs to be applied to clearly delineate gelation, in which case a steady shear test may be appropriate. With such an approach the material is

subjected to a sustained shear, for perhaps a few seconds, at regular intervals in a test of similar duration to those already conducted. It is believed that physical changes occurring during gelation will be more evident in such a test.

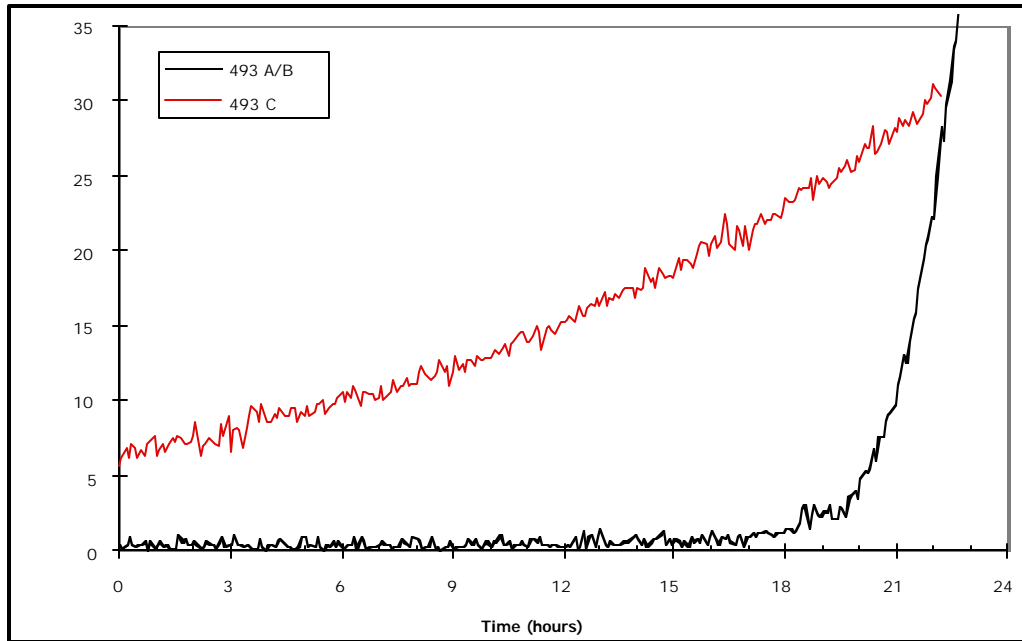


Figure 3.2.1-21 Viscosity as a function of time for Blackglas™ 493A/B and 493C resins

In the case of the COI resin the ‘drying’ process renders the technique unsuitable for determining temporal variations in viscosity. A method such as Brookfield viscometry, in which the shearing tool is completely immersed in the fluid, may solve this problem, provided the moisture loss from the surface is insignificant in relation to the total mass of resin being tested. There remains, of course, the concern that the kinetics of reaction in the bulk resin will not match that in the prepreg material, due to surface and thickness effects. While the Composite Optics material has relatively low compressibility, it may still be applicable in LOM, if curing processes can achieve the fiber volume fractions necessary. It is, in any case, important to determine the practical working life of the prepreg material.

Differential Scanning Calorimetry of BlackglasTM Resins

Changes in compressibility and, to a lesser extent, tack that occurred in previously reported aging studies are likely to be related to advancing cure reactions. Differential scanning calorimetry (DSC) can yield insight into cure kinetics by allowing reaction exotherms to be tracked as a function of exposure time. Samples of 489C and 493C resins were tested after being subjected to various room temperature aging treatments and the DSC results are shown in Figures 3.2.1-22 and 3.2.1-23 respectively. In the time scales considered, significant viscosity changes had occurred. Distinct changes in chemical structure resulting from this treatment would be expected to show up as shifts in position or magnitude of the main reaction exotherm. The temperature of onset of the exotherm is also a significant parameter. In the case of the 489C resin the onset temperature varied by only about 1.5°C and the peak temperature was essentially unchanged. Similarly no definite trends in the magnitude of the reaction exotherm could be identified, suggesting that for this material at least, changes in observed physical behavior cannot be directly related to reaction chemistry, but more likely to surface chemistry or solvent diffusion.

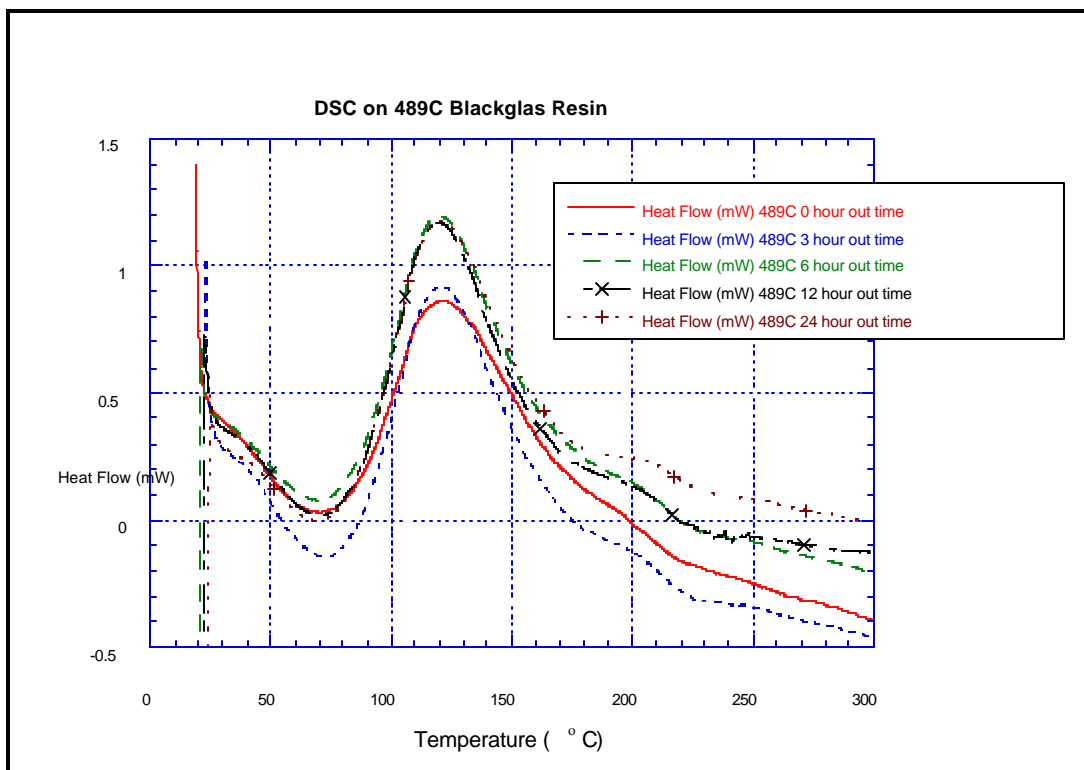


Figure 3.2.1-22 DSC scans on 489C Blackglas™ resin tested after various out times

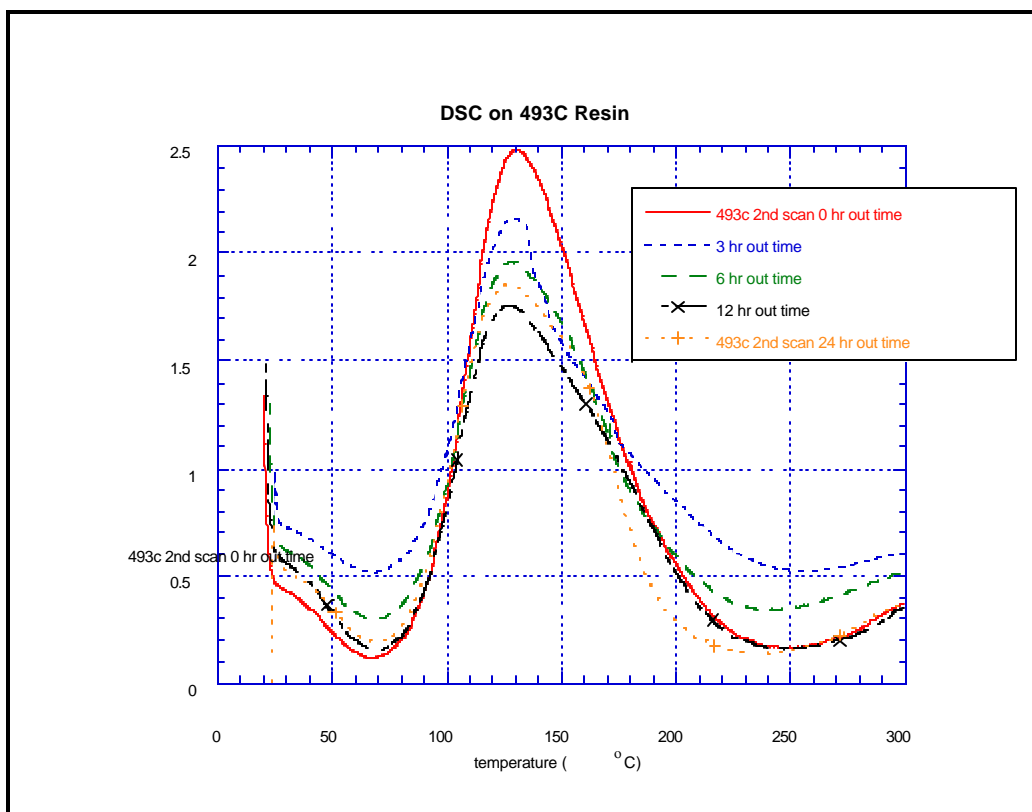


Figure 3.2.1-23 DSC scans on 493C Blackglas™ resin tested after various out times

In the case of the 493C resin reaction onset temperature, peak temperature and exotherm magnitude all seem to show a distinct downward trend. Reduced heat of reaction during DSC scans, as a function of aging time, is indicative of an increasing extent of cure before the scan was carried out. However in light of this the reduced peak and onset temperatures are somewhat surprising. There are a number of chemical mechanisms that could explain this behavior, though none as yet have been verified. FTIR spectroscopy is perhaps the most convenient way to track these chemical changes.

Rheological Testing of BlackglasTM and Composite Optics Resins

Both tack and compressibility are related to matrix resin viscosity. As the resistance to flow increases compressibility is proportionately reduced. The role of viscosity in determining tack properties is not as clear-cut, as surface chemistry will have at least as great an impact. Figure 3.2.1-23 shows viscosity versus time plots for BlackglasTM 493 A/B and C resins. The A/B system has a very low viscosity, remaining below 100 cP until 18 hours of room temperature aging. After about 22 hours the curing reaction begins to progress at a relatively rapid rate. By comparison the 493C material starts at a much higher viscosity (after evaporation of iso-octane) but exhibits a much more gradual climb. These results explain why the compressibility of 493C prepreg materials was dependent on both resin content and relatively short term room temperature exposure time. The 493A/B resin system, on the other hand, was essentially unaffected by resin content and showed no change in compressibility in the 20 hour exposure time employed.

The 489C BlackglasTM resin was also tested. The viscosity was over an order of magnitude higher than the 493C. As with the 493C, testing was carried out after solvent had been allowed to evaporate from the system for about 40 minutes. The very low compressibility of prepreg made using this material, illustrated in Figure 3.2.1-24, is due to the high viscosity. This, of

course does not preclude the possibility of reaching higher fiber volumes with prepregs exhibiting similar properties to 489C. It simply shows that in the lamination timescales expected to be necessary for the LOM process little consolidation can be expected to occur. Later curing process cycles could be designed to address this problem.

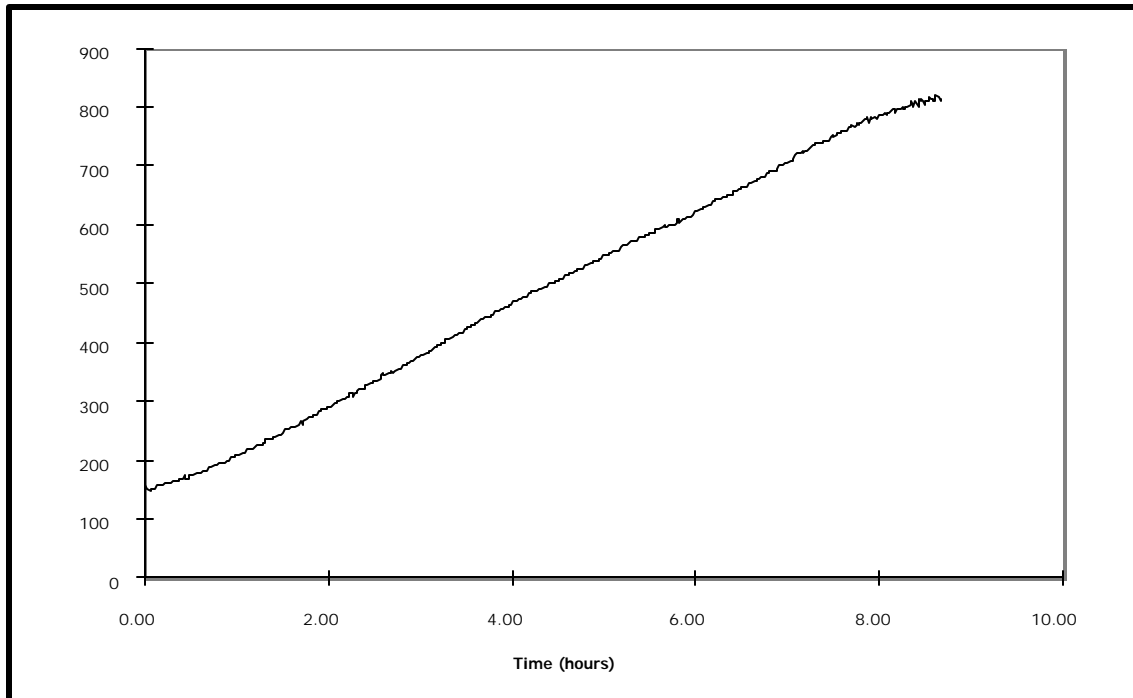


Figure 3.2.1-24 Viscosity as a function of time for 489C resin

LOM Prepreg Development Summary

While progress has been made in characterizing candidate materials for the LOM process a number of issues have arisen that will need to be addressed in future work.

- While Blackglas™ 493A/B prepregs exhibit suitable compressibility and extended out time behavior, their tack properties are inadequate for LOM processing. At the other end of the spectrum is the Blackglas™ 489 material in which the tack is so high it would present a material handling/LOM system automation problem. Since room temperature aging of the Blackglas™ 493 system did not yield a significant improvement in tack properties, a suitable tackifier needs to be selected that does not affect the compressibility of the material and

prevents delaminations from occurring during cure and pyrolysis. Initial tests indicate a Techniweave tackifier developed for the LC³ program may be suitable in this application.

- It was shown in the course of the tackifier work that the compressibility of the BlackglasTM 493A/B material varies over time in the freezer. In order to design a robust process it is important to either eliminate or characterize this behavior.
- Composite Optics prepreg material proved to have low compressibility. This does not mean that the material is unsuitable for LOM application. However its properties are such that it is difficult to determine its behavior over time, and thus establish its useful working life. The kinetics of the water based sol-gel matrix are such that the COI prepreg dries out rapidly in air once its backing sheet is removed. As such it was not possible to determine its viscosity as a function of room temperature aging time. Techniques other than standard torsional rheometry will have to be applied in order to characterize this material for LOM processing. LOM processing of the COI material, though, might actually offer a way of extending the out-time behavior of these materials. As the LOM processing is performed in an enclosed system, some control of the humidity level in the unit is conceivable which could greatly help to reduce the evaporation from these materials and thus extend their working life.

Low Cost LOM Tooling Material Development

The LOM/Forming process developed in the program entails the flat layer lamination of NextelTM / BlackglasTM composite plies and subsequent deformation into part geometry by a diaphragm forming process. To realize the design cycle time and cost reductions promised by the technology, inexpensive tooling materials are required that can withstand both the temperatures (150°C) and pressure (14 psi) involved during forming/cure. While evaluation of other build materials for LOM remains a possibility, development of modification techniques that impart the

required properties to standard LOM paper tools is expected to be the lowest cost and most convenient approach.

To realize the design cycle time and cost reductions for composites prototyping promised by the LOM/Forming process, inexpensive tooling materials are required that can withstand both the temperatures (150°C) and pressure (14 psi) involved during final forming/cure. Though other stronger and more thermally stable build materials are available for fabrication of LOM vacuum forming tools, these tapes are more expensive than adhesive backed LOM paper. In addition, parts made from these stronger materials are more difficult to decube which can often result in damage to the LOM component during the final debulking step. While evaluation of other build materials combined with alternate decubing strategies for LOM remains a possibility, development of modification techniques that impart the required properties to standard LOM paper tools is expected to be the lowest cost and most convenient approach.

The durability of LOM paper mandrels at the temperatures, times, and pressures to be encountered in the curved LOM process was examined. Several blocks and curved mandrels were fabricated with a LOM1015 machine using LOM-paper. The results showed that LOM-paper parts experience an initially high shrinkage (5-15%) through the thickness of the part during the first hour of heated compression. After that point, the through-the-thickness shrinkage is minimal (<2%) for up to 10 hours time. No shrinkage in the X and Y directions was observed. The Z-shrinkage values in this report are considered to be a worst case since rectangular blocks were tested in a through-the-thickness compression mode. In a curved mandrel on the curved LOM machine, the pressure will be distributed normal to the mandrel surface, thus allowing the stiff paper fibers to assume some of the compressive load.

LOM paper parts were tested under a series of temperature, pressure, and hold times in a press to assess dimensional changes and stability. Eight 3” square blocks were fabricated on the LOM1015 using LOM paper. The block thickness was 1” in each case. Following pressing cycles, thickness was measured again. Pressing was done in a press with 1/8” sheets of rubber between the blocks to assure pressure uniformity. The hold time ranged from 1 hour to 10 hour, pressure from 15 psi to 75 psi, and temperature from 60° C to 120° C. Table 3.2.1-2 shows the results of these tests. Based on analysis of the data the following conclusions were drawn:

- Temperature has the most significant effect on shrinkage.
- Most of the shrinkage is seen immediately upon application of the T,P,t, cycle.

Table 3.2.1-2 LOM Paper Mandrel Stability Tests

Trial	t (hour)	P (psi)	T (°C)	% Shrinkage
1	1	15	60	0.00
2	10	15	60	1.14
3	1	75	60	1.72
4	10	75	60	4.07
5	1	15	120	9.56
6	10	15	120	10.79
7	1	75	120	12.81
8	10	75	120	14.78

Development of Forming Tools for Blast Shield

Currently standard LOM paper tooling materials possess properties adequate for room temperature application of forming technology. While it is expected that the final NextelTM/BlackglasTM prepreg material will be adequately formable at room temperature, solidification of the formed part will entail a curing schedule including temperature hold times in the region of 55°C and 150°C, in which the tool will be continuously under vacuum pressure. Because the final cure stage is carried out at a temperature above that which LOM paper parts can provide continuous service, modification methods involving resin impregnation and cure are sought. The basis of this modification is the infusion of low viscosity resin into the LOM paper, since the adhesive layers that hold the paper sheets together are essentially impermeable. The principal challenge was to devise a technique in which the resin would be evenly distributed in the paper layers to a depth adequate to impart the required thermal and mechanical properties. The goals of this task were achieved in a series of sub-tasks as follows;

1. Selection of candidate materials for infiltration of the LOM paper.
2. Evaluation of the wetting characteristics of each of these materials when applied to LOM paper.
3. Infiltration of LOM paper samples using a number of infiltration techniques.
4. Evaluation of thermo-mechanical behavior of resins selected for infiltration experiments.
5. Determination of the basic thermo-mechanical behavior of unmodified LOM paper samples and also those modified by the developed infiltration techniques.
6. Scale-up of infiltration technique to part sizes similar to that needed for the blastshield.

1. Selection of Candidate Infiltration Resins

The principal parameters of concern in selection of infiltration materials are the viscosity, which is desired to be as low as possible, the wetting behavior, which is governed by surface energy factors, and the maximum allowable use temperature for the final cured material. A number of known low viscosity materials with the appropriate thermal stability characteristics were therefore selected for the initial evaluation. These included a photo-resist resin (Shipley Microposit 1400-27), BlackglasTM 493A/B polymer (Allied Signal), Epofix potting epoxy (Struers), and an epoxy based tooling material supplied by Tool Chemical Company designated TCC 630. The latter is the resin system recommended by Helysis for use as a final finish coating to be applied to conventional LOM RP paper models to impart some degree of moisture resistance and improved strength. With the exception of the TCC material, which had a mixed viscosity of about 630 centipoise, all resins had initial viscosities in the range of 100 centipoise.

2. Evaluation of Basic Wetting Characteristics of Infiltration Resins

Initial wetting behavior experiments on strips and small cubes (0.5" X 0.5" x 0.5") of standard LOM LPH042 materials found the Photoresist and BlackglasTM polymer to have much better wetting characteristics compared to the TCC and Struers epoxies. The BlackglasTM resin essentially wet and infiltrated the LOM blocks completely when submerged in a solution of resin. The case was not true for the other resin systems evaluated during the subsequent cure of the BlackglasTM material, though, the resin reacted with the paper adhesive layers leading to severe distortion of the LOM blocks. LOM blocks infiltrated with Photoresist resin also exhibited poor shape fidelity when subjected to excessively higher Photoresist cure temperatures. For these reasons the BlackglasTM and Photoresist resin were not considered suitable as infiltration materials and were dropped from further study.

3. Development of Infiltration Techniques

As mentioned previously, the TCC epoxy is the recommended resin system used to superficially impregnate the surface of standard LOM RP parts to improve their moisture resistance. For this application the resin is simply painted onto the surface of the part and left to stand at room temperature for twenty-four hours. With this method the resin is absorbed into the part to a depth of roughly 1mm. Earlier work had shown that, using a vacuum impregnation technique, LOM parts could be infiltrated with the TCC resin to a depth of about 2mm or so. This was not expected to be adequate for the purposes of providing a tool capable of withstanding standard forming conditions. In order to study the effects of infiltration conditions on the depth of penetration, a series of tests were conducted in which the ambient pressure over the LOM test samples was controlled. Samples of a size suitable for dynamic mechanical analysis (DMA) were prepared from a block of LOM paper material. After being subjected to the various infiltration scenarios the parts were then tested by DMA over the temperature range required for the BlackglasTM polymer cure schedule. Where possible, neat resin samples were also prepared and tested with the same thermal scan.

In an effort to increase the depth of penetration of resin into the LOM samples a pressurization method was utilized. In this technique the DMA samples were fully immersed in the infiltration material, as before, and a pressure of 90 psi applied. This had a significant effect on the depth of penetration into the samples as seen in Figure 3.2.1-25 where results for (a) Photoresist and (b) TCC epoxy are presented. The photoresist material completely penetrated to the center of the part, and the TCC resin, notwithstanding its higher viscosity and demonstrated lower wetting properties, almost reached the part center.

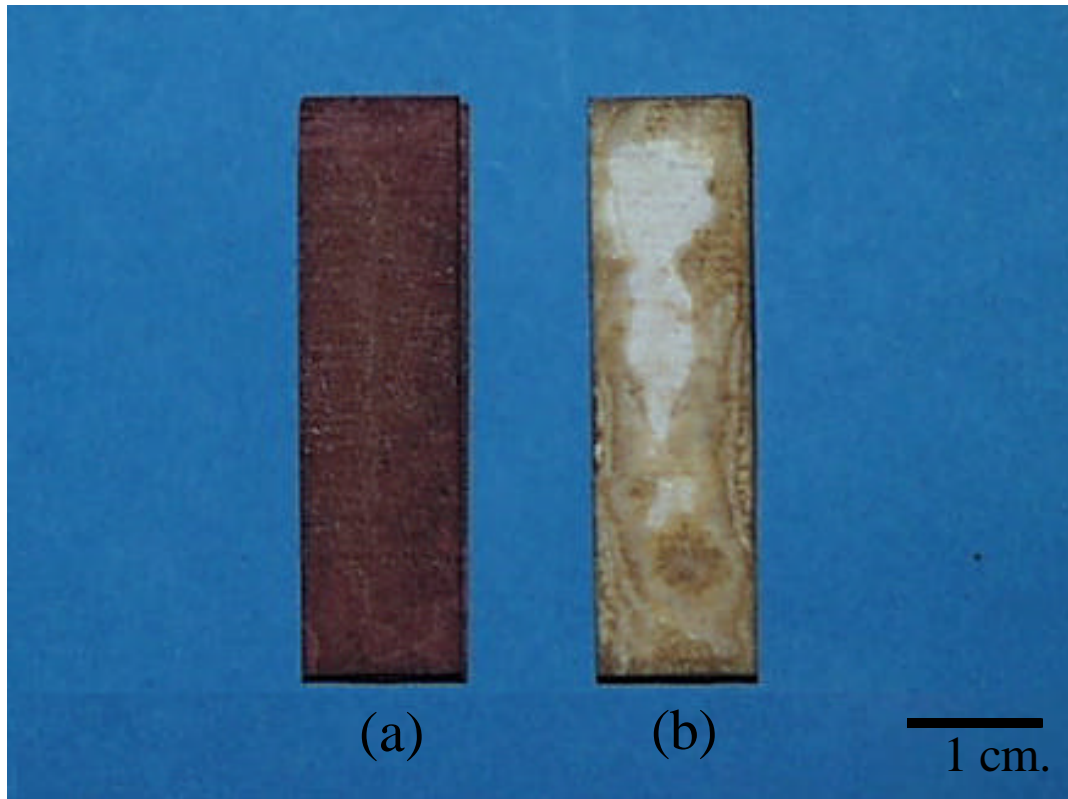


Figure 3.2.1-25 Dynamic Mechanical Analysis samples infiltrated with (a) Photoresist resin and (b) TCC 630 epoxy resin

Because of its expected high temperature performance (up to 148°C), particular focus was then applied to the TCC 630 resin system. The progression of development of the infiltration technique is represented in Figure 3.2.1-26. The procedure for preparing DMA samples was as follows. A piece measuring 45 mm square by 4 mm thick was cut from a LOM paper block. This was cut into samples approx. 13 mm wide. Samples were then infiltrated with resin and cured according to recommended cycles. The surface plies of the samples were removed using a sharp razor blade before testing. This last step is important, since testing of samples with the fully infiltrated surface plies in place would, likely, skew the results of dynamic mechanical testing. The goal of this task reduces to an effort to impede the interply shearing that is favored in the LOM paper parts, especially at higher temperatures at which the adhesive begins to soften. It is therefore important to test in a fashion that emphasizes modification of the interply regions. Figure 3.2.1-26(a) shows a sample infiltrated at room temperature under atmospheric pressure. This

sample was made using the TCC resin mixed according to a modified formula suggested by Helisys. This two-part epoxy system is normally combined in the ratio of 100 parts base resin to 20 parts hardener. However in a effort to enhance infusion the amount of the lower viscosity hardener (100 cP) was increased relative to the base resin (1,600 cP). The resultant penetration into the sample was on the order of a millimeter or so with effects on shear behavior shown in the following section. A similar procedure was employed for the sample shown in Figure 3.2.1-26(b) except that the sample was post cured for 1 hour at 215°F and 1 hour at 250°F. Figure 3.2.1-26(c) shows the same sample compared to that infiltrated with Photoresist resin in Figure 3.2.1-25. It appears from the above that with the application of 90 psi pressure for 1 hour the TCC resin can penetrate about 6 mm into the sample. Samples were therefore prepared in which a grid of 0.5mm diameter holes was drilled with hole center spacing of about 5.8 mm. The results of infiltration under pressure of these samples are shown in Figure 3.2.1-26(d) and (e). As can be seen there is complete infiltration of the samples. In sample (e) a different hardener (116A) formulated by the manufacturer was used with the base TCC resin. This was expected to yield both a resin mix with a lower viscosity and superior high temperature properties in the cured polymer.

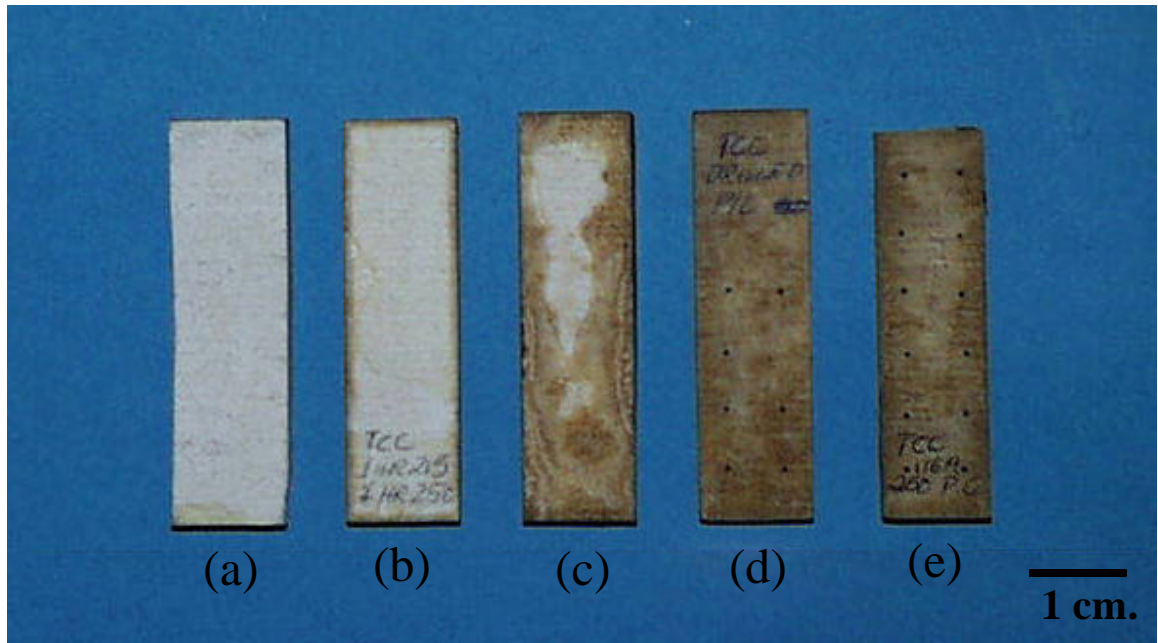


Figure 3.2.1-26 Dynamic Mechanical Analysis samples infiltrated with TCC 630 epoxy; (a) infiltrated under atmospheric pressure without subsequent post cure, (b) atmospheric pressure with post cure (c) 100 psi over pressure and post cured (d) 100 psi over pressure with $\frac{1}{4}$ " center holes (e) 100 psi over pressure with $\frac{1}{4}$ " center holes using high temperature hardener.

4. Evaluation of Thermo-mechanical Behavior of Base Resins

Improvement in thermo mechanical performance by infiltration derives from the thermal properties of the base resin. In an effort to assess the baseline performance of the candidate resins, DMA samples with nominal dimensions of 45mm x 12.5 mm x 2.8mm were cast from the various resins. These were then tested by torsion rheometry in a Rheometrics RDAII Dynamic Analyzer. In this technique samples are gripped at the ends and subjected to a sinusoidal torsion deformation. The amplitude and frequency of deformation are controlled and the resultant torque is recorded. This allows quantities such as shear stiffness and loss factors to be determined. When the test is carried out over a controlled thermal scan, softening points and transitions can be identified. Of particular interest is the shear modulus in the plane orthogonal to the sample length, which, in the LOM samples, will be dominated by the interply shear behavior. The shear modulus in this critical plane is given by;

$$G' = \cos \delta (\tau/\gamma)$$

where;

δ = the phase angle by which the stress lags the strain in a sinusoidal torsion deformation

τ = the torsion stress

γ = the torsion strain.

For the particular test geometry of the Rheometrics RDAII torsion test the stress is given by;

$$\tau = M \times K_{\tau}$$

where;

M = measured torque, and K_{τ} is given by;

$$K_{\tau} = 1000 \left(\frac{3 + 18 \left(\frac{T}{W} \right)}{WT^2} \right) G_c$$

where;

T = sample thickness

W = sample width

$G_c = 980.7$ (for dynes/gm)

= 98.07 (for Pascals).

The strain in this torsion test geometry is given by;

$$\gamma = K_{\gamma} \times T$$

where;

T = angular displacement in radians, and K_{γ} is given by;

$$K_g = \frac{T}{L} \left(1 - 0.378 \left(\frac{T}{W} \right)^2 \right)$$

where;

L = sample length and other symbols are as previously defined.

Figure 3.2.1-27 shows the results of thermal scans carried out on neat resin samples cast from the candidate infiltration materials. The black data points show the behavior of the TCC epoxy material mixed using 50 parts hardener designated 115N per hundred parts resin. The relatively low room temperature stiffness is maintained to about 60°C where it drops off in a fashion typical of that observed at the onset of glass transition temperature (T_g). If T_g is taken to be the inflection point in the shear modulus data, as is commonly quoted, then the value for this baseline is about 65°C. Obviously this is not adequate for the anticipated forming/cure schedule required for the BlackglasTM/NextelTM prepreg system. A higher temperature hardener, designated 116A, combined with the base 630 resin at the recommended ratio of 20 parts per hundred and post cured at 121°C yields both an increase in overall stiffness and a dramatic increase in glass transition. In this case the inflection point is at about 100°C.

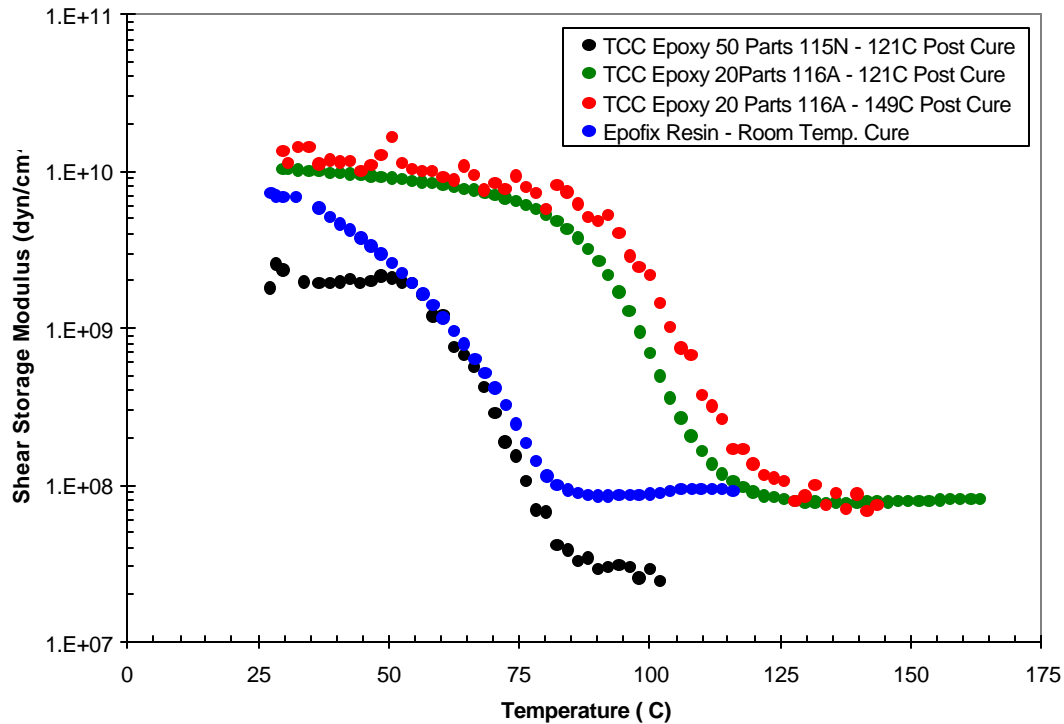


Figure 3.2.1-27 Thermo mechanical behaviors of candidate infiltration resins as evaluated by Dynamic Mechanical Analysis.

Further post cure of the same sample at 149°C provides an increase in the glass transition of about 10°C with a slight stiffness improvement. By comparison the Epofix potting compound, while having a fairly high initial modulus suffers an immediate drop in stiffness when heated, though a heat treatment effect, evidenced by the slight increase in modulus at temperatures above 80°C, is suggested. The results in Figure 3.2.1-27 indicate that the TCC compound, if successfully infused to an adequate depth in LOM paper parts, will provide a viable tooling material.

5. Evaluation of Thermo-mechanical Behavior of Resin Modified LOM Samples

Dynamic mechanical testing was also carried out on LOM paper samples that were infused with the candidate infiltration resins. Figure 3.2.1-28 shows a series of scans for material infused by various methods with the TCC 630 epoxy. A scan on standard LOM material with no infiltration resin present was first generated as a baseline for comparison. The LOM material, though relatively stiff at room temperature, rapidly softens as the temperature is increased. A

simple room temperature ambient pressure impregnation of the LOM paper leads to an apparent increase in stiffness, but the softening point is scarcely affected. Oddly, when a similar impregnation is carried out and followed by a post cure as recommended by the resin manufacturer, the room temperature stiffness appears to go down, but the softening point is increased to about 70°C. In this case the elevated temperature stiffness is consistently higher than in the previous samples. In order to enhance infiltration, a series of holes were drilled through the samples on 5.8mm spaced centers as described previously. This led to an appreciable increase in the room temperature and elevated temperature properties, though the softening point was not further increased. Since all of the above samples were infiltrated with a resin formulation containing a high level of catalyst this result is to be expected as the excess hardener may act as a plasticizer. On the basis of the tests carried out on cast resin samples, there is little difference between the softening point of the hardener rich TCC resin and the LOM paper blocks. However it is evident that, while the incorporation of the resin in the block through the drilled holes does not increase the softening point, it does provide some shear stiffening in the samples. In fact the sample that is infiltrated with the high hardener content TCC resin is almost an order of magnitude stiffer than the base LOM paper block at all temperatures.

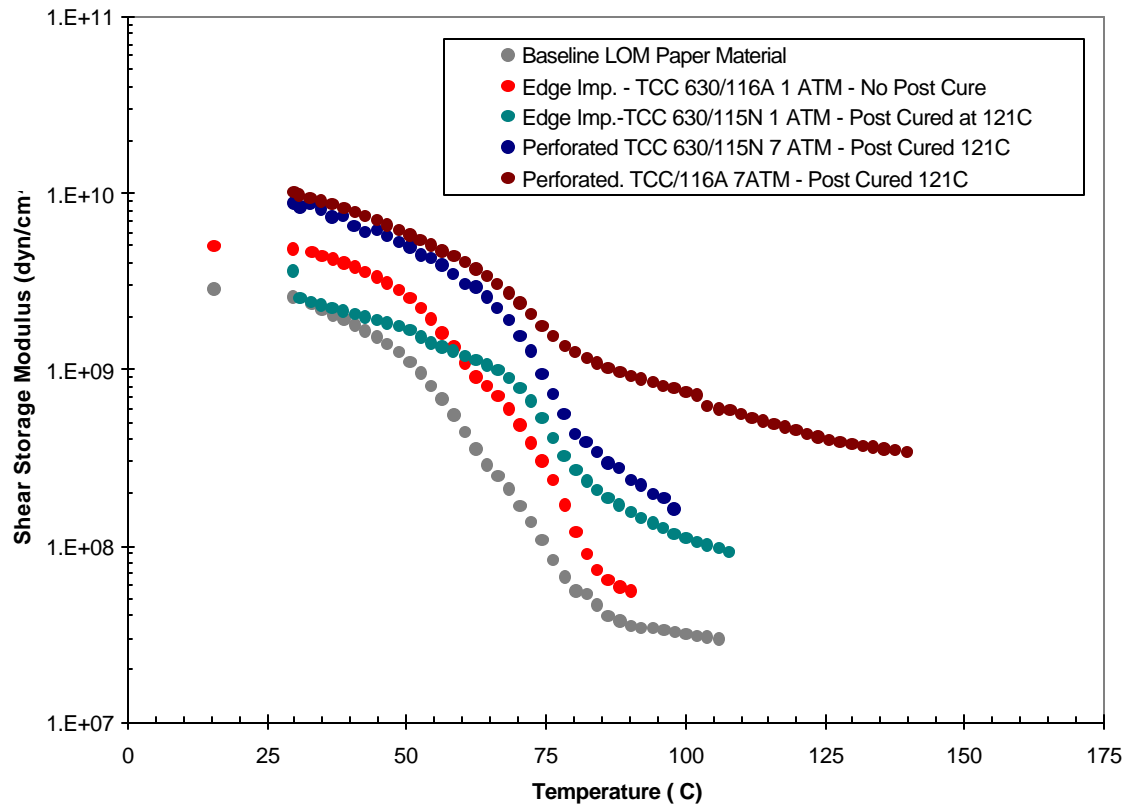


Figure 3.2.1-28 Thermo mechanical behavior of LOM Paper samples infused with TCC 630 Epoxy

When the LOM paper samples were impregnated through drilled holes with a TCC resin formulation containing a higher temperature curative (116A) and post cured at 121°C, the softening point occurred at the same temperature as before but the resulting drop in stiffness was much smaller. A further, less significant transition appears at about 100°C that corresponds to the softening point of the base resin, as shown in Figure 3.2.1-27. Thus a promising LOM paper material modification appears to be available.

There are a few important conclusions that can be drawn from the above work. First, it appears that the mechanical and thermal properties of laminated LOM paper material can be positively impacted by the modification technique developed. Second, the approach of infiltrating the LOM material through a series of small holes seems effective in improving the shear

deformation behavior. While the softening of the existing LOM paper adhesive still exerts a strong influence on the bulk behavior, the ‘shear connection’ forged by the resin network through holes connecting infiltrated paper layers, is effective in increasing the shear modulus of LOM paper parts. Finally, the TCC material provides significant improvement in performance of standard LOM laminates above its glass transition temperature.

Figure 3.2.1-29 shows that increases in thermo-mechanical performance are also provided by the infusion of Epofix potting compound into the LOM paper material. The data shown for BlackglasTM material were obtained from samples that were infiltrated from the edge only without either drilling holes or applying over pressure. Both the softening point and overall mechanical properties are improved, though the drop occurring at the apparent Tg is rapid. Before testing the material was post cured at 50°C for 2 hours and a further 3 hours at 90°C. In line with the results obtained for the cast resin, the sample infiltrated with Epofix potting compound exhibited a very low softening point but an increase in mechanical properties occurring at higher temperatures. This suggests a ‘post cure’ effect, though the property recovery illustrated is minimal.

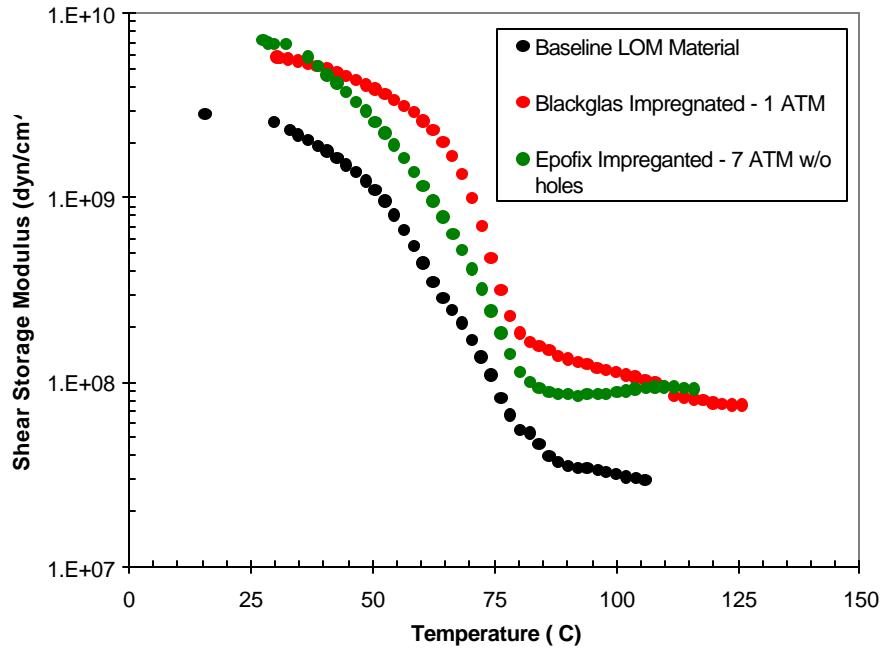


Figure 3.2.1-29 Thermo mechanical behaviors of LOM Paper samples infused with Epofix potting compound and Blackglas™ resin

In summary, thermo-mechanical tests using dynamical mechanical analysis (DMA) were performed on several candidate resin infiltration systems that included a low viscosity polyimide (Shipley 1400-27), Blackglas™ 493A/B polymer (Allied Signal), LOM TCC 630 impregnation epoxy (Tool Chemical Company), and an Epofix metallographic potting epoxy (Struers). The measurements were performed on both neat resin samples and LOM materials that had been pressure infiltrated with the candidate materials and subjected to the temperature-time cure cycles prescribed for each respective system. On the basis of the results of the DMA thermal scans the most promising infiltration resin was found to be the TCC 630 epoxy. It has a fairly unusual combination of low room temperature viscosity but relatively good thermal performance at elevated temperatures (150°C). In addition, an improved hardener was identified for the TCC 630 epoxy system that both further lowered the neat resin's viscosity (improving its ability to infiltrate the LOM paper materials) and further increased its high temperature thermo-mechanical properties compared to the other resin systems evaluated.

Modifying the LOM paper materials with an array of drilled holes through the z-axis of the part was found to both assist in resin infusion into the samples and significantly improve the shear properties of the material at higher temperatures. The shear stiffening effect evident in samples that were infiltrated through drilled holes suggests that the stability required in forming operations may be available to the standard LOM paper system.

6. Scale-up of Infiltration Technique

A tool modification technique involving the infusion of standard LOM paper with an Epoxy resin promises to enhance the thermal capability of this material substantially. However, the concepts evaluated must be extended to larger part scales, and a practicable ‘production-type’ methodology must be developed. It is possible that LOM male tool surfaces could be generated simultaneously with an offset female surface. This latter surface could constitute a holding vessel for the resin that will be infused into the part under pressure. Any potential distortion of the infused part during cure cycles must be fully established, as must its deformation under forming loads. The above-described results illustrate clearly that the adhesive layer in standard LOM paper forms a barrier to through-thickness infiltration.

To gain a better understanding of the critical factors involved in resin infusion into larger volume LOM parts, a series of vacuum and pressure infiltration experiments were performed on a number of progressively larger LOM test blocks. Initial tests focused on 1.7” x 1.7” x .75” LOM blocks followed by 4”x 4” x 0.5” plates and finally 11” x 11” x 0.5” plates. The parameters evaluated included the effects of hole geometry (i.e. diameter, length, number), resin infusion pressure, infusion time, and initial resin/part degassing influence. Figure 3.2.1-30 a,b,c displays examples of LOM infiltration samples (after resin cure) from the three respective test geometry series. Based on the results of these tests a vacuum/pressure infiltration process was devised

which enabled complete resin infiltration into LOM materials. Figure 3.2.1-30d shows a 9" x 9" x 1.5" fully resin infiltrated LOM forming tool which was successfully cured and post cured without suffering any significant warpage or delaminations. The tool represents a 9" x 9" central section of the full scale blastshield surface. A more detailed description of the pertinent issues formulated from the above series of tests to allow successful infiltration of paper-based LOM material follows.

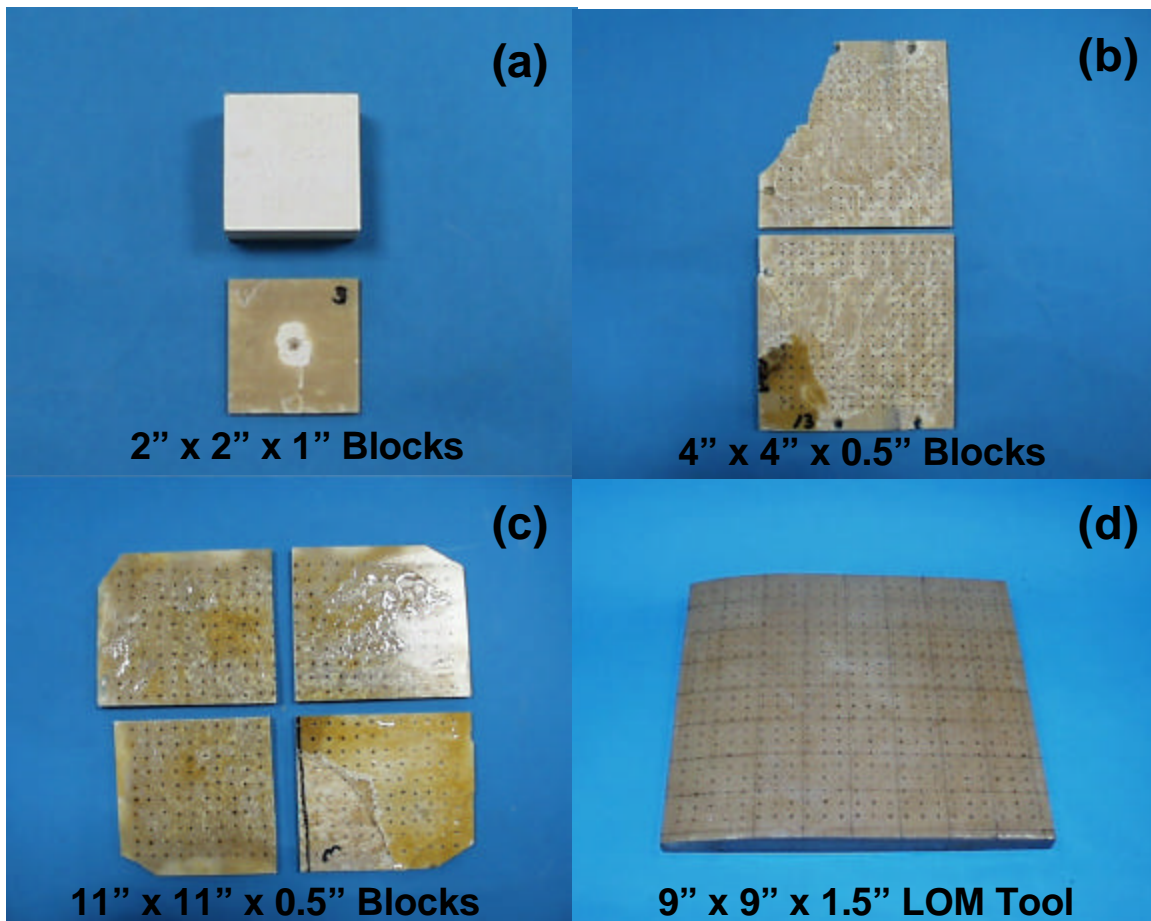


Figure 3.2.1-30 (a) Section of pressure infiltrated (100 psi) LOM test block with single .062" dia. through hole, (b) vacuum/pressure infiltrated LOM test block (sectioned) with through hole array, (c) vacuum/pressure infiltrated 11"x 11" LOM test block (sectioned) with through hole array, (d) vacuum/pressure infiltrated 9"x 9" LOM forming tool

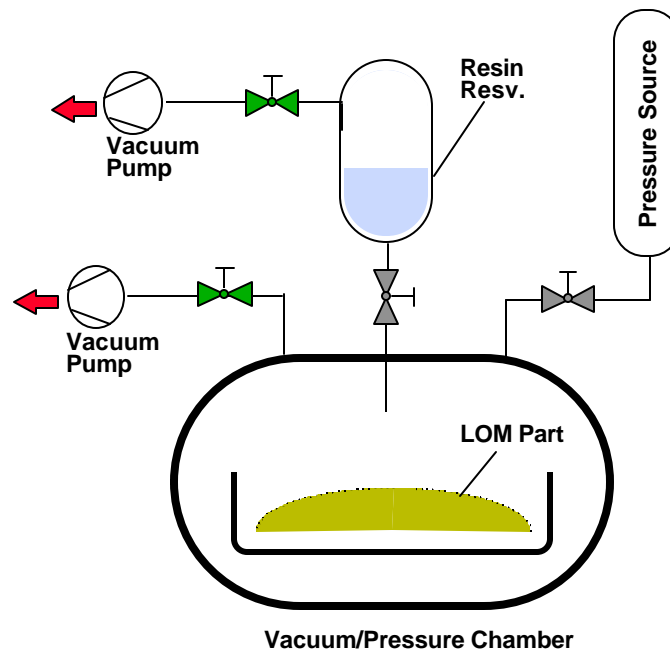
Based on the above results several correlations were discerned which are critical for successful resin infiltration of LOM parts. Drilled holes were found to assist in resin infiltration

only when they completely traversed the entire thickness of the LOM part. As expected the bulk of the resin is infiltrated into the part from its edges as these regions represent the greatest surface area (relative to the drilled holes) and are not obstructed by an adhesive barrier (as are the top and bottom surfaces). For LOM samples without holes resin can be infiltrated up to roughly 1.5” from the edge of the part when overpressures up to 200 psi are applied. As seen in Figure 3.2.1-30a for the small LOM test blocks with a single hole, very little resin infiltration occurs into the part around an individual through hole, due to its limited surface area. This observation was consistent for a variety of hole sizes and combinations of vacuum and/or overpressure infiltration scenarios.

The results were significantly different, though, when an array of through holes is introduced into the part and a two-step vacuum/overpressure process was used to infiltrate resin into the sample (see Figure 3.2.1-30b,c). It is notable that the degree of resin infiltration into the interior of the part cannot be accounted for by merely the summation of the resin fields around individual through holes. The through holes appear to influence the resin flow front in a different manner. The degree of resin infusion into the porous LOM part is a function of the pressure drop from the surface of the part to the flow front of the resin inside the part. Once this pressure gradient equals zero the infiltration stops. It is believed that the benefit of the hole array is to periodically increase the pressure at the moving flow front as the resin penetrates deeper into the part. A secondary benefit of the holes is that they also assist in the removal of air and moisture from the part during the vacuum drying process. This initial degassing of both the resin and the part was found critical to achieving both significant resin infusion into the structure and no delaminations in the part after resin cure. Initial vacuum degassing/drying of the part removes a substantial amount of entrained moisture in the LOM materials. It was surmised that the

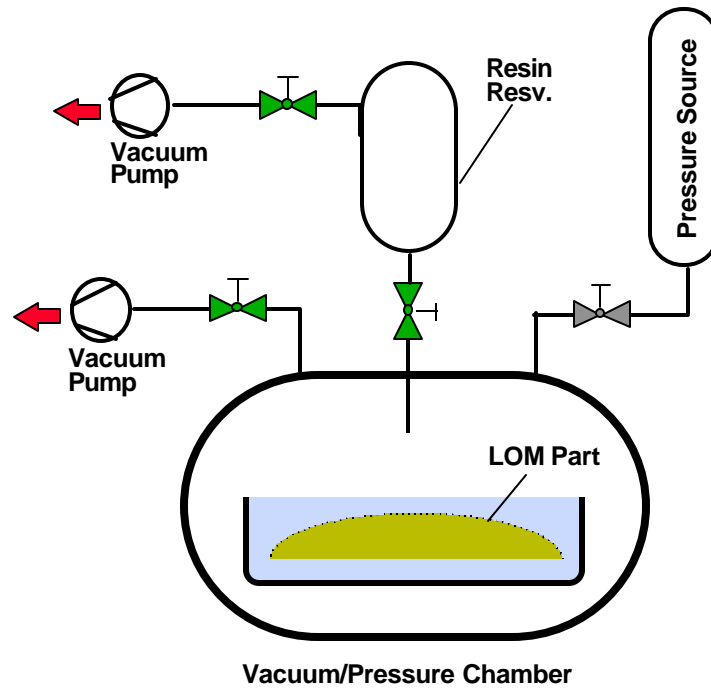
delaminations incurred in the earlier resin infiltrated parts during the final epoxy cure step were a result of the internal pressure build-up caused by the entrapped moisture in the LOM material.

As a result of these findings a combination vacuum/pressure infusion process was developed for injecting resin into the LOM materials and a vacuum chamber modified to perform the injections. The steps involved in the vacuum/pressure resin infusion process are depicted in Figure 3.2.1-31abc. After incorporating an array of holes in the LOM part, it is seated in a reservoir and placed under vacuum to first dry out the part. For large LOM parts that have not been coated after fabrication and have been exposed to the atmosphere for an extended time, this vacuum drying process can take several days. Before resin injection is to take place the infiltration resin is introduced into a separate vacuum chamber and degassed. In the next step (Figure 3.2.1-31b) the degassed resin is introduced into the part chamber and allowed to fill the reservoir until the LOM part is completely covered. Finally, in the third step (Figure 3.2.1-31c) an overpressure is applied to the covered part which further forces the resin into the interior of the sample.



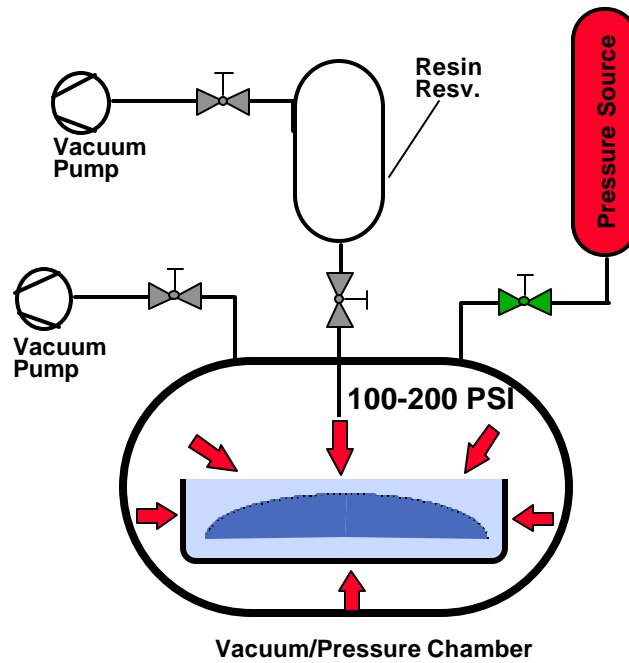
Step 1. Degas Resin & LOM Part

Figure 3.2.1-31a Vacuum/Over Pressure Resin Infiltration Process: Step 1



Step 2. Release Resin Into Chamber

Figure 3.2.1-31b Vacuum/Over Pressure Resin Infiltration Process: Step 2



Step 3. OverPressure Chamber

Figure 3.2.1-31c Vacuum/Over Pressure Resin Infiltration Process: Step 3

Full Scale LOM Tool Infiltration for Blastshield

A full size blastshield-forming tool was fabricated by LOM and successfully resin infiltrated with the TCC 630/116 epoxy. The tool was cured and post cured without suffering any significant delaminations. The infiltrated tool was also subjected to the standard BlackglasTM/NextelTM vacuum cure cycle in the recently completed Vacuum Forming Cell with no adverse effects. A description of the steps in the fabrication of the low cost blastshield forming tool follows:

A forming tool for a full size demonstration blastshield was fabricated by LOM using standard LOM adhesive backed paper. The STL design file for the tool was generated through the following steps. A text file defining a point array of the blastshield IML surface was first generated from the COSMOS/M FEA model of the blastshield. The point file was next imported into Rhino3D CAD software where a lofted surface was produced from the point data. The blastshield forming tool to be fabricated by LOM needs to be scaled and offset in several dimensions from the blastshield IML surface to account for (1) application of a cork damming material around the border of the curved part and (2) offset of the blastshield IML surface to account for the thickness of the elastomer diaphragm material needed between the part and tool surface. A trim boarder of 0.5” was added to the CAD model around the perimeter of the part as well as an IML offset of 0.0625 for the tool surface. The final dimensions of the LOM forming tool are 19” (forward) x 24.5” (long) x 15.7” (aft) x 1” thick. The thickness of the forming tool is limited at this time to 1” as this is the maximum part thickness that has been successfully resin vacuum infused to complete infiltration.

Figure 3.2.1-32a displays the Rhino3D solid model of the final tool. The 3D CAD model was next converted to an STL format and forwarded to the LOM scanner unit for fabrication.

The LOM fabricated tool was next drilled with an array of 0.062" diameter through holes spaced 3/8" apart and placed in the vacuum infiltration chamber for initial vacuum drying/degassing. The vacuum/overpressure technique was then utilized to resin infiltrate the LOM tool after which the part was envelope vacuum bagged and cured/post cured under the temperature/time conditions specified by the epoxy manufacturer. The tool was enveloped vacuum bagged during final cure to help minimize any warpage or delaminations that may occur in the part during the elevated temperature cure. Figure 3.2.1-32b shows the final resin infiltrated blastshield forming tool.

Further thermal analysis work is required for determination of property changes occurring in the infused material during post cure cycles, as well as during anticipated forming schedules. The result of the above work is expected to be a tool modification technique that will provide usable tools for a range of future product and process development activities.

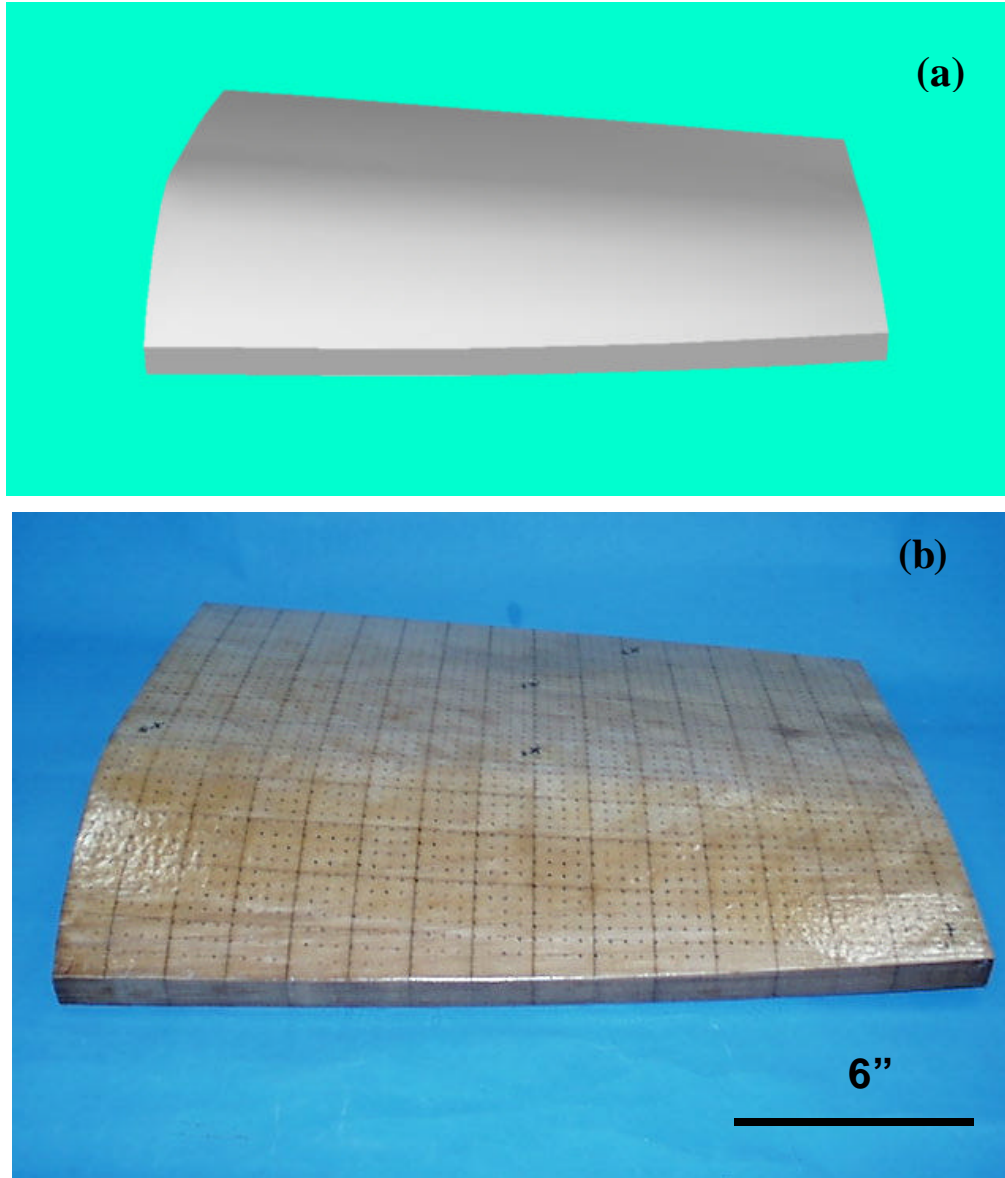


Figure 3.2.1-32 (a) 3D CAD model of LOM blastshield forming tool and (b) final resin infiltrated part.

LOM Blastshield Tool Shape Fidelity Analysis

Details of the vacuum forming/cure simulations performed on the blastshield-forming tool are discussed in Section 3.2.2. The ability of the resin infused LOM forming tool to retain its shape through the elevated temperature consolidation/cure step was also evaluated. The surface profile of the LOM tool was measured on a Coordinate Measuring Machine (CCM) before and after the temperature calibration on the forming system. The point array data from the CMM

measurements was imported into the Rhino3D CAD program where a patched surface was generated of the initial tool surface. A Point/Surface Deviation analysis routine in the software was then utilized to determine the offsets between this initial tool surface and the point array describing the surface after the temperature calibration. Figure 3.2.1-33 displays the results of this analysis. The white points signify measured offsets that were ± 30 mils from the initial tool surface while the blue points indicate offsets greater than ± 30 mils. The measurements indicate the LOM tool suffered a larger amount of distortion around its perimeter. This was not of concern as the tool contains a one inch trim border and thus the distortion would not effect overall part shape. The active tool area offset is below 50 mils, which is considered acceptable for the type of part that is to be formed over the tool. These results indicate that the resin infusion process has the capability to improve the thermal-mechanical properties of large LOM paper based tools for use in realistic composites forming based manufacturing.

Material forms in which the adhesive is applied in a discrete pattern rather than as a continuous film could facilitate application of the principals developed here. Such materials need to be evaluated in order to determine their thermal and mechanical behavior as impacted by the spatial pattern of adhesive.

LOM Tooling Material Development Summary

A tool modification technique involving the infusion of standard LOM paper with the TCC epoxy resin for improving the thermal capability of this material has been successfully extended to larger part scales, and a practicable ‘production-type’ methodology has been developed.

One important issue, which was not completely addressed in the above series of infiltration experiments, was the optimal density of through holes needed. As the density of through holes affects both the degree of resin infiltration into the part and the final part shear

stiffness, a better understanding of this parameter is critical for achieving both strong and easily manufactured forming tools.

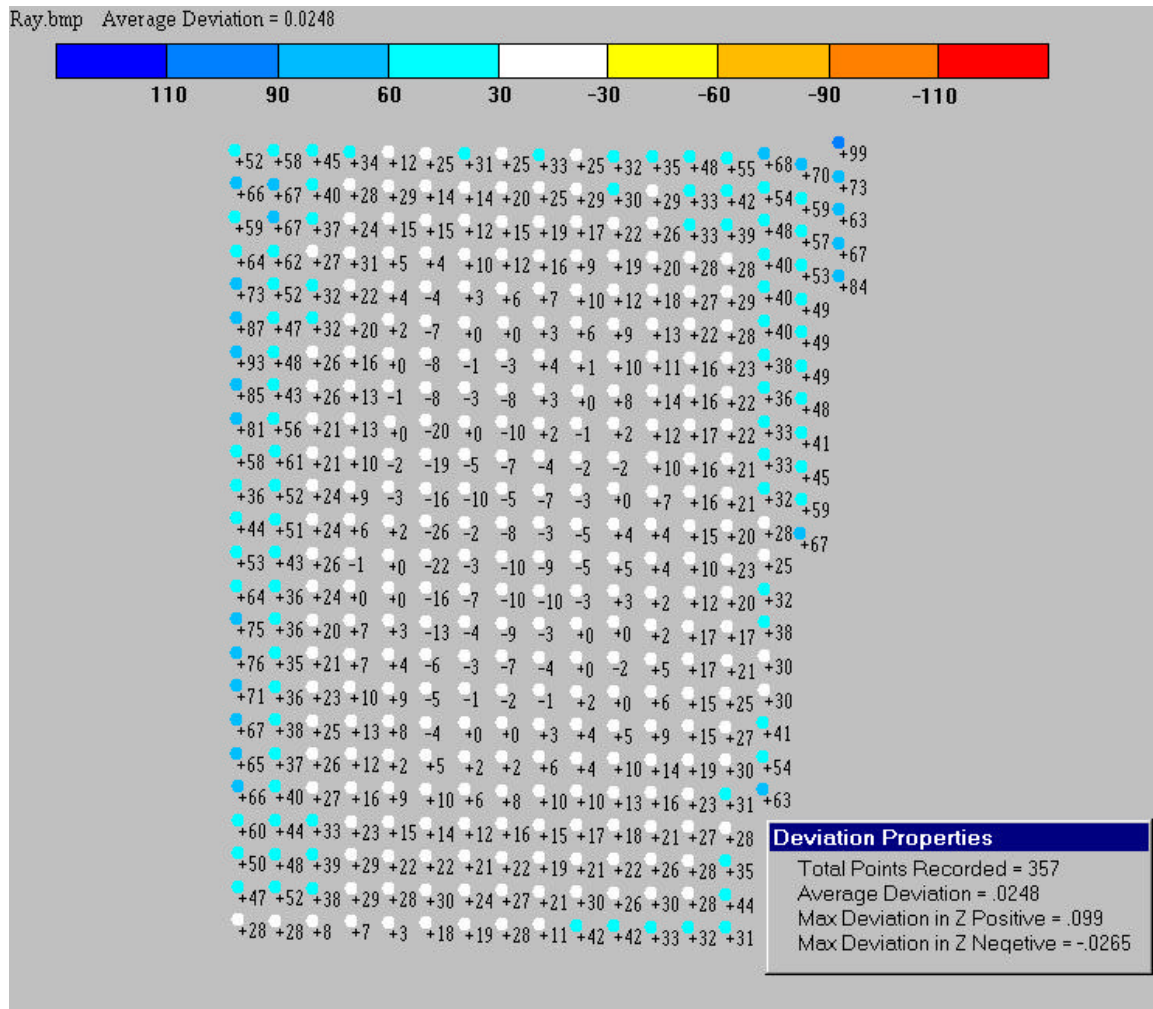


Figure 3.2.1-33 Shape offset analysis of LOM tool before and after temperature calibration on composites forming system (offsets in mils).

A tool modification technique involving the infusion of standard LOM paper with the TCC epoxy resin promises to enhance the thermal capability of this material substantially. However, the concepts evaluated must be extended to a practicable 'production-type' methodology. It is possible that LOM male tool surfaces could be generated simultaneously with an offset female surface. This latter surface could constitute a holding vessel for the resin that will be infused into

the part under pressure. Any potential distortion of the infused part during cure cycles must be fully established, as must its deformation under forming loads. Work performed in this reporting period illustrates clearly that the adhesive layer in standard LOM paper forms a barrier to through thickness infiltration. Material forms in which the adhesive is applied in a discrete pattern rather than as a continuous film could facilitate application of the principals developed here. Such materials need to be evaluated in order to determine their thermal and mechanical behavior as impacted by both the infiltration process and final application environment.

The necessity of drilling a large number of holes in the part to achieve total resin infiltration is a concern, especially for large parts as it is an additional manufacturing step. The feasibility of using the LOM scanner system (described in Section 3.2.2) to introduce the holes in the part as it is being fabricated needs to be evaluated. The increased speed of the scanner system (especially for building paper based parts) should help to offset the additional build time needed to drill holes in each build layer.

One important issue that was not completely addressed in the above series of infiltration experiments was the optimal density of through holes needed. As the density of through holes affects both the degree of resin infiltration into the part and the final part shear stiffness, a better understanding of this parameter is critical for achieving both strong and easily manufactured forming tools.

3.2.2 LOM System Development

The overall goal of the LOM System Development Task (Task 1.2.2) was to incorporate hardware and software upgrades to a commercial Helisys LOM unit to improve laser cutting accuracy, speed, and quality for processing fiber reinforced CMC materials (with a specific demonstration on the NextelTM/BlackglasTM preceramic polymer system). Under a contract redirection plan, this overall goal was updated to development of a LOM/Forming system that included addition of a Composites Diaphragm Forming module to the LOM processing scenario. The program successfully implemented and evaluated the following hardware and software improvements to a commercial Helisys 2030H LOM unit:

- 200 W Coherent CO₂ Laser Installation
- General Scanning Laser Scanner Implementation
- Quadrant Cutting Software Development
- CCD Based Laser/Scanner Automated Calibration Routine
- Fiber Orientation Mechanism Installation
- Updated User Software Interface
- Composites Diaphragm Forming Module

The above combined hardware and software upgrades resulted in a significant technical advancement in LOM for processing CMC and other composite material systems. Through laser and scanner upgrades an improved LOM process was developed that is 2-4 times faster for parts processing with additional improvement in component surface finish and dimensional precision. A major technical achievement involved extending the cutting field of the laser scanner to large build areas without compromising scanner accuracy and cutting quality. This achievement was accomplished through a new quadrant cutting based LOM processing mode combined with a sophisticated CCD camera based calibration protocol for the laser scanner. The hardware and software upgrades also were designed such that they could be easily adapted to existing LOM

systems enabling current LOM users to extend their capabilities with a LOM/Forming process. A summary of the specific hardware and software upgrades implemented in Task 1.2.2 now follows.

LOM System Platform Upgrade

Early in the program it was determined that hardware deficiencies with the Helisys model 2030E LOM unit that was to be upgraded (as planned in the proposal) severely limited technical development plans. The 2030E LOM system was an earlier generation Helisys model that by the time of contract award was no longer produced by the vendor. By dedicating further development work to this machine, the program would have drastically increased the amount of effort and expense needed for eventual commercialization, as all technical upgrades and documentation would eventually need to be transferred from a 2030E to 2030H system. In addition, the program realized that replacing the standard LOM X-Y gantry drive mechanism with a galvo mirror positioning system offered major advantages in increased laser positioning accuracy and speed which would result in more exact parts built in less time. The benefits of a laser scanner, though, can only be realized if these precision optics are mounted on a rigid, stable platform. The benefits of the 2030H upgrade stems largely from the improvements in frame stability and laser control software that this unit provides. Integrating this latest software with the precision laser scanner helped to significantly rectify the laser cutting problems, which initially impeded further process development activities on the program.

Several important points should be also mentioned. The LOM 2030E and 2030H machines are substantially different. The 2030H system is designed to be a much more precise and stable machine (a major limitation with the 2030E unit for the program's hardware upgrades). The unit has an improved, welded machine tool frame as opposed to the weak and more compliant 2030E bolted frame. The optical and vertical stage frames on the 2030E unit are separate and connected through a sheet metal cabinet, which contributes to mechanical instability. In the improved 2030H series all of the optical, fuser (heated roller) and Z stage components are now attached to the welded frame that significantly improves the stability of optical alignment.

In contrast, the optics on the 2030E typically need to be adjusted and calibrated frequently, thus limiting the improvements in laser cutting accuracy provided by a scanner. Finally, improvement in cutting accuracy and stability are also obtained on a 2030H machine by utilization of a single Z stage mechanism. In the earlier 2030E design, two vertical stages were utilized which were not always synchronized. This sometimes led to wedge shaped imprecise parts.

Another advantage of scanner implementation stems from a heightened awareness of the issues associated with decubing of LOM parts made from new, stronger materials such as composites. As stronger build materials are used for LOM fabrication, the final decubing step becomes more difficult. Excess force can be required to remove decube regions which can induce delaminations. Surface damage from manipulation with decubing tools, surface material pullout, and edge/corner damage are also encountered during the decubing process, which can more seriously degrade part surface finish and tolerance. This important issue was not addressed in the original proposal. Scanner based adaptive cross-hatching and ablative decubing are two methods Helisys has conceived to mitigate the above decubing problems. The current program did initial exploration of these enhanced decubing strategies. Further work, though, is needed beyond the scope of that evaluated in this completed program.

The 2030H system was not considered as an option in the initial contract proposal as the unit was not yet developed. The unit was engineered during the same time frame as the current LOM program. This base LOM platform substitution thus represented a unique opportunity to reap the benefits of this state of the art LOM technology developed with Helisys' internal funds.

Though it was anticipated that basic laser cutting problems of CMC materials could be reduced by using the standard 2030H model (as this system utilizes an updated laser power/motion control algorithm) additional upgrades were also required to the machine for optimal processing of composite materials. The standard 2030H commercial system is equipped with a 50W laser that does not provide adequate laser power for cutting of composite materials. The machine also does not take advantage of beam stability and speed of cutting offered by laser

scanner technology. The unit also lacks the software for processing part ply orientation data and the necessary hardware for orienting composite plies before lamination and laser cutting. The upgrades described below effectively eliminated these drawbacks.

200 W Laser / Laser Scanner Upgrade

An initial scanner module was developed which consisted of a 100-Watt (Synrad) laser and a General Scanning scanner jointly installed on a modified Y Gantry of a standard 2030H LOM unit. Both the laser and the scanner were borrowed from another LOM prototype machine currently being developed by Helisys. Although not suitable for use in a final commercial system these components (and their optical set-up) were considered adequate for evaluation of an initial “proof of principle” prototype unit. Subsequent laser cutting evaluations performed on Nextel™/Blackglas™ prepreg materials showed substantial improvement in laser cut edge quality and damage reduction. While demonstrating the potential of scanner-based laser cutting of composite materials by the LOM system, this early prototype design, though, suffered from the substantial weight of the laser/scanner module (due largely to the significant mass of the 100W laser which was translated with the scanner mirrors). This resulted in a significant inertia of the XY positioning gantry, which reduced processing speed and reliability. Other drawbacks of the prototype system were 1) low laser power for cutting composite materials, 2) lack of a mechanism for ply orientation, and 3) limited software capability for both extending cutting performance over the full build envelope of the machine as well as processing of LOMNEF files of composite parts.

After initial testing of the “proof of principle” LOM scanner system it was decided to move the 100-Watts laser off the moving Y gantry into a stationary position on the LOM 2030H frame. Though this design significantly reduced the inertia of the scanner/gantry assembly it introduced an additional challenge in laser beam alignment between the stationary laser and “flying optics” arrangement of the scanner module. An improved optical alignment system was

developed for the unit, which included a suspension system for the laser with improved beam alignment components, incorporated into the design. The Y gantry of the machine was also redesigned to accommodate the scanner assembly. The new gantry was manufactured with two guiding rails and a belt driven carriage. The design incorporated the same servomotors that were previously used in the conventional LOM 2030 system but upgraded with more powerful DC and RF power supplies and driver electronics for the system.

A new scanner assembly was also developed and the mechanism installed on the gantry. Although the Synrad laser was more powerful than the conventional laser used on the commercial 2030H unit, 100W still proved insufficient for effectively cutting composites. In fact the measured delivered power was only 80 Watts due to the power losses on the lenses and mirrors of the older model scanner. To achieve more appropriate processing power and cutting speed a 200W Diamond 64 laser from Coherent Inc. was acquired and installed on the machine. The laser not only delivered a significantly higher power output but also was capable of higher modulation frequency, higher pulse peak power, and better energy distribution mode than its Synrad made predecessor. The new laser was mounted on stationary mounting brackets attached to the frame of the XY system to keep stable alignment. Incorporation of the RF power unit was somewhat challenging because of its size. Finally it was located on the backside of the upper deck of the machine. Figure 3.2.2-1 displays the current configuration of the modified LOM 2030 unit with the attached laser scanner and 200W Coherent laser.

Figure 3.2.2-2 shows the current General Scanning scanner module attached to the modified Y gantry on the system. As expected, alignment of the laser and scanner was a challenging task. A special beam alignment fixture was developed in order to make the beam alignment less of an art. A modified gantry mechanism was also devised for mounting interchangeably the scanner as well as a special beam alignment fixture for optical beam path calibration. A beam expander also was added between the laser source and scanner assembly to decrease the final focal spot size thereby improving the cutting efficiency of the system.



Figure 3.2.2-1 Modified LOM2030H system with laser scanner subsystem

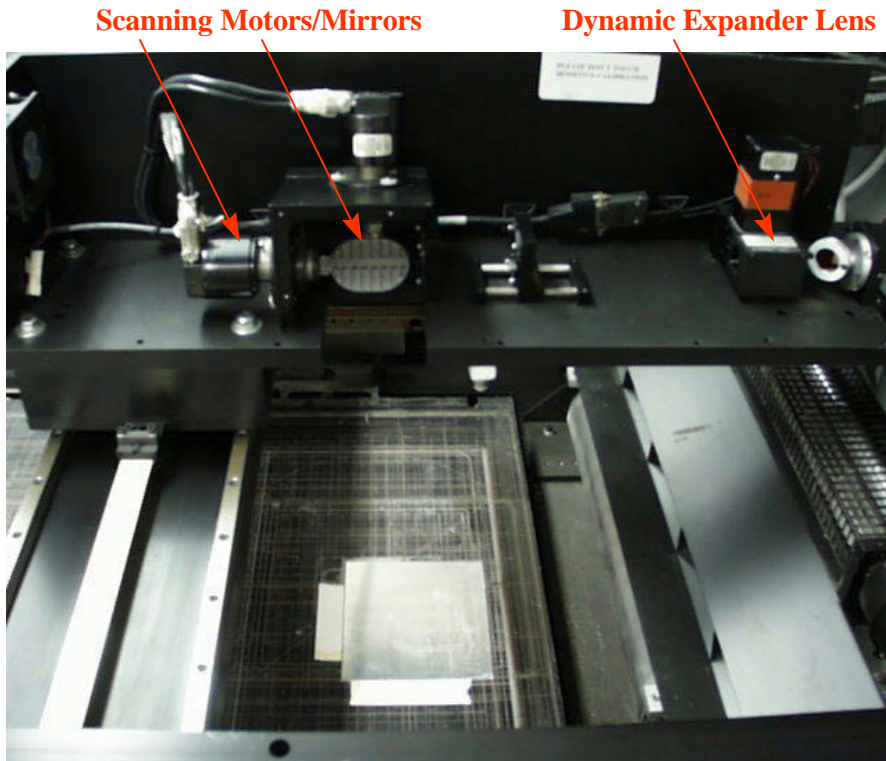


Figure 3.2.2-2 Laser Scanner Module on LOM 2030H system

Quadrant Cutting Development

A fundamental issue evaluated in the initial proof of principle device was the manner in which the scanner would be utilized to laser cut over a large build area. The scanner X and Y positioning mirrors have a limited range of angular motion, which sets the total area over which the device can scan. To increase the effective scan area one must increase the distance between the scanner and the build surface. For large build areas this distance is quite large which introduces unacceptable design limits for a viable commercial system. In addition, due to the separation of the X and Y mirrors in the 2-axis scanner module, the positioning accuracy of the system is non-linear. A grid scanned in such a system will show pincushion like distortion and must be corrected for in the scanner control software to achieve laser cutting accuracy. Laser scanner controllers typically contain sophisticated interpolation algorithms and Look-Up-Tables (LUT) to correct for such distortions but only over a limited scan area which for the current

system is 10" x 10". Scanning over a much larger area makes calibration significantly more difficult.

The solution implemented in the program was to divide the build surface into 10" x 10" quadrants then calibrate the scanner first for each quadrant then each quadrant relative to the ones it borders. During laser cutting the scanner module would be translated on the X-Y gantry to each specifically calibrated quadrant to achieve laser-positioning accuracy over the entire LOM built area. The software and hardware modifications necessary to implement this novel form of scanner based laser cutting are documented below.

Scanner Software Development Overview

Conventional LOMSlice 2.0 software was first adapted to operate in conjunction with the scanner controller. An algorithm for flexibly changing the laser speed during scanning was created and a new laser control interface developed and tested with the scanner. A procedure and software was developed to perform cutting calibration within one quadrant of the cutting field, which is 10"x10". The calibration consists of a 5x5 point look up table and establishes precise positioning of the beam within the field. Implementation of a multi-quadrant intra-regional calibration routine based on a field consisting of six 10" x 10" quadrants covering the field of 20"x30" was also devised. The procedure is based on shooting targets with a laser on lined paper. The developed software has the capability to move the scanner into the center of each quadrant. The operator interactively aligns the quadrants by assuring that the laser shoots at the same point at the corner of each quadrant independently on the quadrant in which the scanner is positioned. An automated CCD based image acquisition system is utilized to perform the above scanner intra-regional calibration.

Additional software was also developed which divides the image of a slice of the part into portions, which belong to each respective quadrant. The software also controls the mechanical motion of the system, which directs intra-quadrant moves of the XY gantry and the operation of the scanner within each quadrant. As laser scanner cutting tests have established that

multiple high velocity cuts on a NextelTM/BlackglasTM prepreg sheet generate less edge charring than a single, low velocity cut performed with higher power, LOMSlice software was also modified to allow the flexibility of automatically re-cutting a given layer multiple times. Laser cutting results on NextelTM/BlackglasTM prepreg using the prototype scanner system are detailed more fully in the LOM Process Development section below.

Additionally, software was created that generates an interface between the LOMNEF file format and internal operations of the LOMSlice 2.0 program. The code automatically recognizes the LOMNEF format and uses it in the multi-quadrant mode. The visual interface shows the specific LOMNEF defined plies on the screen as they are being produced. A rotary table has been incorporated onto the LOM machine to allow orientation of the ply as defined by the LOMNEF part data file (described below).

CCD Based Intra-regional Automated Calibration

The automated calibration routine to allow accurate LOM based multi quadrant laser cutting consists first of dividing the build surface into 10" x 10" quadrants, then calibrating the scanner first for each quadrant then each quadrant relative to the ones it borders. During laser cutting the scanner module would be translated on the X-Y gantry to each specifically calibrated quadrant to achieve laser-positioning accuracy over the entire LOM build area. The necessary software was developed which divided the CAD image of a slice of a part into portions, which would be located in each respective build quadrant. Software that also controls the mechanical motion of the system, i.e. Inter quadrant moves of the X-Y gantry followed by operation of the scanner in each quadrant, was also optimized.

The calibration routine consists of first sectioning the LOM build envelope of 20x30 inches into 6 main quadrants and 3 additional quadrants, which are centered and overlap these main quadrants. Traces of laser shots are made onto a clean sheet of LOM paper, which covers the entire LOM, build area at the peripheries of the quadrant boundaries. The DVT image analysis system records the image of the dots produced by the laser on a target in a specific

quadrant and compares their actual position to their desired position. Then the software makes appropriate corrections to the calibration look up table for that quadrant. When the same target is shot from an adjacent quadrant it will have to coincide with the mark produced by shooting from the center of a previous quadrant. The software needs to remember which mark represents the result of which shot to perform the final calibration to align the peripheries of the scanning quadrants. One of the most challenging tasks is to incorporate the CCD camera into the calibration procedure for aligning quadrants. The camera will need to be able to grab the image of the dots produced by the laser on a target and compare their actual position to their desired position. Then the software will need to make appropriate corrections to the calibration look up table. When the same target is shot from a different quadrant it will have to coincide with the mark produced by shooting from the center of a previous quadrant. The software will need to remember which mark represents the result of which shot.

Calibration Software Development

Z-Axis Calibration

In order to achieve proper focal distance within a large scanning field, one needs to change the location of the Z lens of the scanner in correspondence with the current position of the turning mirrors. Without calibration of the Z lens location relative to the mirror positions, the line width of the laser path varies as a function of position in the 10"x 10" scan field. This anomaly results in the width of laser cuts in material varying in different regions of the LOM build envelope. The GS scanner control software as supplied by the vendor contains a Z-axis lens look-up table (LUT) to accomplish this goal. This vendor supplied Z-axis lens calibration, though, was found to be less than satisfactory, especially at the edges of the 10" x 10" scan field. Precise z-axis lens calibration is especially critical at these edges for successful alignment of adjacent quadrants.

A new calibration look up table was developed to extend the accuracy of the Z -axis lens correction over the full 10"x 10" scan field for each quadrant of the build envelope. To develop

the new LUT an improved mathematical model was formulated relating the Z-axis lens position to other scanner geometric properties/constraints. The following geometric equations were developed to determine the coordinate for the Z lens relative to these other scanner parameters:

$$\text{Corr} = L_0 - k * (L_1 + L_2 - D_x)$$

$$L_0 = 65535$$

$$L_1 = (D_x - D_y) / \cos(\alpha_x)$$

$$L_2 = D_y * (\text{SQRT}(1 / \cos(\alpha_x)^2 + \text{tg}(\alpha_y)^2))$$

Where:

Corr – correction for the absolute coordinate of a Z lens

L0 – max. travel of a Z lens

L1 – length of the beam path between the X and Y turning mirrors. (It changes in accordance with the X mirror angle)

L2 – length of the beam path between the Y mirror and given point on the scanning field.

Dx – distance from X turning mirror and scanning field.

Dy – distance from Y turning mirror and scanning field.

$\alpha_{x,y}$ – angle of the corresponding turning mirror.

Using the above model, the Z-axis lens position look-up tables were calculated for each quadrant. Figure 3.2.2-3 displays for one quadrant a plot of the required Z-axis lens position relative to the scanner X and Y mirror steps or positions (Note: the X and Y axes are multiplied by 1000). Figure 3.2.2-4 shows the offset between the newly calculated Z axis lens LUT positions and the original LUT values supplied with the scanner. The considerable variation in accuracy at the edges of the scan field is clearly evident. The new LUT's making it possible to implement the Inter-Regional Calibration routine now compensates for these discrepancies.

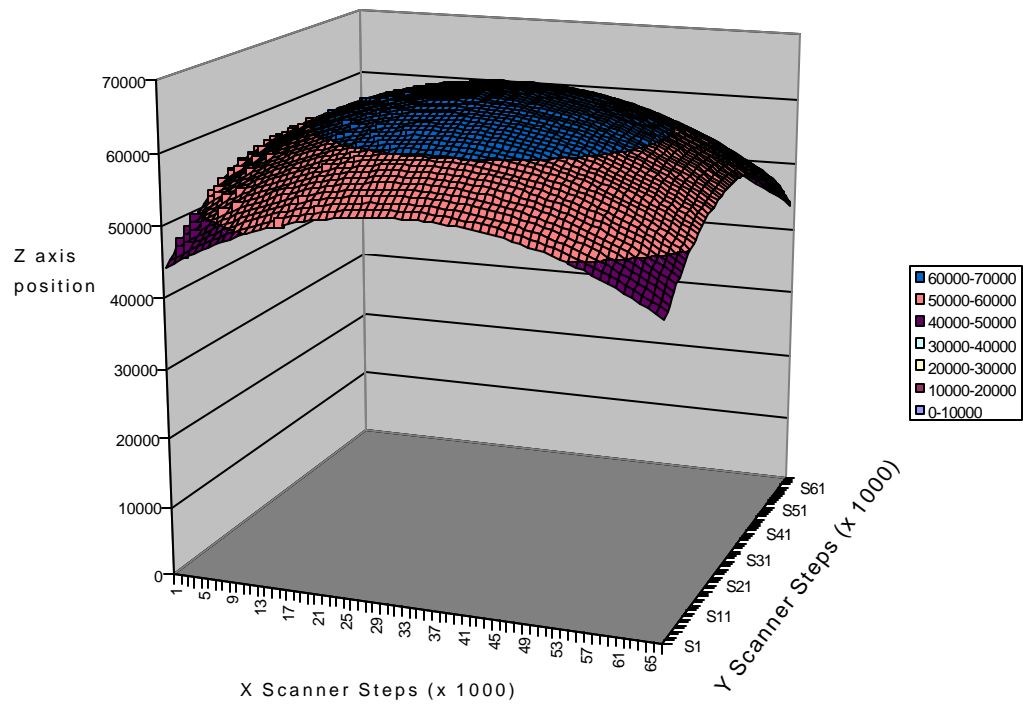


Figure 3.2.2-3 3D representation of the calculated Z-axis Look Up Table.

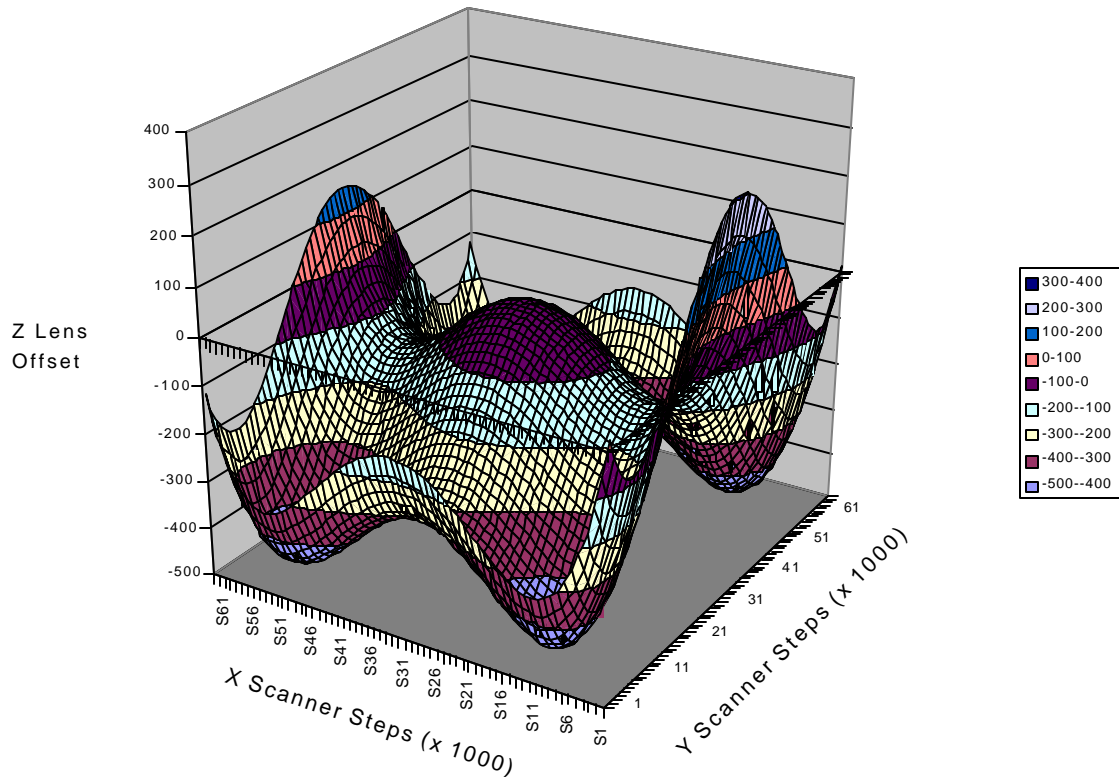


Figure 3.2.2-4 Difference between calculated and original Z-axis lens Look-up Table.

CCD Camera based Scanner Calibration

The DVT video system software and firmware packages allow one to program the unit to perform automated image recognition, which in our case entails finding traces of laser shots made into a white sheet of paper at specified quadrant boundary locations. The shots are produced by pulsing the laser at low power at a single scanner position such that the paper is only slightly singed (discolored) and not cut through. The camera sees these shots as dark spots roughly 0.010-inch in diameter. The entire LOM build envelope of 20x30 inches has been divided into 6 main quadrants (0 thru 5 in Figure 3.2.2-5) and 3 overlapping quadrants centered down the middle of the platform (6 thru 8 in Figure 3.2.2-6). Each quadrant contains a 5x5 array of look-up points. The control points are located at the grid intersections and the corners of this array (see Figure 3.2.2-6).

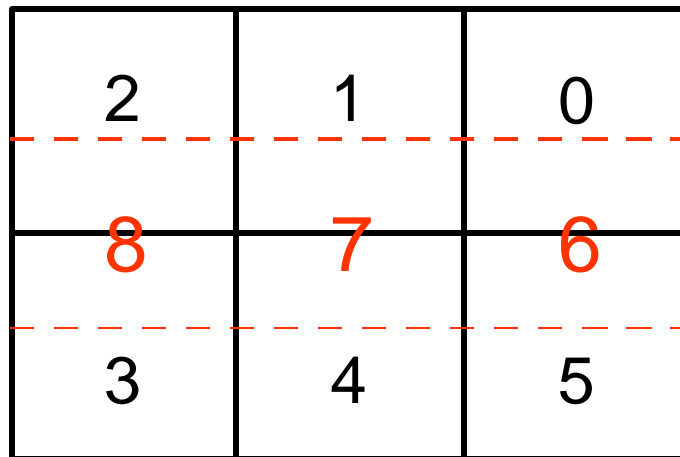


Figure 3.2.2-5 Division of the working field into quadrants.

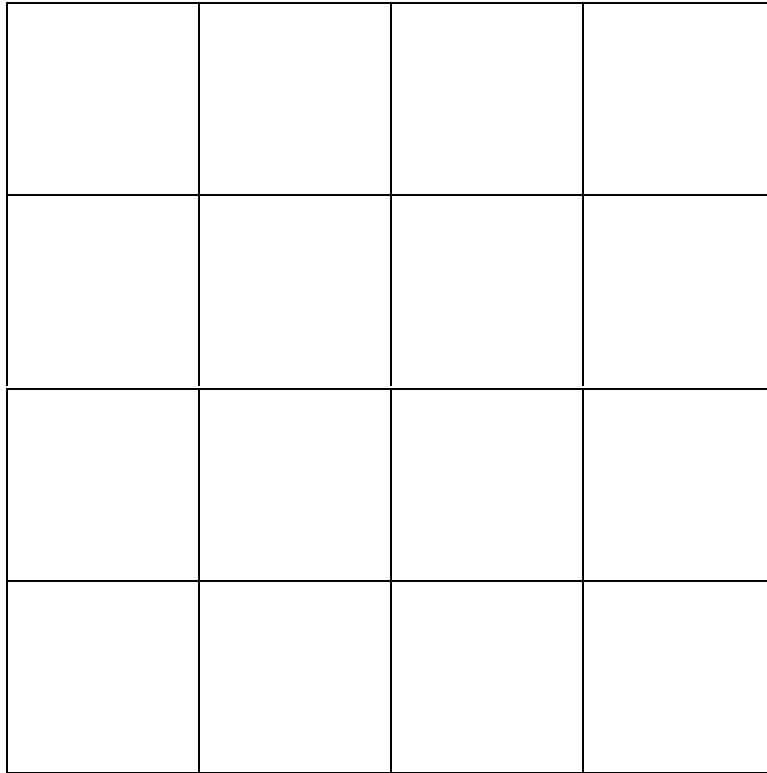


Figure 3.2.2-6 Division of a quadrant into 5x5 array of control points.

Figure 3.2.2-7 shows a screen image of the new user visual interface dialog box developed in LOMSlice which allows the operator to choose the quadrant in which to perform the calibration, set the scanner calibration parameters, and view the laser shots images collected by the CCD video system. Figure 3.2.2-8 displays a typical laser shot profile collected from one quadrant of the LOM build envelope. Red point calibration positions (two shots per lookup point per quadrant) are intentionally deviated from the origin lookup points

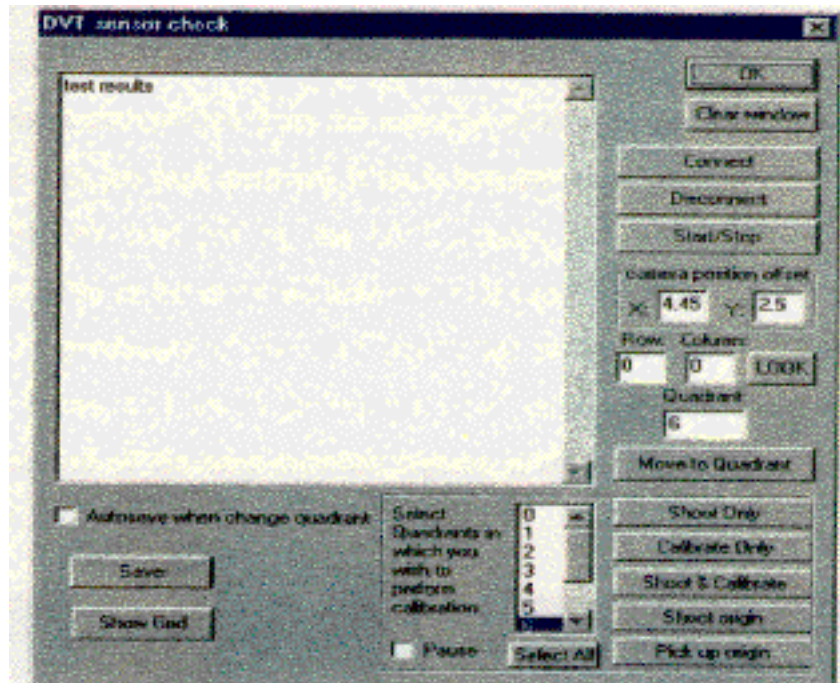


Figure 3.2.2-7 Visual Interface Dialog Box for scanner calibration.

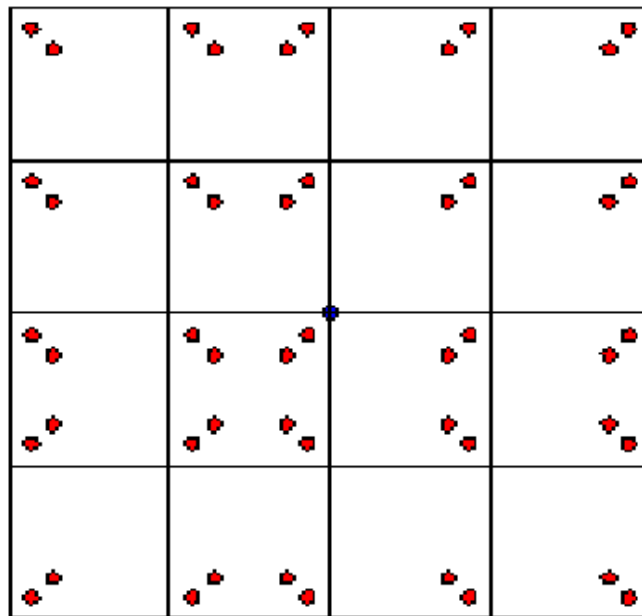


Figure 3.2.2-8 Image of target calibration points shot by the laser into one quadrant.

located at the corners of the grid location. The eventual position of the control point is extrapolated from the locations of the two red points located near each corner. One shot, per each quadrant, is made into the middle origin point. The coordinates of this point are recorded by the DVT camera and served as the camera origin coordinates. After all the shots had been made the camera is moved from one lookup point to another. Coordinates of the shot points are recorded and correction coefficients calculated. Figure 3.2.2-9 shows an example of a collected camera image of calibration points within one of the most crowded regions of the build envelope at the junction of quadrants 1,2,3,4,7,8 as viewed on the LOMSlice software screen.

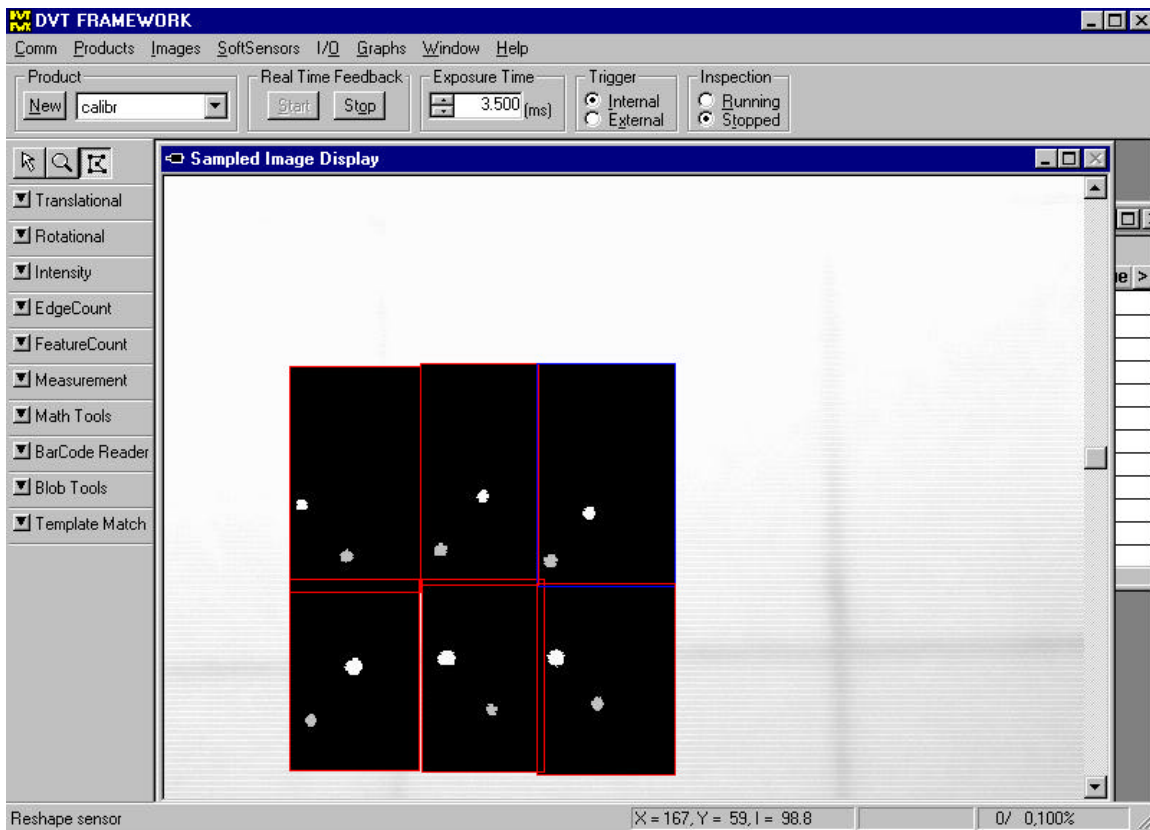


Figure 3.2.2-9 CCD camera data at the junction of quadrants 1,2,3,4,7,8.

Figure 3.2.2-10 shows a central view above quadrant number 8, which included one shot into the point of the quadrant origin. The reason why shots into every origin are avoided is due to the possibility of shots overlapping with each other and thus not being clearly distinguished.

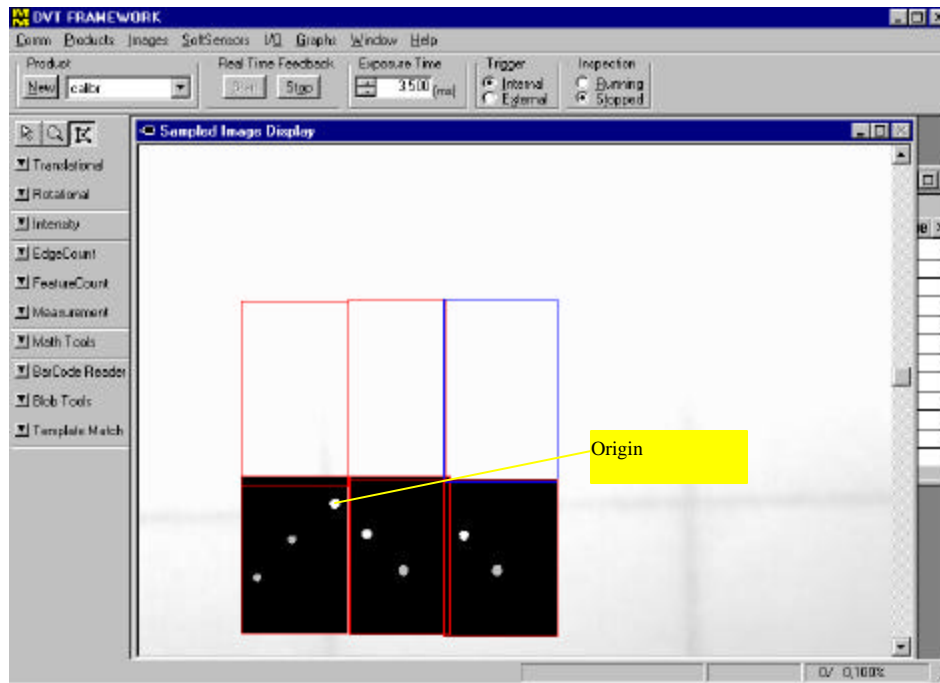


Figure 3.2.2-10 Verification of calibration by detecting the coordinate of a shot delivered into a quadrant origin.

The above calibration method allows one to achieve good matching of the quadrant edges. This success is easily verified through visual inspection of the boundary regions of grid patterns laser scribed into adjacent quadrants. The grid lines are produced similar to the calibration shots by scribing the laser scanner at low power over white paper covering the LOM build envelope such that the material is not cut but only discolored. Figure 3.2.2-11 displays grid patterns made in adjacent quadrants before the Inter Regional Automated Calibration routine was performed on the system. Misalignment is clearly shown along both the top grid and right edge grid relative to the center grid in the image. Figure 3.2.2-12 shows images of laser shots made in one quadrant during the calibration routine while Figure 3.2.2-13 that of grid lines made after the calibration was completed. No visible offset is discernible at the quadrant boundaries.



Figure 3.2.2-11 Example of grid misalignment at quadrant boundaries before Inter-Regional Calibration procedure.



Figure 3.2.2-12 Example of laser calibration shots on LOM paper used for Inter-Regional Calibration procedure.

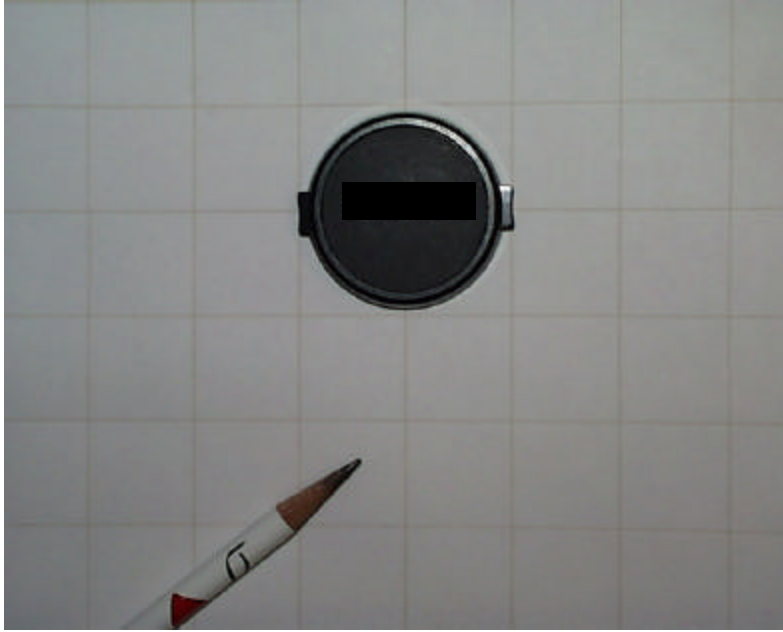


Figure 3.2.2-13 Grid alignment at quadrant boundary after Inter-Regional Calibration procedure.

The consistency of the scanner calibration procedure initially was evaluated by performing a series of laser cutting trials on successive layers of fiberglass cloth (no matrix resin). The design file for the laser cutting was a full blastshield STL model which had been generated earlier in the program. Figure 3.2.2-14 displays a series of images of the laser cutting of one layer of cloth in which the scanner is translated through each quadrant to complete the stiffener profile. Visual analysis of quadrant boundary connectivity after multi-quadrant laser cutting of multiple plies of the glass fabric sheets found no obvious anomalies. Quadrant calibration was considered satisfactory for fabrication of the full size Nextel™/Blackglas™ laminate required to form the blastshield demonstration component.

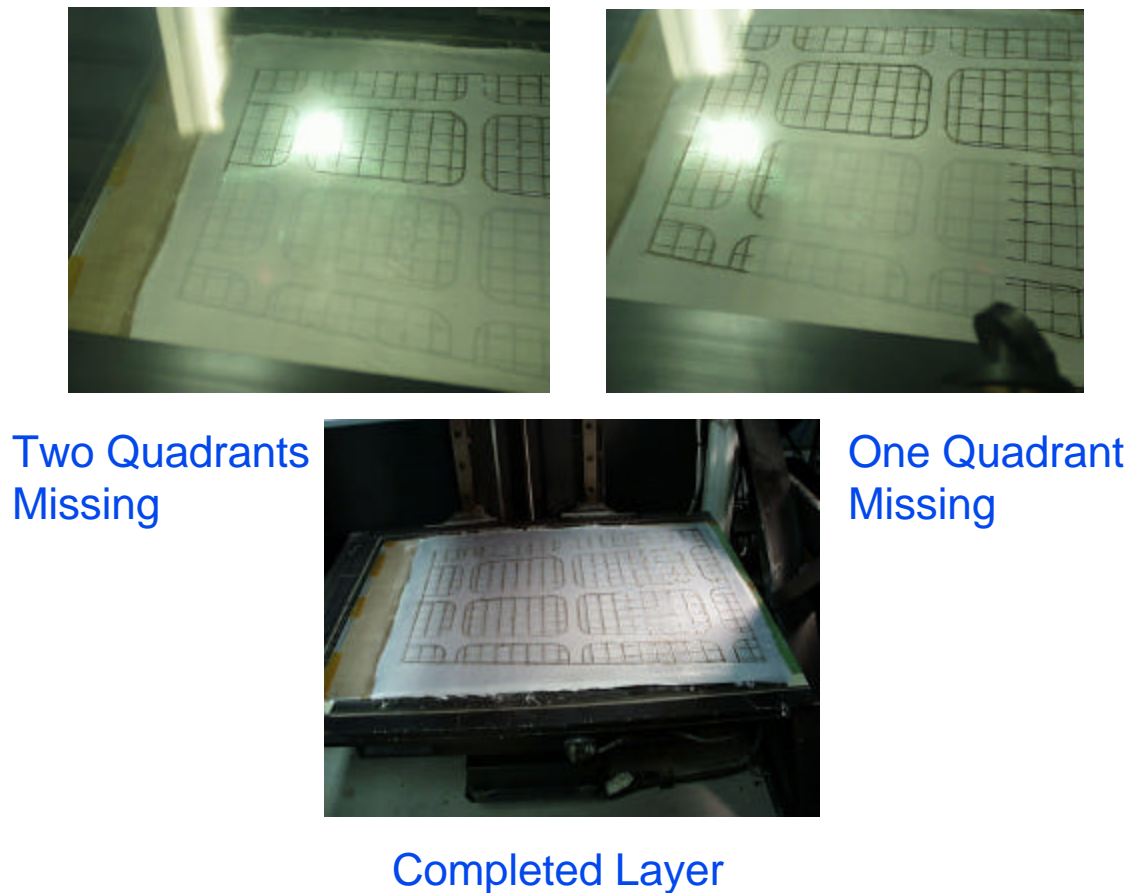


Figure 3.2.2-14 Multi-quadrant laser cutting evaluation on glass fiber fabric after Inter-Regional Calibration procedure.

Initial experiments evaluated visual methods for inter-quadrant scanner calibration. A manual, visual calibration procedure first was developed. However, this method proved quite labor intensive with too many time consuming steps. In order to automate the calibration process it was decided to use a new, industrial type CCD video camera system developed by DVT Corp. DVT's SmartImage sensors are compact (1.5" x 3" x 5"), complete image analysis units that incorporate all imaging elements including CCD camera, image-acquisition electronics, and computer into one package.

The CCD-based sensors capture images similar to that of a video camera. The resulting image is then processed in the system's internal processor, which is co-located directly with the CCD chip. A user simply teaches the system what to look for using a Windows-based interface and then the system stores those parameters and reports its findings to the control system. The

sensor achieves a high level of stability for reading each individual pixel element of the CCD, which allows for direct analysis of feature characteristics such as size, orientation, and feature position relative to other features.

The main advantage of this latest CCD imaging technology is that it eliminates the signal conversion electronics, fixed frame rates, and limited gray-scale quantization of traditional machine vision systems. The CCD cameras unique image acquisition design allows dynamic access of the charge -coupled device with no horizontal image jitter. Dynamic image acquisition is accomplished by transferring the image of the CCD directly into the memory (RAM) of the embedded microprocessor. Horizontal jitter in frame grabber based vision systems can result in image movement of more than ten times the desired accuracy for an inspection. This can result in distorted geometric shape recognition and position offsets as well as poor repeatability of performance. The direct, digital image acquisition method utilized in the SmartImage Sensor also captures images to 256 gray scale levels compared to a limited 64 gray scale used by most machine vision systems complying to the RS-170 standard. In addition to providing measurement precision to 1/2000 of the field of view, the system can track and measure a moving part up to 360°, count features of a specified size, store and manage hundreds of image files, and read 2D matrix codes. It supports SPC and motion control interfacing and inspection rates of 4000+ images/min., with no need for a dedicated PC during operation.

A DVT CCD camera was integrated with the scanner assembly to assist with the calibration of the working field of the system. Figure 3.2.2-15 displays the location of the installed DVT CCD Imaging System on the scanner gantry. Due to the mechanical constraints the camera view was rotated 90 degree CW relative to the XY plane. The maximum view field provided by the camera is 1 x 1 inch. The DVT camera provides 243 x 324 pixel image over this 1"x 1" area. The position of the camera was adjusted to cover all quadrants of the system's motion. An RS232 communication link also was established between the DVT sensor and the LOM 2030H computer. The DVT software and firmware packages permits one to easily program

an automated image recognition routine, which for our particular application entails locating and recognizing traces of laser shots into a white sheet of paper. The image acquisition functions

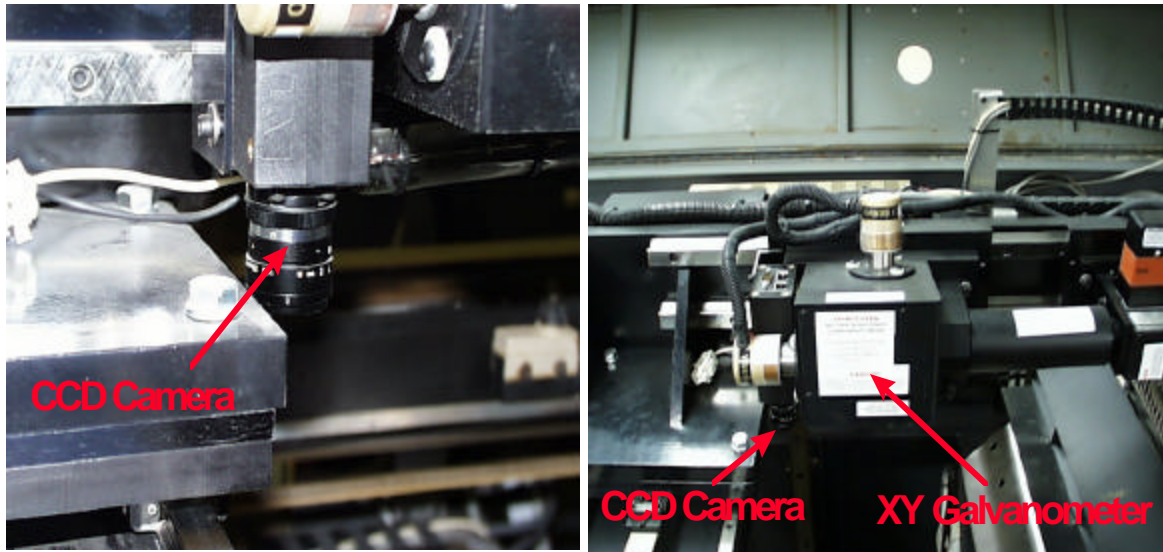


Figure 3.2.2-15 DVT CCD camera system mounted on scanner gantry

for this procedure were written into the software responsible for the calibration of the scanning quadrants and a sophisticated calibration software routine that aligns the peripheries of scanning quadrants was also implemented.

Fiber Orientation Mechanism

A rotary table needed for orientation of composite layers was installed on the LOM unit, interfaced with a stepper motor, and provided with an upper plate for carrying the composite stack during the building of the flat laminate. Software was created that generates an interface between the LOMNEF file format and internal operations of the LOMSlice 2.0 program. The code automatically recognizes the LOMNEF format and uses it in the multi-quadrant mode. A user visual interface was created in LOMSlice that shows the specific LOMNEF defined plies on the screen (and its required orientation) as they are being produced. Software was also devised which generates a circular rather than square boundary around the part and that enables laser cutting of separate sections of the circle that are located in different quadrants.

To demonstrate the fully automated lamination, fiber orientation, and multi-quadrant laser cutting of a fiber reinforced material, a polyethylene backed fiberglass fabric was prepared for use on the LOM scanner system (Note: the high cost of Nextel™ 312 fabric prohibited its use for such a demonstration). A two mil thick layer of polyethylene was thermally bonded onto a 100' long x 30" wide roll of fiberglass fabric and installed on the LOM scanner system. Using the thermal roller on the system for lamination, a 0.5x scaled version of a 0°/45°/90° cruciform stiffened blastshield was LOM fabricated from the fabric using a LOMNEF design file. Figure 3.2.2-16 displays assorted images taken during the fabrication of the fiberglass part.

Figure 3.2.2-16a shows the heated roller bonding the fiberglass fabric onto the underlying ply on the build layer. Figure 3.2.2-16b displays the multi quadrant laser cutting of the circular boundary around the part for the ply. Figure 3.2.2-16c and -16d show the final laser cut ply patterns for a layer which just has been rotated into position for bonding of (c) a + 45° orientated and (d) -45° oriented ply. After careful adjustment of fabric tension, heater temperature, and roller speed, multiple plies were successfully laminated, rotated, and laser cut in an automated

fashion to build the total fiberglass ply stack. Figure 3.2.2-17 exhibits the final, LOM fabricated fiberglass blastshield after decubing.

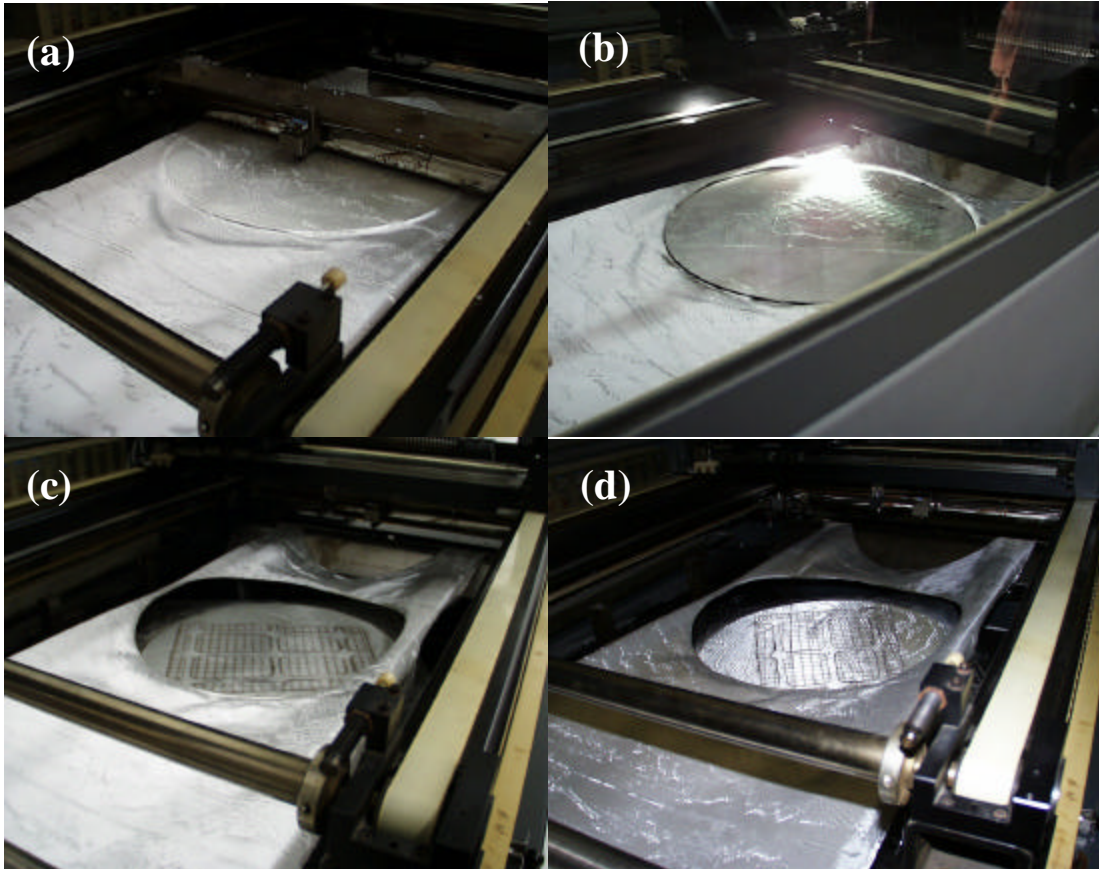


Figure 3.2.2-16 Processing steps for LOM fabrication of half scale fiberglass blastshield laminate: a) lamination of fabric with heated roller, (b) multiquadrant laser cutting of part circular boundary, (c) $+45^\circ$ rotation of ply stack, d) -45° rotation of ply stack

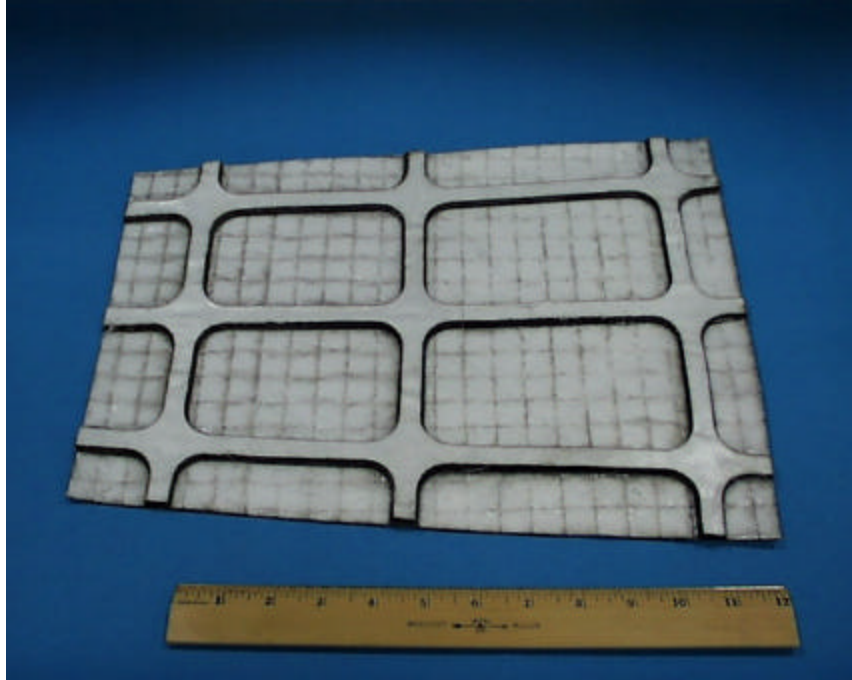


Figure 3.2.2-17 LOM fabricated half scale, fiberglass blastshield laminate after decubing

Laser Scanner Cutting Evaluations

A series of laser cutting tests were performed on NextelTM/BlackglasTM prepreg sheets using the prototype scanner system. An initial series of tests utilized the scanner system with the stationary 100W Synrad laser configuration. The experiments were repeated using the 200W Coherent laser after its installation on the unit. Cutting evaluations were performed on single sheets of dry NextelTM 312 fabric, dry fabric with applied tackifier, standard resin content NextelTM/BlackglasTM prepreg (45% resin by weight) and a low resin content prepreg (22.5% resin by weight), both with and without the application of tackifier to the bottom surface of the ply. Both straight and corner cuts were evaluated.

For all cutting tests the laser power was held constant at maximum power while the scanner velocity was varied for each cut. Due to power losses from the scanner optics the maximum power delivered to the samples was typically 85 watts for the Synrad laser and 153W for the Coherent laser. The range of scanner velocities evaluated was from a minimum of 18 mm/sec to a maximum of 576mm/sec (the scanner controller increases scan speed in increments of 9 mm/sec). Typically, for scanner speeds above 63mm/sec multiple laser passes were required over the ply before the sheet was totally cut through. On average 4 passes were required for scan speeds up to 135 mm/sec and as many as 20 passes for the maximum velocity of 576mm/sec.

Figure 3.2.2-18 displays photomicrographs of two corner cuts made in single sheets of NextelTM/BlackglasTM prepreg using the prototype scanner with the Synrad laser. Uniform kerf widths are maintained through the entire length of both types of cuts with no indication of excessive char build-up around corners as found with the earlier 2030E curved LOM system. The corner edge retention in the high-speed 90-degree cut clearly shows the advantage of scanner-based cutting versus the previous x-y gantry based method.

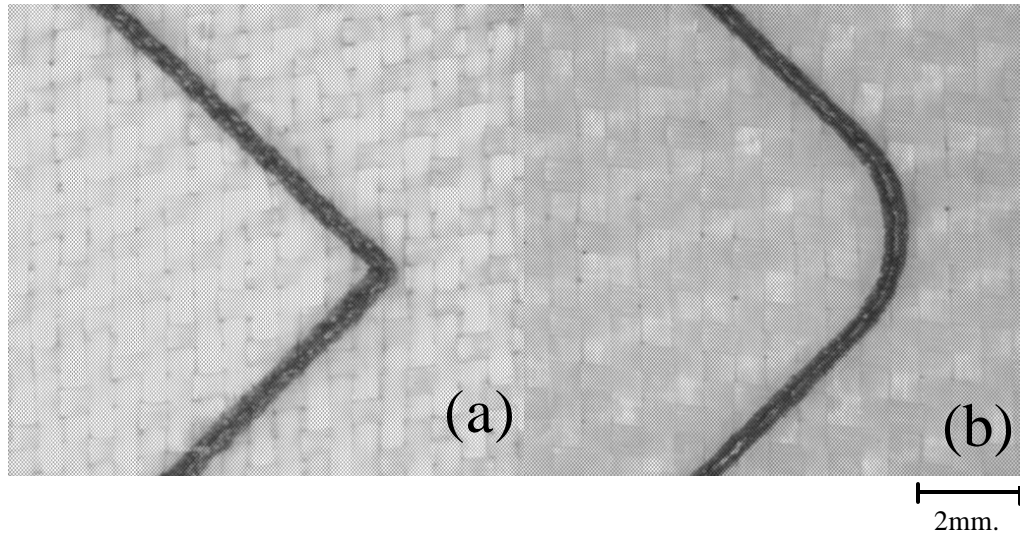


Figure 3.2.2-18 Corner cuts in Nextel™312/Blackglas™493AB prepreg sheet utilizing laser scanner on LOM 2030H prototype unit: (a) 90° corner, (b) .0625" corner radius

For the scanner system it was also found that for a fixed laser power both the width and char zone along a laser cut was significantly reduced at higher scan velocities. Figure 3.2.2-19 displays photomicrographs of laser cuts in 45%resin content Nextel™/Blackglas™ prepreg utilizing a scanner speed of 18, 36, 81, 135, 270 and 576 mm/sec and maximum laser power of 153W (Coherent laser). In general, for both laser power settings, 83W (Synrad laser) and 158W (Coherent laser), increased scan speed resulted in narrower laser cuts decreasing in width from a maximum of 400 microns at 18mm/sec to roughly 100 microns at 576 mm/sec.

The perimeter of the laser cuts at low scan speeds were scattered with 100-200 micron diameter spherical droplets that decreased in size with increased scan speed to a diameter of 20-50 microns. The spheres also increased in density along the perimeter of the cut with increasing cutting speed. Though the char zone was also significantly reduced at the higher cutting velocities, the width of the laser cut became increasingly non-uniform. The sidewalls down through the cut also became irregular at these speeds. A large portion of this visual effect, though, can be attributed to both the kerf width approaching that of the fabric tows and the increased density of smaller spheres along the edges of the cut producing a somewhat jagged appearance.

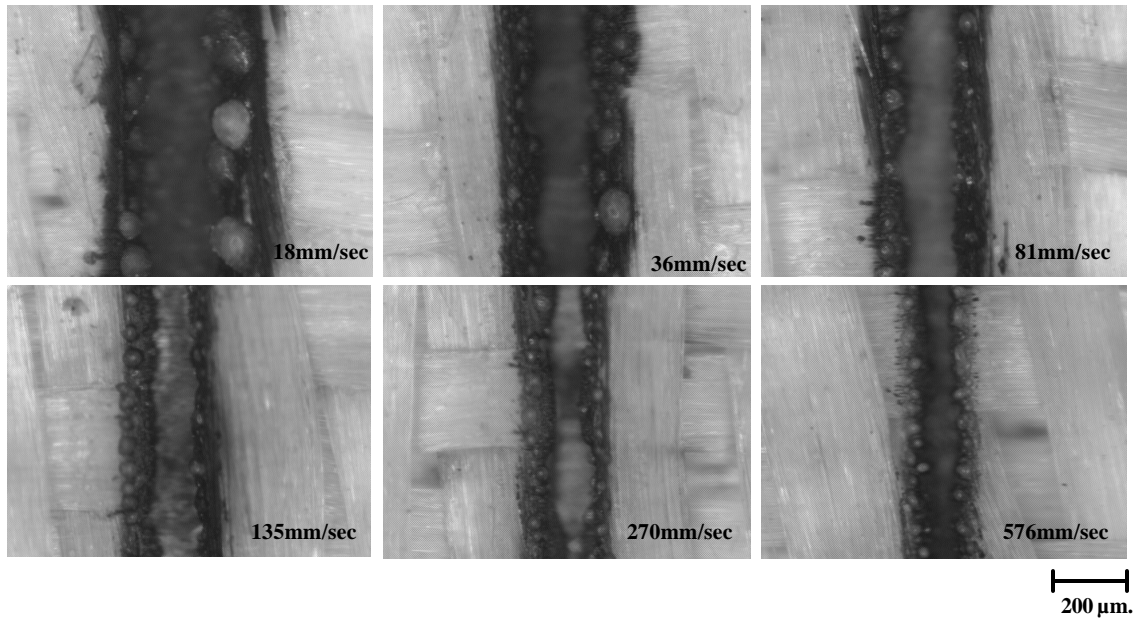


Figure 3.2.2-19 Laser cutting tests at various scanner velocities in 45% resin content Nextel™/Blackglas™ prepreg

Figure 3.2.2-20 shows laser cuts in standard resin content prepreg sheets taken at roughly the same scan velocity but with different laser and laser power settings. Figure 3.2.2-20a displays an incomplete cut made with three passes at 126mm/sec using the Synrad laser at 84.6W. Figure 3.2.2-19b shows a complete laser cut made with three passes at 135mm/sec with the Coherent laser at 153W. As expected, for a given scan velocity fewer laser passes were required to cut through a single prepreg sheet at the higher laser power. More importantly, the cuts made with the higher power Coherent laser exhibited greatly reduced char zones and density of remelt spheres as well as straighter wall profiles through the cut when compared to those made with the Synrad laser.

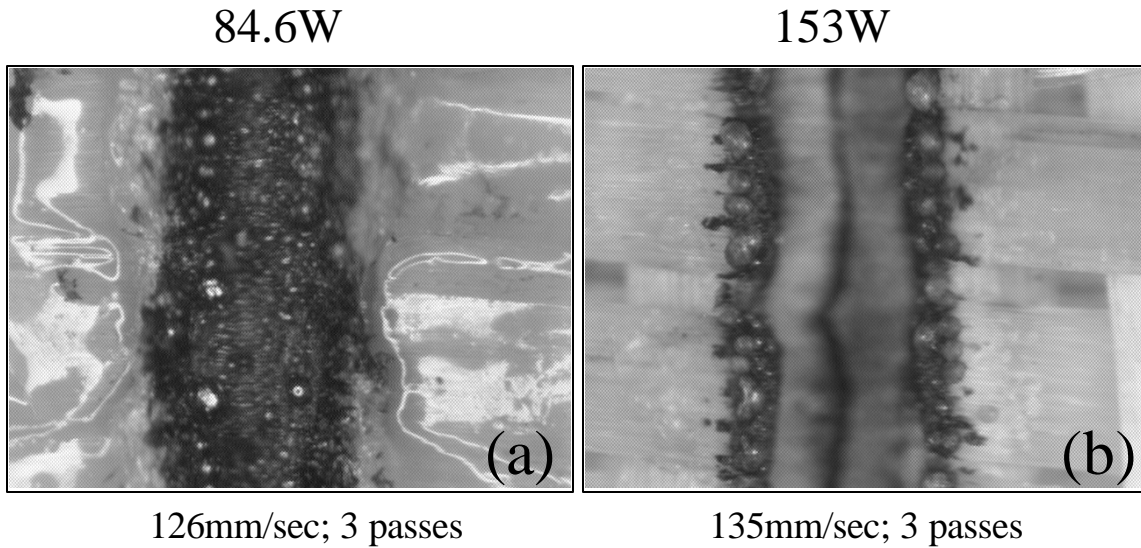


Figure 3.2.2-20 Laser cuts made in standard resin content prepreg with (a) Synrad and (b) Coherent laser.

The black char along the edge of the cut became more pronounced with each successive laser pass. This effect is displayed in Figure 3.2.2-21 for four consecutive cuts made in the 45% resin prepreg at 270mm/sec and 153W in which the progressive charring along the cut becomes evident as the ply is sliced through. A portion of this increased char can be attributed to the tackifier layer on the underside of the ply. This is borne out in another series of laser cutting experiments on dry fabric with and without the application of a tackifier layer and also on prepreg sheets without tackifier. These studies indicate that to a large degree the black residue remaining along the edge of a laser cut is generated from the pyrolysis of the thin tackifier layer bonding the ply to the platform. It is likely the ejected laser plume contains pyrolysis residue from the tackifier that coats the above sidewalls and spherical particulates as it exits from the laser cut.

The increased generation of char with successive laser passes, though, is also observed during laser cutting of prepreg sheets that contain no tackifier. Figure 3.2.2-22 displays four successive laser cuts in a 45% resin prepreg sheet whose underside has not been coated with tackifier. The progressive increase in char as the ply is cut through is also evident (but to a lesser

degree). One possible explanation is that the resin in the fabric is not evenly distributed through the ply's thickness. When the ply is first attached to the metal support on the LOM build platform a large portion of resin in the fabric might wet out to the bottom surface of the ply. The top surface would be relatively resin poor and not generate as much charring along the laser cut. More charring results as successive laser passes reach the bottom "resin rich" portion of the ply. Laser cutting evaluations on multiple ply layers need to be performed to further study this effect.

Comparison of laser cuts generated with the high power laser on the standard and low resin content materials (without tackifier) found a lower level of black char along the laser cut for the 22.5% resin prepreg over the range of scanner velocities. The density of resolidified spheres, though, was similar. This suggests that the spheres result largely from the resolidification of melted alumina fibers along the edge of the laser cut. This is borne out in laser cuts made in dry Nextel fabric which have similar sized edge features though they are not as spherical as those found in the prepreg samples. Also, the resolidified material typically formed bridges between the opposite edges of the cut in the dry fabric, which was not seen in the prepreg materials. This suggests that the resin component contributes to producing a cleaner cut in the prepreg. As found in earlier laser cutting studies, no black char is generated during cutting of dry Nextel fabric. The variation in char between the standard and low resin content prepreg was not as evident in the samples that also contained a tackifier layer. Any variation is difficult to gauge, though, as the char zone is considerably reduced using the higher power laser and is likely dominated by the laser cutting properties of the bottom tackifier component.

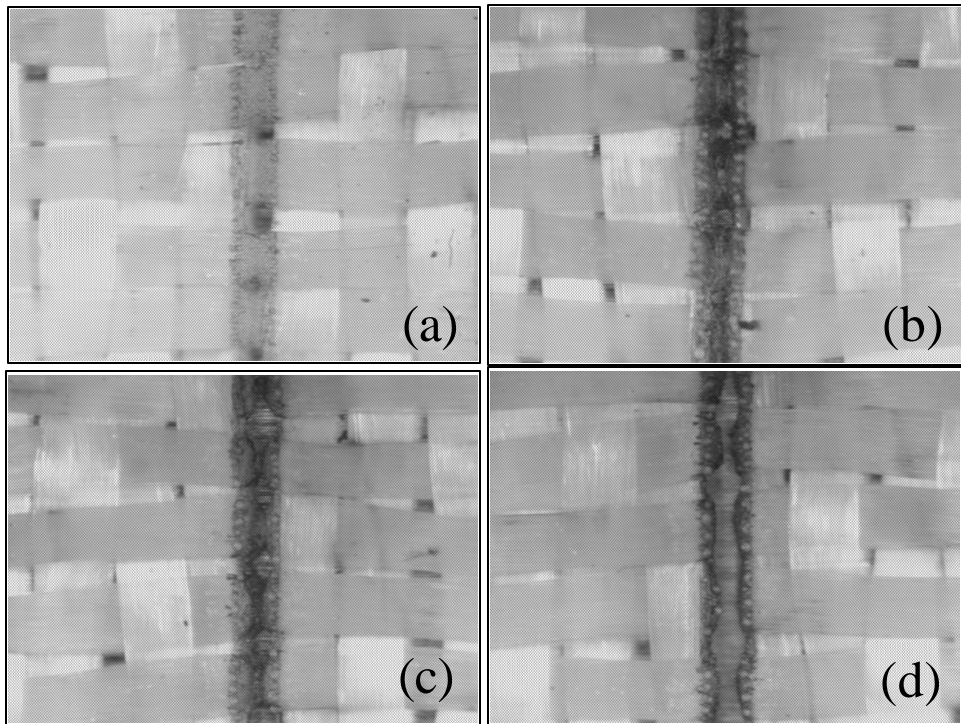


Figure 3.2.2-21 Multiple scanner passes in Nextel™/Blackglas™ prepreg (45% resin content) with tackifier: (a) first pass, (b) second pass, (c) third pass, (d) fourth pass

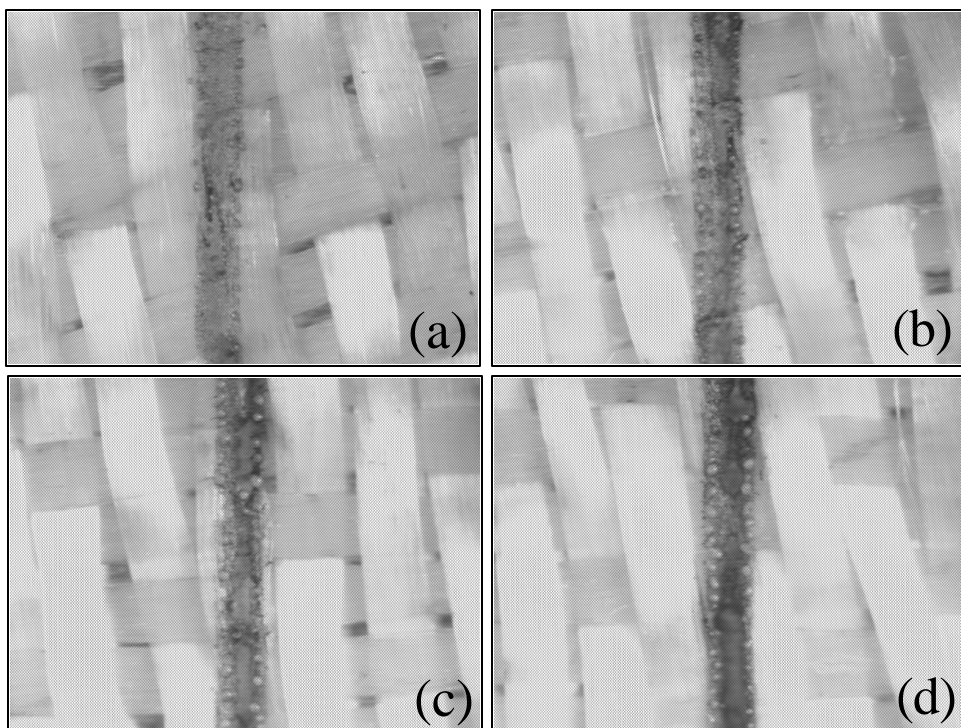


Figure 3.2.2-22 Multiple scanner passes in Nextel™/Blackglas™ prepreg (45% resin content) without tackifier: (a) first pass, (b) second pass, (c) third pass, (d) fourth pass

Subsequent to the above laser cutting studies, a new GS laser scanner was acquired for the project and incorporated into the LOM/Forming system. This new laser scanner design eliminated many of the drawbacks of the older model unit being utilized. It has a different layout for the electrical control modules, which are positioned directly on the scanner head assembly. This led to less electrical interference affecting the device and resulted in a smoother scanning pattern. The new scanner also allowed the full power range of the Coherent laser to be utilized for laser cutting of composite materials. Based on the laser cutting results described above it is anticipated that further improvements in laser cut quality will be achieved for NextelTM/BlackglasTM prepreg used to fabricate the final demonstration component with the higher laser power available.

In summary, the quality of the laser cuts in NextelTM/BlackglasTM prepreg material can be greatly improved by operating the scanner system at the highest available laser power and scanner velocities. Multiple laser passes, though, are required to completely cut through a single ply with increasing scanner velocity. The drawback of this cutting approach is that the part build time increases substantially; especially when high scanner velocities are used which may require up to 10-20 passes for complete cutting. For a fairly large or intricate part (which might be fabricated using an out-time limited thermosetting composite system) an extended build time might be unacceptable. Based on build time measurements from initial LOM fabrication trials of an 8"x 8", 32 ply cruciform stiffened subcomponent panel, an estimate can be made of the time required to generate the full blastshield. These estimates indicate that by using a scanner setting requiring a maximum of four cutting passes, the full blastshield can be fabricated in well under the 20 hour out-time limit for the BlackglasTM 493A/B resin system.

3.2.3 LOM System Demonstration

The overall objective of this task was to use the subcomponent design descriptions generated in Task 1.1.3 (Design Methodology Validation) to fabricate increasingly complex CMC sub-elements from the optimized NextelTM/BlackglasTM prepreg and low cost tooling materials developed in Task 1.2.1 (LOM Materials Development) utilizing the hardware and software upgrades incorporated on the LOM system in Task 1.2.2 (LOM System Development). The following task was performed in an iterative fashion with several series of subcomponent panels LOM fabricated and characterized in conjunction with progressive hardware and software upgrades to the LOM system.

An initial series of 4"x 4", 10 ply NextelTM 312/BlackglasTM 493A/B panels were fabricated with and without the application of tackifier and either hand cut (control) or laser cut with the LOM system to serve as a materials properties baseline for future process development activities. All the panels were then post processed through the same number of pyrolysis/re-infiltration cycles to determine the critical effect of both process variables on CMC quality. The objective of the study was to elucidate the influence of several specific LOM process variables on sample post processing (pyrolysis/re-infiltration cycle) behavior, CMC microstructure, final CMC mechanical properties, and scanning electron microscope (SEM) fractography. Test specimens were prepared from the final CMC panels and their flexural mechanical properties measured as well as fracture surfaces analyzed with SEM. Polished cross-sections of the test specimens were then prepared and microstructures examined.

Table 3.2.3-1 displays the process variables and mechanical test results for the initial flat panels. The overall measured modulus of the laminates laser cut on the LOM system was lower than that for the samples built from plies which was cut by hand. It would seem unlikely that the laser char zone along the edge of the panels would influence the flex results as the mechanical test specimens were cut from the samples far from the edge. One possibility is that a combination of excess tackifier and improper lay up procedure contributed to the lower values of modulus for

the laser cut samples. A more consistent method of tackifier application was implemented to improve the mechanical properties of the panels..

Figure 3.2.3-1 displays the fracture surface from a flex specimen prepared from Panel 990203. The fracture surfaces of this specimen showed fiber pullout behavior and distributions of fiber fracture lengths similar to those obtained from other Nextel™312/Blackglas™ 2D composites produced by Northrop Grumman.

Panel ID	Cutting Method	Tackifier ?	Specimens Tested	Peak Stress (KSI)	Modulus (MPSI)	% Strain (%)
021799-1	Hand	No	2	36 (0)	10.6 (0.1)	0.4 (0.0)
021799-2	Hand	No	2	32 (0)	10.6 (0.1)	0.3 (0.0)
021799-3	Hand	Yes	2	39 (2)	10.4 (0.4)	0.4 (0.0)
0990202	Laser	Yes	2	33 (0)	8.9 (0.2)	0.4 (0.0)
0990203	Laser	No	2	29 (1)	9.3 (0.3)	0.4 (0.0)
0990208	Laser	Yes	2	33 (0)	8.9 (0.2)	0.4 (0.0)

Table 3.2.3-1 Mechanical test results for Nextel™/Blackglas™ panels

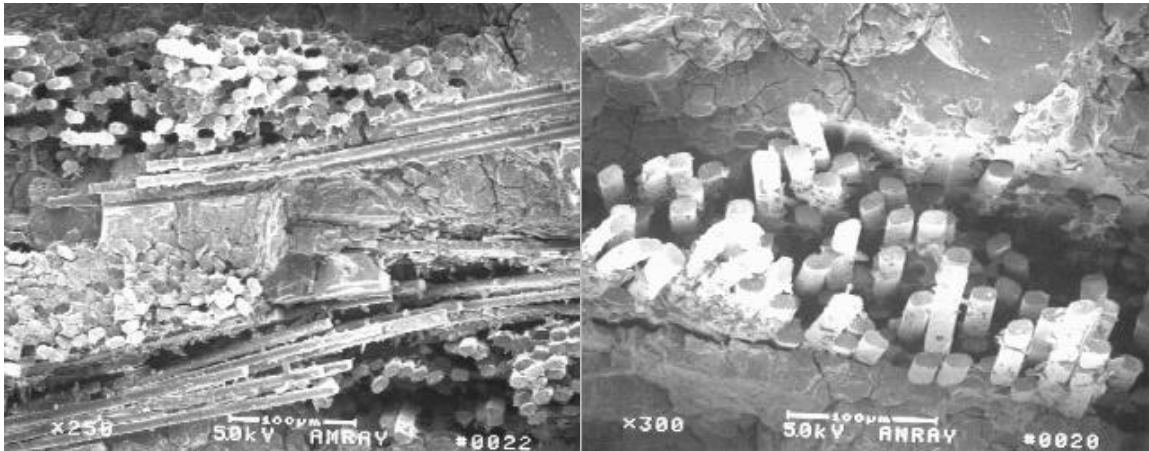


Figure 3.2.3-1 SEM photomicrographs of fracture surface of Nextel™ 312/Blackglas™ panel LOM 990203

Figure 3.2.3-2 shows the microstructure of Panel LOM 21799-3 which is similar to that obtained from other 2D Nextel™/Blackglas™ CMC materials prepared by Northrop Grumman, as

expected. All panels exhibit dense nesting of plies and porosity levels consistent with the baseline Nextel™ 312/Blackglas™ 312 CMC system.

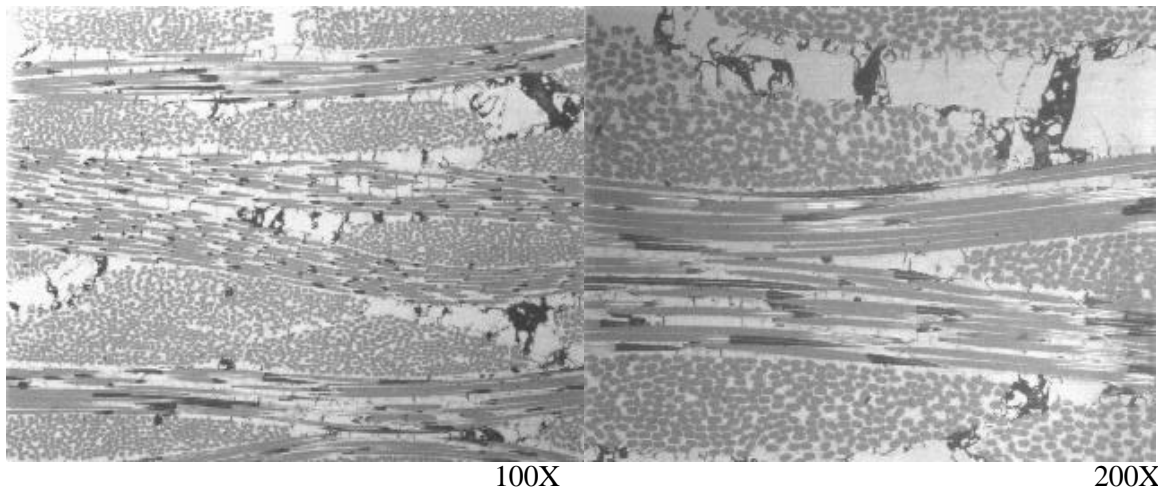


Figure 3.2.3-2 Photomicrographs of microstructure of Nextel™ 312/Blackglas™ panel LOM 21799-3

CMC Subcomponent Panel Fabrication & Characterization

The first series of subcomponent panels (for which the LOMNEF data files were described in section 3.1.4) were fabricated on a conventional (gantry based) LOM system equipped with a Synrad 200W pulsed CO₂ laser. Subsequent sub-element panels were fabricated on the scanner based LOM system through progressive machine improvements. The initial series of flat and curved Nextel™/Blackglas™ sub-component panels consisted of a 4"x 4" flat and curved panel, a flat and curved panel with a single stiffener, a flat and curved panel with a cruciform stiffener, and an 8" x 8" flat and curved panel with a cruciform stiffener. All files were composed of 32 plies in 0°, 45°, 90° orientations. The crosshatch dimensions in the design files, though, needed to be increased (from 0.2"x 0.2" to 0.5"x 0.5") as delaminations occurred during laser cutting in the decube regions at the smaller crosshatch dimensions.

Flat Panel Fabrication

All flat panels were fabricated on metal plates that were attached to the LOM platform with tape. This allowed the uncured laminates to be easily removed from the LOM unit and cured off-line. To help reduce the amount of potential laser cutting damage to the ply drop off regions of the stiffener elements, the flat panels were fabricated upside-down on the LOM platform. In this manner any material damage to the region beneath the top ply being laser cut will be in an area which will later be removed during decubing (see Figure 3.2.3-3). The design files for the flat and curved panels initially incorporated crosshatch dimensions of 0.2" x 0.2". In the course of fabricating the panels on the LOM unit it was determined that the close spacing of the cross-hatch regions contributed to additional charring along the laser cut, delamination of individual decube regions, and also significantly increased the part build time.

The reason for the excess charring was likely due to the fact that as the number of laser cuts during part fabrication increases a greater amount of laser power/energy is dissipated into the material. The laser energy causes the local region around the laser cut to increase in temperature. With multiple laser cuts generated in rapid succession in close proximity, the Blackglas resin is heated substantially in the crosshatch regions resulting in excess material damage and delaminations. To remedy this problem the remaining part design data files were modified to increase the crosshatch area to 0.5"x 0.5" (which explains the variations in cross-hatch dimensions displayed in the images of the various fabricated panels which follow). This problem was greatly reduced when greater cutting speeds became available on the LOM Scanner system.

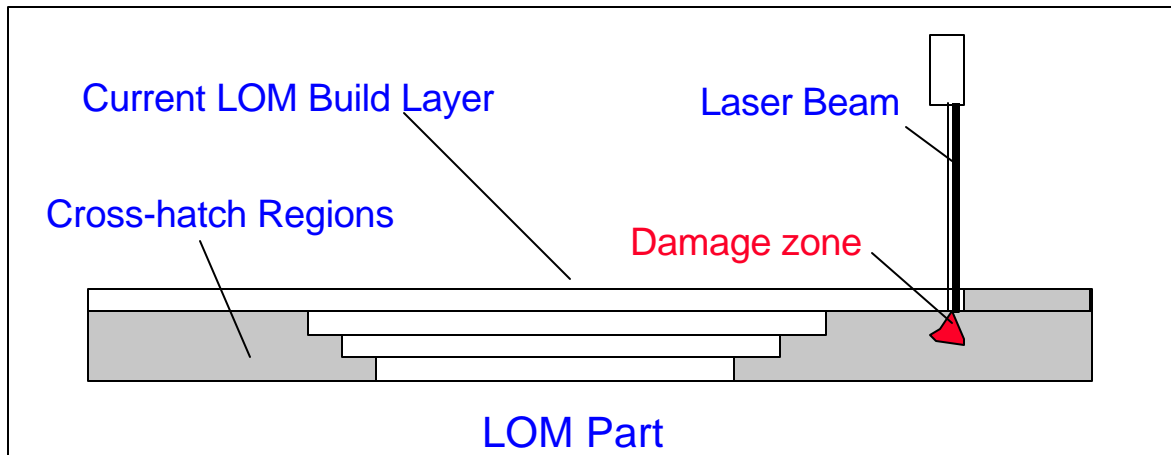


Figure 3.2.3-3 Illustration of laser cutting damage minimization through LOM fabrication of part top to bottom Curved Panel Fabrication

To fabricate the first series of curved sub-component panels a quasi LOM/Forming fabrication process was utilized. A 2mm thick sheet of silicone rubber was first attached to a metal plate with a thin layer of vacuum grease. The metal plate was next attached to the LOM build platform with tape and a mold release agent applied to the silicone rubber surface. Successive layers of prepreg were next laminated (with tackifier) onto the silicone sheet then laser cut to fabricate a flat ply stack-up. The metal plate with uncured laminate was removed from the LOM platform and the silicone sheet with laminate was detached from the metal plate by running a thin wire between the plate and silicone sheet. The silicone sheet with attached laminate was next vacuum formed over an Al tool surface and consolidated and cured in a conventional oven using standard aerospace vacuum bagging techniques (see Figure 3.2.3-4). For these initial subcomponent LOM fabrication trials, the LOM tooling materials had not yet been optimized so an Al tool was machined instead. The curvature of the Al tool surface was NC machined to represent a roughly 8" x 8" area of the full blastshield tool surface and to also incorporate the necessary edge features to the tool such that it could also be used as a part re-infiltration fixture (which required the additional machining of a matched female tool). Figure 3.2.3-5 shows the final decubed 8" x 8" curved cruciform panel before final pyrolysis/reinfiltration processing. The

other 4" x 4 " curved sub-components were cured/consolidated on the Al tool with the same procedures as described above for the 8"x 8" panel.

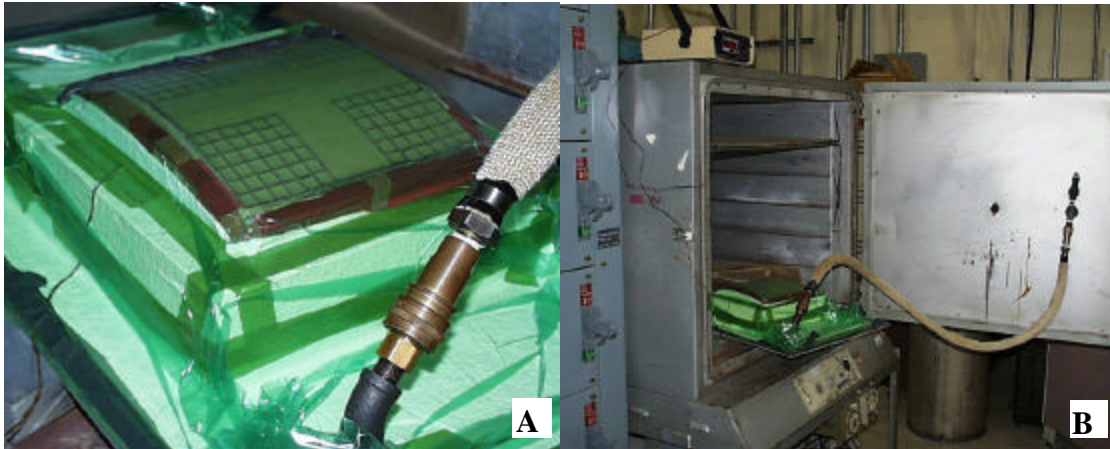


Figure 3.2.3-4 A) Uncured 8" x 8" Curved Cruciform Panel Vacuum Bagged on Al Forming Tool; B) Vacuum Curing Oven with LOM Part/Forming Tool

Pyrolysis / Reinfiltration

After consolidation/cure and decubing all panels were subjected to repeated cycles of pyrolysis and reinfiltration. During pyrolysis Nextel™/Blackglas™ parts typically need to be moderately constrained to minimize possible panel warpage. For flat panels a simple Inconel weight or lightly bolted Inconel plates are utilized. For the curved panels graphite pyrolysis tools were machined for use as constraining fixtures.

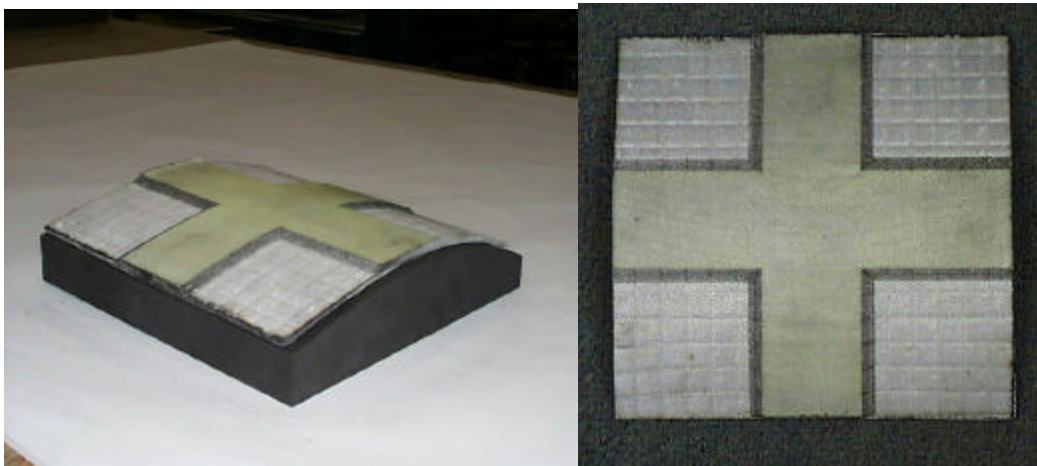


Figure 3.2.3-5 8" x 8" Curved Cruciform Panel after cure/consolidation and decubing

The thickness of the panels in the cruciform areas were much greater than that for any other NextelTM/BlackglasTM sample Northrop Grumman has pyrolyzed. The laser charring along the edges of the panels was a concern as any damage developed in this area could induce delaminations in the panel during pyrolysis. To reduce the risk of delaminations occurring during repeated pyrolysis, an optimized pyrolysis cycle recently developed and validated in the DARPA LC³ program was used for all subsequent densifications. The cycle was developed as a means to improve the mechanical properties of NextelTM/BlackglasTM panels without increasing pyrolysis-processing time. To date no panel has ever delaminated using the optimized cycle developed in the LC³ program. By using controlled heating rates and hold times over specific temperature ranges that coincide with increased evolution rates for specific gas species, panels with improved mechanical properties could be produced while reducing processing times by 50% compared to the lowest heating rates evaluated. During pyrolysis the conversion of the Blackglas polymer to a ceramic leads to the evolution of hydrocarbon gases such as methane, ethane, and hydrogen from the composite. By minimizing the outgassing rate of these volatiles both matrix microcracking can be decreased (resulting in improved mechanical properties) and potential delaminations mitigated. Decreasing the outgassing rate by simply decreasing the pyrolysis-heating rate, though, increases processing times and deteriorates the NextelTM fiber, which negatively impacts the mechanical properties and overall cost of the process.

A mechanistic model of the pyrolysis process was developed in the LC³ program, which took into account the effects of heating rates, temperatures, and temperature duration on outgassing kinetics. Using this model one could accurately predict an effective window of processing variables to optimize the properties of the final composite. The maximum rate of gas evolution of particular volatile components was found to occur over a limited range of temperatures. The model could accurately predict this temperature range and the decrease in the pressure rate due to gas evolution as a function of heating rate (see Figure 3.2.3-6). The model was validated in the LC³ program with experimental tests and proved quite accurate in predicting

measured outgassing rates as a function of heating rates and hold times. To identify an optimal pyrolysis schedule an extensive pyrolysis model evaluation matrix was designed using a Taguchi method for the purpose of identifying accelerated time/temperature cycles with low outgassing rates. Using this approach controlled heating rates over specific temperature ranges and controlled hold times (which corresponded to regions of maximum outgassing rates by specific volatile species) were identified that led to significant reductions in processing for the same outgassing rate. Figure 3.2.3-7 shows an example of one such cycle identified that was subsequently experimentally verified in the LC³ program. A similar process cycle was used for pyrolysis of the LOM sub-component panels. Figure 3.2.3-8 depicts the first series of subcomponent panels fabricated on the standard (gantry based) LOM system with a Synrad pulsed 200W laser.

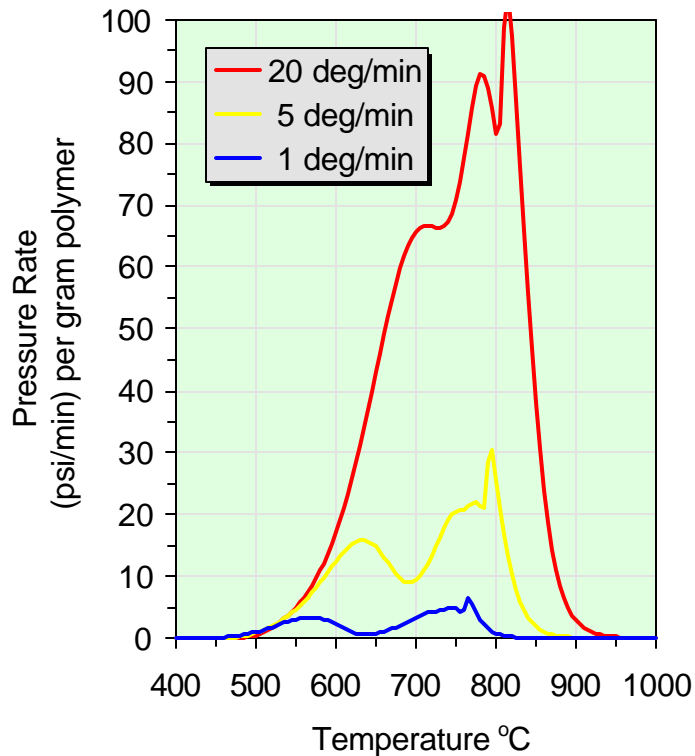


Figure 3.2.3-6 Pyrolysis model simulation of pressure rate variation due to accumulated gases in a closed system at three heating rates

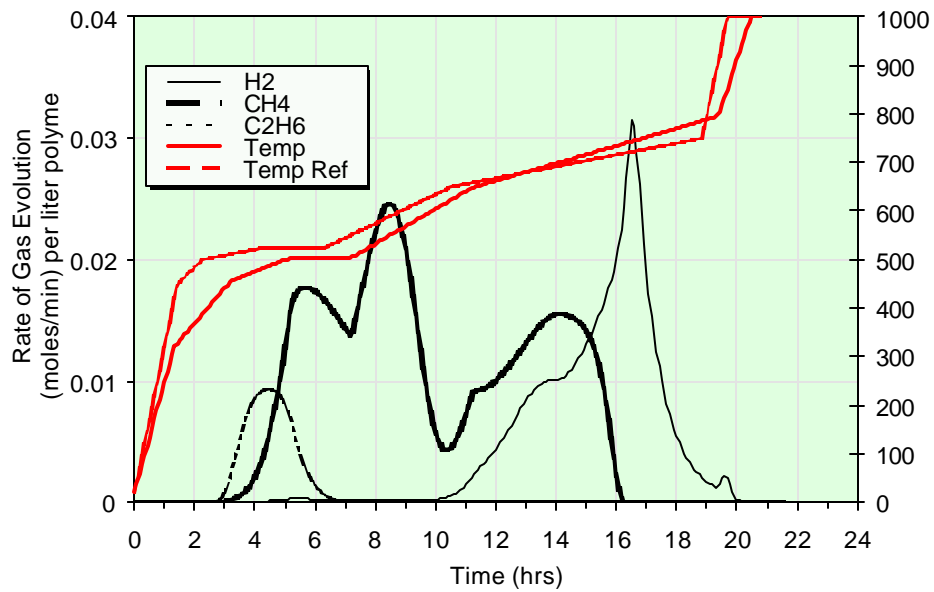


Figure 3.2.3-7 Pyrolysis Cycle Rate of Gas Evolution (Beta Cycle: Lab Implementation)

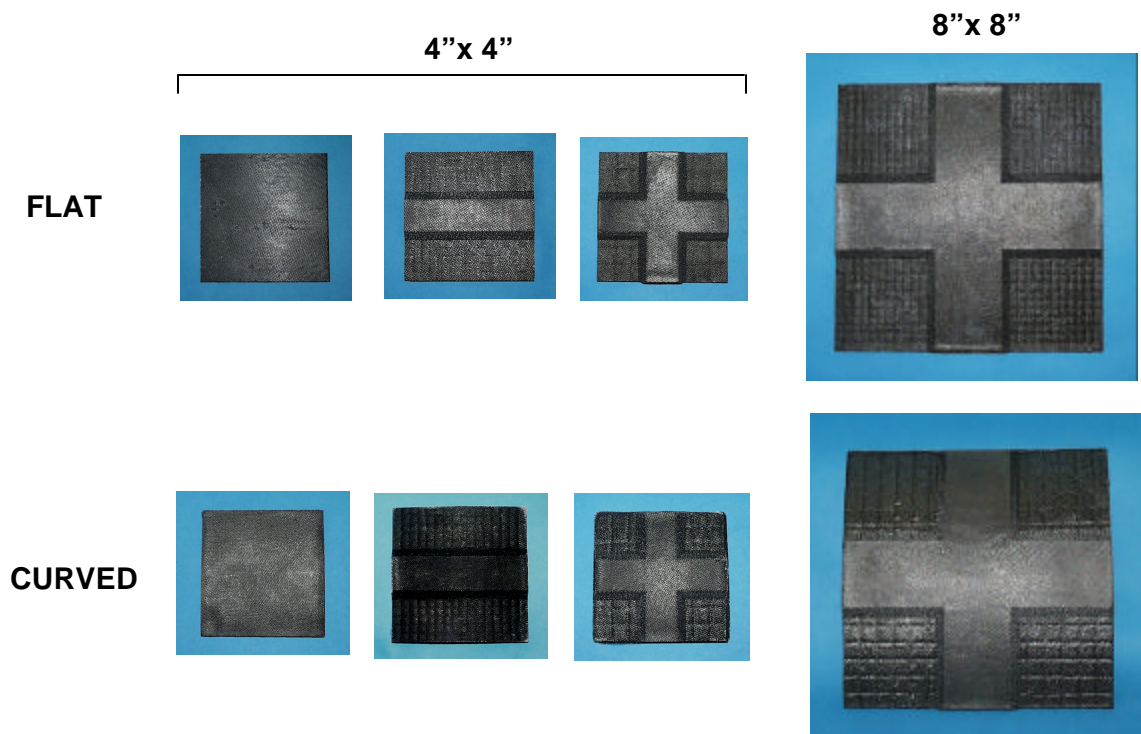


Figure 3.2.3-8 Initial LOM fabricated Nextel™ 312/Blackglas™ 493 sub-component panels

Laser Cutting Edge Effects

Several problems were identified during the LOM fabrication of the initial series of flat and curved sub-component panels. The most serious problem was the generation of unwanted edge and surface features in the final consolidated panels due to excess material damage along the perimeter of the laser cuts. This effect had not been found in previous LOM processing studies performed by Helisys on other fiber reinforced polymer systems such as glass/epoxy and glass/phenolic system. During laser cutting a portion of uncured BlackglasTM polymer along the cut appears to be pyrolyzed. This “char zone” produces a lower value of material compressibility along the edge of a laser cut compared to that of the overall prepreg material. This non-uniform compressibility over the laminate volume results in two effects. During final laminate compaction the edges of the part do not compress to the same thickness as the interior resulting in a final panel with thicker edges (see Figure 3.2.3-9). The other effect is found in the crosshatch regions. In the current panel geometry the crosshatch regions, which define the outline of the stiffener elements, lie above several layers of uncut prepreg. During final panel compaction the edges of the decube regions preferentially depress into the more compliant prepreg layers beneath resulting in the crosshatch pattern becoming imbedded in the surface of the decubed part (see Figure 3.2.3-9). The effect appears to be specific to the BlackglasTM resin system which, of course, has been specifically optimized by its vendor Allied Signal to easily convert from a polymer phase to hard glass ceramic.



Figure 3.2.3-9 Green State 4"x 4" Curved Panel with edge/surface irregularities due to laser char zone

For the current part geometries, though, the non-uniform edges can be removed by simply trimming of the panels after final pyrolysis. All NextelTM/BlackglasTM CMC parts typically require a final edge trimming to improve the mechanical properties of the part as the edge region typically contains high porosity, damaged regions. One can envision, though, certain part geometries (i.e. stiffener elements with vertical sidewalls) where a final trimming step is not feasible. Staggering the crosshatch positions between each ply in the laminate can mitigate the cross-hatching defect. During panel compaction the laser cut edges in each ply now will not be aligned on top of each other, which might help to lessen the effect (as exhibited by the stiffener drop off regions which show little indication of these edge depressions). The staggered cross-hatching would not be a problem during final panel debulking as each crosshatch in a NextelTM/BlackglasTM part is currently removed one ply at a time. Effective use of an offset decube pattern is described more fully in the discussion of panels fabricated with the LOM scanner system.

The earlier laser cutting studies found that the BlackglasTM resin and not the NextelTM fibers in the prepreg produced the char zone along the laser cut. To help reduce the char zone further, the resin content in the prepreg for elements made with the scanner system was decreased to the minimum required to produce a green part.

Specimens were cut from the border of the consolidated CMC panels and polished cross-sections prepared to determine the nature of the raised edge features. There was concern that during laser cutting the ends of the fiber tows were being fused together limiting the ultimate compaction achievable at the part edges even with the use of caul plates. Figure 3.2.3-10 displays a cross-section of the edge region taken from the pyrolyzed 8"x 8" curved cruciform panel. The tows that intersect the edge of the sample appear to be cleanly cut with no indication of fiber sintering. In addition, the spherical remelt particulates found along the edge of the laser cuts for single plies are also not evident. The spheres most likely were removed from the edge of the panel during the vacuum compaction/cure step or through the subsequent pyrolysis/reinfiltration cycle. This is borne out by microscopic probing of the edge of a laser cut in a single ply which finds the spheres to be rather loosely bonded to the fiber tow ends. The lower compressibility of the prepreg along the laser cut edge is more likely due to both partially

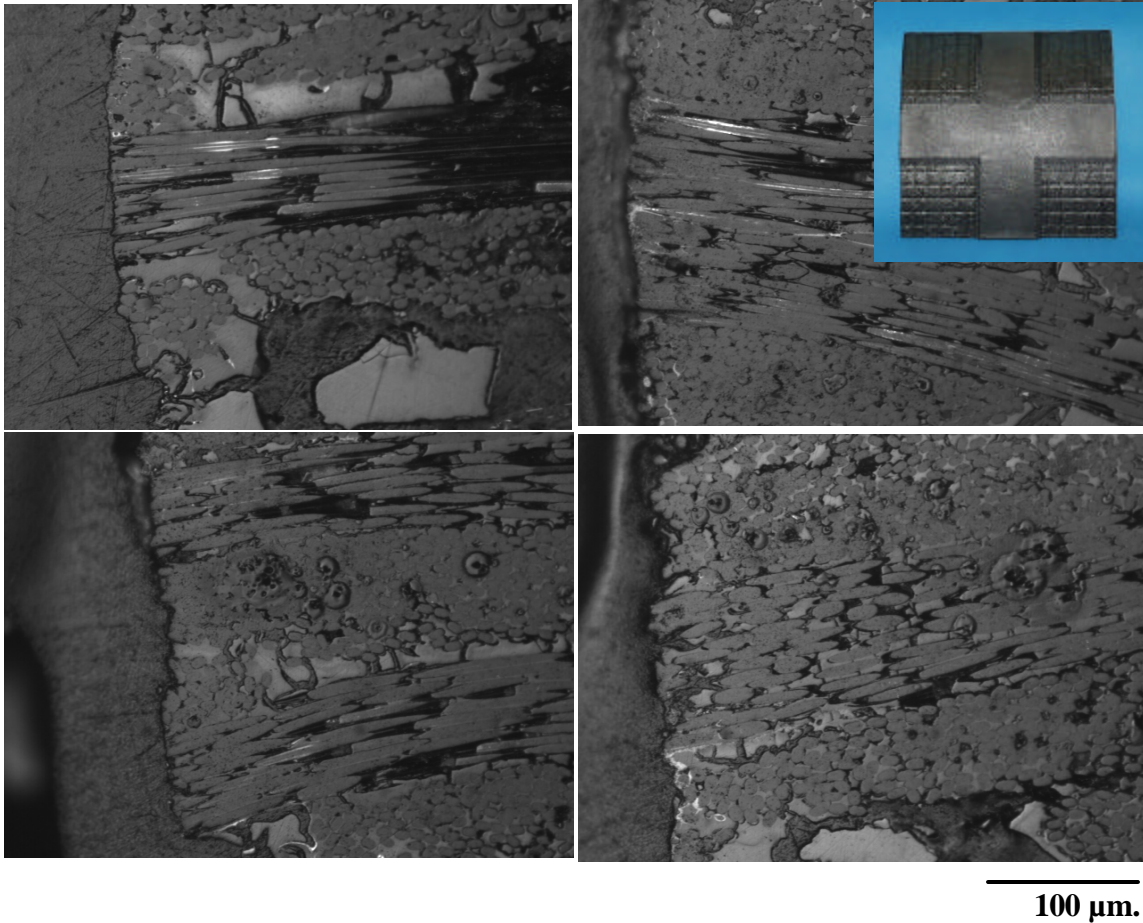


Figure 3.2.3-10 Cross-sections taken from raised edge of 8''x 8'' curved cruciform Nextel™/Blackglas™ CMC subcomponent panel (shown in insert)

cured and pyrolyzed resin restricting further nesting of the fiber tow ends. Depending on the extent of this affected zone along the edge of the panel, utilization of caul plates during compaction/cure might be a suitable solution to eliminate effect.

Evaluation of Laser Ablation Based Cutting

To serve as a comparison to the laser cuts obtained with the CW and pulsed CO₂ laser on the LOM systems, a limited series of cutting experiments also were performed on Nextel™ 312/Blackglas™ 493 A/B prepreg using an ablative laser cutting process. The CO₂ lasers used on LOM systems (which operates at a wavelength of 10⁶ microns) removes sample during the cutting process by delivering enough concentrated energy in a small area to effectively melt and vaporize away material. The laser/material interaction is largely a thermal process. As one moves

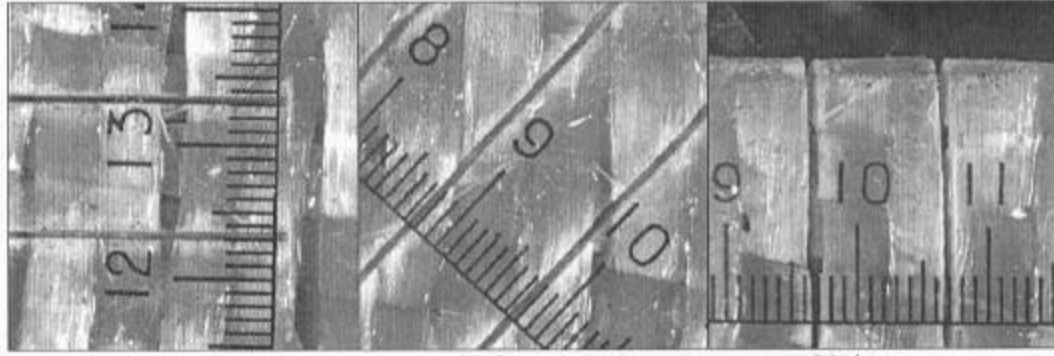
from laser systems operating at IR wavelengths to those using visible (typically < 533nm) and UV excitation lines and shorter pulse widths (nano, pico, femtoseconds), the laser/material interactions become dominated by photochemical (electronic) processes wherein laser energy is now absorbed by valence electrons in the material. Laser ablation stems primarily from the pressure buildup due to the absorption of laser energy by the valence electrons in a material. At high enough laser fluence an ablation threshold is achieved wherein the intense electric field generated in the laser pulse ionizes the atoms of the irradiated material. These highly excited ions are ejected or “explode” at high velocity from the material surface in what is essentially a high velocity plasma plume.

The advantage of an ablative-based laser cutting process is that the damage zone along the cut can be significantly decreased by minimization of thermal degradation effects. Lasers used for ablation (Excimer, Nd-YAG) do not operate at IR excitations and the short pulse widths (femtosecond, picosecond) typically used do not allow enough time for a high density of thermal energy to be absorbed and diffused into the material. The major disadvantages of laser ablation based cutting methods are: (1) the high cost of the high power, pulsed laser systems required, (2) the limited reliability and duty cycle of such systems (not “commercially hardened”), and (3) difficulty of integrating laser power control with xyz positioning control to allow for effective high speed cutting.

A series of laser cuts were made in NextelTM312/BlackglasTM493 A/B prepreg samples using a pulsed femtosecond laser operating at a wavelength of 795 nm at various laser fluence and power levels. The objective was to discern if different lasers operating at other frequencies and rep rates could diminish the pyrolyzation/charring of the matrix resin in the prepreg during cutting. The laser cuts were typically 10 mm long at 0°, 45°, and 90° orientations to the sample edge.

Laser fluences of 1.0, 2.7, 3.1 and 9.7 J/cm² were investigated using a spot size of 80 microns and pulse width of 400fsec. 1, 3, 5, 10, 15 and 25 passes were made for each fluence and orientation.

Figure 3.2.3-11 and 2.21 show photomicrographs of the best quality laser cuts obtained for the laser operating parameters investigated. The best cut was obtained with the lowest per pulse energy level but with the highest fluence of the series. For the laser parameters investigated cut widths ranged from 50 to 150 microns with minimal char zone evident. Visual inspection of the various cut regions reveals that BlackglasTM resin has been removed from the adjacent fiber regions roughly 100-150 microns from the edge of the cut. As laser/material interactions during ablation are fairly complex and not very well understood, there are many possible explanations for the cause of the resin displacement. The above laser ablation cutting trials demonstrate that it is technically feasible to laser cut NextelTM/BlackglasTM prepreg without pyrolyzing the edge of the material (which was found in early CO₂ laser cutting trials to lead to irregularities in the final CMC parts. Though the char zone was eliminated in the cuts obtained by laser ablation, the program did not pursue further studies in this area. Changing to an ablative mode of laser cutting would significantly decrease the system's cutting speed resulting in increased build times. The high laser costs and technical challenges associated with integrating ablation based laser cutting with the current LOM process limited the commercial viability of such an RP/SFF system at this time.



(a)

(b)

(c)

Figure 3.2.3-11 Pulsed (400fsec) laser cut in Nextel™312/Blackglas™ 493 A/B prepreg: laser cuts at (a) 0°, (b) 45°, and (c) 90° orientations to ply edge, 15-25 passes per cut, 485μJ/pulse with a fluence of 9.7 J/cm² (Scale: 1 graduation = 100μm.)

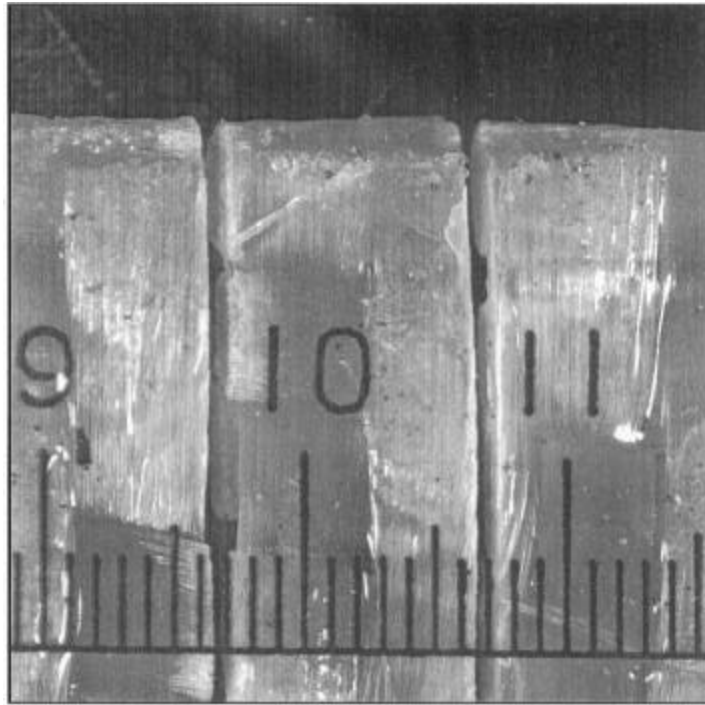


Figure 3.2.3-12 Detail of femtosecond (400fsec) laser cut in Nextel™/Blackglas™ prepreg at 90° orientation to ply edge (Scale: 1 graduation = 100μm.)

Subcomponent Fabrication on LOM Scanner System

Several CMC subcomponent panels were fabricated on the LOM scanner system to evaluate machine performance with each major hardware/software upgrade. The results of the laser scanner cutting trials on individual plies (described in section 3.2.2) determined that the quality of the laser cuts in NextelTM/BlackglasTM prepreg material can be greatly improved by operating the scanner system at the highest available laser power and scanner velocities. Multiple laser passes, though, are required to completely cut through a single ply with increasing scanner velocity. The drawback of this cutting approach is that the part build time increases substantially; especially when high scanner velocities are used which may require up to 10-20 passes for complete cutting. For a fairly large or intricate part (which might be fabricated using an out-time limited thermosetting composite system) an extended build time might be unacceptable. Based on build time measurements from initial LOM fabrication trials of an 8"x 8", 32 ply cruciform stiffened subcomponent panel, an estimate can be made of the time required to generate the full blastshield. These estimates indicate that by using a scanner setting requiring a maximum of four cutting passes, the full blastshield can be fabricated in well under the 20 hour out-time limit for the BlackglasTM 493A/B resin system.

Based on this estimate two CMC subcomponent panels were initially fabricated on the prototype scanner system using the optimized cutting parameters determined in section 3.2.2. One panel was a flat, 4" x 4", 32 ply, cruciform stiffened panel and the other a curved 8"x 8" cruciform stiffened element. Both panels were fabricated from the standard prepreg formulation (45% resin) using the scanner system with the lower power Synrad laser and scanner setting of 135mm/sec:4 passes for each ply. The silicone rubber attachment scheme used earlier for bonding of the plies to the LOM build platform for the curved parts was not used for these trials. The previous processing trials found the silicone rubber (which was attached to the metal plate with vacuum grease) was difficult to remove from the plate without damaging the attached uncured prepreg laminate. The BlackglasTM resin was also found to react with the silicone rubber over

time causing the material to warp. This warpage resulted in shifting of the registration of the individual plies of the uncured laminate. The alternate attachment procedure used consisted of first attaching with tape a sheet of non-porous Teflon (coated with mold release) to the LOM build platform then bonding the first ply to the Teflon sheet with tackifier. The final laminate is removed from the LOM build platform by cutting around the edges of the Teflon sheet and placed on the curved LOM forming tool and cured/consolidated with the Teflon sheet attached. This attachment procedure was only suitable for the 8" x 8" panels or smaller. A more involved attachment scheme was required for larger laminate sizes (i.e. final blastshield) to ensure the plies did not move during successive laminations. This more advanced attachment scheme used for fabrication of the blastshield is described in section 3.3.2 of this report.

The post LOM processing steps for the panels were the same as that described in the previous section of this report. The 4" x 4" panel was vacuum consolidated and cured using a caul plate that further helped to eliminate the raised edges found in earlier processed panels, as shown in Figure 3.2.3-13(b). Due to using the optimized scanner cutting parameters to reduce the char zone in the layers, the ridges in the crosshatch regions were also greatly diminished in the panel but not totally removed. A caul plate was not used during consolidation of the 8"x 8" curved panel, which resulted in slightly higher raised edges than the flat panel. Figure 3.2.3-13 displays the final pyrolyzed 4" x 4" cruciform panel and Figure 3.2.3-14 the 8" x 8" curved cruciform panel.

The LOM fabricated panels with the raised edges did not appear to generate any delaminations in the final pyrolyzed CMC parts. As a trimming step is required for all composite parts, the edge features will not remain in the final subcomponent panels and thus may not be a critical issue. The vacuum-forming step may also be contributing to the generation of the edge perturbation as the sidewall of the part is subjected to a normal force causing the relatively compliant prepreg stack to buckle slightly. Further vacuum consolidation tests will need to be performed to determine to what degree this may be a factor in generating the edge features.

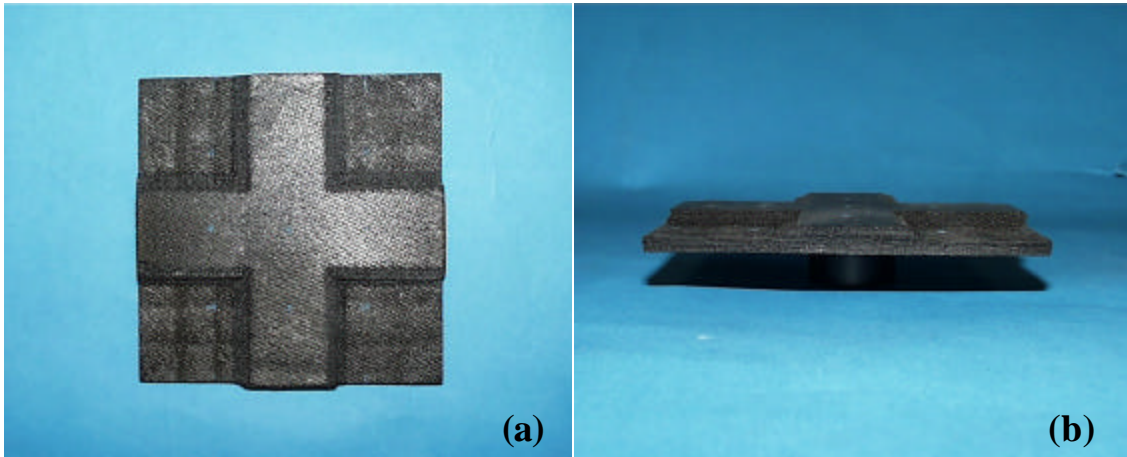


Figure 3.2.3-13 (a) Top and (b) side view of 4'' x 4'' Nextel™/Blackglas™ cruciform panel fabricated on prototype LOM scanner system

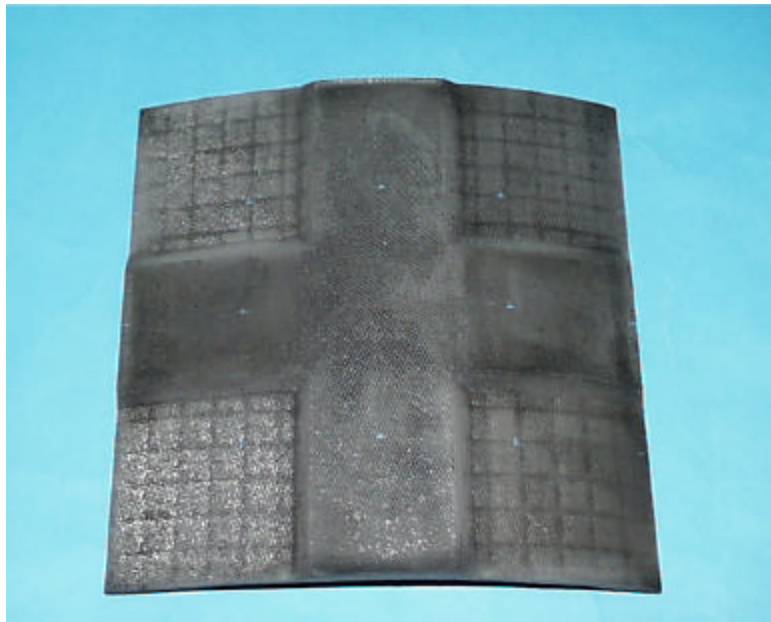


Figure 3.2.3-14 8'' x 8'' Nextel™/Blackglas™ curved cruciform panel fabricated on prototype LOM scanner system

The earlier laser cutting tests on single prepreg plies demonstrated that further improvement in cutting is obtained using the higher power 200W CW Coherent laser and a lower resin content prepreg formulation. The scanner optics on the LOM system used to fabricate the previous subcomponent panels, though, limited the maximum power that could be utilized for cutting. After the new laser scanner optics was installed on the system and the full laser power

became available, a final series of subcomponent panels were fabricated with the lower resin content prepreg formulation. By this time in the program the LOM tooling materials had been developed and optimized for use with the Blackglas material system.

Based on an initial blastshield design trade studies, several Blackglas/Nextel subcomponent panels were designed and subsequently fabricated on the LOM scanner system and consolidated/cured on the 9"x 9" resin infused LOM forming tool (described previously in section 3.2.2). The 8" x 8" subcomponent panels (all with alternating 0/90 ply orientations) included two single-stiffener flat panels, a curved cruciform-stiffened panel, and a curved cruciform panel with 2" wide stiffener. The single-stiffener flat panels represent blastshield design Case 6 of heatshield dynamic analysis, i.e., 0.135"-thick skin, 0.405"-thick skin-plus-stiffener, and 1.0"-wide stiffener (refer to Section 3.3.1 of this report for full description). Figure 3.2.3-15 shows images of the panels in various stages of the CMC conversion cycle. The stiffener regions of the single-stiffened panels were LOM fabricated from narrower strips of prepreg than the skin plies to minimize waste. The border area of the stiffener section was removed from the panel before consolidation/cure, hence, no remnants of crosshatching is visible on the skin ply as found for the cruciform subcomponents (Figure 3.2.3-15c, -15d). Mechanical tests were performed on the single-stiffener panels to obtain strength data for the demonstration component design analysis task. These results are discussed in Section 3.3.1.

The utility of offsetting the decube elements from ply to ply to minimize the indentations produced in the stiffener cutout regions during part consolidation/cure was also evaluated on the curved subcomponents. Helisys had previously developed a mode of cross-hatching called “diamond decubing” in which crosshatch lines are gradually shifted through each consecutive slice of a part. Figure 3.2.3-16 displays a schematic of the diamond decube offset pattern. The technique was developed for standard commercial LOM RP to make the post-LOM decubing step quicker and easier to perform. In Figure 3.2.3-15(c) one can see remnants of the initial diamond crosshatch pattern in the skin sections of the green state, curved cruciform panel. Offsetting the crosshatching between plies by “diamond decubing” was found to broaden and significantly reduce the depth of the indentations but not completely remove them. It is believed that the laser cuts are still too closely aligned between adjacent plies using the diamond decube mode to completely remove the effect. Forming the part over a curved tool surface also probably contributes to diminishing the advantage of the decube offset by causing slight shifting of

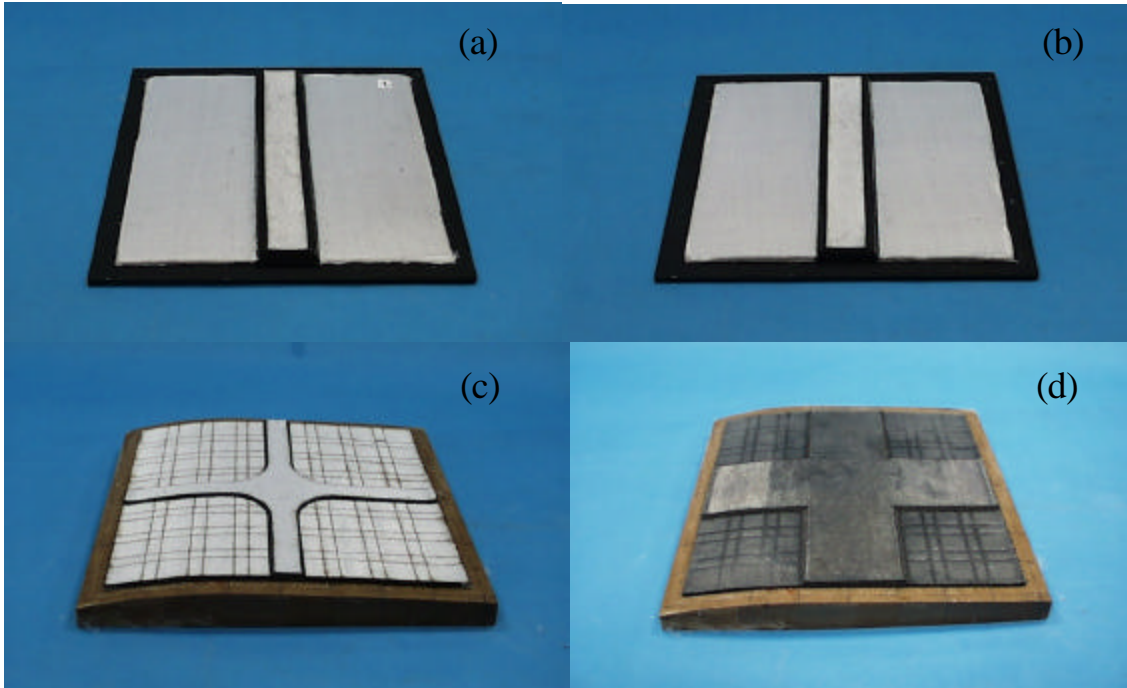


Figure 3.2.3-15 8" x 8 " Single Stiffener Mechanical Test Panels (a) 1 and (b) 2; curved cruciform panels (c, d) formed/cured on resin infused LOM tool (Notice the remnants of diamond decubing pattern in skin sections of c and d).

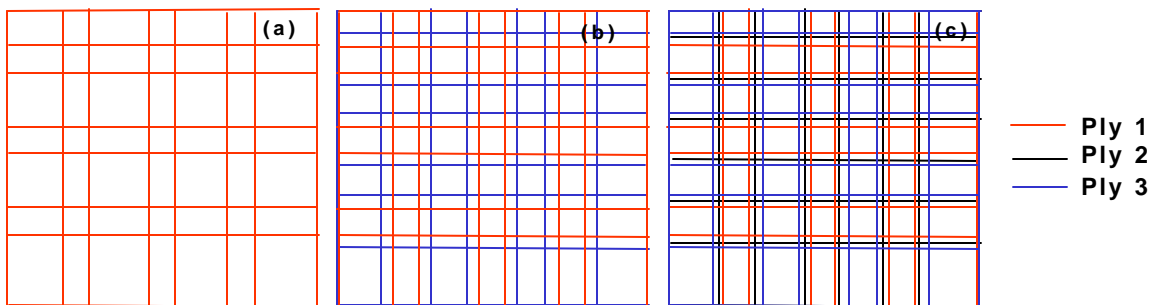


Figure 3.2.3-16 "Diamond" decube offset pattern for (a) ply 1, (b) ply 2, and (c) ply 3.

the cuts in adjacent plies such that they are more closely aligned. An alternate crosshatch offset geometry was devised which further separates the laser cut lines from ply to ply. Figure 3.2.3-17 displays a schematic of this alternate decube offset pattern. It was found that by using a larger

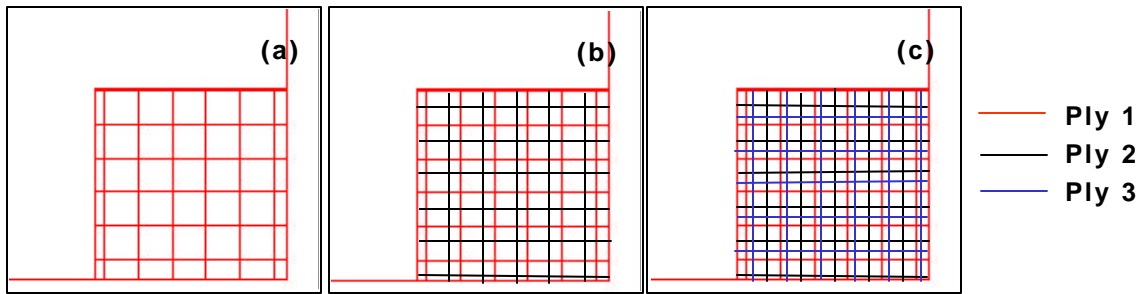


Figure 3.2.3-17 Alternate decube offset pattern for (a) ply 1, (b) ply 2, and (c) ply 3.

crosshatch dimension and this alternate offset pattern the effect could be largely eliminated. This new decube offset subroutine was written into the CCDP/LOM translator software for LOMNEF file generation and was successfully utilized in the design and processing of the final blastshield demonstration component. These results are presented in Section 3.3.2 of this report.

Future Recommendations

Previous CO₂ laser/material damage studies performed by Northrop Grumman in a previous program found that performing the laser cutting under an inert atmosphere such as nitrogen significantly reduced the amount of charring in various types of polymer impregnated fabrics. The benefit of performing the laser cutting of NextelTM/BlackglasTM prepreg under nitrogen on the LOM unit needs further evaluation. Purging the LOM unit would not be difficult as the system is already designed to operate in a sealed enclosure.

Further work is also needed in using caul plates during post LOM consolidation/cure of the laminates to more evenly distribute the compaction force across the part surface. Caul plates are commonly used in polymer composite processing to achieve uniform compaction over a part volume. The caul plates could be easily generated by LOM just as are the curved part tool mandrels. Further compaction pressures can also be achieved by curing the LOM parts in an autoclave (though this is considered a last resort as it adds further complexity to the LOM fabrication sequence). Utilizing one or a combination of material and process modifications it is

hoped the indentation effects resulting from laser induced charring can be eliminated in the LOM processing of NextelTM/BlackglasTM CMC.

3.3 CMC PROTOTYPE DEMONSTRATION

3.3.1 Design of Demonstration Component

3.3.1.1 Background and structural description

This section addresses vibration and stress analysis of a LOM CMC design for the AV-8B blastshield structure. This is the second CMC design proposed for replacement of the production metal article.

The first, or baseline CMC design, was completed by NGC (Vought) in 1997, Ref. 3.3.1-1. The baseline CMC design has the same geometry and aircraft installation as the AV-8B production metal blastshield. Figure 3.3.1-1 illustrates the current metallic structure and the 1997 baseline CMC replacement design.

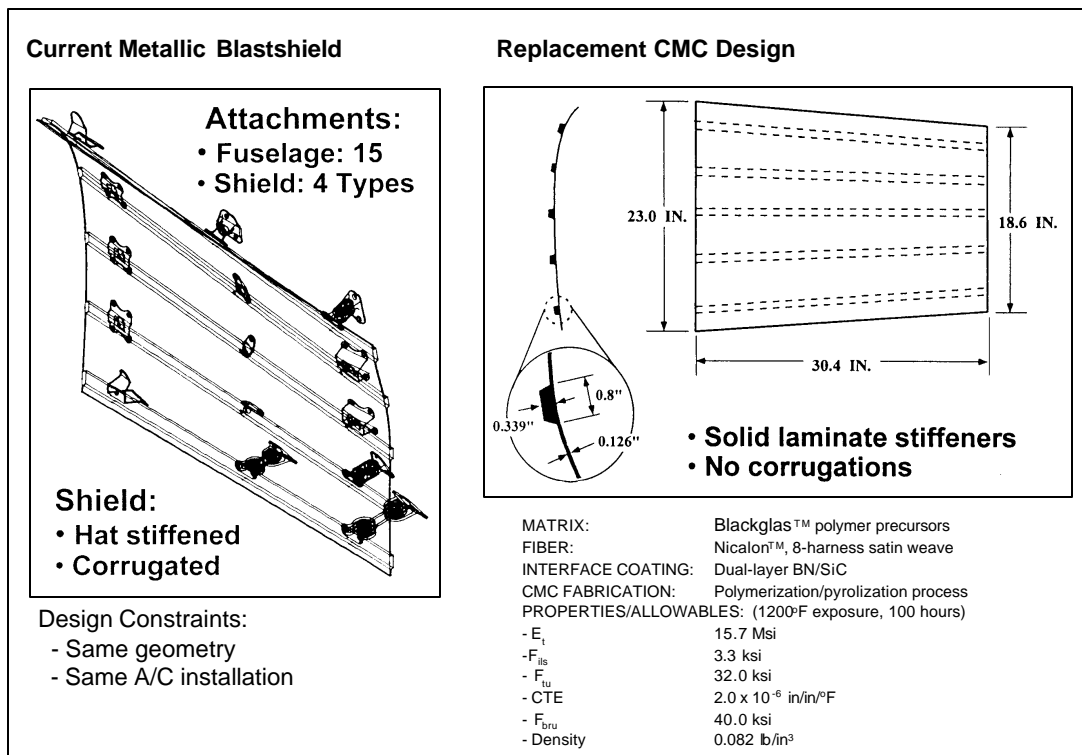


Figure 3.3.1-1 AV-8B Metal production blastshield and 1997 baseline CMC blastshield

Ground tests and flight tests were conducted on the baseline blastshield, Refs. 3.3.1-1 and 3.3.1-2. Stress and vibration analyses of the baseline design are contained in Refs. 3.3.1-2 and

3.3.1-3. Structural loads and temperatures for the baseline design are given in Ref. 3.3.1-2. Revised loads and temperatures based on the test data are contained in the appendices of Ref. 3.3.1-2.

The present program conducted by NGC and Helisys, 1998-2000, addresses rapid, reduced cost, CMC development by exploiting the laminate object manufacturing (LOM) process and the NextelTM312/ BlackglasTM material. The LOM CMC blastshield design concept also explores the weight advantages of a modified aircraft installation wherein the number of fuselage attachments is reduced from 15 to 9. Equipment and budget constraints dictated a reduced size (24" x 18" x 14.6") demonstration component, but the preliminary design analysis (no structural tests, no flight qualification) was addressed to the full size component geometry (30.4" x 23" x 18.6") and loads. Figure 3.3.1-2 shows the LOM CMC blastshield.

3.3.1.2 CMC properties

A preliminary set of design properties for NextelTM312/BlackglasTM was derived from LC3 program data. No LOM-processed material test data was available until mid-July 2000, too late to be included in the analyses carried out during this program. For comparison, NicalonTM/BlackglasTM data used to design the 1997 baseline CMC blastshield and the NextelTM312/BlackglasTM data are both included in Figure 3.3.1-3.

3.3.1.3 Static analysis

The approach taken for all the static, dynamic, and thermal structural analyses here is to compare the performance of the baseline and LOM designs against the test-modified loads and temperatures using finite element analysis (FEA).

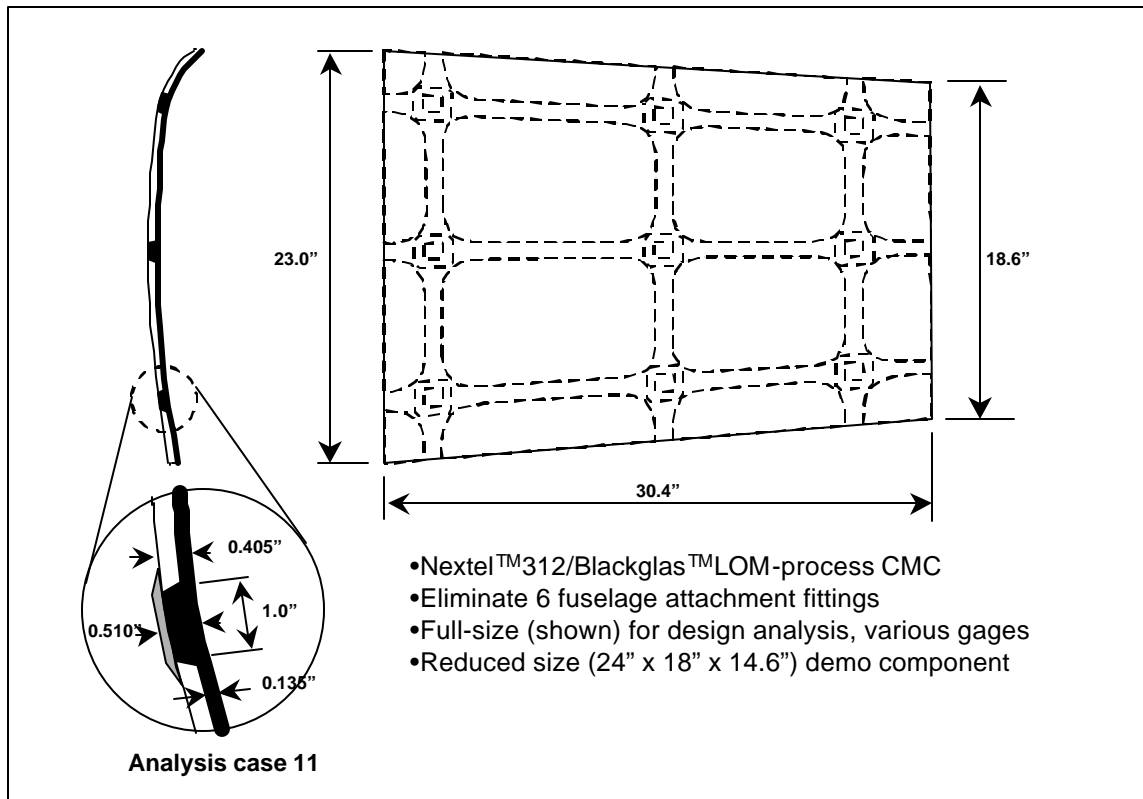


Figure 3.3.1-2 LOM CMC blastshield

Cross-ply Laminate Property	Baseline Nicalon/Blackglas	Nextel312/Blackglas
$E_1 = E_2$, msi	12.0 - 15.7*	9.6
ν_{12}	0.14	0.11
G_{12} , msi	4.7 - 6.08*	3.64
F_{tu} , ksi	32.0	25.7
ρ , lb/in ³	0.082	0.077
α , 10^{-6} in/in/°F	2.0	2.0
*Used for 1997 acoustic rms analysis		

Figure 3.3.1-3 CMC Properties

Initially, fine PATRAN models (grids, or meshes), were prepared from the CATIA mold description, but two practical issues arose. First, the COSMOS/M FEA code accepts members and nodes from PATRAN, but surfaces and other features essential for describing thickness variations, etc., are lost in the translation. Second, no automated method was at hand to derive

and transfer the correct local variation of material orientation to the several thousand individual finite elements. Consequently, models were developed in COSMOS/M by constructing splines and surfaces from an array of points describing the mold surface and by parametrically generating the elements to have one side parallel to the local material axis in a similar manner to that used in Refs. 3.3.1-2 and 3.3.1-3.

Quadrilateral laminated shell elements were used to model the structures. Stiffeners were represented as groups of elements with increased thickness and offset to maintain the outboard mold contour. Figure 3.3.1-4 illustrates the arrangement of elements to represent the LOM CMC blastshield stiffeners.

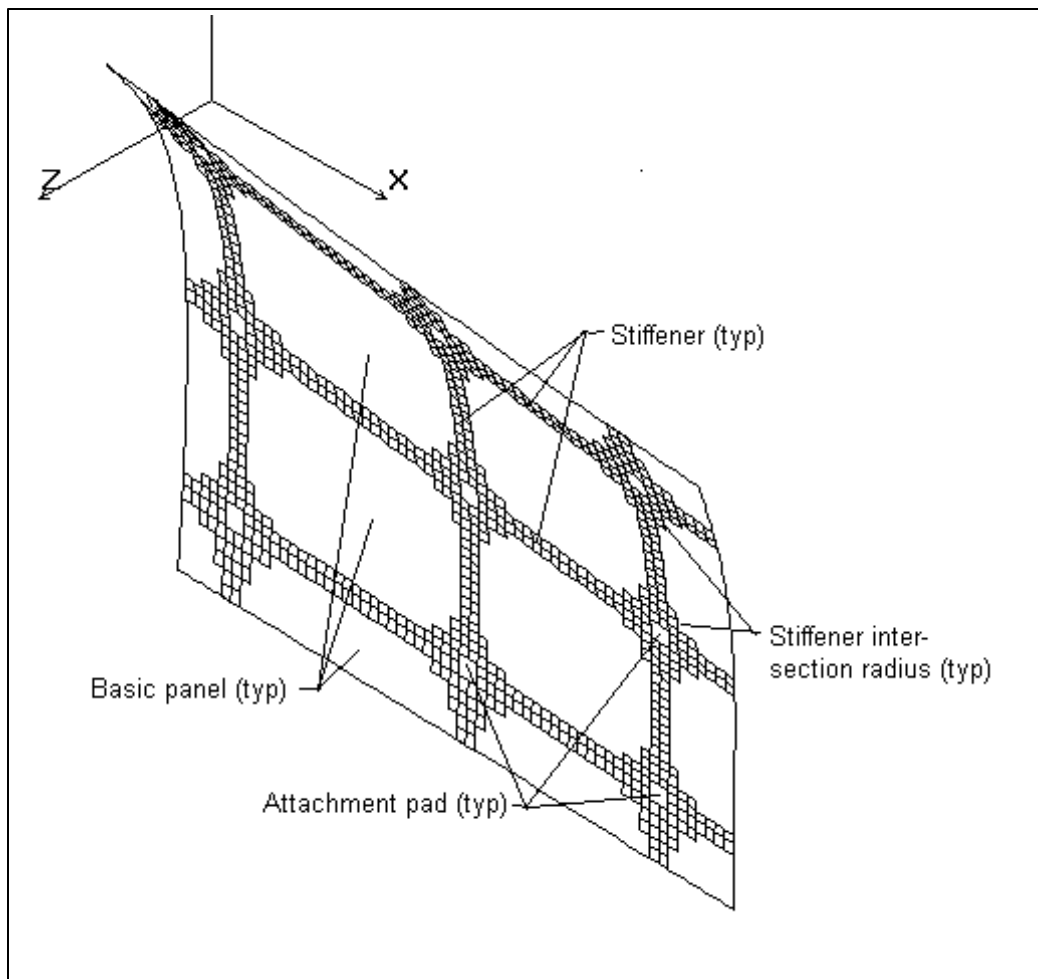


Figure 3.3.1-4 Arrangement of stiffener elements on LOM CMC model.

Boundary conditions have a significant impact on natural frequencies and stresses. The element arrangement and the attachment boundary conditions of Ref.3.3.1-2 were maintained for the baseline model, Figure 3.3.1-5. Flexural constraint had to be approximated by pairs of translational constraints for the low-order tetrahedral brick element used for the stiffener in Ref. 3.3.1-2. This approximates the differing fixities imposed by the various attachment arrangements shown in the left-hand side of Figure 3.3.1-1.

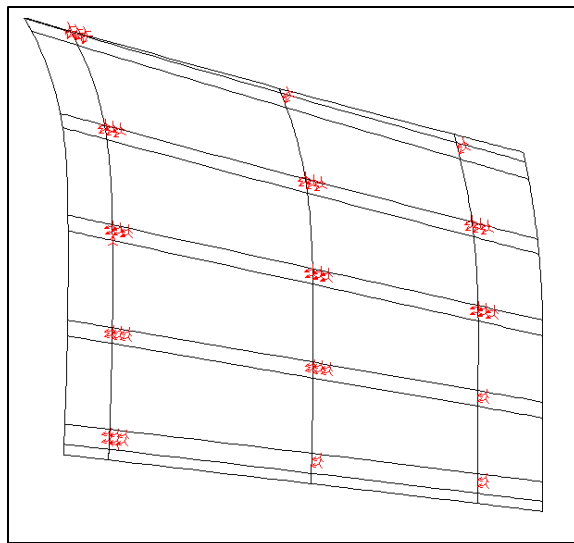


Figure 3.3.1-5 Boundary conditions for baseline CMC model.

For the alternate 9-attachments arrangement proposed for the LOM CMC design, it was assumed that the greater fixity (full flexural fixity) hardware be used at all nine locations. Further, it was assumed that inplane fixity be relaxed as much as possible, the same as in the baseline case, to reduce differential expansion loading from the airframe. The flexural fixities are approximated by rotational constraints, Figure 3.3.1-6.

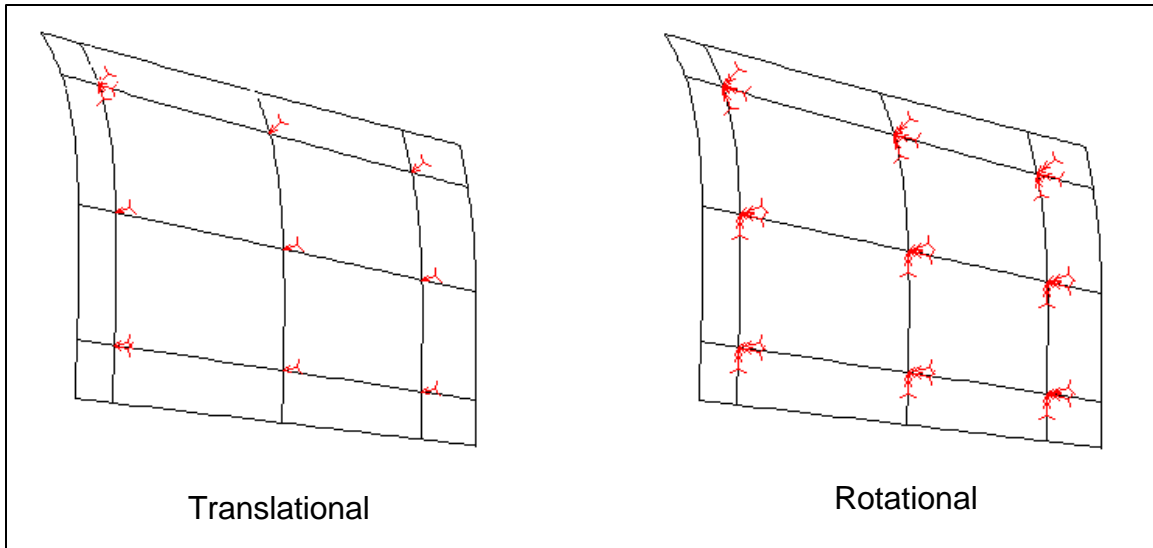


Figure 3.3.1-6 Boundary conditions for LOM CMC model.

The static ultimate pressure distribution as modified by the ground and flight tests is shown in Figure 3.3.1-7 (Ref. 3.3.1-2, appendices). An approximation of these pressures was applied to the FEA models in stepwise blocks of constant pressures corresponding to the subpanels (COSMOS/M surfaces) visible in Figures 3.3.1-5 and -6.

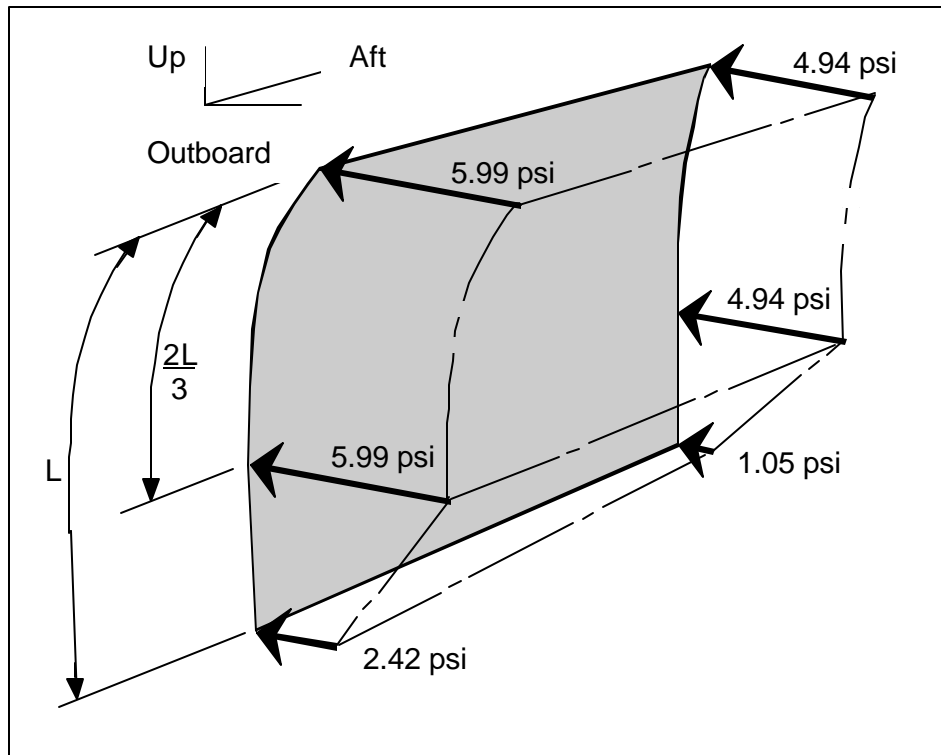


Figure 3.3.1-7 Modified ultimate static pressure distribution

17 variations of the LOM CMC design were examined for natural frequency and model weight. Those results are described later. One candidate, called case 11, was selected for stress analysis. The static pressure loading FEA results are summarized in Figure 3.3.1-8 for both the baseline CMC and the LOM CMC design. The stresses illustrated in all cases are at the outboard surface in the material coordinate system. The critical flex stresses are about 30 per cent lower for the LOM CMC design.

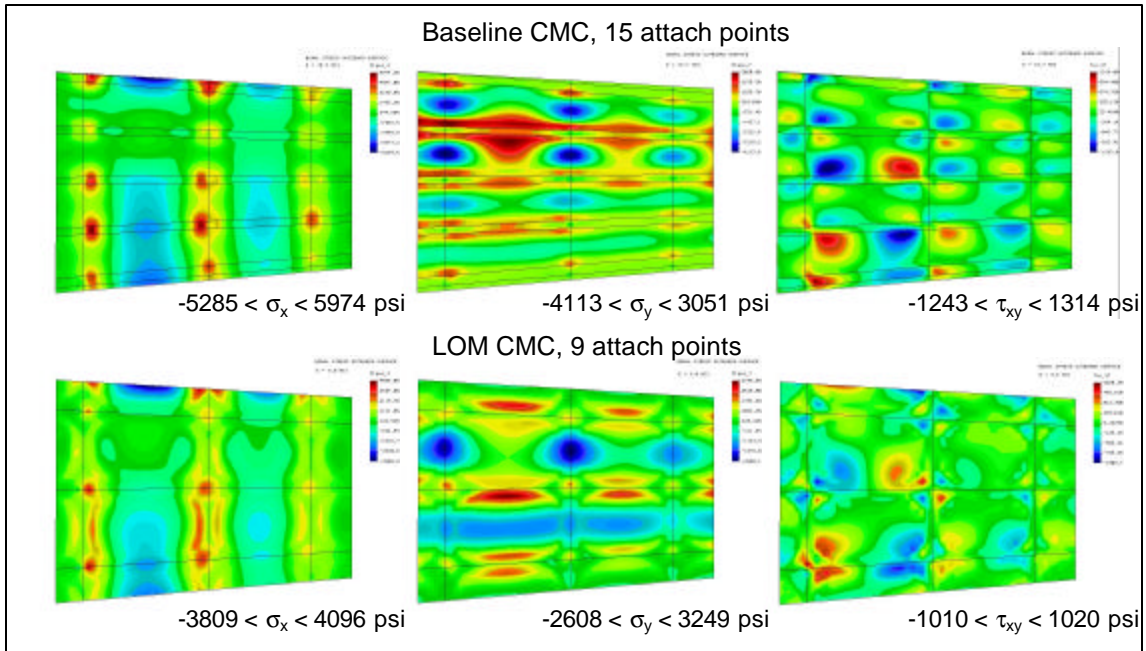


Figure 3.3.1-8 Static stresses

The thermal profile for the hot day adjusted ground test measured temperatures (Ref. 3.3.1-2, Figure A.26) is taken from 35 points and given in temperature contours on the surface. These have to be smoothed else unrealistically high gradients (and stresses) result at the contour boundaries. This smoothing was accomplished in a “natural” way by inputting constant temperatures within the contours as initial temperatures in a transient adiabatic process. After a few steps, corresponding to 100 seconds, the temperatures were reasonably faired over the surface while the peak temperature remained within 10 degrees of the maximum. The resulting thermal profile is shown in Figure 3.3.1-9.

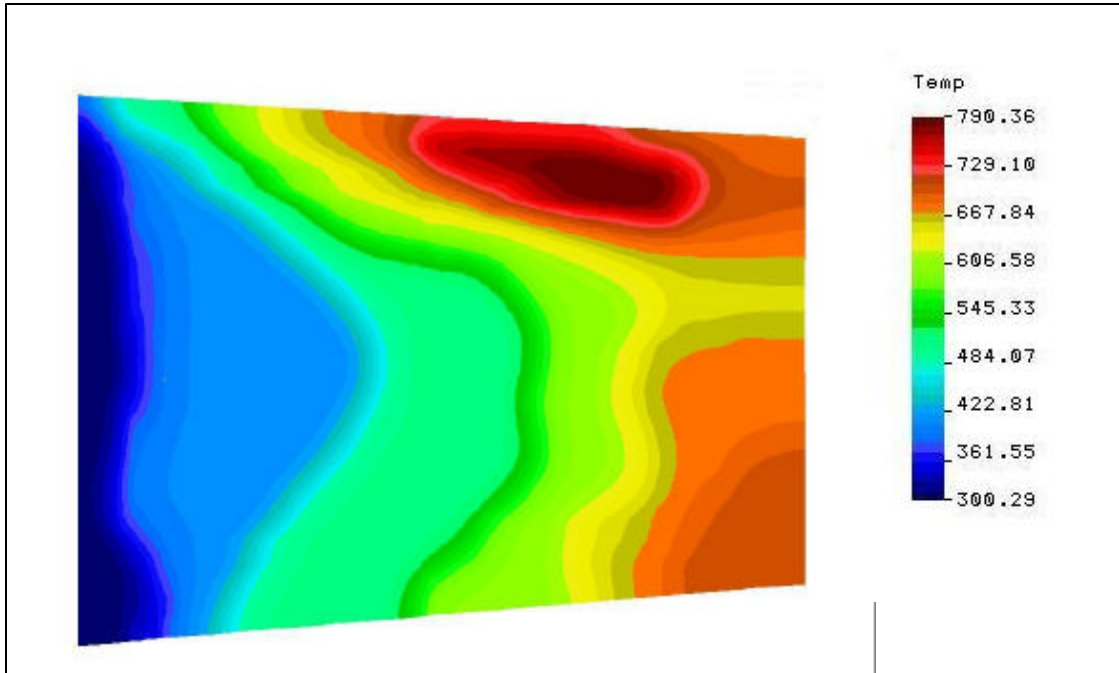


Figure 3.3.1-9 Thermal profile—hot day adjusted ground test measured temperatures, after smoothing.

The temperatures in Figure 3.3.1-9 were next applied as a thermal load on the two FEA models. The resulting thermal stresses at the outboard surface in the material axes are summarized in Figure 3.3.1-10.

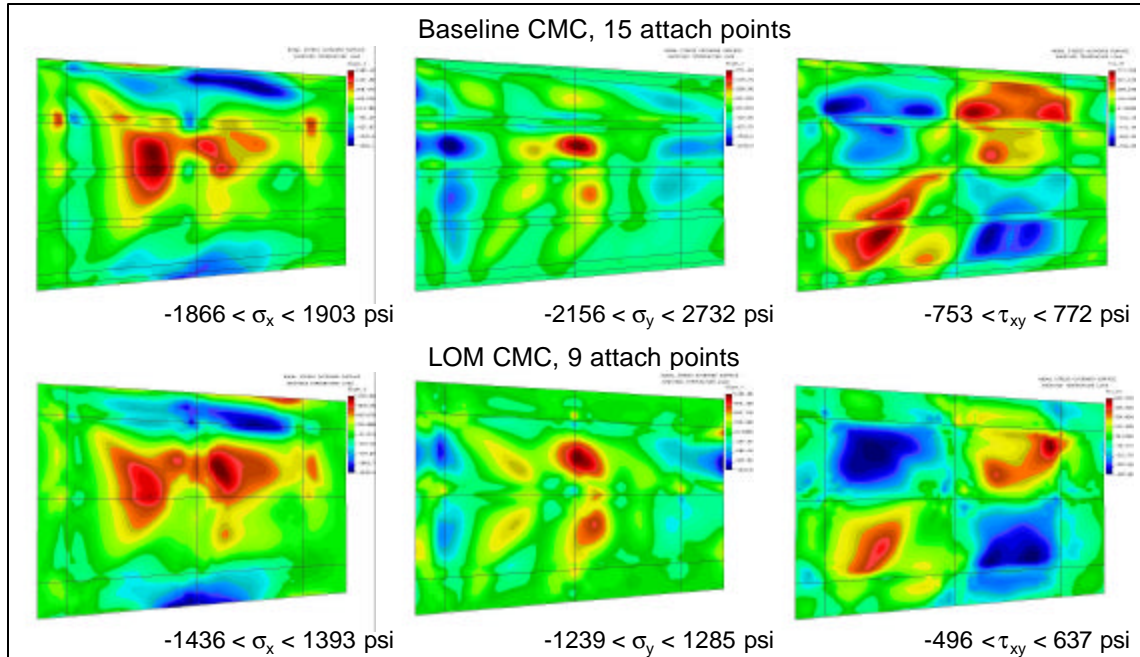


Figure 3.3.1-10 Thermal stresses.

3.3.1.4 Frequency analysis

The first five natural frequencies were obtained for the baseline CMC model and 17 variations of the LOM CMC model. Figure 3.3.1-11 illustrates a typical result. The results are summarized in Figure 3.3.1-12. The effect of relaxing the flexural fixity of the attachments is seen in the cases with the “ss” suffix, denoting simple support conditions. Comparing cases 6 and 7 and 6ss and 7ss shows that the effects of in-plane flexure coupling are negligible.

Case 7 - 0.135" skin, 0.405" x 1.0"
stiffener, no pads, in-plane flexure
coupling included

Freq/Modeshape #	Frequency, Hz
1	416.2
2	461.4
3	494.4
4	520.9
5	565.9

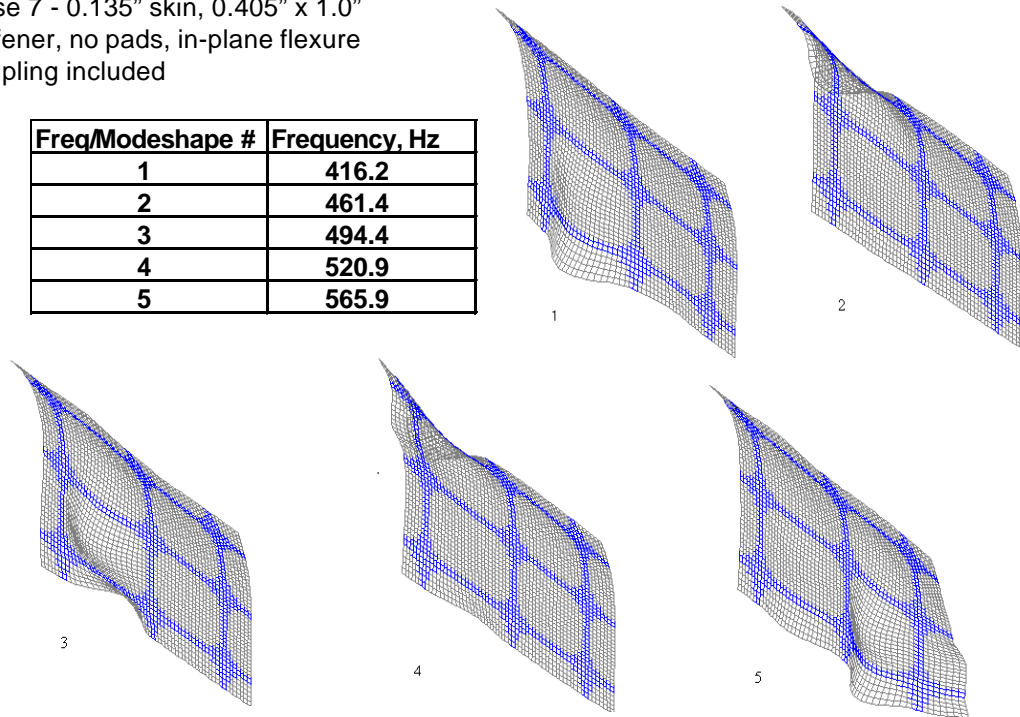


Figure 3.3.1-11 Frequency and mode shape analysis, case 7 LOM CMC model.

3.3.1.5 Random vibration analysis

The acoustic environment is described in Ref. 3.3.1-2. The modified acoustic pressure load is shown schematically in Figure 3.3.1-13. (In random vibration analysis, the exciting pressure is taken to be oscillating about zero mean pressure, so the direction of the pressure is not meaningful.)

Case	Tskin, in	Tstif, in	Stif width, in	Radius, in	Model Weight, lb.	Freq1, Hz
Baseline	0.126	0.339	2x1, 3x0.8	N/A	9.13	362.0
2000-1	0.15	0.375	1	-	10.00	361.8
-2	0.15	0.400	1	-	10.27	385.0
-3	0.15	0.375	1	2	10.76	385.4
-3ss	0.15	0.375	1	2	10.76	244.5
-4	0.15	0.400	1	2	11.11	410.0
-4ss	0.15	0.400	1	2	11.11	258.0
-5	0.15	0.405	1	2	11.18	414.8
-5ss	0.15	0.405	1	2	11.18	260.7
-6	0.135	0.405	1	2	10.63	418.2
-6ss	0.135	0.405	1	2	10.63	262.4
-7	0.135	0.405	1	2	10.63	416.2*
-7ss	0.135	0.405	1	2	10.63	262.9*
-8	0.135	0.405	2	2	12.81	445.6
-9	0.135	0.375	2	2	12.14	413.6
-10	0.135	0.375	2	2	12.14	412.9*
-11	0.135	0.405	1	2	10.70	444.6**
-11ss	0.135	0.405	1	2	10.70	263.6**
*In-plane flexure coupling included. **Padded up to 0.510 in. locally at attachments.						

Figure 3.3.1-12 Frequency analysis summary

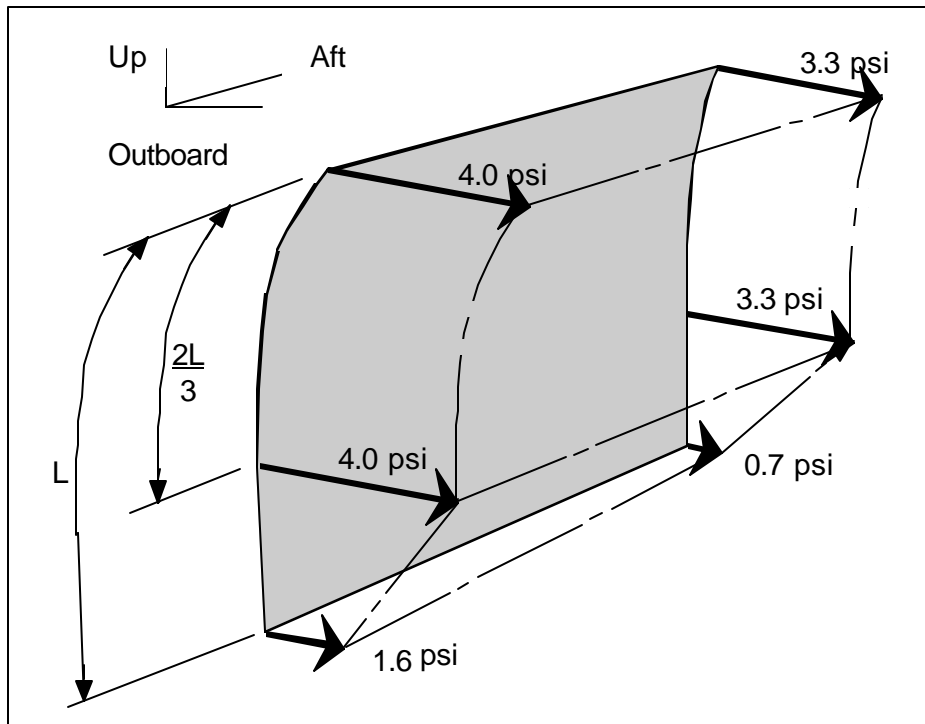


Figure 3.3.1-13 Acoustic pressure load.

Figure 3.3.1-14 illustrates the power spectral density for the acoustic loading. Notice that the frequency range is from 250 Hz to 2500 Hz. 58 modes for the baseline CMC model and 78 modes for the LOM CMC model had to be computed to cover the upper limit of this frequency range. Fewer modes were tried (Ref. 3.3.1-2 used only 25 modes) but this was found to have a significant effect on the rms stresses. Damping of 0.05 between modes was assumed. RMS stresses were obtained for both models and found to be very high, particularly for the baseline CMC model. The highest stresses in most cases were not at the attachment points. In some cases the high stresses occurred in the narrow overhang at the top of the baseline panel. In Ref. 3.3.1-2, all the attention was directed to the attachment points and stresses in other locations were not published. In any event, it was evident that the peak stresses were lower for the LOM CMC design, though they were unrealistically high in both models. Given that the baseline CMC flight article survived both ground and flight acoustic tests, it was concluded that the LOM design was

likely to be adequate. Figure 3.3.1-15 compares the rms stress results of random vibration analysis at 166dB for both CMC designs at the outboard surface in the material axes.

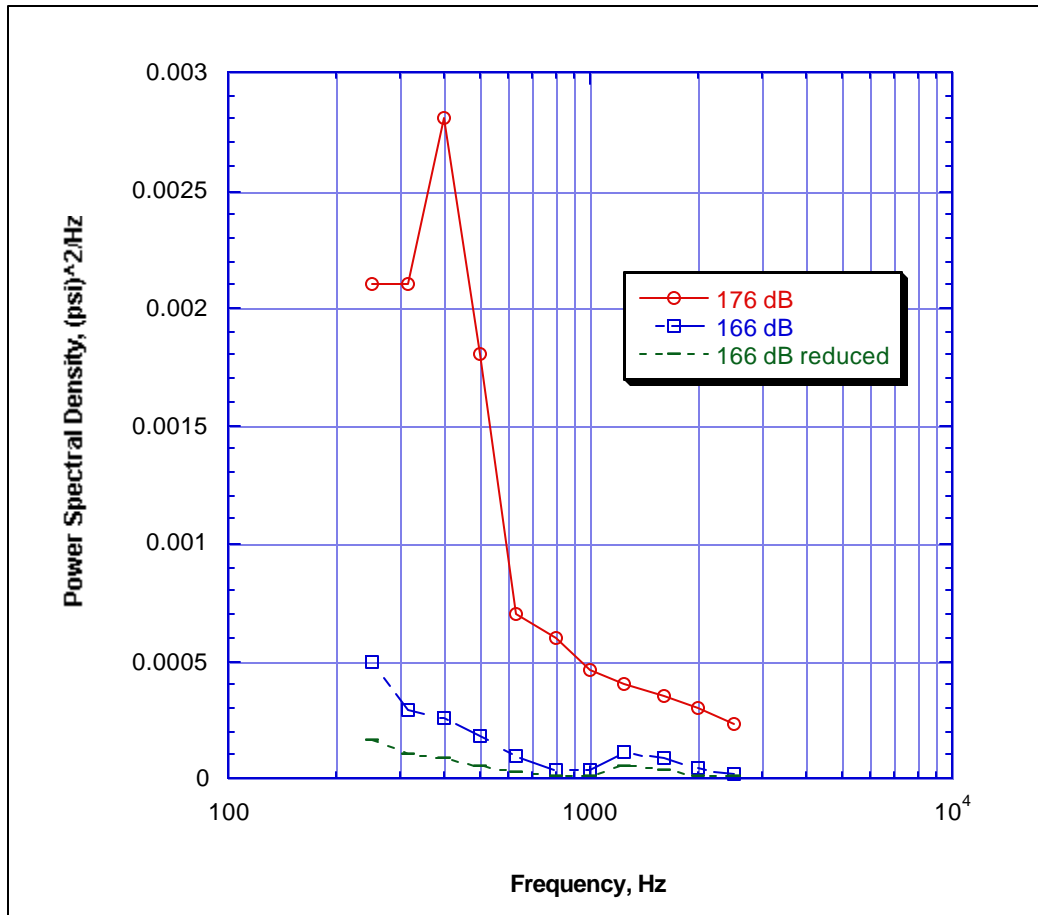


Figure 3.3.1-14 Power spectral density—acoustic loading.

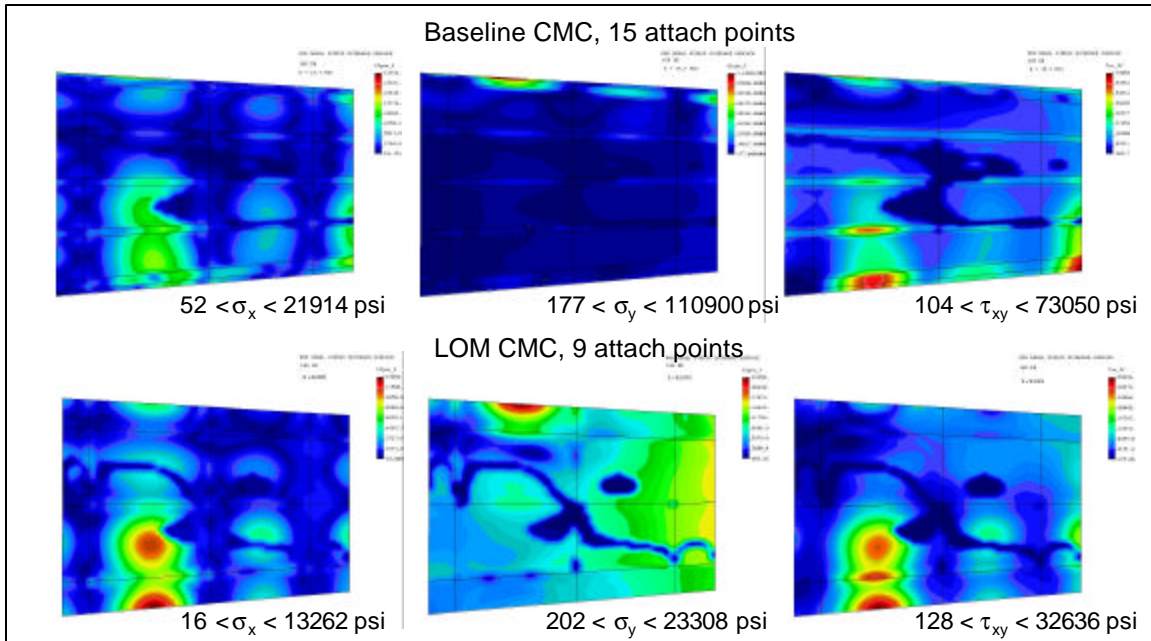


Figure 3.3.1-15 Acoustic stresses

3.3.1.6 Weight summary

According to Ref. 3.3.1-1, the production metal blastshield weighs 11.7 lb., and the baseline CMC flight article weighed 9.5 lb., which grew to 10.4 lb. after repair doublers were added. The baseline CMC model used here weighs 9.13 lb., and the LOM CMC model weighs 10.70 lb. (case 11). Note that panel model weights are typically a few percent low due to the simplification of details such as fillets (2.9-3.9% here).

It is estimated that using a 9-attachment design could eliminate an additional 2.0-2.6 lb. of hardware (2 threaded posts, 3 brackets/nutplates, and 1 linkage/clevis).

3.3.1.7 Structural analysis conclusions

- Working stress / allowable stress levels are adequate for the two CMC design concepts.
- Both CMC designs are lighter than the production metal heatshield.
- An alternate attachment concept can produce the lowest total weight.

- Detailed failure modes such as ply-ply delamination, stiffener-skin separation, bearing, etc., require considerable testing beyond the scope of the present program, but the LOM process can facilitate test elements manufacture.

3.3.1.8 Mechanical Testing

Flexure of basic skins

Flexure specimens were cut from two panels of LOM-processed Nextel™312/Blackglas™ CMC cross-ply woven composite. The raw data are reported in Appendix 5.1. The test results are summarized in Figures 3.3.1-16 and 3.3.1-17.

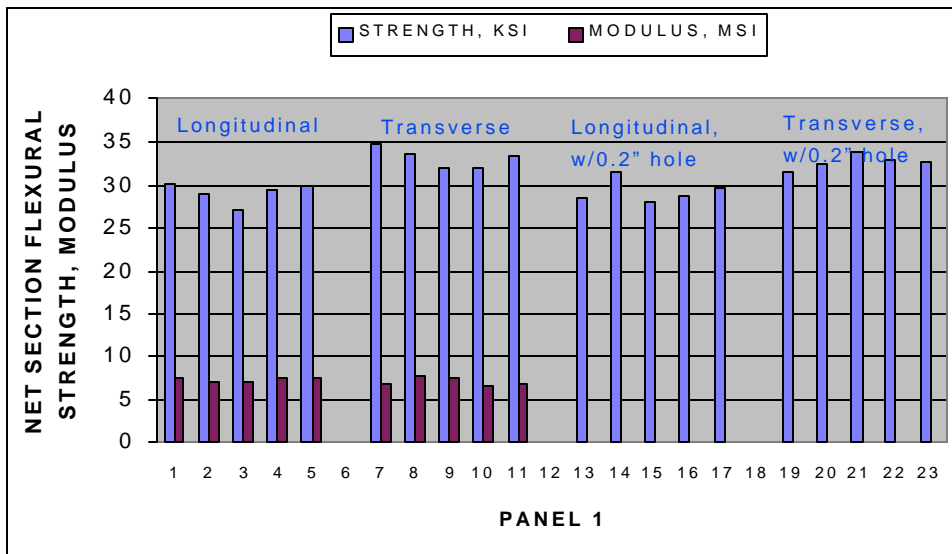


Figure 3.3.1-16 Skin flexure strength and modulus, with and without hole—Panel 1.

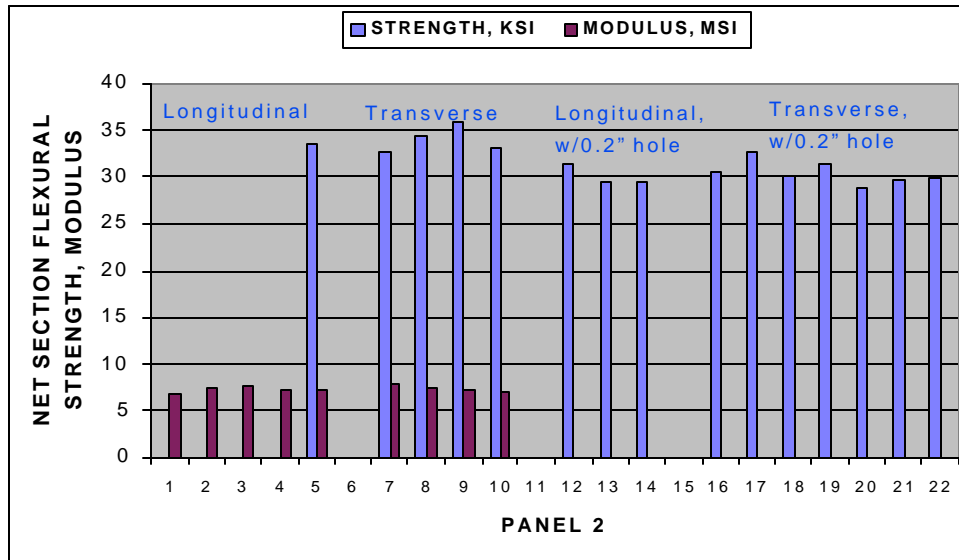


Figure 3.3.1-17 Skin flexure strength and modulus, with and without hole—Panel 2.

The flex strengths and moduli, Figures 3.3.1-16 and –17, are somewhat below those achieved in the LC³ program. For example, referring to Figure 4.1-3, unnotched tensile strength and modulus was expected to be 25.7 ksi and 9.6 msi, respectively, and approximately 10-20% higher for flex strength, and approximately 10-20% lower for flex modulus. Notch strength, however, is encouraging, indicating that overall static strength is possibly adequate. Dynamic performance may need to be reevaluated in view of the modulus values found here.

Flexure of skin-stiffener

Figure 3.3.1-18 illustrates the test arrangement and includes the test data on skin-stiffener transverse sections. Failure occurred at low values of basic skin flexural stress, generally around 50 percent or less of the plain skin specimens. This implies that skin-stiffener failure modes will be critical and must be addressed in design and process development.

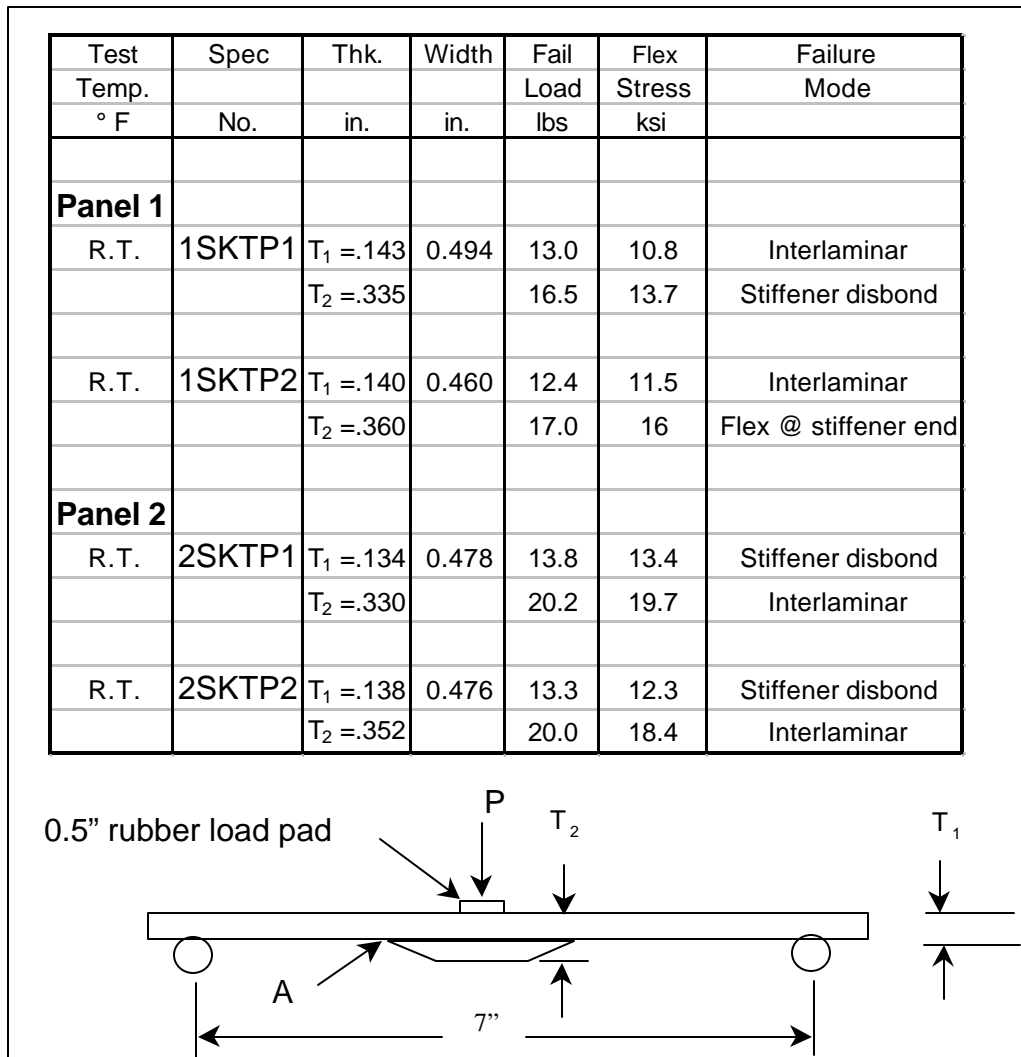


Figure 3.3.1-18 Skin-stiffener flexure tests results

Flexure of stiffener

Figure 3.3.1-19 includes the test data and shows the test arrangement for flexure of longitudinal stiffener sections. Flexural stresses at failure ranged from about 50 to 100 percent of the values obtained in the basic skin flexure tests. This is an issue that should receive further attention and development. The microstructural quality of the stiffener sections should be

determined. If the thick sections are found to be of acceptable quality, this suggests a strength size effect may be involved and the implications of that need to be considered in design.

Test	Spec	Thk.	Width	Fail	Flex	Failure
Temp.				Load	Stress	Mode
° F	No.	in.	in.	lbs	ksi	
Panel 1						
R.T.	1STB1	0.335	0.575	95.0	13.2	Interlaminar
			0.616	116.0	15.1	Flex Tension Side
			0.631			
Panel 2						
R.T.	2STB1	0.328	0.628	130.0	17.3	Noise: No visible damage
				152.0	20.2	Interlaminar
				154.0	20.5	Flex Tension Side
				198.0	26.4	Multiple Interlaminar

Figure 3.3.1-19 Stiffener section flexural tests.

References for 3.3.1

- 3.3.1-1 Box, Don M., Charles R. Foreman, Steven L. Pauletti, John E. Ramon, and Kendall G. Young, "Structural Design of the AV-8B Ceramic Matrix Composite (CMC) Heatshield," Report No. N380/7R-01, Northrop Grumman Corporation, November 1997. (*Proprietary report*)

- 3.3.1-2 Box, Don M., Charles R. Foreman, Steven L. Pauletti, John E. Ramon, and Kendall G. Young, “Structural Analysis for the AV-8B Ceramic Matrix Composite (CMC) Heatshield,” Report No. N380/6R-01, Northrop Grumman Corporation, August 1996. *(Proprietary report)*
- 3.3.1-3 Buesking, Kent, Brian Sullivan, Shannon Casey, Hans Jensen, Terry Barnett, Don Box, and John Madsen, “Repair of Ceramic Matrix Composites for Exhaust Washed Structures,” Final Report MR&D AW01 (NAWC Contract N68335-99-C-0025), Materials Research & Design, Inc., July 1999. *(ITAR/EAR report)*

3.3.2 Fabrication of Demonstration Component (Task 1.3.2)

Introduction

This section describes the procedures employed for the fabrication of the final design for the blastshield demonstration component by the LOM/Forming process. The final optimized design for the demonstration article was down-selected from the set of test cases evaluated in the structural analysis described in Section 3.3.1. The procedures described below incorporate the optimized prepreg and low cost LOM tooling material described in Section 3.2.1, with the hardware improvements implemented on the LOM scanner system described in Section 3.2.2, to LOM fabricate a 2-D laminate which was subsequently formed/cured into the green state blastshield demonstration article. The cured Nextel™312/Blackglas™ blastshield is then decubed and subjected to successive pyrolysis/reinfiltration procedures to convert and densify the component into CMC.

The final design case blastshield demonstration article design specifications were input into the CCDP system, which generated the LOMNEF file description for the final composite flat ply stack. A subroutine was written into the LOMNEF file translator to offset the decube regions of adjacent ply layers to eliminate the indentations which were found to form in the skin regions of the cured components due to overlapping laser cuts. The ply stacks for two blastshield demonstration articles were fabricated on the LOM scanner system, formed/cured on an appropriate forming tool and decubed. Both green state demonstration articles were next subjected to five pyrolysis/reinfiltration cycles.

Generation of Demonstration Component LOMNEF File

The minimal geometric descriptors for a 2D laminate composite required by the CCDP system to generate ply cut-out and stacking sequence data for part fabrication (using the PLYDEF and CADCOMP subroutines) are 1) an array of points defining the part IML surface, 2) set of points defining the part IML edge boundary, 3) set of points defining center of attachment locations on part IML surface, 4) final (CMC) ply thickness 5) final (CMC) skin thickness, and 6)

stiffener width, thickness & taper angle. The CCDP system accepts the above point data in a variety of formats (ASCII, CSV, EXCEL spreadsheet). Based on the dynamic structural analysis results, Test Case 6 was chosen for the final blastshield demonstration component design. The appropriate point array file descriptors for the blastshield IML surface were generated in COSMOS/M from the blastshield solid model. The points were defined as comma delineated ASCII files for input to the CCDP system. Figure 3.3.2-1 displays the corresponding point files delineating the blastshield IML surface nodes (3038 points) while Figure 3.3.2-2 the IML edge boundary and attachment node locations. Due to corporate liability issues (the original AV-8B blastshield is a Boeing part) coupled with material budget constraints (mainly the cost of nitrided Nextel™ 312 fabric), it was decided to fabricate a dimensionally scaled down (0.8x) demonstration component with a size of (18"W x 24"L x 14.6"). The point files were scaled accordingly in the Rhino3D modeling program and exported as CSV (comma separated values) files to the CCDP system.

Utilizing the PLYDEF subroutine in CCDP the flat ply patterns for the demonstration component were generated which included the necessary debulking elements. An added subroutine was written into the program to automatically offset the decube regions in adjacent plies based on the specified crosshatch dimensions. Figure 3.3.2-3 displays

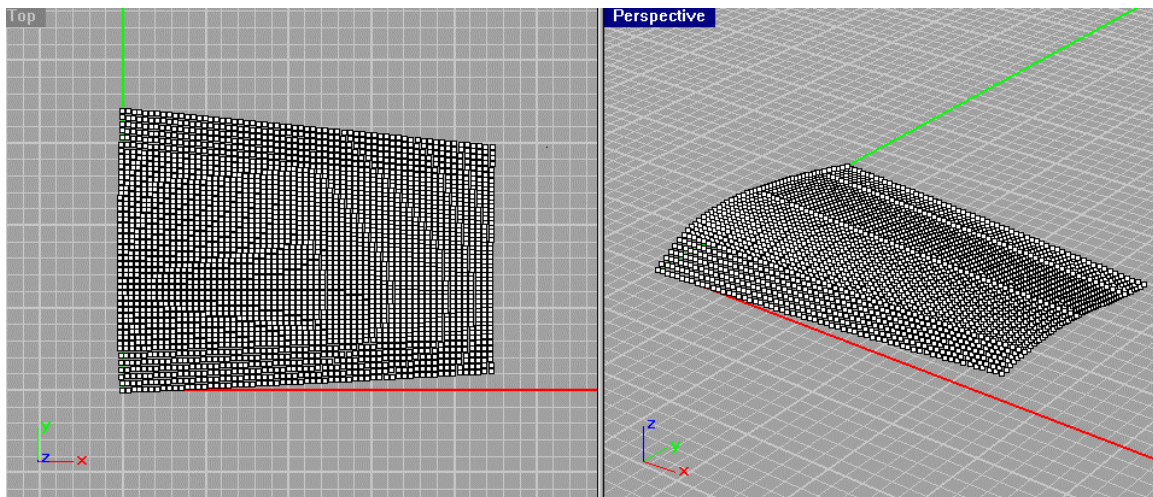


Figure 3.3.2-1 Surface nodes for blastshield demonstration component

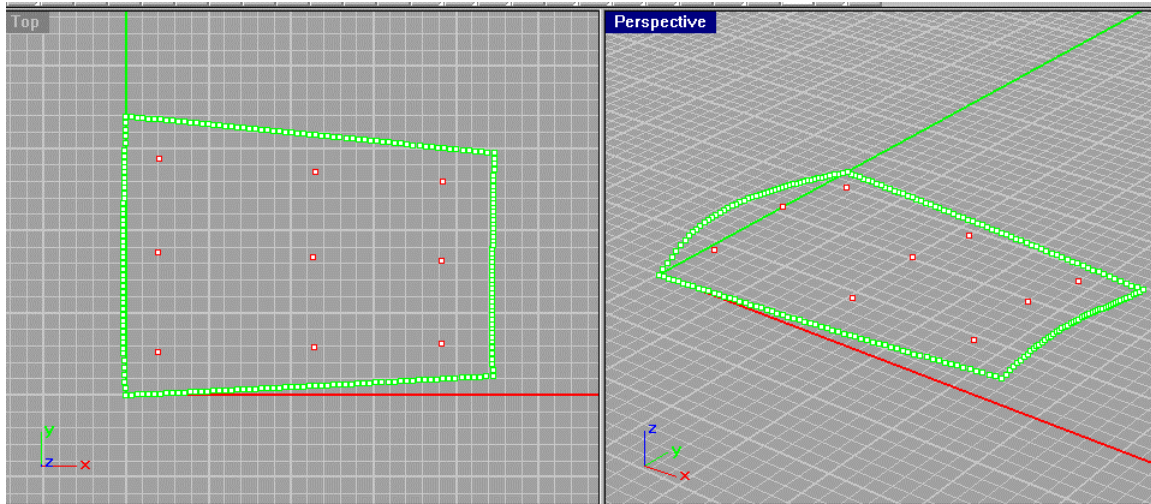


Figure 3.3.2-2 Edge and attachment nodes for blastshield demonstration component

the CCDP screen output for the demonstration component (0/90) flat ply patterns with the overlapping offset decube pattern. The crosshatch dimension for each ply was 1"x 1" (Note: As the image is a supposition of all plies in the laminate, the cutout regions appear meshed due to the simultaneous view of all shifted decube boundaries). Finally, the flat ply pattern data with debulking paths was converted into the LOMNEF file format and outputted from CCDP to the LOMSlice program of the LOM scanner system. Figure 3.3.2-4a displays the LOM scanner system screen image for a skin ply of the demonstration component; Figure 3.3.2-4b the screen image of a stiffener ply.

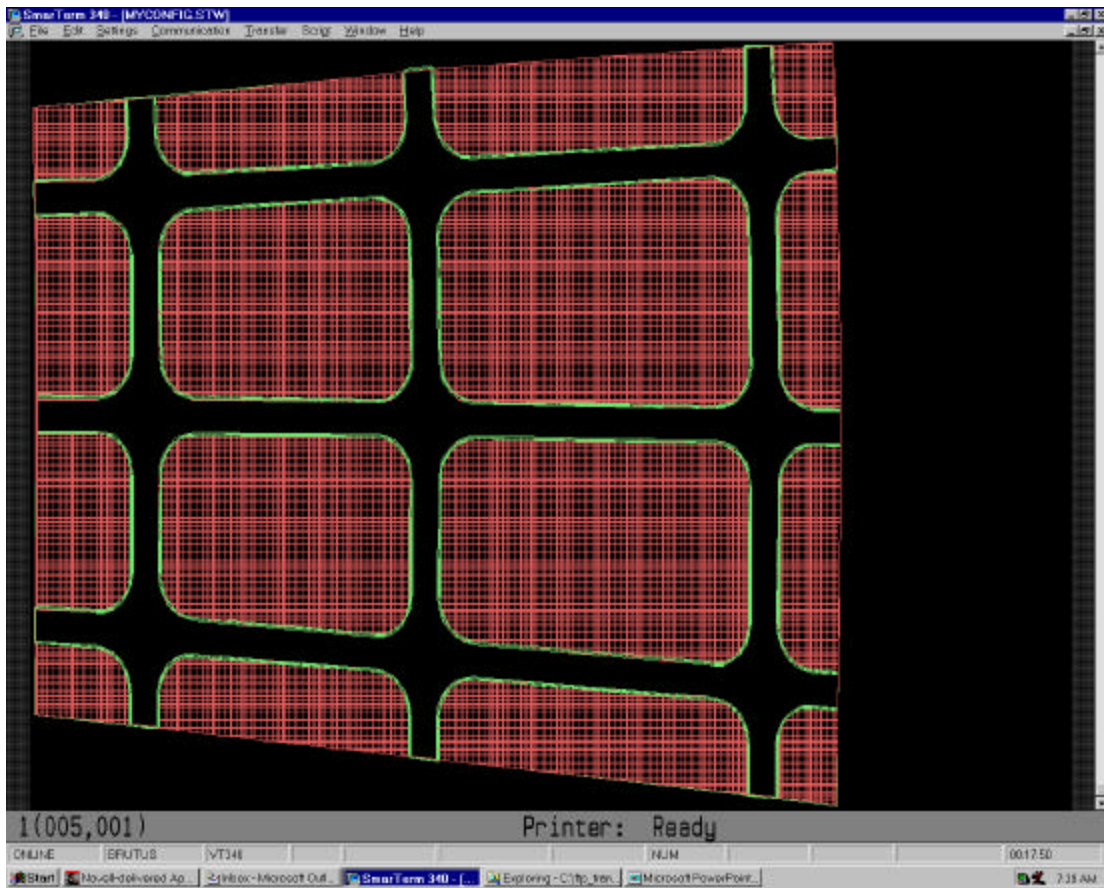


Figure 3.3.2-3 CCDP screen display of blastshield flat ply patterns with offset decube pattern

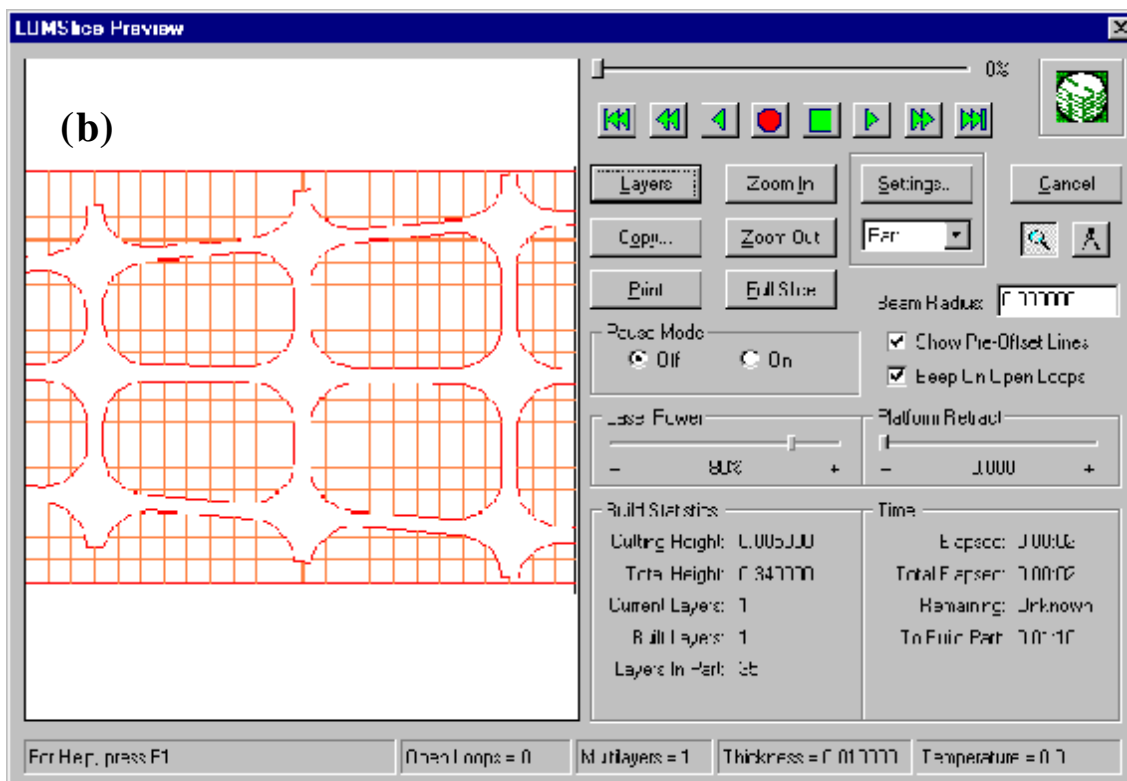
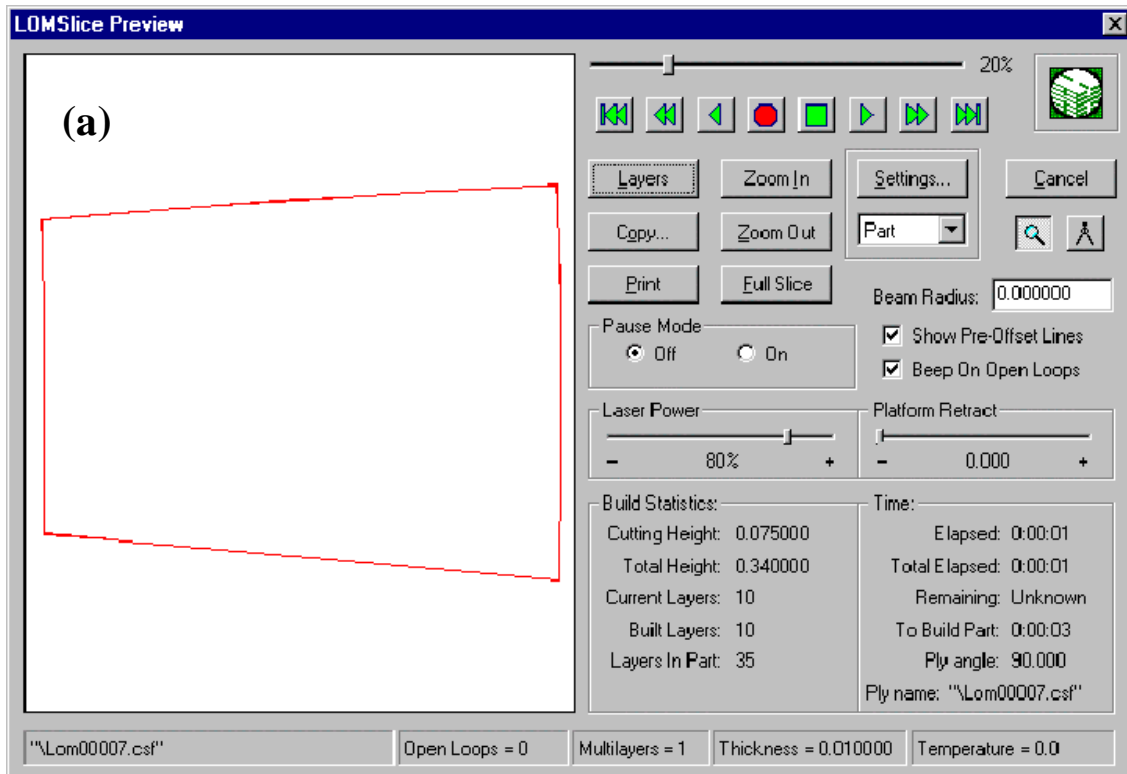


Figure 3.3.2-4 LOMSlice screen display of demonstration blastshield (a) skin ply and (b) stiffener ply

Fabrication of Demonstration Component

Utilizing the LOMNEF design file, two (0/90), 16 ply Nextel™ 312/Blackglas™ 493 A/B laminates were fabricated on the LOM scanner system utilizing the optimized prepreg formulation and scanner cutting parameters determined earlier in the program. It was decided to LOM fabricate two blastshield laminates as a precaution in the event that one did not survive post processing (as 2D Nextel™/Blackglas™ laminates of this size had not previously been pyrolyzed/reinfiltrated by Northrop Grumman). To firmly secure the prepreg ply stack to the LOM build platform for successive lamination/laser cutting (while also allowing the final laminate to be easily removed from the unit), the following initial ply attachment scheme was utilized. A stiff metal plate was first attached to the LOM build platform with tape. A layer of Freecoat was applied to the plate, then a sheet of non-porous TX1040 Teflon (of a size much greater than blastshield dimensions) was tightly stretched over the plate and secured at its edges with tape. Two plies of fiberglass cloth impregnated with 20 wt.% Blackglas™ 493A/B polymer were next attached to the Teflon sheet with tackifier (with tackifier between each layer of fiberglass cloth) followed by another layer of non-porous Teflon sheet. Finally, the first prepreg ply of the Nextel™/Blackglas™ laminate was attached to the Teflon sheet with tackifier.

To remove the final LOM processed laminate from the build platform; the tape holding the metal plate to the unit was cut and the plate removed. The border around the first Teflon layer was next cut from the metal plate to allow the laminate to be lifted and transferred onto the forming tool. As expected, during the first pyrolysis run, the Teflon layers attached to the cured laminate burned off causing the fiberglass sheets to debond from the final Nextel™/Blackglas™ demonstration component.

The two Nextel™/Blackglas™ ply stacks for the demonstration component were fabricated on the LOM scanner system located at Helisys Inc. in Torrance, CA. The Composites Forming Module needed to cure/form the uncured laminates into the designated blastshield shape, though, was still located at the Northrop Grumman Bethpage NY site. Due to the inherent risk

involved with shipping (while chilled) the uncured laminates back to Bethpage, it was decided to cure/form one laminate at the nearby Northrop Grumman El Segundo facility while shipping the second laminate back to the Northrop Grumman Bethpage, NY site for post processing.

Blastshield Demonstration Component 1 Post Processing

The initial plan was to cure/form one of the LOM fabricated blastshield laminates on the Composites Forming System utilized in the Northrop Grumman F/A-18 production facility in El Segundo, CA. Thermal calibration tests on the El Segundo system, though, revealed that the upper temperature required for cure of the BlackglasTM polymer could not be reached on the unit without potentially damaging the system's Plexiglas viewing ports. Unlike the Composites Forming module in Bethpage, which uses heat lamps, the El Segundo Composites Forming System utilizes forced hot air to heat the composite ply stack during forming. To contain the forced air over the part/tool (while still allowing the part to be visually monitored) a cover with Plexiglas windows is mounted over the top of the Forming Device. Calibration tests revealed that the Plexiglas windows would melt if the unit's hot air blower system was forced to heat the laminate to 150°C. As an alternative, the uncured NextelTM/BlackglasTM ply stack was formed by vacuuming bagging the laminate over the blastshield Richlite tool and cured (under vacuum) in a conventional walk-in oven. Figure 3.3.2-5a displays the initial vacuum bagged laminate while Figure 3.3.2-5b the laminate after cure.

After cure the blastshield was shipped back to the Northrop Grumman Bethpage site for decubing followed by pyrolysis/reinfiltration. Figure 3.3.2-6 displays a section of the partially decubed blastshield in which the decube offset pattern is revealed. Figure 3.3.2-7 displays the final, fully decubed blastshield before the first pyrolysis run. Figure 3.3.2-8 shows a close-up image of a stiffener section in the decubed component. No dimpling of the surface of the skin cutout regions of the blastshield was found when using the optimized decube offset pattern. The dark lines in the cutout regions of the skin are not depressions but remnants of the laser cut char zone on the surface of the ply. Wrinkling was also evident in the surface ply of the stiffener

section located in the region of the blastshield with the greatest curvature (top forward).

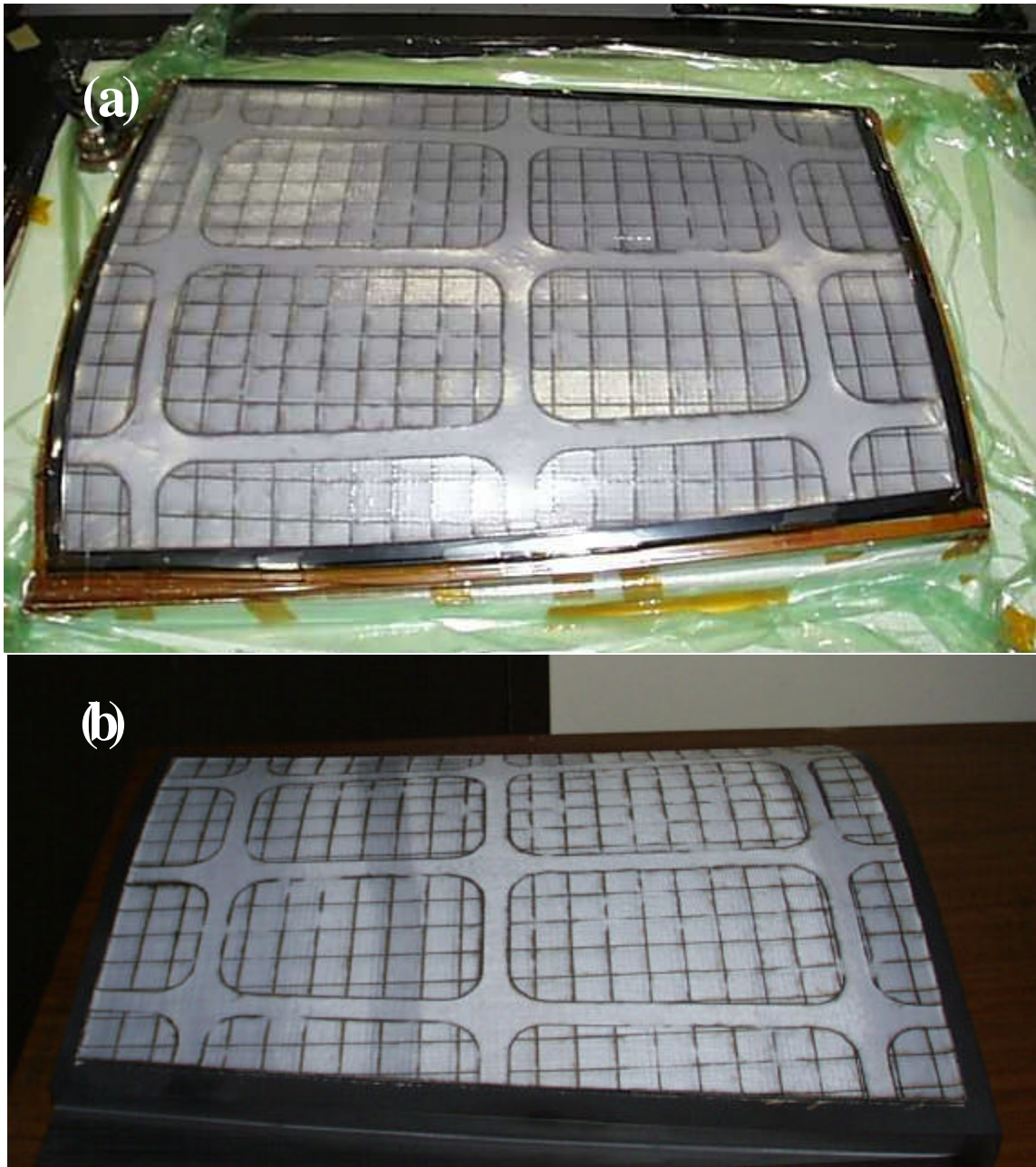


Figure 3.3.2-5 Nextel™/Blackglas™ prepreg laminate (a) vacuum bagged over blastshield tool and (b) after cure in oven



Figure 3.3.2-6 Partially decubed section of cured blastshield showing offset decube pattern

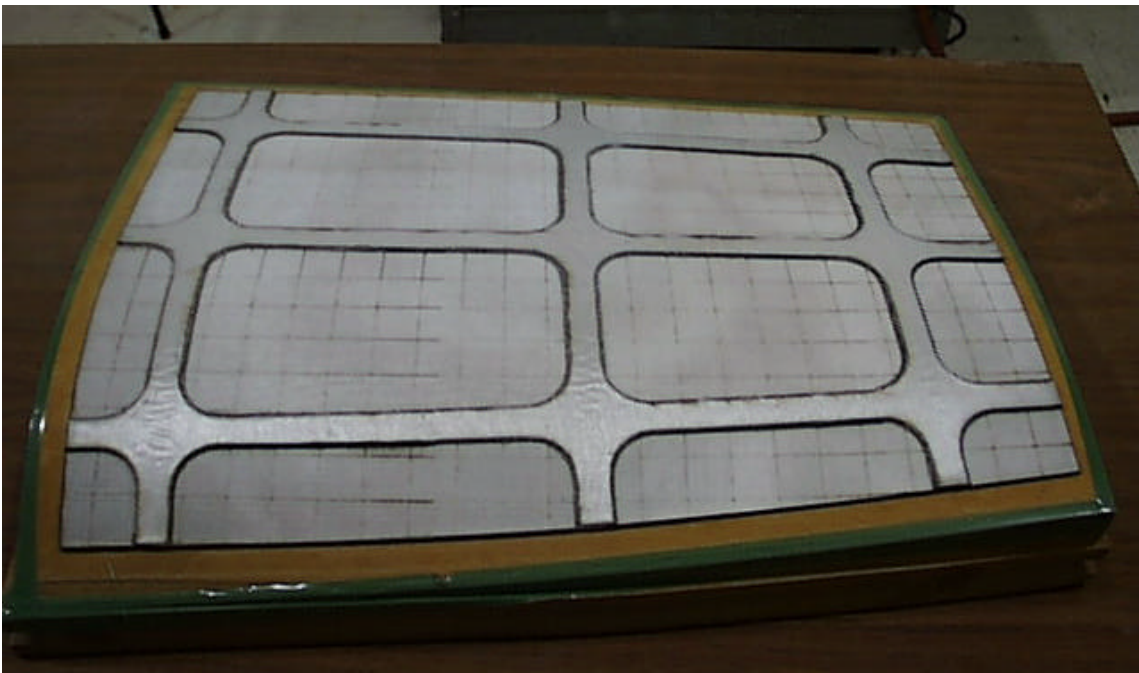


Figure 3.3.2-7 Blastshield Demonstration Component 1 after decubing

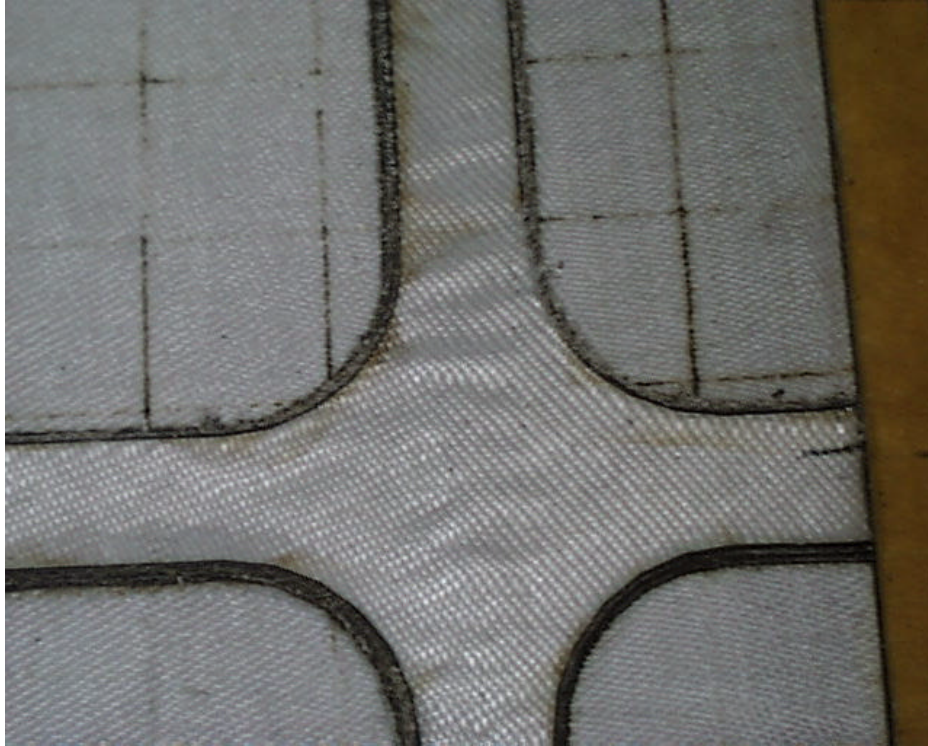


Figure 3.3.2-8 Detail of stiffener section of decubed blastshield Demonstration Component 1 showing ply wrinkling

The reason for the ply wrinkling is unclear. Though the formability curvature analysis indicated that this section of the blastshield had the greatest degree of complex curvature, the amount was not at a level that would indicate the area could not be formed. The role of the laser cuts making up the crosshatch regions around the stiffener section cannot be ruled out. The shear force exerted by the vacuum bag combined with the compliant nature of the decubed fabric and curvature of the part could have resulted in wrinkling of the plies. The wrinkling has been eliminated in the second Nextel™/Blackglas™ laminate by using the Bethpage composite double diaphragm forming module in which better control of the shearing force can be obtained during the forming step.

After decubing, the blastshield was subjected to the multiple pyrolysis and reinfiltration steps to convert the Blackglas™ polymer into a ceramic and densify the final Nextel™/Blackglas™ CMC blastshield. A (proprietary), optimized pyrolysis schedule developed under the previous DARPA LC³ program was used for all pyrolysis runs. No CMC panel was

ever found to delaminate during this optimized pyrolysis schedule. A reinfiltration fixture was initially used to reinfiltrate the blastshield after the first pyrolysis. Great difficulty was encountered, though, in removing the (at this point) partially densified and thus fairly pliable blastshield from the mold. Removal from the fixture also resulted in considerable waste of unused Blackglas™ resin.

Out of concern for inducing delaminations in the partially densified part, the fixture was not utilized for further reinfiltrations. Taking advantage of the low viscosity of the Blackglas™ 493 A/B resin, the reinfiltration instead was accomplished by simply applying the resin to the surface of the blastshield with a brush (while examining the underside of the part to note when the resin diffused to the other side). Previous Northrop Grumman Blackglas™ CMC development programs had determined this to be a suitable infiltration method for thin, simply shaped composite parts. These studies found no discernable difference in strength between thin 2D panels re-infiltrated with the above method compared to panels infiltrated by RVI, closed mold techniques. The blastshield tool was used as a support structure during oven cure of the component after the Blackglas™ polymer reinfiltration. The tool was first vacuum bagged, though, before placement of the reinfiltrated blastshield as the Blackglas™ resin reacts at the cure temperature with the tooling material.

Figure 3.3.2-9 displays the fully densified Nextel™/Blackglas™ CMC demonstration blastshield 1. No visual delaminations or other defects were discerned in the part (except for the wrinkles which were generated during cure). The wrinkled zones along the stiffener elements also did appear to increase in size after successive pyrolysis runs.



Figure 3.3.2-9 Pyrolyzed Nextel™/Blackglas™ Blastshield Demonstration Component 1.

LOM/Forming of CMC Blastshield Demonstration Component 2

The second LOM fabricated Nextel™/Blackglas™ prepreg laminate for the demonstration blastshield was shipped from Helisys Inc. to the Northrop Grumman Bethpage site for cure on the Composites Forming Module. The LOM fabricated and resin infused blastshield tool prepared earlier in the program was used for the forming/cure step. The tool was placed in the module and a vacuum pulled between the tool and the first diaphragm. The frame was next removed from the perimeter of the uncured blastshield laminate and the prepreg stack then transferred to the tool surface with the (still attached) underlying Teflon release ply. The prepreg laminate was centered on the tool, trimmed with a cork dam, and configured with the appropriate thermocouple gages. A single sheet of non-porous TX 1040 Teflon release ply was used to isolate the surface of the prepreg stack from the upper transparent silicone diaphragm as the Blackglas™ polymer reacts with silicone at the upper cure temperature.

The combined low viscosity of the Blackglas™ resin and loose weave of the AF10

Nextel™ fabric made the prepreg laminate readily drapable over the blastshield tool. It is for this reason that the prepreg laminate was not first constrained through application of a vacuum between the two elastomeric diaphragms followed by deformation over the tool by applying a vacuum between the tool surface and bottom diaphragm. The latter procedure is typically performed for composites forming of thermoplastic and thermoset based polymer matrix composites in which the prepreg forms are typically less flexible.

Figure 3.3.2-10 shows, consecutively, the composites forming module with the a) initial blastshield prepreg laminate on the resin infused LOM tool, b) transparent diaphragm under initial vacuum, c) laminate under partial vacuum, d) laminate under full vacuum; e) blastshield laminate during cure under the heat lamps and f) final cured component before decubing. No wrinkling was observed after cure in the outer plies of the stiffener sections of the laminate as found for blastshield demonstration component 1. It is hypothesized that this is due to the more controlled vacuum consolidation achieved in the forming module. Figure 3.3.2-11 displays the final, cured blastshield demonstration component after decubing (before initial pyrolysis). Figure 3.3.2-12 shows a detail of a stiffener element of the part in which no ply wrinkling/buckling is evident. Note also the smooth surface of the cutout regions of the skin as a result of using the offsets decube pattern. After decubing, the blastshield was subjected to pyrolysis and reinfiltration cycles as described above in “Blastshield Demonstration Component 1 Post Processing”. Figure 3.3.2-13 displays the fully densified Nextel™/Blackglas™ CMC Demonstration Blastshield 2. No visual delaminations or other defects were discerned in the part.

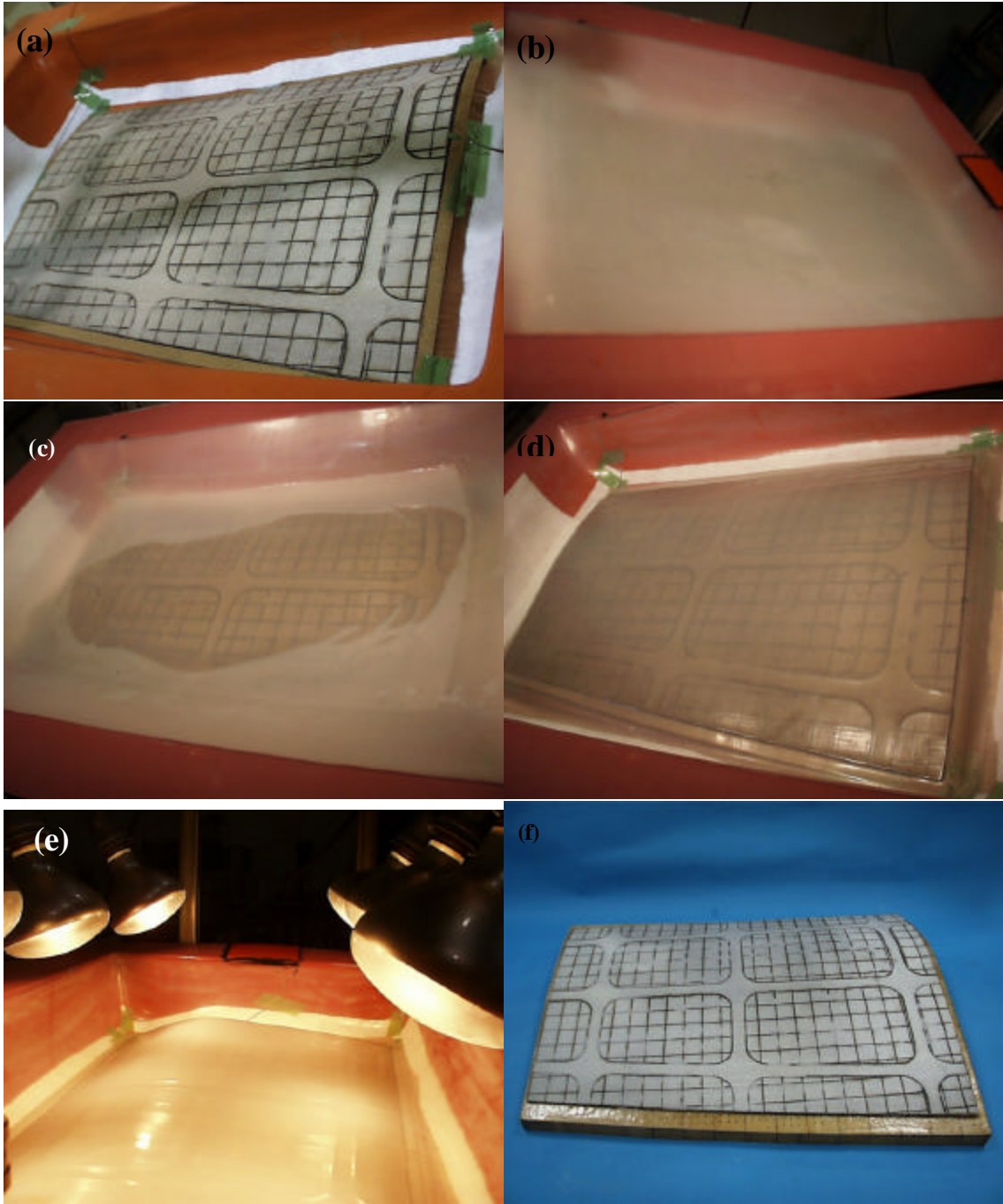


Figure 3.3.2-10 Composites forming module with a) uncured blastshield prepreg laminate on resin infused LOM tool, b) transparent diaphragm under initial vacuum, c) under partial vacuum, and d) under full vacuum; e) curing of blastshield laminate under heat lamps and f) final, cured Demonstration Component 2 before decubing.

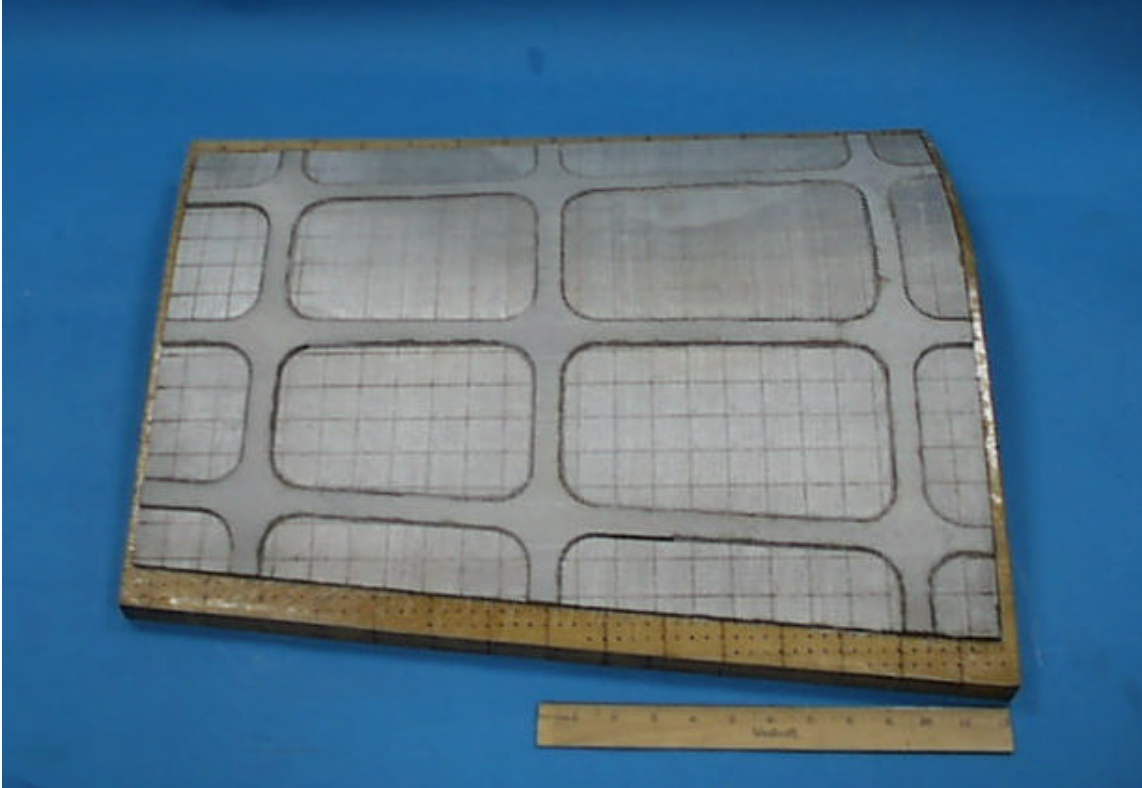


Figure 3.3.2-11 Nextel™/Blackglas™ Blastshield Demonstration Component 2 after decubing (before first pyrolysis).

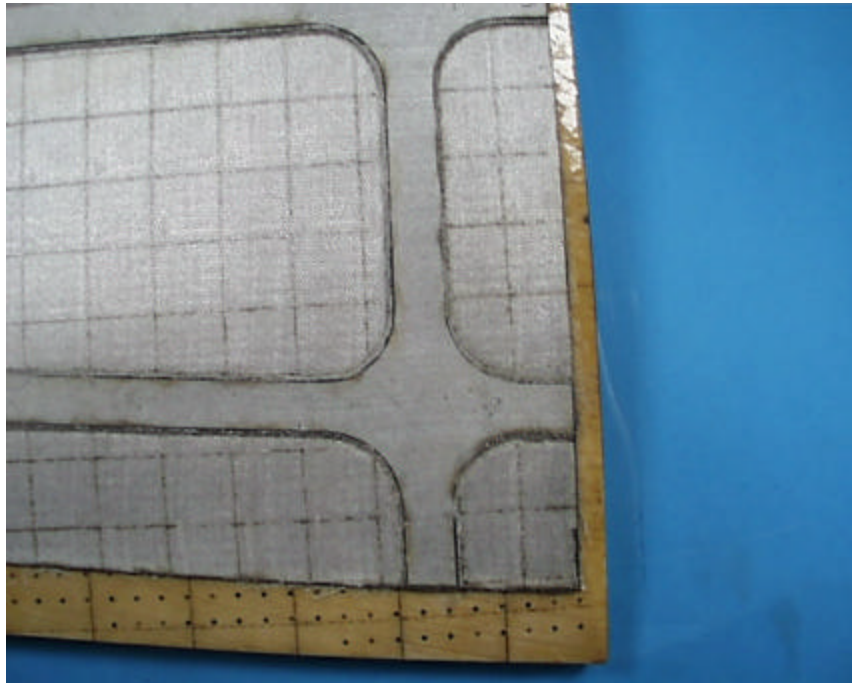


Figure 3.3.2-12 Detail of stiffener elements in cured Nextel™/Blackglas™ Blastshield Demonstration Component 2 after decubing (before first pyrolysis)



Figure 3.3.2-13 Nextel™/Blackglas™ Blastshield Demonstration Component 2 after pyrolysis.

4.0 OVERALL SUMMARY & CONCLUSIONS

As reported upon herein, program goals to develop LOM processing of CMC materials and processing technology, and to fabricate a CMC demonstration blastshield component were achieved. Significant advances were made in the development of LOM processing of preceramic polymer Blackglas™ CMC, in the design, and manufacture of a CMC blastshield demonstration component, and in the successful utilization the capabilities that exist within different organizations to achieve these goals. Some of the major program accomplishments were:

- Evaluated low-cost 2D Nextel™ 312(BN)/Blackglas™ systems for LOM processing
- Developed science-based processing methodology for LOM of Blackglas™ preceramic polymer
- Completed detail design of a demonstration blastshield component
- Designed low cost tooling for LOM/forming processing and fabricated two demonstration CMC blastshield components
- Integrated the SFF LOM/Forming Prototyping Process With the CCDP Composite Laminate Design System
- Formulated a Design Methodology for the New LOM/Forming Prototyping Process
- Developed & Demonstrated LOM/Forming for Fabrication of CMC With the Low-Cost, Nextel™/Blackglas™ Ceramic Precursor Synthesis Route
- Developed Processes for Generating Low Cost, Composites Tooling Via LOM
- Developed & Demonstrated LOM/Forming for Fabrication of Large, Curved CMC Structures
- Demonstrated the Validity of SFF Design Approach by Design, Fabrication, & Test of an Aircraft CMC Demonstration Blastshield
- Developed a Brand New LOM System/Process that:
 - Can Process CMC and Other Composites

- Is 2-4 Times Faster for Parts Processing
- Improved Surface Finish and Precision
- Has Convenient Users Interface Based on Latest LOMSlice 2.0 Software
- Features User Friendly CCD Camera Based Calibration
- Is Easily Adaptable to Existing LOM Platforms.

Figure 4-1(a) and (b) illustrate the design/build flow of the LOM CMC process developed here.

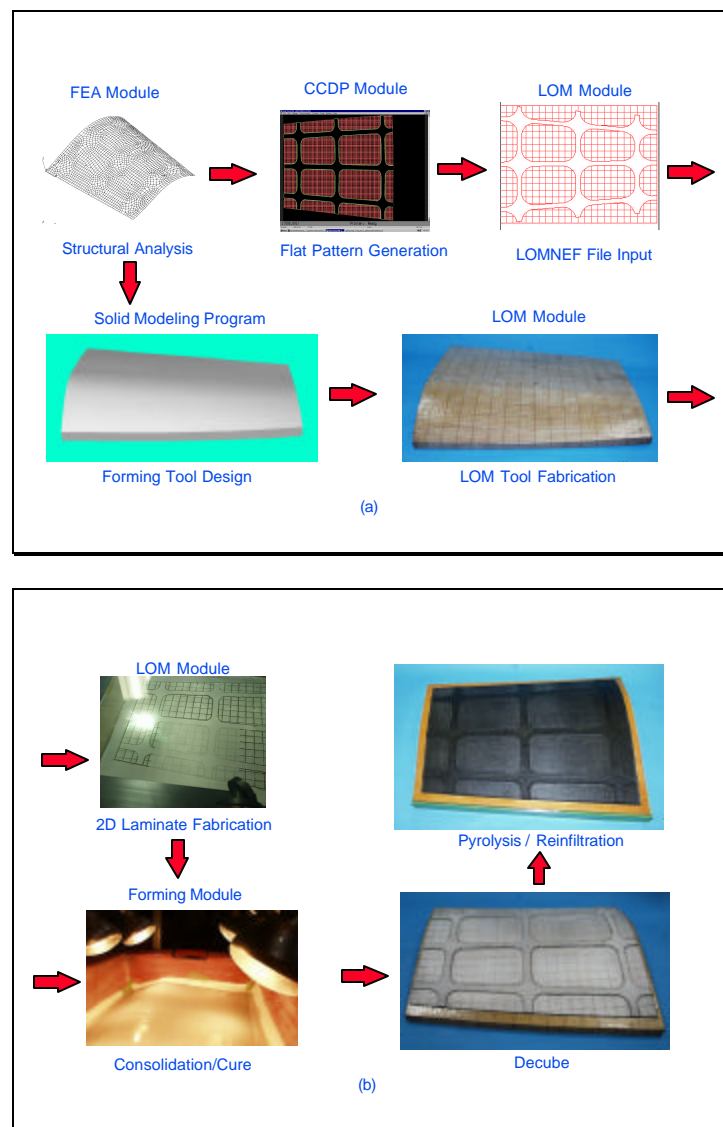


Figure 4-1 Elements of LOM-Based CAD/CAM Procedure for CMC Blastshield

5.0 APPENDICES

5.1(a) Basic Skin Flexure Test Report – Panel 1

LABORATORY REPORT - MATERIAL TEST

EMTL

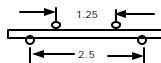
REQUESTED BY G. Dillon				DATE 7/13/00					
JOB NO.				SPECIFICATION ASTM D-790					
JOB TITLE Laminated Object Mmainence - Material				TESTING MACHINE TO-Lo Cap					
MATERIAL				INSTRUMENTATION D-2					
TEST CONDITIONS NORMALIZED THICKNESS: 16 Plies @ 0.0075 = 0.120				SPAN as noted CROSSHEAD RATE, IN./N 0.06 SOAK TIME, MIN. N/A					
Test Temp. ° F	Spec. No.	Thk. in.	Width in.	Fall Load lbs	Stress ksi Act.	Mod msl Act.	Load Config	ID Dir	Failure Mode Notes
Panel 1									
Longitudinal									
R.T.	1SKLB1	0.141	0.473	75.5	30.1	7.63	3	(2)	Flex / Tension side
R.T.	1SKLB2	0.145	0.481	77.8	28.8	6.94	3	(2)	Flex / Tension side
R.T.	1SKLB3	0.143	0.479	70.8	27.1	6.90	3	(2)	Flex / Tension side
R.T.	1SKLB4	0.142	0.481	76.0	29.4	7.69	3	(2)	Flex / Tension side
R.T.	1SKLB5	0.143	0.463	75.0	29.7	7.55	3	(2)	Flex / Tension side
Transverse									
R.T.	1SKTB1	0.141	0.478	87.6	34.6	6.76	3	(2)	Flex / Tension side
R.T.	1SKTB2	0.142	0.479	86.8	33.7	7.70	3	(2)	Flex / Tension side
R.T.	1SKTB3	0.141	0.480	81.2	31.9	7.60	3	(2)	Flex / Tension side
R.T.	1SKTB4	0.144	0.490	86.8	32.0	6.48	3	(2)	Flex / Tension side
R.T.	1SKTB5	0.143	0.480	87.0	33.2	6.82	3	(2)	Flex / Tension side
R.T.	1SKTB6	0.144	0.478				3	(2)	
R.T.	1SKTB7	0.142	0.474				3	(2)	
Open Hole (Nominal .200 diameter hole)									
Longitudinal									
R.T.	1SKLB8	0.142	0.512	48.0	17.4	N/A	3	(2)	Flex / Tension side
R.T.	1SKLB9	0.140	0.506	50.5	19.1	N/A	3	(2)	Flex / Tension side
R.T.	1SKLB10	0.140	0.488	42.2	16.5	N/A	3	(2)	Flex / Tension side
R.T.	1SKLB11	0.143	0.496	46.2	17.1	N/A	3	(2)	Flex / Tension side
R.T.	1SKLB12	0.136	0.485	41.5	17.3	N/A	3	(2)	Flex / Tension side
Transverse									
R.T.	1SKTB8	0.139	0.473	44.2	18.1	N/A	3	(2)	Flex / Tension side
R.T.	1SKTB9	0.139	0.479	46.5	18.8	N/A	3	(2)	Flex / Tension side
R.T.	1SKTB10	0.140	0.470	47.8	19.5	N/A	3	(2)	Flex / Tension side
R.T.	1SKTB11	0.140	0.479	48.0	19.2	N/A	3	(2)	Flex / Tension side
R.T.	1SKTB12	0.141	0.478	48.2	19.0	N/A	3	(2)	Flex / Tension side
R.T.	1SKTB13	0.142	0.480			N/A	3	(2)	
R.T.	1SKTB14	0.141	0.484			N/A	3	(2)	

Notes:

- (1) Identification side tested in compression
- (2) Identification side tested in tension

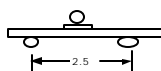
Loading Configurations

Configuration 1 (4 point loading @ quarter points)



Configuration 2 - Same as #1, except utilized .063 x .190 Fiberglass Pads load pads.

Configuration 3 (3 point loading) w/ .063 x .190 Fiberglass load pad



5.1 (b) Basic Skin Flexure Test Report – Panel 2

LABORATORY REPORT - MATERIAL TEST

EMTL 00-17

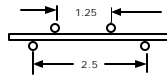
REQUESTED BY G. Dillon (6-6830)					DATE 7/13/00				
JOB NO.					CONDUCTED BY Fidnarick				
JOB TITLE Laminated Object Maintenance - Material Ev					TYPE TEST Flexure				
MATERIAL					TESTING MACHINE TO-Lo Cap				
TEST CONDITIONS					INSTRUMENTATION D-2				
NORMALIZED THICKNESS: 16 Piles @ 0.0075 = 0.120					SPAN, as noted CROSSHEAD RATE, IN 0.06 SOAK TIME, MIN. N/A				
Test Temp ° F	Spec No.	Thk IN.	Width IN.	Fail Load lbs	Stress, ksi Act	Mod, msi Act	Load config	ID Dir	FAILURE MODE NOTES
Panel 2									
Longitudinal									
R.T.	2 SK L B7	0.130	0.410	71.2	19.3	6.70	1	(1)	Comp under load point / Flex Ten
R.T.	2 SK L B8	0.135	0.485	52.0 / 55.5		7.44	3	(1)	Flex / Tension side
R.T.	2 SK L B9	0.136	0.486	50.0 / 53.5		7.68	3	(1)	Flex / Tension side
R.T.	2 SK L B10	0.134	0.486	48.5 / 49.0		7.29	3	(1)	Flex / Tension side
R.T.	2 SK L B11	0.136	0.483	80.0	33.6	7.05	3	(2)	Flex / Tension side
R.T.	2 SK L B12	.126-.135	0.482	75.8			3	(2)	Flex / Tension side
Transverse									
R.T.	2SKTB8	0.135	0.481	77/98			2	(1)	nterlam : Flex Ten side
R.T.	2SKTB9	0.135	0.484	38.5/46.8		7.56	3	(1)	nterlam : Flex Ten side
R.T.	2SKTB10	0.135	0.484	40/49		7.39	3	(1)	nterlam : Flex Ten side
R.T.	2SKTB11	0.133	0.486	75.0	32.7	7.85	3	(2)	Flex / Tension side
R.T.	2SKTB12	0.133	0.486	79.0	34.5	7.35	3	(2)	nterlam : Flex Ten side
R.T.	2SKTB13	0.133	0.484	82.0	35.9	7.15	3	(2)	Flex / Tension side
R.T.	2SKTB14	0.133	0.486	76.0	33.2	6.94	3	(2)	Flex / Tension side
Open Hole (Nominal .200 diameter hole)									
Longitudinal									
R.T.	2SKLB1	.128-.135	0.489	39.8			3	(2)	Flex / Tension side
R.T.	2SKLB2	0.134	0.485	43.0	18.5		3	(2)	Flex / Tension side
R.T.	2SKLB3	0.132	0.484	38.8	17.3		3	(2)	Flex / Tension side
R.T.	2SKLB4	0.132	0.486	39.2	17.4		3	(2)	Flex / Tension side
R.T.	2SKLB5	0.132	0.485	22.5 / 27.0			3	(2)	Flex / Tension side
R.T.	2SKLB6	.125-.131	0.485	36.8			3	(2)	Flex / Tension side
Transverse									
R.T.	2SKTB1	0.132	0.485	40.5	18.0		3	(2)	Flex / Tension side
R.T.	2SKTB2	0.132	0.482	42.8	19.1		3	(2)	Flex / Tension side
R.T.	2SKTB3	0.133	0.486	40.5	17.7		3	(2)	Flex / Tension side
R.T.	2SKTB4	0.133	0.482	41.8	18.4		3	(2)	Flex / Tension side
R.T.	2SKTB5	0.134	0.484	39.2	16.9		3	(2)	Flex / Tension side
R.T.	2SKTB6	0.134	0.481	39.8	17.3		3	(2)	Flex / Tension side
R.T.	2SKTB7	0.134	0.481	40.2	17.5		3	(2)	Flex / Tension side

Notes:

- (1) Identification side tested in compression
- (2) Identification side tested in tension

Loading Configurations:

Configuration 1 (4 point loading @ quarter points)



Configuration 2 - Same as #1, except utilized .063 x .190 Fiberglass Pads load pads.

Configuration 3 (3 point loading) w/ .063 x .190 Fiberglass load pad

